Master's thesis

NTNU
Norwegian University of Science and Technology
Faculty of Engineering
Department of Civil and Environmental Engineering

Jan Alexander Tubid Myhrvold
Alf Eirik Valle Kopperud

Consolidation and Stress History in Shallow Sediments in the Northern North Sea

Master's thesis in MTBYGG
Supervisor: Rao Martand Singh
Co-supervisor: Seyed Ali Ghoreishi Amiri
June 2023

NTNU
Norwegian University of
Science and Technology

Jan Alexander Tubid Myhrvold
Alf Eirik Valle Kopperud

Consolidation and Stress History in Shallow Sediments in the Northern North Sea

Master's thesis in MTBYGG
Supervisor: Rao Martand Singh
Co-supervisor: Seyed Ali Ghoreishi Amiri
June 2023

Norwegian University of Science and Technology
Faculty of Engineering
Department of Civil and Environmental Engineering

NTNU
Norwegian University of
Science and Technology

Abstract

Acknowledging CO_2 as the main greenhouse gas driving the climate change, many international projects have been initialized to drive innovations and solutions to cut emissions from the worldwide industry. A research project, SHARP, aims to provide investors with data to reduce the associated risks of carbon sequestration in the Northern North Sea. Two dimensional numerical model, oedotriaxial and Atterberg limit tests on Onsøy clay anagolous to Troll were conducted.

Oedotriaxial tests were conducted on clay retrieved from the Onsøy NGTS site provided by NGI. The aim of this testing was to create a basis of comparison between the laboratory assessed K_0 values of the Onsøy clay and the recommended K_0 values from the Troll field. This extended into an assessment of whether the Onsøy clay has analogous properties to Troll which would enable.

Atterberg limit tests were conducted to put the Onsøy samples into the context of the previous characterization of the soil, and to provide documentation in relation to the testing. It also provided a basis for assessing whether changes in the soil had occurred due to time in storage. The results from Atterberg limit tests conducted in conjunction with this thesis fell into what could be expected from previous characterization.

Numerical simulations were conducted in PLAXIS to improve simulations to K_0 and OCR in Troll characterized by Lunne in Unit IIIA (74 – 110). A new thermodynamically sound constitutive model, called Hyper-viscoplastic Cam Clay model, (HVMCC) developed by Dadras-Ajirloo, Grimstad and Amiri (2022) was applied. Remaining layers was calculated with Soft Soil Creep as a continuation of previous thesis work from Jalali (2022). HVMCC adds flexbility in the yield surface by setting the relative location of the effective mean stress, and twist by fricitonal dissipation parameter to address the dilative behavior better.

The flexbility was demonstrated by improving K_0 from 0.8 to near 1 with increasing spacing ratio, while maintaining OCR. Taken into account model limitations and existing studies on spacing ratios of clay, a spacing ratio of 5 with associated flow was determined. Inability to simulate the field recorded K_0 ranging between 1.0 and 1.2, suggests that Unit IIIA is still unloading, or been subjected to anisotropic conditions, which of both the model is unable to recreate. The model have great uncertainties on ice thickness and creep index as field recorded data in these depths vary across the Troll area.

Sammendrag

Mange internasjonale prosjekter har tatt sikte på å fremme innovasjoner og løsninger for å redusere de globale klimagassutslippene. Blant disse er SHARP som sikter på å redusere risikoene knyttet til karbonlagring i den nordre delen av Nordsjøen. En to-dimensjonal numerisk modell, ødotreaksiale og Atterberg-grensetester på analogt materiale ble gjennomført.

Ødotreaksiale tester ble utført på Onsøy-leire levert av NGI. Målet med disse testene var å etablere et sammenligningsgrunnlag mellom laboratoriebaserte K_0-verdier for leiren fra Onsøy og de anbefalte K_0-verdiene fra Troll-feltet. Dette inkluderte også en vurdering av om Onsøy-leiren har analoge egenskaper til Troll-feltet.

Atterberg-grensetester ble gjennomført for å sette prøvene av Onsøyleire i sammenheng med tidligere karakterisering av materialet. Det kan også anses som en ytterligere dokumentasjon i forbindelse med de ødetreaksiale testene og for å vurdere hvorvidt prøvene har tatt skadesom følge av sin tid i oppbevaring. Resultatene fra Atterberg-grensetestene som ble utført i forbindelse med denne avhandlingen var som forventet basert på tidligere karakterisering.

Numeriske simuleringer ble kjørt i PLAXIS for å gjenskape K_0 og OCR i Enhet IIIA (74-110 m) i Troll-feltet undersøkt av (Lunne, Long and Uzielli, 2006). En ny termodynamisk sikker konstitutiv modell, kalt hyper-viskoplastisk cam clay-modell (HVMCC) utviklet av (Dadrasajirlou, 2022) ble brukt som en videreførelse av tidligere masterarbeid av Jalali (2022). HVMCC øker til fleksibiliteten i flyteoverflaten ved å angi den relative plasseringen av den kritiske spenningstilstanden (avstandsforhold), samt vridning via en fiksjonell dempningsparameter for å bedre håndtere dilatansen i materialet.

Med dette økte K_0 fra 0.8 til nær 1, samtidig som OCR ble opprettholdt. Avstandsforholdet ble bestemt til 5 med assosiativ flyt. Avviket fra feltdata for $K_0 = [1, 1.2]$ knyttes til ødometerforholdene modellen er satt i. Resultatene antyder dermed at Enhet IIIA er under avlastning eller vært usatt for passiv belastning, hvilke modellen ikke kan gjenskape. Modellen har stor usikkerhet når det gjelder isbretykkelse og krypindeks, ettersom feltregistrerte data i disse dybdene varierer over Troll-feltet.

Preface

This master's thesis on stress history in the Northern North Sea aims to add new insight by laboratory testing and improving existing models. It is a continuation of a Northern North Sea modelling from a master thesis by Ramin Jalali in 2022 and contribution to research project SHARP.

This master's thesis was conducted in tandem as the conclusion of a five-year master's degree in Civil and Environmental Engineering at NTNU, spring 2023. The topic was chosen on the interest of practical work and alluring prospects of Carbon Capture Storage in conjunction with the ongoing international research project SHARP. The problem is formulated by laboratory testing procedures and numerical simulation using a finite element software, PLAXIS. The thesis is also written in cooperation with the Norwegian Geotechnical Institute (NGI).

Many thanks to our supervisor Dr. Rao Martand Singh for extensive help and giving us confidence in our work. The work has been interesting with many practical hurdles. Therefore, we want to thank Gudmund Reidar Eiksund and Espen Andersen for the diligent assistance. We want to express our gratitude to our partner Lars Grande at NGI for providing material to the laboratory work and helping with literature studies, along with providing support in developing the oedotriaxial test scheme.

Additionally, we thank our supervisor Dr. Seyed Ali Ghoreishian Amiri Seyed for technical assistance on the modelling work. We want to express our gratitude to Dr. Davood Dadrasajirlou's for helping us understand his work and provide support for his constitutive model within hyper viscoplasticity. We have had many helpful discussions which we highly appreciate.

Contents

List of Figures

List of Tables

Nomenclature

Abbreviations

API	Application Programming Interface
GUI	Graphical User Interface
GDS	Global Digital Systems Ltd
GDSTAS	GDS Triaxial Automated System
IURL	Isotropic unloading-reloading line
INCL	Isotropic normal compression line
MCC	Modified Cam Clay (model)
SSC	Soft Soil Creep (model)
HVMCC	Hyper-viscoplastic Modified Cam Clay (model)
NGTS	Norwegian Geo-Test Site
NGI	Norwegian Geotechnical Institute
NGF	Norwegian Geotechnical Society
NTNU	Norwegian University of Science and Technology
PDF	Portable Document Format
PLAXIS	Geotechnical finite element analysis software
NaN	Not a Number, Non-associated number, Undefined number
CCS	Carbon Capture Storage
SINTEF	The Foundation for Industrial and Technical Research
ka	Thousand years

Symbol

σ'_{v0}	Effective initial vertical stress. Sometimes referred as p'_0 in the literature.
σ'_c	Effective vertical preconsolidation stress. Sometimes referred as p'_c in the literature.
σ'_3	Effective principal minor stress
σ'_r	Effective radial stress
σ'_h	Effective horizontal stress
σ'_d	Effective deviatoric stress
ε_q^p	Plastic shear strain
ε_p^p	Plastic mean stress strain
$\dot{\varepsilon}_p^v$	Viscoplastic mean stress strain
ε_V	Volumetric strain
ε_r	Radial strain
ε_a	Axial strain
ε_1	Strain on the major principal axis
ε_3	Strain on the minor principal axis
K_0	Coefficient of lateral earth pressure at rest
K_0^{NC}	Coefficient of lateral earth pressure at rest in normally consolidated condition
c	Cohesion
r	Radius
L_{dr}	Length of drainage path
H	Sample height
D	Sample diameter

a	Attraction
t	Time
τ	Intrinsic reference time, normally 1 d or 24 h
ψ	Dilatancy angle
ν	Poisson's ratio
υ	Specific volume
V	Volume
g	Dimensionless shear stiffness factor
γ	Frictional dissipation parameter
I_p	Plasticity index
ϕ	Critical friction angle
q	Deviatoric stress
p_a	Reference pressure (atmospheric pressure)
p'	Effective mean stress
p'_o	Initial effective mean (isotropic) stress
p_0	Initial mean (isotropic) pre-consolidation pressure
p'_{eq}	Equivalent effective mean stress on IURL
η	Ratio between deviatoric and mean stress
n	Rate sensitivity parameter, regulates spacing between isotaches
M	Slope of critical state line in $p':q$-space.
λ	Slope of IURL
κ	Slope of INCL
μ	Creep index
r	Norm of an arbitrary reference volumetric strain rate
R	Spacing ratio
I_P	Plasticity index
w	Water content
w_L	Liquid limit
w_P	Plastic Limit
e	Void ratio
c_v	Coefficient of consolidation
OCR	Overconsolidation ratio
OCR_0	Initial overconsolidation ratio
u	Pore pressure
u_b	Pore pressure at top cap drainage point

Note: Dotted accent indicate rate dependency. E.g.: $\dot{\varepsilon} = d\varepsilon/dt$

1 Introduction

This chapter introduces the background of the thesis. The thesis is inspired by an international innovation project to enable Carbon Capture Storage called SHARP by mainly quantifying risks. The project aims to meet the targets of the Paris Agreement. Stress conditions in the shallow sediments in Troll East Field are studied.

Investigations from 1980s show a steady increase in stresses in line with recorded glacial history and sedimentation rates down to around 74 m depth from the seabed. A sharp increase in OCR and K_0 is recorded, assumed to be a significant ice loading event from Weichselian glacial period. Deeper layers show series of erosion material and glacial activities. This can be demonstrated through auxiliary climatic records in Europe and Scandinavia. Overall, at these depths the chronology of the sediments and ice loading history are uncertain, thus a recommended values are given. Here, K_0 increases along with a recommended constant OCR.

The greatest enabler of off-shore installations in Trolls comes from analogous material in Onsøy on-shore Norway. It is demonstrated that Onsøy share similar stress properties to Troll to around 30 m depth. Due to this, field experiments were carried out on Onsøy before applying it in Troll. By demonstrating that similarities extend beyond 30 m of Troll by consolidation, one removes the costly measure of offshore sampling in the Northern North Sea.

A PLAXIS numerical model simulating ice load and sedimentation rates in Troll have managed to adequately simulate OCR to the field data. However, it underestimates K_0 in Unit IIIA, located between depths 74-110 m of the borehole. This discrepancy is pointed to limitations in the constitutive model used for simulations that is Soft Soil Creep model (SSC). Therefore, new constitutive model under the framework of hyper-viscoplasticity is applied, by introducing new parameters that changes the yielding surface more flexibly than SSC. Calibrating these parameters may couple OCR and K_0 to field data, thus simulating a more accurate model of the stress states recorded in Troll.

One of the most central sources used in the thesis are from (Lunne, Long and Uzielli, 2006), (Sejrup *et al.*, 1995), (Olsen *et al.*, 2013) and (By and Skomedal, 1993).

1.1 Carbon Capture Storage

The World Climate Summit reports have consistently called on tackling the urgent global issue of climate change. The Paris Agreement, effective in 2016, has resulted in the commitment to achieve 50-85 % CO_2 reduction by 2050. One approach is achieving net-zero emissions – i.e., equally removing greenhouse gasses emitted from human activity. A method with great potential is by carbon geosequestration – by capturing and storing CO_2 in oil and gas depleted reservoirs. This is commonly known as Carbon Capture Storage (CCS)

To meet the targets of the Paris Agreement, CO_2 emissions must be reduced by 50-85 % by 2050, according to the IPCC[1]. 14 % of the total emissions by 2060 must come from CCS., according to the IEA[2] (SINTEF).

Addressing this, rapid development on CCS is ongoing with funding from ACT[3], an international initiative to establish CO_2 capture, utilization, and storage as a tool to combat global warming. ACT is a part of Horizon Europe, an EU research and innovation funding program to strengthen efforts in tackling global challenges. This ensures longevity on CCS research. A particular project funded by ACT is SHARP (Stress History and Reservoir Pressure for improved quantification of CO_2 storage containment risks).

1.2 SHARP

SHARP's mission is to reduce the risks of subsurface CO_2 storage to an acceptable level for commercial and regulatory interests. The uncertainties related to the geomechanical responses to injection can be quantified by, among other things, improving and integrating stress models (NGI, 2023). An international consortium representing investors and universities combine work to gain knowledge about the North Sea stress system before running risk quantification at the end of 2024 (Figure 1). They identified Horda Platform Area as a region of great potential for CCS. Contributing to the data set of stress modeling, a fully quantitative CO_2 containment risk method can be developed (Larsen, 2023)

The soil characterization by (Lunne, Long and Uzielli, 2006) represents Troll well and serves as the most publicly accessible data covering a representative range of sediments in the Troll field. Because of this it will be one of the main sources to the thesis. Obtaining other geotechnical records is difficult. According to the project manager in NGI, applying is required.

Direct access to borehole data in the North Sea enhances companies' competitiveness in offshore industry by enabling more cost-effective foundation design. One example is to reduce costs of offshore wind seabed installations which is a hot research topic (UiB, 2023). Due to its sensitive nature, any new geotechnical characteristics of the sediments are likely to be treated as confidential information.

This thesis can be regarded as a contribution to Task 3.2, regarding the stress and burial history impact on present stress state, within Work Package 3.2 in the SHARP project. One of the goals of this work package is to utilize already existing data to examine the

[1] IPPC: International Panel on Climate Change
[2] IEA: International Energy Agency
[3] ACT: Accelerating CCS Technologies

impact of stress history on the coefficient of lateral earth pressure. The delivery to this work is two parted, consisting of laboratory work and numerical work.

Figure 1: Events on the SHARP Storage project. Excerpt from (NGI, 2023)

1.3 Troll

Troll is one of the largest offshore gas fields in the world. It is in the Northern North Sea, in the bottom of the Norwegian Channel outside the western coast of Norway (Figure 2). The Norwegian Channel is a trench stretching from the Oslo fjord, around the southern coast towards the continental margin off the western coast, before fanning out in the Norwegian Sea northbound.

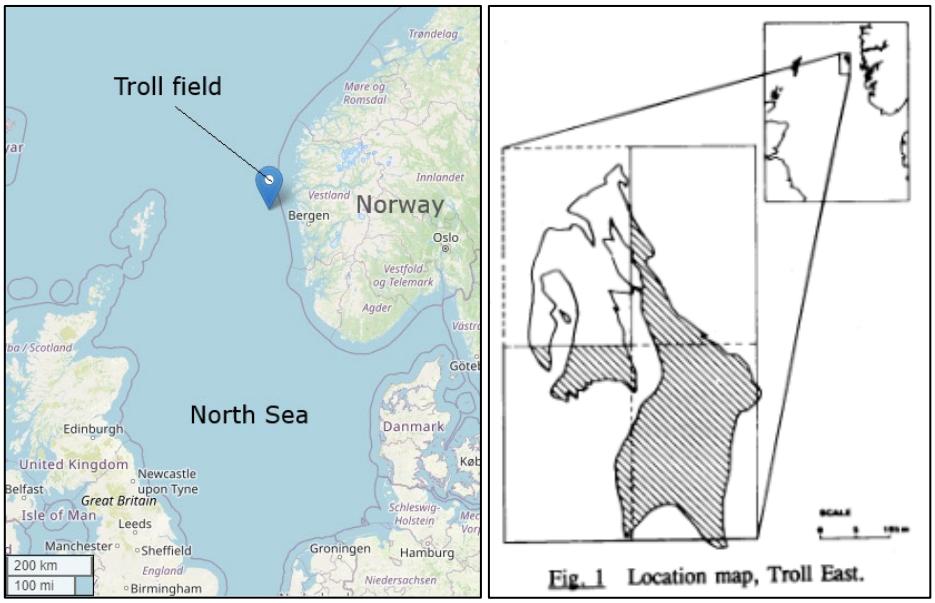

Figure 2: North Sea and Troll field. Courtesy of OpenStreetMap and (By and Skomedal, 1993).

The study area is Troll Field East, one of the most thoroughly investigated offshore sites in the North Sea and possibly in the world (By and Skomedal, 1993). The investigation from (By and Skomedal, 1993) has divided the sediments into five units each describing the soil in detail. One of the most interesting findings are as follows:

- Unit II (16.5-74 m) and Unit IV (120-160 m) are probably very similar in its marine environment.
- Unit IIIA (74-110) is exceptionally overconsolidated with erosional surface caused by glacial advance, composed of coarser glacial till.

Neighboring boreholes near Troll describing the Norwegian Channel's glacial history and lithology are combined with more accurate biostratigraphical records from the Netherlands (Sejrup et al., 1995). In all, it provides a good overview of the geotechnical parameters, chronology of the sedimentation, and ice loading from the cycles of glacial advances and retreats. These records are combined by (Jalali, 2022), where some parameters are described in the methods chapter in 3.2. Figure 3 shows the profile of OCR and K_0 in Troll by (By and Skomedal, 1993).

The main challenges in these records are that uncertainties are not quantified, and data points becomes increasingly scarce by depth. Noticeably, in Unit IIIA, K_0 is recommended to equal or greater than unity which is rarely observed for clay in the geotechnical field. Raw data are currently not available for the recommended values for OCR and K_0.

Since these are used in the soil characterization by (Lunne, Long and Uzielli, 2006) in a larger context, these diagrams and results will from now on be referred to as (Lunne, Long and Uzielli, 2006).

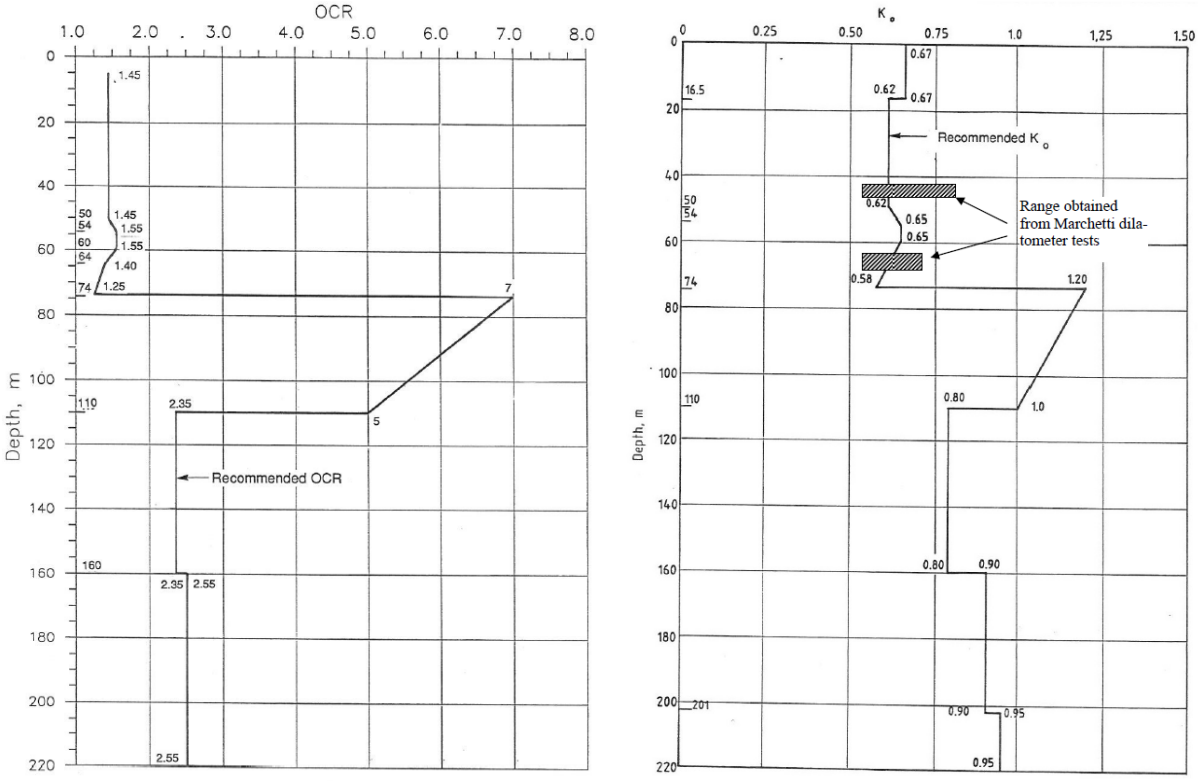

Figure 3: OCR and K_0 down to 220 m depth from seabed at Troll.

The sharp increase of OCR and K_0 in Figure 3 show a significant glacial loading and unloading over time. The extent of Unit IIIA to the Northern North Sea is mixed. Unit IIIA is connected to Eemian interglacial[4] event and is most dominant in the Norwegian Channel, compared to the shallower regions in the southwestern parts of the Northern North Sea.

The sedimentation sources show spatial and temporal variability (Bellwald *et al.*, 2020). Sediments from Fennoscandinavian Ice Sheet, Norwegian Channel, are likely main contributors. Figure 4 depicts a plausible mechanism of Troll during significant glacial advance. Imagine the persistent ice margin oscillations, creating several erosion surfaces and various till and glaciomarine deposits (Olsen *et al.*, 2013). Subsurface seismic surveys suggests that the layers are homogeneous in the shallowest parts like Unit I, but increasingly heterogenic from Unit IIIA, which can be attributed to erosional surfaces, postglacial rebounds, faults and changing sea levels.

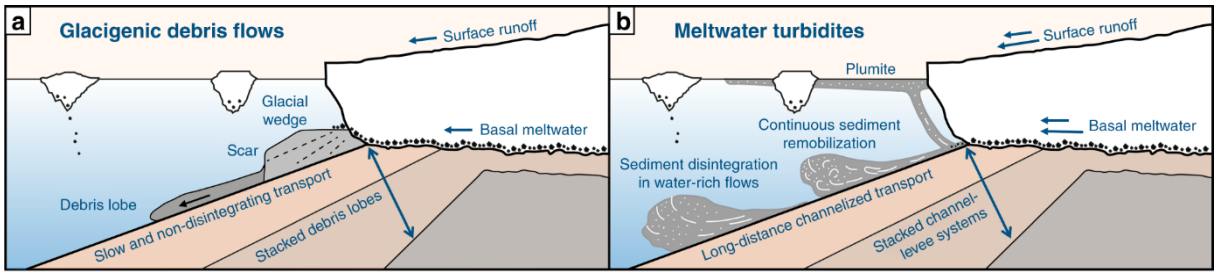

Figure 4: Conceptualized sedimentation from the Norwegian coast to the Norwegian Channel (Bellwald *et al.*, 2020).

Figure 5 shows the effective vertical and preconsolidation stresses with depth. These estimates illustrate the magnitude of stresses in the soil. The ice thickness is estimated to range between 226 m and 778 m (Jalali, 2022), demonstrating the magnitude of uncertainties involved.

[4] Interglacial: Period of warmer climate to temperate conditions within an ice age, lasting around 10 000 year or more.

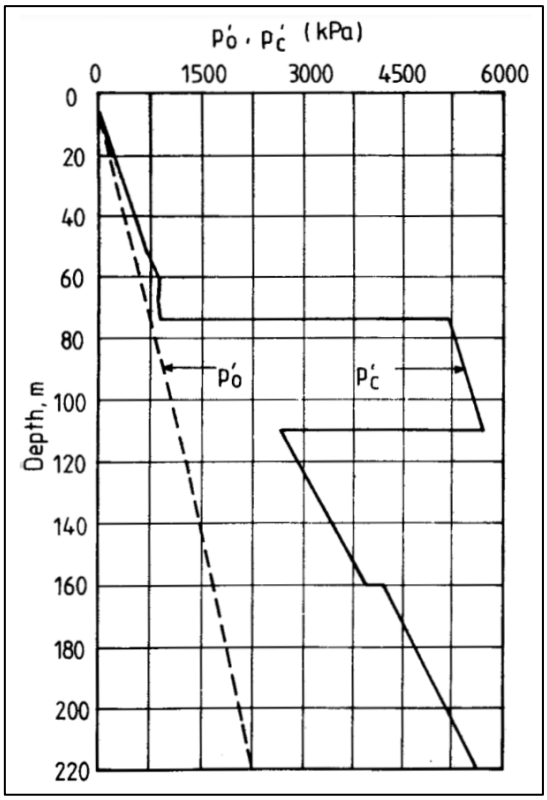

Figure 5: Effective vertical initial stress and effective vertical preconsolidation stress.

1.4 Onsøy clay

Onsøy clay is soft clay from the NGTS test site in Onsøy, which is in the municipality of Fredrikstad in southeastern Norway. NGTS is a research consortium led by NGI, and further consisting of NTNU, SINTEF/UNIS, and The Norwegian Public Roads Administration (L'Heureux, no date). Among the goals for NGTS is for the sites to function as benchmark areas. As such, the Onsøy clay has been shown to bear similarities with Units I and II in Troll field (Lunne, Long and Uzielli, 2006) (Gundersen *et al.*, 2019). Onsøy share similar K_0, OCR and I_p with Troll to around 30 m. Both have not experienced significant ice loading, but there are possibly creep effects on preconsolidation stresses.

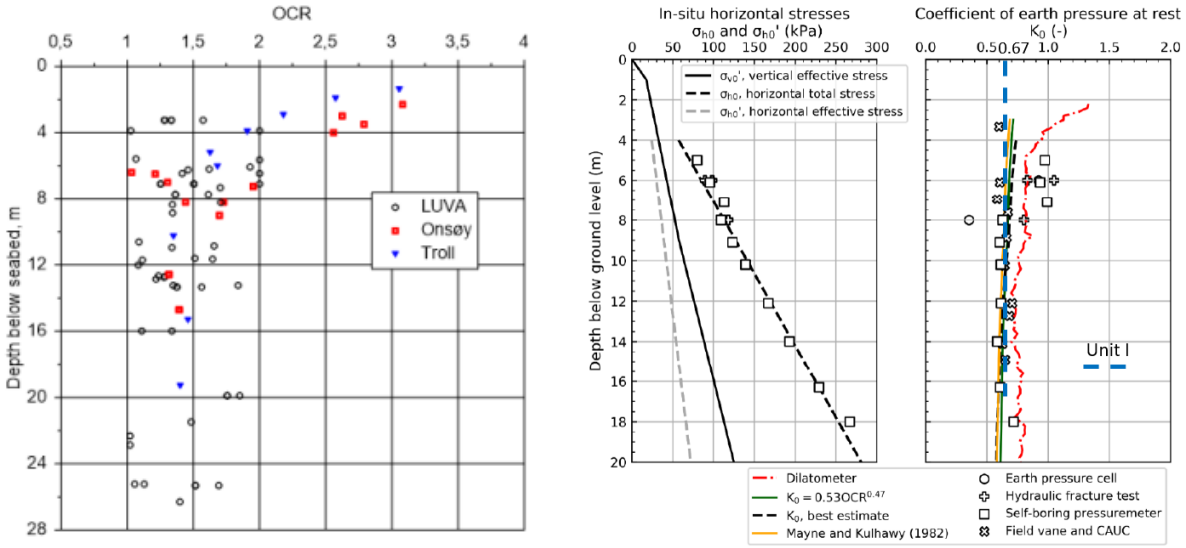

Figure 6: OCR and K_0 for Onsøy. Notice the resembling OCR between Troll and Onsøy (Gundersen *et al.*, 2019).

From Figure 5 and Figure 6 a connection between Onsøy and Unit I can be made in OCR and K_0, possibly due to both Unit I and Onsøy being deposited in Holocene[5]. Onsøy clay is thought to originate from glacial erosion and glaciofluvial deposits while submerged. It was notably located downstream of Glomma, the longest river in Norway, contributing to steady flow of sediments. Due to the mentioned similarities between Unit I and IV, a possible connection to Unit IV can be made as well.

1.5 Previous works and recommendations by Ramin Jalali

Starting from 2021, an extensive literature study resulted in a 2D PLAXIS model, aimed at recreating sedimentations and stresses based on Figure 6. The chronology of sedimentation, ice loading of Troll was constructed in several phases, with horizontal layers and uniform vertical loads. This gave the model oedometer conditions in practice. Soft Soil Creep (SSC) was the constitutive model for all layers. Despite great advances in crossing multiple evidence and calibrating parameters to field data, SSC has been shown not to sufficiently describe the field recorded K_0 (Jalali, 2022). When it comes to Unit IIIA, creep index was increased to raise the OCR by attributing the increase of OCR boost the time-depended behavior over the course of millions of years.

[5]Holocene: Geological time age about 13 000 – 8 000 years ago, a general warmer period where glaciations did not advance into the Northern Channel.

For further work, Ramin made two recommendations:

- Get more data – perform or get access to lab tests to see time dependent behavior on K_0 and improve λ^* and κ^*.

- Use models that uses kinematic hardening concept.

The time evolution, in this case creep, of K_0 is contested within the geotechnical community. Existing tests that attempt to demonstrate this remain highly uncertain (Grimstad *et al.*, 2021). Ramin recommends conducting high-quality and long-term laboratory tests on Troll clay. In terms of the model, he suggests using constitutive models that incorporate the concept of kinematic hardening. The concept builds on soil stress memory relating to permanent volume changes with preconsolidation stresses. Regarding the soil parameters, he noted that the results were especially sensitive to the modified compression indexes λ^*, κ^*. The number of accessible laboratory tests of Troll was insufficient to make an accurate simulation. To address this, he suggests collaborating with relevant companies to gain access to more recent test results.

1.6 Problem

The shared issue appears to lie in the lack of new insights into stress states in the shallow sediments in Northern North Sea.

The problem in this thesis consists of the following questions:

- What impact does the glaciation history have on the stresses in the quaternary sediments of the Northern North Sea?
- Can Onsøy clay, as an analogous material, replicate similar stress states and Atterberg limits found in deeper sediments of Troll?
- How can a new constitutive model accurately simulate OCR and K_0 in tandem?
- How do the results contribute to the project goals in the SHARP project?

1.7 Summary

The SHARP project has identified Troll East as a potential site for Carbon Capture Storage. A region of highly consolidated material with relatively high lateral earth pressure is recorded in Unit IIIA (74-110 m). Onsøy clay is brought as an analogous material to Troll which may provide more insights via experimental tests in the geotechnical lab in NTNU. Numerical work on SSC has successfully simulated OCR and K_0 apart from Unit IIIA where K_0 is underestimated. Further development of the numerical model may help understand the glaciation history of Troll and contribute to the SHARP project.

2 Theory

This chapter introduces the various geotechnical concepts that are important for the evaluation of the results of the thesis. Here, coefficient of lateral pressure at rest (K_0) and overconsolidation ratio (OCR) are introduced. Then the numerical models are presented. In here, the new constitutive model called hyper-viscoplastic cam clay model (HVMCC) is introduced. In addition, principles in the experimental part of the thesis are mentioned.

2.1 Coefficient of lateral earth pressure at rest (K_0)

The coefficient of lateral earth pressure at rest (K_0) is the ratio of in-situ effective horizontal stress (σ'_{h0}) to in-situ effective vertical stress (σ'_{v0}) at the state of zero strain (Knappett and Craig, 2019), shown in equation 2.1.

$$K_0 = \frac{\sigma'_{h0}}{\sigma'_{v0}} \tag{2.1}$$

Aas and Lacasse (2022) describes K_0 as an important geotechnical design parameter. In practical design is it especially used in earth retaining structures like sheet piles. In advanced numerical modelling, it aids in generating initial stress conditions. K_0 is usually determined via a standard oedometer test or a triaxial test. To save time on laboratory testing, numerous empirical relationships with other soil parameters have been derived to estimate K_0.

According to (Grimstad *et al.*, 2021), the empirical relationships are of the form of

$$K_0 = K_0^{NC} \cdot OCR^m \tag{2.2}$$

where m specifies the type of clay. This could be related to plasticity, creep, etc. Its values are typically in the range 0.4 - 0.5. For these ranges, it overpredicts the developments of K_0 compared to the hyper-viscoplastic model which be discussed in 2.6

Soil properties like poison ratio (ν) are directly linked to K_0 due to the tendency of transversal expansion, especially in oedometer conditions.

- Plasticity index (I_p) is related to soil's compressibility and ability to retain water. Higher I_p means a higher interparticle bonding with higher water content, leading to increased resistance to lateral pressures. This can be related to the void ratio, its specific organization of the particles.

- Critical friction angle (ϕ) impacts K_0 due to its resistance against shear stresses, which have a lateral stress component, Jaky (1944).

- Overconsolidation ratio (OCR) has an influence on K_0 since it reflects the stress history. An overconsolidated soil with be in a denser state, which could lead to some anisotropy with higher resistance against lateral stresses. Estimations with I_p and OCR have been shown notably by Brooker and Ireland (1965)

The K_0 ratio is thus linked to the stress history of the soil through its effective horizontal stress (Sivakumar *et al.*, 2002). Unlike the effective vertical stress, the effective horizontal stress state is not fully recoverable after unloading. This is illustrated in a deposition to erosion sequence in Figure 7. Much like OCR, the K_0 coefficient may then reflect a maximum load that the soil has taken. It is also clear that the unloading K_0 should be higher than the loading K_0.

Despite of this, the reliability of laboratory or in-situ estimates still are uncertain. They also point out that many previous relationships between K_0 and clay types and soil history are not well suited with Norwegian conditions.

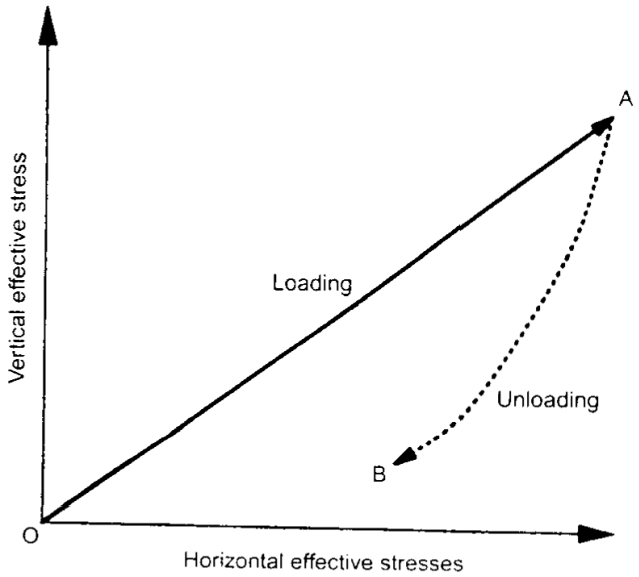

Figure 7: Typical stress path with unrecoverable horizontal stress (Sivakumar *et al.*, 2002)

An estimation established by a database of K_0 measurements from laboratory and in-situ testing on Norwegian clays, including from Onsøy and Troll, by L'Heureux *et al.* (2017) is highlighted in equation 2.3 as to remedy this. The estimation is shown in the equation 2.3 underneath. Among other soils, Troll and Onsøy soils were part of the data utilized for the design of this estimation.

$$K_0 = 0{,}53 \cdot OCR^{0{,}47} \qquad \textbf{2.3}$$

The estimation of L'Heureux *et al.* (2017), however, only considers the OCR, as I_p was shown to have a negligible impact on K_0.

It is important to know whether K_0 is based on loading or unloading conditions in the soil. Empirical relationship between K_0 and OCR are often based on unloading due to available high-quality datasets (Grimstad *et al.*, 2021).

2.1.1 K_0 in oedometer conditions in Cam Clay

This section demonstrates that K_0 in compression cannot exceed unity in oedometer conditions.

When translating Mohr-Coulomb failure line to $p':q$ space, the critical line for triaxial compression is defined by the equation:

$$M = \frac{6 \cdot sin\phi}{3 - sin\phi} \qquad \textbf{2.4}$$

From the definition of one-dimensional normal compression line is defined as follows in the $p':q$ plane (Wood, 2007):

$$\eta_{K_{NC}} = \frac{d\epsilon_p}{d\epsilon_q} = \frac{d\epsilon_p^e + d\epsilon_p^p}{d\epsilon_q^e + d\epsilon_q^p} = \frac{3(1 - K_0)}{1 + 2K_0} \overset{oed.}{=} \frac{3}{2} \qquad \textbf{2.5}$$

By superposition of elastic and plastic strain increments the following expression is obtained:

$$\eta_{K_{NC}} \cdot \frac{(1+\nu)(1-\Lambda)}{3(1-2\nu)} + \frac{3\eta_{K_{NC}} \cdot \Lambda}{M^2 - \eta_{K_{NC}}^2} = 1 \quad , \qquad \Lambda = \frac{\lambda - \kappa}{\lambda} < 1 \qquad \textbf{2.6}$$

K_0 is determined by solving equation 2.5 with respect to $\eta_{K_{NC}}$ and evaluated in terms of ν, Λ and $M = f(\phi)$. Figure 8 show that zero friction angle will result in a material that flows with lateral force equal to overburden stress, that is $K_0 \to 1$ (Wood, 2007). The relationship turns increasingly divergent when $\nu \to 0.5$ for some ranges of Λ, stressing the importance of having consistent parameters in Cam clay-based model.

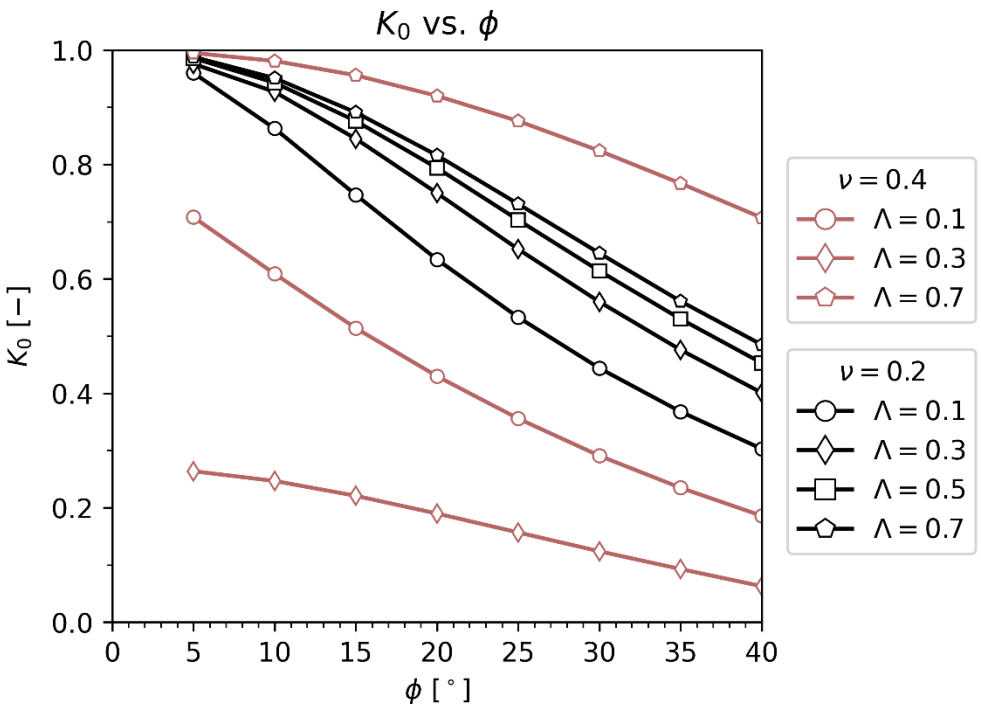

Figure 8: Dependence of K_0 for normally compressed soil on friction angle according to Cam clay model, plot regenerated from (Wood, 2007).

2.1.2 K_0 on creep

Creep is observed in materials that accumulate strains over time under the influence of constant effective stress. This phenomenon is also known as aging.

Due to the large span of seabed in the Northern North Sea, one can assume 1D creep conditions, also known as oedometer conditions. A fundamental question within the geotechnical community is how K_0 evolves under 1D creep deformation and unloading for clay. Knappett and Craig (2019) defines secondary compression, or creep, as a process where soil is compressed under a constant effective stress after the excess pore pressure has dissipated during the primary consolidation. The primary and secondary consolidation is thought to occur simultaneously during loading.

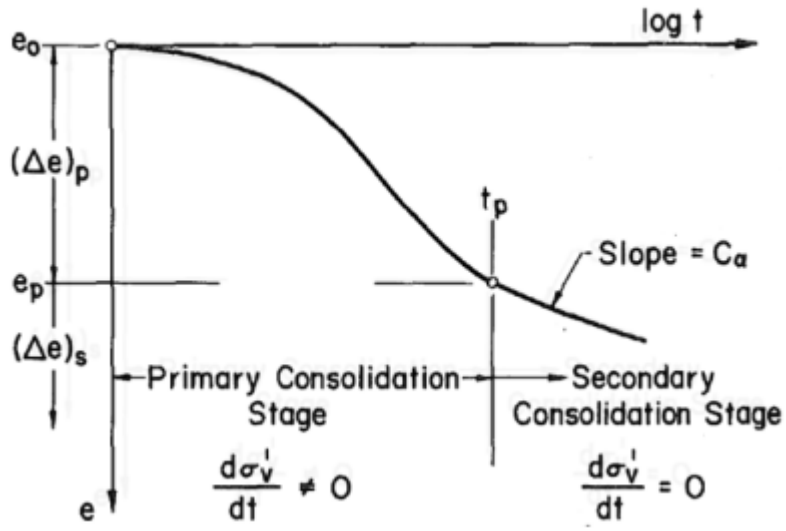

Figure 9: Diagram illustrating the compression over time under constant pressure separate from pore pressure dissipation.

The process of creep may lead to an increase in K_0 (Mesri and Castro, 1987). This increased K_0 can be predicted with equation 2.7. It must be noted that the evolution of K_0 with time is disputed among geotechnical engineers (Grimstad *et al.*, 2021). The interaction between creep and K_0 in equation 2.7 must therefore only be regarded as an input in the discussion, and a possibility within the realm of time dependent K_0.

$$K_0 = [K_0]_{primary} \cdot \left(\frac{t}{t_p}\right)^{[(C_a/C_c)/(1-\frac{C_r}{C_c})] \cdot sin\varphi'} \quad \textbf{2.7}$$

2.1.3 Mineral content on creep and thixotrophy

A reduction of K_0 over time can be the result of a cementation effect. When subjected to effective stresses, the material liquefies due to breakage of contacts between weakly adhering particles. During resting, fragments dissolved reconnects and becomes more plastic.

The behavior and resting time are highly dependent on the clay dispersion content. Minerals like kaolin, smectite are common dispersions with observed thixotropy depending on the solid content. These are also known to affect geotechnical parameters like plasticity index (I_p) and K_0.

2.2 Overconsolidation ratio (OCR)

Knappett and Craig (2019) defines the overconsolidation ratio (OCR) as the maximum effective vertical stress that a soil has been subjected to (σ_c'), divided by the in situ effective vertical stress (σ_{v0}'). Equation 2.8 shows the mathematical definition of OCR. The maximum effective vertical stress that a soil has been subjected to (σ_c'), is termed preconsolidation stress.

$$OCR = \frac{\sigma_c'}{\sigma_{v0}'} \quad in\ 1D \tag{2.8}$$

$$OCR = \frac{p_0'}{p_{eq}'} \quad in\ 3D \tag{2.9}$$

OCR is a central parameter in expressing the stress history of a soil. An overconsolidated (OC) soil is defined as having an $OCR > 1$, while a normally consolidated (NC) soil has an $OCR = 1$. Drawing an example from Troll, a previous ice load atop the soil, now melted, will result in a higher value of OCR, and the soil is defined as overconsolidated.

Higher values of OCR may occur without higher values of previous load than present (Statens Vegvesen, 2022). An example of this is that the OCR values in Norway are seldomly found to be below 1.4, often due to a phenomenon called creep. The creep phenomenon will be explained further in chapter 2.3. Evaporation of pore water and oxidation is among other mechanisms that may increase OCR but are not relevant at Troll.

2.3 Modified Cam clay Model

The new constitutive model is based on Modified Cam clay model (MCC) – therefore a short presentation of the Modified Cam Clay Model follows, based on (Wood, 2007) and lectures notes by (Nordal, 2020). Illustrations are based on these as well.

Many elaborate models are derived from the MCC to give a more accurately description of specific soil behavior. MCC addresses basic clay behavior and critical state soil mechanics through elastic and plastic properties via the flow rule and volumetric hardening. Critical state is a state where large shear strains may be applied without any change in effective stresses or in volume. It employs an elliptic yielding surface to represent the transition from elastic to plastic strains in axisymmetric stress conditions, usually represented in $p'{:}q$ plane, where

$$F = q^2 - M^2[p'(p_0' - p')] = 0 \tag{2.10}$$

$$M = \frac{6\sin\phi}{3 + \sin\phi}$$

2.11

The yield surface can be seen as displaying the current memory the preconsolidation stress and is mapped by M in equation 2.10. The total strain has an elastic component inside the surface, and a plastic component when the stress path pushes the yield surface.

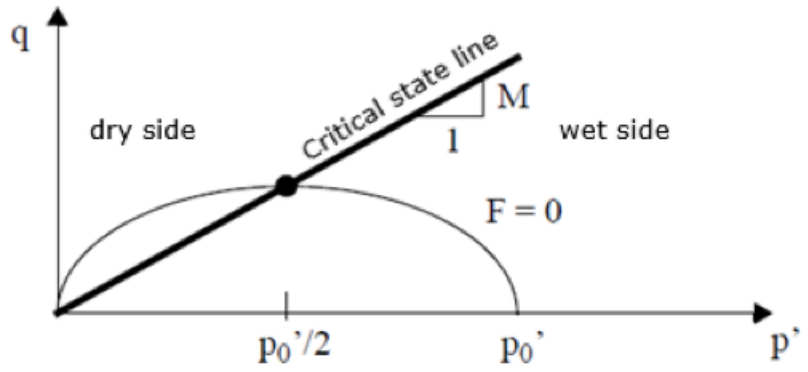

Figure 10: The Cam clay yield surface modified from lecture notes.

The critical state is for centered on the ellipsis. However, it is important to note that this is a gross simplification, and the location of the critical state varies greatly around the world. Elaborate models address this limitation in section 2.6.

The soil behavior is described by an isotropic normal compression line (INCL) and an isotropic unloading reloading line (IURL). In a sense, INCL shows the flow behavior and IURL show the recoverable relaxation behavior.

The responses are linear with the slope λ , equation 2.12, and κ, equation 2.13, respectfully when plotting the specific volume against the logarithm of the effective vertical stress as shown in Figure 11. This gives a simple physical description of the soil's plastic and elastic behavior, which can be easily determined in a standard oedometer test.

$$\lambda = \frac{v}{m_{OC}} = \frac{1+e}{m_{NC}}$$

2.12

$$\kappa = \frac{v}{m_{OC}} = \frac{1+e}{m_{OC}}$$

2.13

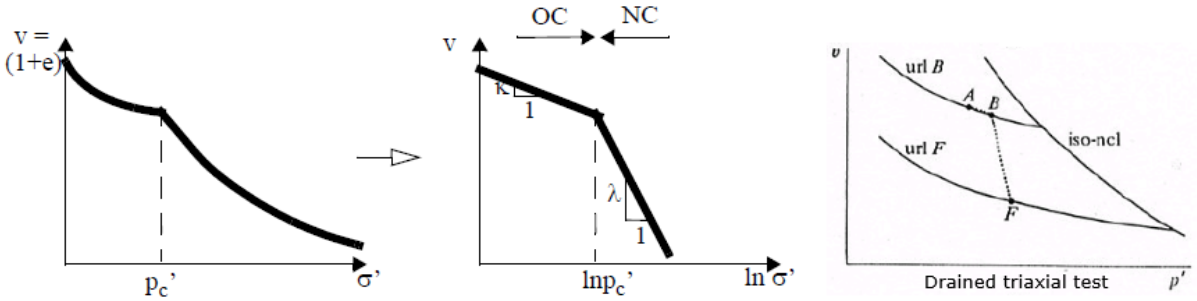

Figure 11: Illustrating the compression indexes λ and κ, compiled from lecture notes.

The development of the NC plastic stress path is governed by the flow rule. The flow rule describes the proportion of plastic deviatoric and isotropic strain. In Figure 10: The Cam clay yield surface modified from lecture notes. Figure 12 the volumetric isotropic strain flow is positive in the wet side and negative on the dry side. The soil behavior is illustrated in plane strain by points A, B, C and D.

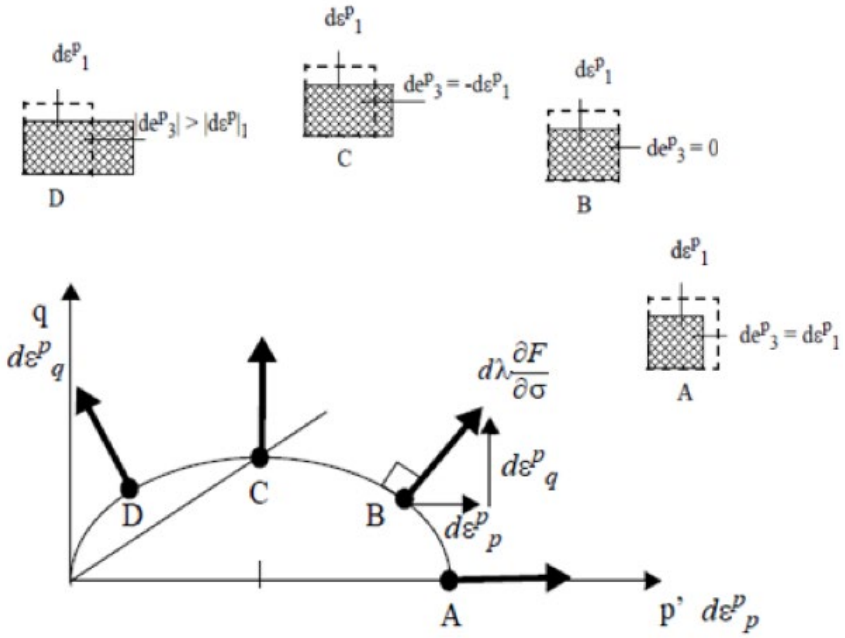

Figure 12: Associated flow rule and yield patterns, modified from lecture notes.

Noticeably, point A is flowing purely isotropic with a $K_0 = 1$.

2.4 Soft Soil Creep Model

The modelling work by Ramin was based on Soft Soil Creep Model (SSC). Sources here come from lectures notes by (Nordal, 2020) and PLAXIS' Material Models Manual (Bentley, 2022).

The Soft Soil (SS) model expands upon the Modified Cam Clay (MCC) model by accommodating analysis of very soft, compressible, soils. Very soft soils are here defined as $E_{oed}^{ref}/E_{50}^{ref} < 0{,}5$. The Soft Soil Creep (SSC) model is a further expansion, taking into consideration the time-dependent effect of creep.

The stiffness parameters of the SSC model can be found amongst those of the MCC model but utilizes modified swelling and compression indexes, in addition to the modified creep index. The modified indexes are defined as $Modified\ index = \frac{index}{1+e}$, as such they are defined in terms of the void ratio. The modified swelling and compression indexes may be evaluated by plotting the logarithmic vertical effective stress against void ratio from an oedometer test, as shown in the picture below (Karstunen and Amavasai, 2017). The modified creep index may be evaluated from a plot of axial strain against the natural logarithm of time, as shown in the picture below (Karstunen and Amavasai, 2017).

SSC considers the effects of time in the behavior of soil. This means, as time elapses, an additional compression mode is prevalent. This effect is known to be called secondary compression, usually by the name creep. Creep is elaborated in section 2.3.

It incorporates hardening soil rule, which essentially combines two plastic yield surfaces. The first one is the Coulomb-criterion based on the mobilized friction angle. When the effective stresses increase, the mobilized friction, ρ, increases towards plasticity ϕ, it gradually "tilt" itself on the pivot of attraction based on the currently mobilized friction ρ towards a failure ϕ. The second one is the ellipsis, the cap, controlled by the preconsolidation stress like in MCC. In SSC, however, the crown of the ellipsis (M) is not related to equation 2.11, but instead mapped a function of ν, λ^*,κ^* and K_0^{NC}, where K_0^{NC} is dominant. This was made to make reasonable K_0 values during simulations.

This washes away the clear visual distinction between elastic and plastic behavior of soil. Instead elasto-plastic stiffness parameters are used to resemble a smooth stress strain development commonly observed in soft plastic soil behavior.

SSC uses the modified version of the indexes κ^* and λ^* compared to the original MCC's κ and λ. The ordinate axis is replaced with volumetric strains instead of specific volume, which is related to the classical void ratio as seen in Figure 14. Obtaining the void ratio is strictly not needed if the results are meant for conventional settlement calculations.

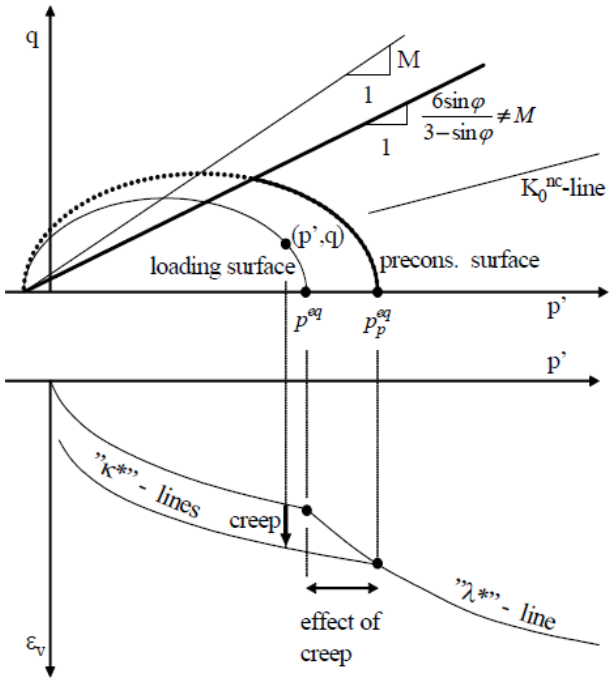

Figure 13: SSC yielding surface with the ellipsis mapped by control line $M = f(K_0^{NC})$ and cut by a Coulomb surface by ϕ.

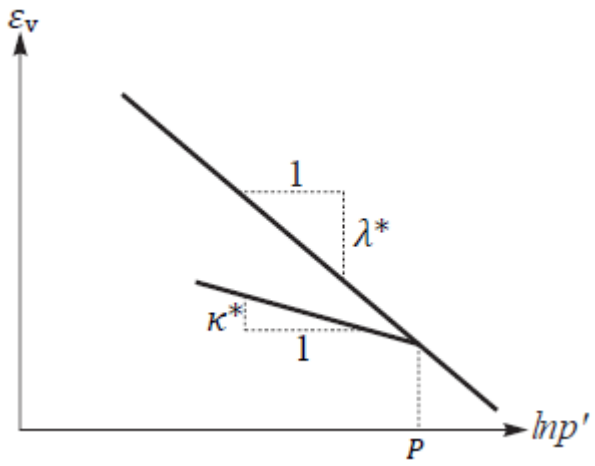

Figure 14: INCL and IURL show linear relationship between volumetric strain against the logarithm of effective mean stress.

In oedometer conditions, the volumetric strains can be replaced with axial strain.

Rough estimates of the modified model parameters are suggested by Bentley (2022). This may be useful for verifying the ability of Dadrasajirlou model for getting reasonable values of both the K_0 and OCR values. The estimates are as follows: $\lambda^* \approx I_P/500$, $\lambda^*/\mu^* = [15, 25]$ and $\lambda^*/\kappa^* = [2{,}5, 7]$.

2.5 Hyper-viscoplasticity Modified Cam Clay Model

A generalized hyper-viscoplastic constitutive model for clay was developed by (Dadrasajirlou, 2022; Dadras-Ajirloo, Grimstad and Amiri, 2022). The model incorporates the effect of time dependency and critical state soil mechanics through versatile thermodynamically sound potential functions that addresses the time dependent plastic behavior of clay. It is a family of MCC and adds flexibility to the yield surface in two ways:

- Freedom to set the location of the critical state stress.
- Further versatility of the flow rule by the viscoplastic shear strain weighted by the mean effective stress dependent frictional parameter ($\bar{M}$).

The proposed model is based on the isotache concept based on which a unique relation between stress, strain and strain rate exist (Suklje, 1957).

2.5.1 Isotache concept

The isotache concept is introduced to address rate-dependent response of clay. The Greek name isotache means iso- (equal) and rate (speed) and refers to lines (compressional behavior of clay on bi-logarithmic compressional plane) of equal rate of strain (Figure 15).

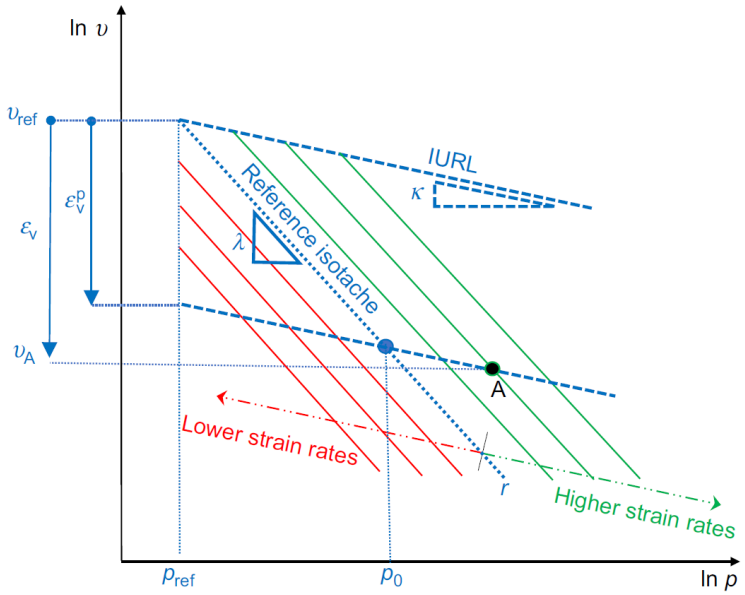

Figure 15: Illustration of isotropic consolidation. Parallel INCL and IURL demonstrating uniqueness of λ and κ on different strain rates in the bi-logarithmic plane between specific volume and mean stress.

The relation that governs the spacing between the isotaches is regulated by:

$$n - 1 = \frac{\mu}{\lambda - \kappa}$$

2.14

2.5.2 Helmholtz free energy potential

A thermodynamic potential, called Helmholtz free energy is employed in the model to describe the reversible, elastic behavior of clay (Houlsby, Amorosi and Rojas, 2005). To keep in line with the critical state soil mechanics, the bulk modulus was set to vary linearly with stresses, so that there is a linear relation for IRUL on the logarithmic compression plane. This potential reads as:

$$f = (p_a \kappa) \exp\left[\frac{1}{\kappa}\left(\varepsilon_V - \varepsilon_V^p\right) + \frac{3g}{2\kappa}\left(\varepsilon_s - \varepsilon_s^p\right)^2\right]$$

2.15

Based on the definition, the derivatives of the Helmholtz potential with respect to the volumetric strain and the shear strain give the mean effective stresses (p) and the deviatoric stress (q), respectively:

$$p = \frac{df}{d\varepsilon_V} = (p_a) \exp\left[\frac{1}{\kappa}\left(\varepsilon_V - \varepsilon_V^p\right) + \frac{3g}{2\kappa}\left(\varepsilon_s - \varepsilon_s^p\right)^2\right] = \frac{p}{\kappa}$$

2.16

$$q = \frac{dp}{d\varepsilon_s} = 3g(p_a)\exp\left[\frac{1}{\kappa}\left(\varepsilon_V - \varepsilon_V^p\right) + \frac{3g}{2\kappa}\left(\varepsilon_s - \varepsilon_s^p\right)^2\right] = 3gp$$

2.17

Now, the differential of p and q is computed with respect to the increment of volumetric and shear strains, the elastic matrix D can be obtained as:

$$\boldsymbol{\sigma} = \boldsymbol{D^e} d\boldsymbol{\varepsilon} \Rightarrow \begin{bmatrix} dp \\ dq \end{bmatrix} = \begin{bmatrix} \frac{\partial^2 f}{\partial \varepsilon_V^2} & \frac{\partial^2 f}{\partial \varepsilon_V \partial \varepsilon_s} \\ \frac{\partial^2 f}{\partial \varepsilon_V \partial \varepsilon_s} & \frac{\partial^2 f}{\partial \varepsilon_V^2} \end{bmatrix} \begin{bmatrix} d\varepsilon_V \\ d\varepsilon_s \end{bmatrix} = \begin{bmatrix} \frac{p}{\kappa} & \frac{q}{\kappa} \\ \frac{q}{\kappa} & 3gp + \frac{q^2}{\kappa p} \end{bmatrix} \begin{bmatrix} d\varepsilon_V \\ d\varepsilon_s \end{bmatrix}$$

2.18

The familiar MCC bulk is recognized in the elastic matrix in equation 2.18. Therefore, the above form of the Helmholtz is chosen. Based on the free energy function a constant Poisson's ratio for isotropic compression can be employed for the elastic moduli:

$$\frac{G}{K} = g\kappa = \frac{3(1-2\nu)}{2(1+\nu)} = 0.75$$

2.19

It is recommended to use equation 2.19 for estimation of g if no proper data for small strain (elastic) conditions are available.

2.5.3 Force potential and dynamic yield surface

The force potential is introduced to address the plastic behaviour of the soil by (Grimstad, Dadrasajirlou and Ghoreishian Amiri, 2020). It is based on plastic work done during isotropic consolidation at an arbitrary isotache. The force potential reads as:

$$z = \frac{rp_0}{n}\left[\frac{\sqrt{\left(T\dot{\varepsilon}_V^p\right)^2 + \left(\bar{M}\dot{\varepsilon}_s^p\right)^2} + \dot{\varepsilon}_V^p}{Rr}\right]^n$$

2.20

$$\bar{M} = M\sqrt{1 - \gamma + \gamma\left(\frac{Rp}{\bar{p}_0}\right)} \;\; ; \;\; n = 1 + \frac{\mu}{\lambda - \kappa} \;\; ; \;\; T = \frac{R}{2} + \left(\frac{R-2}{2}\right)\tanh(S) \;\; ; \;\; S = \left(\frac{M}{\eta}\right)^2 - \left(\frac{\eta}{M}\right)^2 \;\; ; \;\; \eta = \frac{q}{p}$$

2.21

The first factor outside the bracket in equation 2.20 represents a reference power made of multiplication of a reference strain rate (r) and the critical state soil mechanics hardening stress (p_0). n is the homogeneity order of the equation 2.21. The power term, comprised of the base inside the bracket and the exponent (n), scales the reference power resulting in the current dissipative power as a function of the rate of plastic strain. Since the general form of the force potential is similar to the MCC dissipation function (Houlsby and Puzrin, 2006), the dissipative or plastic response would be similar to the MCC model but with different rate (due to the isotache scaling).

Inside the bracket, the parameter R in the denominator is called the spacing ratio. It sets the relative position of the critical state on the effective mean stress axes. For MCC, the spacing ratio is 2. However, higher critical state for clay has been observed (Chen and Yang, 2017) leaving R to handle these cases.

In the numerator, the volumetric plastic strain rate is set to be non-negative by putting it under the square root. This comes from the definition of the exponentiation of n. But also, it reflects the isotache concept which sees creep as a compressive phenomenon with the progress of time.

The terms plastic volumetric and plastic shear strain inside the square root are scaled by factors T and $\bar{M}$ respectively. S is a state variable, T is a transition function and $\bar{M}$ is a modified version of M as seen in 2.3.

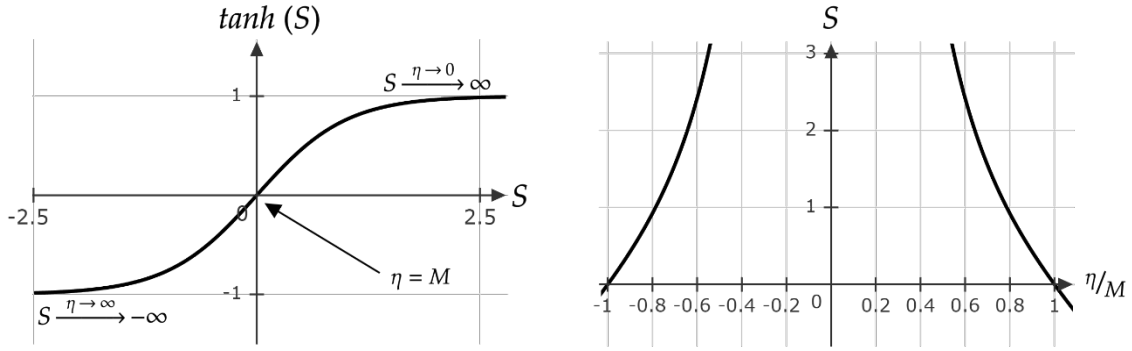

Figure 16: Exponential behavior of S changes the hyperbolic tangent function rapidly to accommodate a new eccentricity of the yield surface on the dry side.

$\bar{M}$ is a modified critical state to make the plastic shear stresses dependent on the mean stress, analogous to the coefficient of friction. It contains the frictional dissipation parameter (γ), spacing ratio (R) and $OCR = p_0/p$ (implied). When $\gamma = 0$, then $\bar{M} = M$.

Introducing pressure-dependent frictional dissipative mechanism with in equation 2.20 twists the shape of the dynamic yield surface. Having $\gamma = 0$ and $R = 2$ implies associative flow. Associated flow means the volumetric and shear components of the plastic strain are orthogonal on the yield surface like the MCC model.

In order to understand the performance of the transition function, the yield surface can be seen as a composite of two ellipses (Figure 17). The stress state follows the red square marks as the mobilized friction increases and approaches the critical state. At the critical state the stress state transitions to the blue circle marks. The plastic volumetric strains decrease and turns negative, to address the dilative behavior of the soil.

Mathematically, the state variable (S) increases exponentially as $\eta/\bar{M} \to 1$. Passing $\eta/\bar{M} = 1$, the hyperbolic tangent function in the transition function (T) gradually but quickly (Figure 16), change signs, which reduces the eccentricity of the ellipse (T) towards a smaller ellipse resembling the shape of an egg in Figure 17. A special case is when $R = 2$ which centers the ellipse to be in line with the MCC. Equation 2.20 provides a smooth and differentiable surface. It holds true to the CSSM where dilation is controlled by the mobilized friction and spacing ratio.

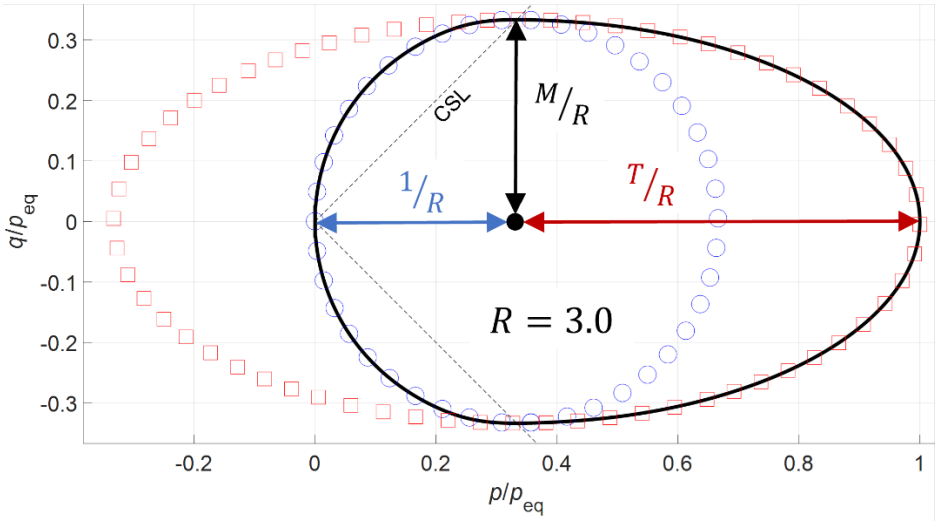

Figure 17: Yield surface (bold line) constructed by two ellipses R=1.5 and R=3. merging at critical state for M=1 ($\phi = 25.4$).

Now, when γ is increased, it scales up the plastic volumetric strains (dilatancy) at the wet side, twisting the yield surface as seen in Figure 18. This flexibility enables better numeric modelling of laboratory results for more overconsolidated type of material which has dilative tendency on the compression side.

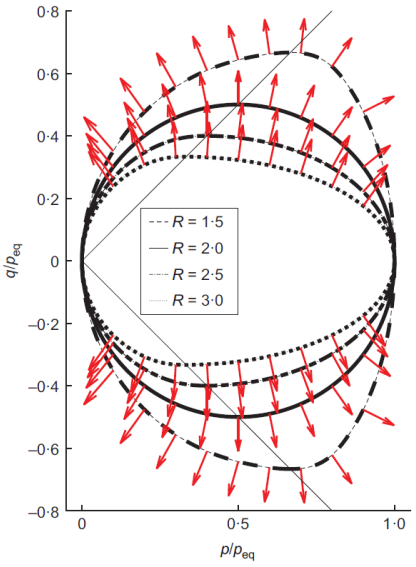

Figure 18: Yield surface in normalized stress space for different spacing ratios with $M = 1$ (Dadras-Ajirloo, Grimstad and Amiri).

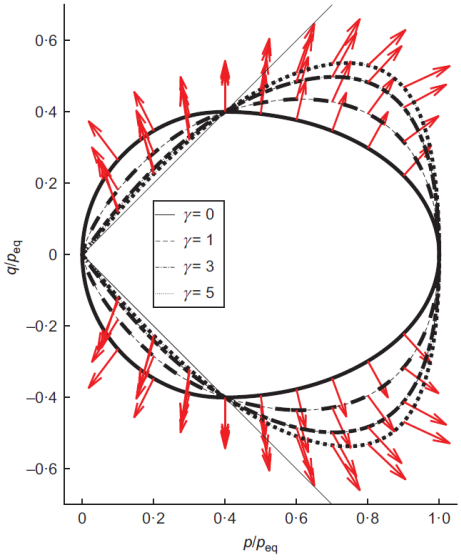

Figure 19: Yield surface in normalized stress space for different frictional dissipation parameter with M=1 and $R = 2.5$ (Dadras-Ajirloo, Grimstad and Amiri).

2.5.4 Model parameters and summary

The model parameters are summarized in Table 1.

Table 1: HVMCC model parameters with description

Parameters	Description
κ	Slope of the isotropic unloading-reloading line (IURL) in the bi-logarithmic compression plane
λ	Slope of normal compression line (INCL) in the bi-logarithmic compression plane
g	Dimensionless shear stiffness factor
M	Slope of the critical state line (CSL) in the $p'{:}q$ stress plane
R	Spacing ratio
γ	Parameter for non-associated flow rule due to frictional dissipation
μ	Creep index
ν	Constant Poisson's ratio
τ	Reference time – must be in consistent unit (typically 24 hours)
K_0	Initial coefficient of lateral earth pressure at rest
OCR_0	Initial overconsolidation ratio.

The frictional dissipation parameter (γ) determines the intensity of the frictional dissipative mechanism (the mean effective stress dependency of shear dissipation), i.e., the intensity of the twist and non-associative plastic flow direction. The value of γ can be estimated from the experimentally obtained yield surface.

The slope of the CSL (M) follows the definition from MCC as the Coulomb line. However, modified version ($\bar{M}$) is scaled by the spacing ratio (R) and incorporates stress-dependency and frictional dissipation.

The spacing ratio (R) controls the relative location of the critical state on the mean effective stress axis. Its value varies within 1.5 - 4 (Chen and Yang, 2017) and can be estimated with the same methodology for γ.

The creep index (μ) follows the definition from SSC, which can be obtained as the inverse of the slope of fitted straight line through the creep data (oedometer test) presented on the plane of the time resistance (inverse of strain rate) against time (Nilmar, 1969).

The slopes of IURL (κ) and INCL (λ) are interpreted in a $\ln v : \ln p'$-plot which incurs a negligible error compared to SSC's κ^* and λ^* that are interpreted in a $v{:}\ln'$-plot.

The dimensionless shear stiffness factor (g) sets the elastic moduli depending on the constant Poisson's ratio (ν).

The initial coefficient of lateral earth pressure at rest (K_0) and initial overconsolidation ratio (OCR_0) sets the initial variables in the numerical computation. If the computed layer is in a normally consolidated condition, then $K_0 = K_0^{NC}$ and $OCR_0 = 1$ by definition. However, for settlement calculations for NC clays, it is recommended to increase OCR_0 to check for premature creep deformations. For stress calculations in NC clays, it sets the iterative terms as the young development of the equivalent effective mean stress is dependent on the shape of the yield surface.

2.5.5 Parametrical relationship between SCC and HVMCC

Given that HVMCC is a family of the MCC, it can be useful to discern the parametrical relationship between SSC and HVMCC. Importantly, the slope of the INCL and IURL between SSC and HVMCC are not identical**.** In HVMCC, it is interpreted in a bi-logarithmic plane in a $\ln v : \ln p$-plot compared to $v : \ln p$-plot in SSC. The error between them would only amount to 1-2 %. Using this SSC parameter would then be practically applicable. The critical state line in SSC is based mostly on K_0^{NC}.

Table 2: List over similar parameters and differences between HVMCC and SSC.

HVMCC	SSC	Relationship
λ	λ^*	$\lambda \approx \lambda^*$
κ	κ^*	$\kappa \approx \kappa^*$
μ	μ^*	$\mu = \mu^*$
$\bar{M}$	M	$\bar{M}_{HVMCC} = M\sqrt{1-\gamma+\gamma\left(\frac{Rp}{\bar{p}_0}\right)}, \quad M = \frac{6\sin(\phi)}{3-\sin(\phi)}$ $M_{SSC} = \sqrt{\frac{(1-K_0^{NC})^2}{(1+2K_0^{NC})^2} + \frac{(1-K_0^{NC})(1-2\nu_{ur})\left(\frac{\lambda^*}{\kappa^*}-1\right)}{(1-2K_0^{NC})(1-2\nu_{ur})\left(\frac{\lambda^*}{\kappa^*}\right)-(1-K_0^{NC})(1+\nu_{ur})}}$
ν	ν_{ur}	$\nu = \nu_{ur}$
γ	ψ	$\gamma = 0$ implies $\psi = \phi$. No mathematical relationship for $\gamma > 0$.
g	E_{ur}	$g = \frac{3(1-2\nu)}{2(1+\nu)} \cdot \frac{1}{\kappa}$ $E_{ur} = 3(1-2\nu_{ur})K_{\mathrm{ur}}, \quad K_{ur} = -\frac{p'+c\cdot cot(\phi)}{\kappa^*}$
ϕ	ϕ	$\phi_{HVMCC} = \phi_{SSC}$

2.6 Atterberg limits

The Atterberg limits consists of the liquid limit w_L and the plastic limit w_P, where the plasticity index I_P is defined as the difference between the liquid limit and the plastic limit, $I_P = w_L - w_P$ (Head and Epps, 2011). The Atterberg limits tests are conducted in a laboratory and is a common tool for geotechnical soil characterization. There are two main methods of conducting the liquid limit test, the falling cone method and the Casagrande method, whereas the plastic limit test is conducted by rolling threads of the soil to be classified.

The liquid limit occurs at the water content at which the soil enters its liquid state, leaving its plastic state, whereas the plastic limit is found at the water content at which the soil leaves its plastic state for its solid state. As a rule, it follows that the liquid state will be of higher magnitude than the plastic state, as the water content is higher in this

state. In the instance that the soil does not follows this rule, that the plasticity index is zero, the soil is classified as non-plastic.

2.7 Consolidation

Anisotropic consolidation and K_0 consolidation will be performed in the laboratory part of this thesis. An understanding of consolidation will make it possible to estimate the time usage of the lab phases. Knappett and Craig (2019) defines consolidation as "the gradual reduction in volume of a fully saturated soil of low permeability due to change of effective stress". This may be understood as the drainage of excess pore water due to some loading.

An estimation of the time of consolidation is shown in equation 2.22. The time calculated will be the time of the vicinity of 90% consolidation and follows the consolidation theory presented in Craig's Soil Mechanics by Knappett and Craig (2019). The time estimate considers the length of drainage L_{dr} and the coefficient of consolidation c_v. The length of drainage is the distance the excess pore water must travel to be drained. The coefficient of consolidation reflects the permeability of the soil. A higher permeability facilitates faster consolidation, and a higher coefficient of consolidation.

$$t = {L_{dr}^2}/{c_v} \tag{2.22}$$

In equation 2.22, the length of drainage is of a higher order than the coefficient of consolidation. The length of drainage may be manipulated using different drainage schemes, while the coefficient of consolidation is a characteristic of the. It follows then that the length of drainage is the only term that may be manipulated, as well as being the term that will have the biggest impact on the estimated time of consolidation.

The length of drainage may be manipulated through different drainage schemes, of which two will serve as examples. Consider a cylindrical sample, as illustrated in Figure 20. If the drainage is restricted to being one-sided, which is the case in the leftmost illustration in Figure 20, excess pore water must travel from the bottom of the sample to the drainage at the top of the sample. The length of drainage is equal to the height of the sample H. Consider then a case in which drainage is allowed at either end of the sample. Water at the center of the sample can now reach drainage at either the top or the bottom of the sample. The length of drainage is half the height of the sample.

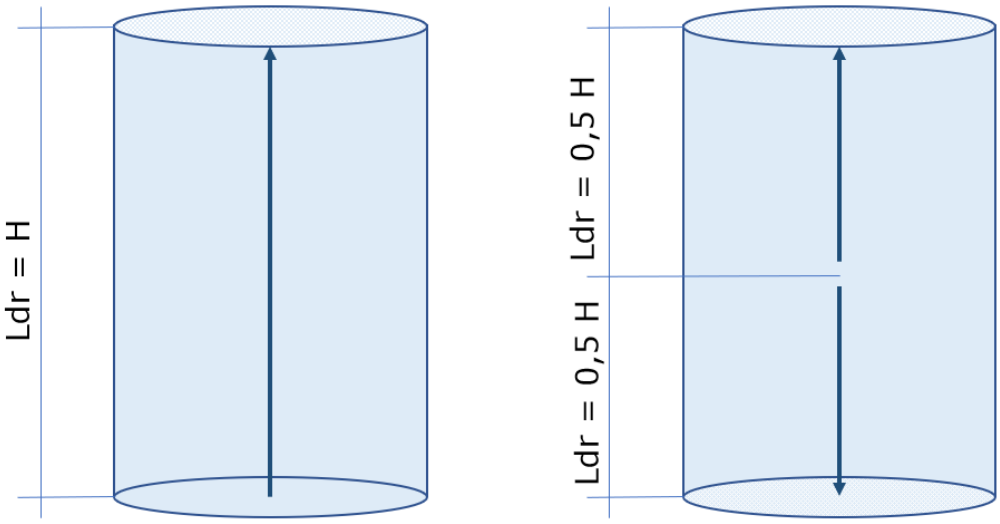

Figure 20: One-sided and two-sided drainage

It follows from equation 2.22 that the sample with one-sided drainage will have an estimated consolidation time t equal to H^2/c_v, while two-sided drainage will result in an estimated time of consolidation equal to $0{,}25 \cdot H^2/c_v$. Consolidation of samples where only one-sided drainage is permitted will take four times longer than if two-sided drainage is allowed.

The drainage time may be reduced by dressing the sample with vertical drainage papers**.** Excess pore water can now migrate radially towards the drainage paper along the periphery of the sample, as illustrated in Figure 21. The pore water then migrates through the drainage paper towards the sample drainage. Considering equation 2.22, the radius of the sample can now be considered as the length of drainage. The diameter of a sample is typically in the vicinity of half the height of the sample. The radius is half the diameter of the sample. Put into equation 2.22, radial drainage gives the expected time of consolidation equal to $0{,}0625 \cdot H^2/c_v$, a significant decrease in consolidation time when compared to strict one-sided drainage. It must be noted that the radial drainage does not lead directly to the drainage of the sample, the excess pore water must still travel along the drainage paper towards the sample drainage. The estimated consolidation time of $0{,}0625 \cdot H^2/c_v$ only considers the migration of pore water from the center to the periphery of the sample.

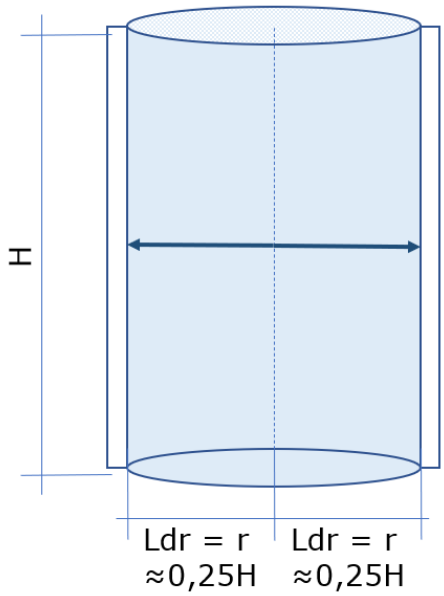

Figure 21: Pervious drainage paper

It is established that vertical drainage papers will reduce the time of consolidation, but considering the radius as the length of drainage does not reflect the whole path of drainage. An attempt at quantifying the importance of the vertical drainage papers were done by Mackinnon *et al.* (2010). For the tests conducted on clay, the consolidation finished 2,5 to 6,4 times faster for samples dressed in a single vertical drainage paper. For samples dressed in a double layer of drainage paper, the consolidation went 4.9 to 16.7 times faster than samples without drainage papers.

Another consideration is the change in rate of consolidation throughout the test. Consider equation 2.22 and the importance of length of drainage. As tests are ran, the samples will experience axial displacement and thereby a decrease in length of drainage. This will contribute to a decrease in the time of consolidation. At the same time, the coefficient of consolidation will increase as the vertical axial load increases (Yeo, Shackelford and Evans, 2005). This will contribute to a prolonging of the time of consolidation.

2.8 Oedotriaxial testing

Oedotriaxial testing, also commonly referred to as K_0 testing or K_0 consolidation, is a form of drained triaxial testing without shearing, under the condition of zero radial strain (Piriyakul and Haegeman, 2005). The testing condition would resemble a soil condition where lateral strains cancel each other, leaving only the vertical strain as the only deformation direction. These conditions are often observed in wide and flat area.

Zero radial strain can be achieved by controlling the cell pressure and deviatoric pressure individually. Two common testing methods are used to achieve essentially what is called oedometer conditions:

- Increase axial strain → measure response → adjust radial stress.
- Increase radial pressure → measure response → adjust axial stress.

It is important that the response is measured and adjusted quickly to avoid unnecessary shearing of the sample. Under ideal conditions, the sample should not fail during consolidation.

The response can be measured by a radial displacement transducer or a back volume controller. Radial displacement transducer method offers a direct response to the actual sample behavior and radial stress can be set accordingly. Back volume controller method offers an indirect response by relating the expulsed pore water with the sample volume change. The volume change is calculated via the product of original surface area with the required axial displacement illustrated in Figure 23. The axial stress can set accordingly.

The K_0 evaluated after the slope of the stress path in a $\sigma_1' : \sigma_3'$ plot as shown in Figure 22 with clay (Piriyakul and Haegeman, 2005). For graphical evaluation, both axes must have the same stress increments. The results should represent a stable and representative stress region. Non-linear behavior commonly observed in unloading needs extra attention.

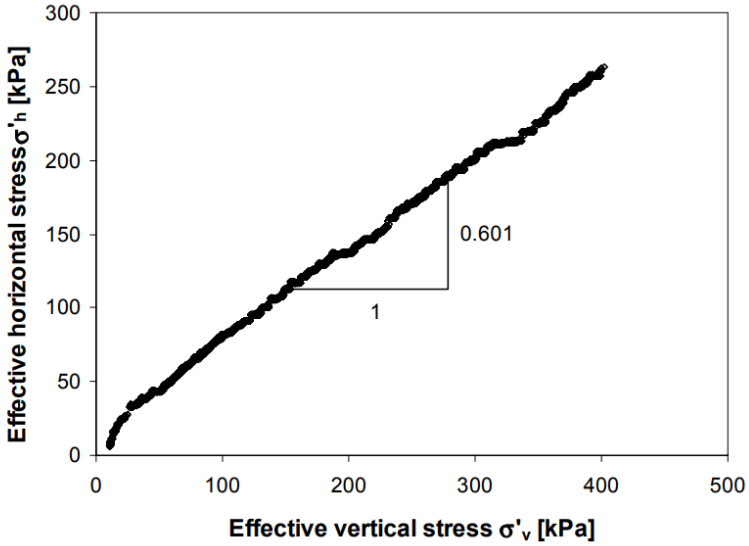

Figure 22: Plot of a stress path of oedotriaxial test with slope reading $K_0 = 0.601$.

The test is only suitable for fully saturated soils and must begin without excess pore water pressure. An increase in excess pore water pressure must not be allowed throughout the test.

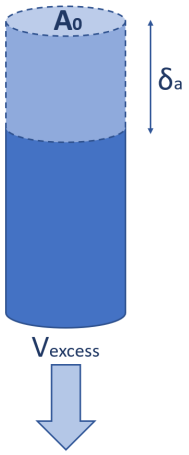

Figure 23: Idealized sketch of the relationship between volume change and axial displacement to keep original cross-section area of the sample.

Being a variant of a drained triaxial test, it is vital for the viability of the results that excess pore pressure is drained throughout the consolidation. This brings to question the rate of strain, or alternatively the rate of loading which facilitates this. While it depends on the unique soil behavior, it is considered better to have slow loading rates to reduce the buildup of excess pore pressure in the sample.

2.9 Pore pressure distribution

Effective stresses are used for calculating K_0 values, as outlined in chapter 0. To achieve dependable effective stress values within a sample, it is vital to have good estimates of the pore pressure and its distribution within a sample. In image (a), (b), and (c) in Figure 24, Head and Epps (2014) outlines how the pore pressure water migration reacts to different drainage schemes. This is discussed further in chapter 2.8. It also illustrates an expected development of pore pressures within a sample with passing time, shown in (e).

In picture (e) in Figure 24, line (i) signifies the initial pore pressure distribution within the sample, before drainage is opened in the top cap. At this point, the pore pressure is uniform with a value u_i. As the drainage in the top cap is opened, the pore pressure in the top of the sample decreases to a value u_b, which approaches zero. The development in the pore pressure distribution is followed sequentially through lines (1) through (5), before showing an ideal endpoint in line (f). It shows that the pore pressure read from the sensor at the pedestal will be of the highest magnitude within the sample. This brings to question how the read pore pressure should be treated to best reflect the actual distribution within the sample, through a mean value.

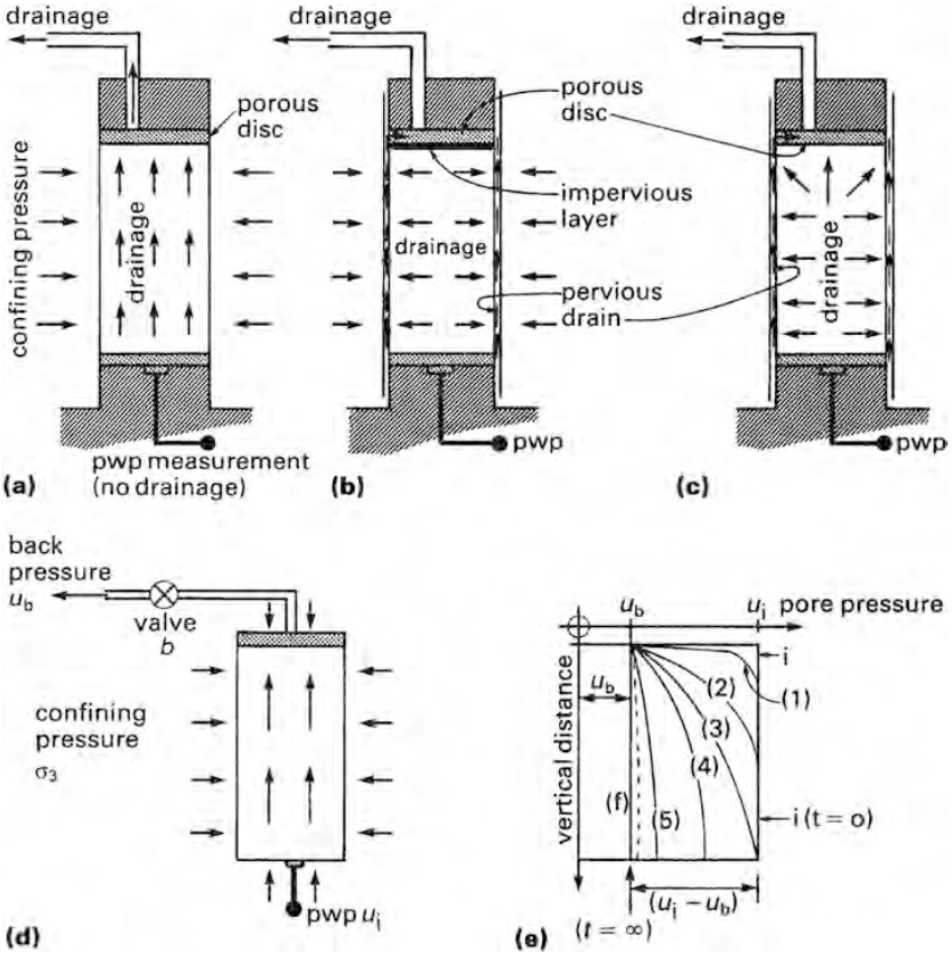

Figure 24: Drainage schemes and pore pressure distribution (Head and Epps, 2014)

To be able to approach an answer to how the read pore pressure should be treated, the impact of different drainage schemes on the pore pressure can be examined.

For a drainage scheme consisting of only top cap drainage, as shown in (a) in Figure 24, the pore water has a long way to migrate from the bottom of the sample. This is discussed further in chapter 2.8. As the pore water takes long to dissipate, one can expect the read pore pressure to reduce slowly. A good reflection of the pore pressure distribution within the sample would then lie in line (2) or (3) in image (e) in Figure 24. The distribution in this instance is assumed by Head and Epps (2014) to be parabolic, giving a mean pore pressure $\bar{u}$ as shown in equation 2.23, where u is the pore pressure value read from the sensor, and u_b is the pore pressure at the top cap drainage, assumed to approach zero.

$$\bar{u} = {}^{2}/_{3}\, u + {}^{1}/_{3}\, u_b \qquad \textbf{2.23}$$

If a pervious side drain paper is mounted, radial drainage is allowed, as discussed in chapter 2.8. As pore water can be radially drained from the bottom of the sample as soon as drainage starts, and the same goes for the whole length of the sample, one can expect the pore pressure distribution to approach that of line (4) or (5) in image (e) in Figure 24 sooner. As the difference between the pore pressure read at the pedestal u

approaches that of u_b at the top cap drainage, which approaches zero, Head and Epps (2014) suggests a linear distribution for practical purposes. This is shown in the equation 2.24.

$$\bar{u} = {}^{1}/_{2}\, u + {}^{1}/_{2}\, u_b \qquad \textbf{2.24}$$

2.10 Effects of storage time

It has been shown that the mechanical and index properties of clays can change markedly, even within the first 10 days of storage (Jean-Sebastien and Kim, 2013). The changes generally stem from pore fluid migration, moisture loss, chemical effects, and temperature and moisture changes. The effects of storage may be difficult to disconnect from the effects of sample disturbance, for instance in sampling or transportation.

For clays, the changes in index properties are largely found in the liquid limit (w_l) and the sensitivity. The sensitivity decreases with time after sampling, while the liquid limit increases. The changes in mechanical properties are largely found in decrease in undrained strength and preconsolidation pressure.

2.11 Summary

The theoretical chapter defines K_0 as the ratio between initial effective lateral stress and initial effective vertical stress, which are in varying degree determined by Poisson's ratio (ν), friction angle (ϕ), plasticity index (I_p), and overconsolidation ratio (OCR). There is not a clear scientific consensus on how K_0 develops with creep. Some proposed empirical relationships between these parameters are introduced.

The hyper-viscoplastic cam clay model (HVMCC) is a family of modified Cam clay Model (MCC) which follows the laws of thermodynamics and considers time dependent plasticity. Compared to Soft Soil Creep (SSC) the yield surface in $p'{:}q$-space is more flexible and can simulate experimental more precisely. It includes the control of the critical state on the mean effective stress via a spacing ratio (R) and the level of flow attributed to shear stresses via frictional dissipation (γ).

Oedotriaxial tests or K_0 testing, compresses the sample while maintaining the original cross-section. Compared to a standard oedometer test, it can measure the applied cell pressure. K_0 is greater during unloading than loading due to the immediate vertical relaxation of the sample compared to the lateral side.

Consolidation speed is and pore pressure distribution were discussed as important factors in determining the actual stress condition inside the sample. Most noticeably, correct application of drainage papers can reduce the consolidations speed significantly, but also make pore pressure distribution more uniform. Plasticity index (I_p) describes the soils water content between a liquid, plastic, and solid state. It is central soil characteristic which has shown empirical relationship with K_0.

The effect of storage time of samples affects the undrained strength, preconsolidation pressure, liquid limit, and sensitivity.

3 Method – Numerical

The methodology involves implementation of a new constitutive model within a hyper-viscoplasticity (HVMCC) framework developed at NTNU (Dadrasajirlou, 2022) that improves the simulation of K_0 in Unit IIIA.

Chapter 3.1 presents the numerical modelling software and systems used for the computation. It briefly explains how the previous model is imported into an older version of PLAXIS from which the kernel of the HVMCC is designed on. Chapter 3.2 presents the numerical model itself and justifies the modelling choices to suit the Troll field. Chapter 3.3 presents a fairly new type of calculation in PLAXIS using Python. Here, it presents the computational advantages with Python in regard to repeated processes. Chapter 3.4 presents the chosen approach to improve the simulation of K_0. It discusses how the approach is beneficial for the task. Chapter 3.5 presents a summary of the chapter.

3.1 PLAXIS

The numerical modelling was conducted with the geotechnical engineering software PLAXIS 2D. PLAXIS is a geotechnical numerical analysis tool using finite element method.

The HVMCC user-defined model was applied in PLAXIS. The kernel (hvpmcc64.dll) provided was placed into the udsm-folder (user-defined soil model). An empty folder named *temp* was created in C Drive to interpret any error outputs.

The inherited model is saved on a newer 1078 released in October 2022 while the kernel for HVMCC is based on build 452, released in May 2022. Between the builds, PLAXIS' internal codes have changed to integrate with Bentleys systems. Adapting HVMCC to be compatible with the latest build entails an overhaul of the code. At the same time, PLAXIS files on newer builds are not compatible with older builds.

The remedy is to regenerate the commands of the project in build 452. By entering *Expert* tab using *Examine commands*, all commands except calculations are activated and saved as a p2dxlog file. The file is opened and executed using *Commands runner*. This enables the regeneration of geometry, structures, mesh, phases, and all its associated parameters and settings of the project.

Calculations were run on build 452 to avoid any version-related issues with the kernel during simulation and automation.

The calculations were run on two different systems, from personal and office computer:

- Yoga Slim 7 with AMD Ryzen 7 4800U CPU at 18 CPUs ~ 1.8Ghz and 16 GB RAM with Windows 11 Home 64 bit, 10.0. Build 22621. Personal.

- ThinkPad E580 with Intel Core i5-8250U, CPU at 8 CPUs ~ 1.8Ghz and 8 GB RAM with Windows 11 Home 64 bit, 10.0. Build 22621. Office.

3.2 Numerical model

The model is a simplified 2D model of the borehole characterized by (Lunne, Long and Uzielli, 2006) that was based on (Jalali, 2022). The geotechnical parameters, geological characteristics, ice load chronology and are all extracted from his work. The additional background information connected to the parameters are sourced from (Sejrup *et al.*, 1995) and (Olsen *et al.*, 2013).

The model is essentially set in elastoplastic drained oedometer conditions. The layers are horizontal and based on interpreted lithology and geotechnical units by isotope and biostratigraphy studies. Each glacial advances are represented by uniform vertical loads. The glacial loads are based on estimated ice thicknesses. The identified depth, time interval and presence of ice sheet can be found in Appendix 7. The units are then divided into several phases to match loading and unloading from glacial and interglacial events.

Separating the sedimentation and glacial loads has given the most accurate estimations. For each new layer that is constructed by sedimentation, the loading of the preceding layer is removed. Then, a loading is applied without sedimentation during the same time interval. This process begins bottom up, starting from Unit V until the final layer in Unit I.

All the layers are calculated with SSC except Unit IIIA. Instead, Unit IIIA is calculated with HVMCC. This model has additional flexibility, which theoretically greater ability to simulate the field data as discussed in chapter 2.6. All units are assigned parameters and can be seen in Appendix 7. Due to numerical issues, the estimated older sea levels effect on pore pressures is addressed in the submersed unit weight (Lunne, Long and Uzielli, 2006). The general model information is described are summarized in Table 3.

Table 3: Model information. For more, see chapter 3.4.2 and Appendix 7.

Model information	Description	Value
Contour	From SSC	100x220 m
Loading type	From SSC	All plastic, except gravity loading (Unit V)
Drainage type	From SSC	Drained
Time unit	From HVMCC	Day
Time intervals	See Appendix 7	Order 10^6 days from Unit IV.
Flow conditions	Dry	Pore pressures reflected in unit weight.
Numerical control p.	Default, except. Unit IV and V.	Tolerated error = 0.03
Initial phase	Unit V	Gravity loading
e_0	From SSC, Unit IIIA.	0.44

Note that Unit IIIA is calculated in two parts. During the sedimentation of the layer, the $OCR_0 > 1$ based on suggestions from the SSC (Nordal, 2020). Then, in the next phases, $OCR_0 = 1$ to simulate normal consolidation conditions.

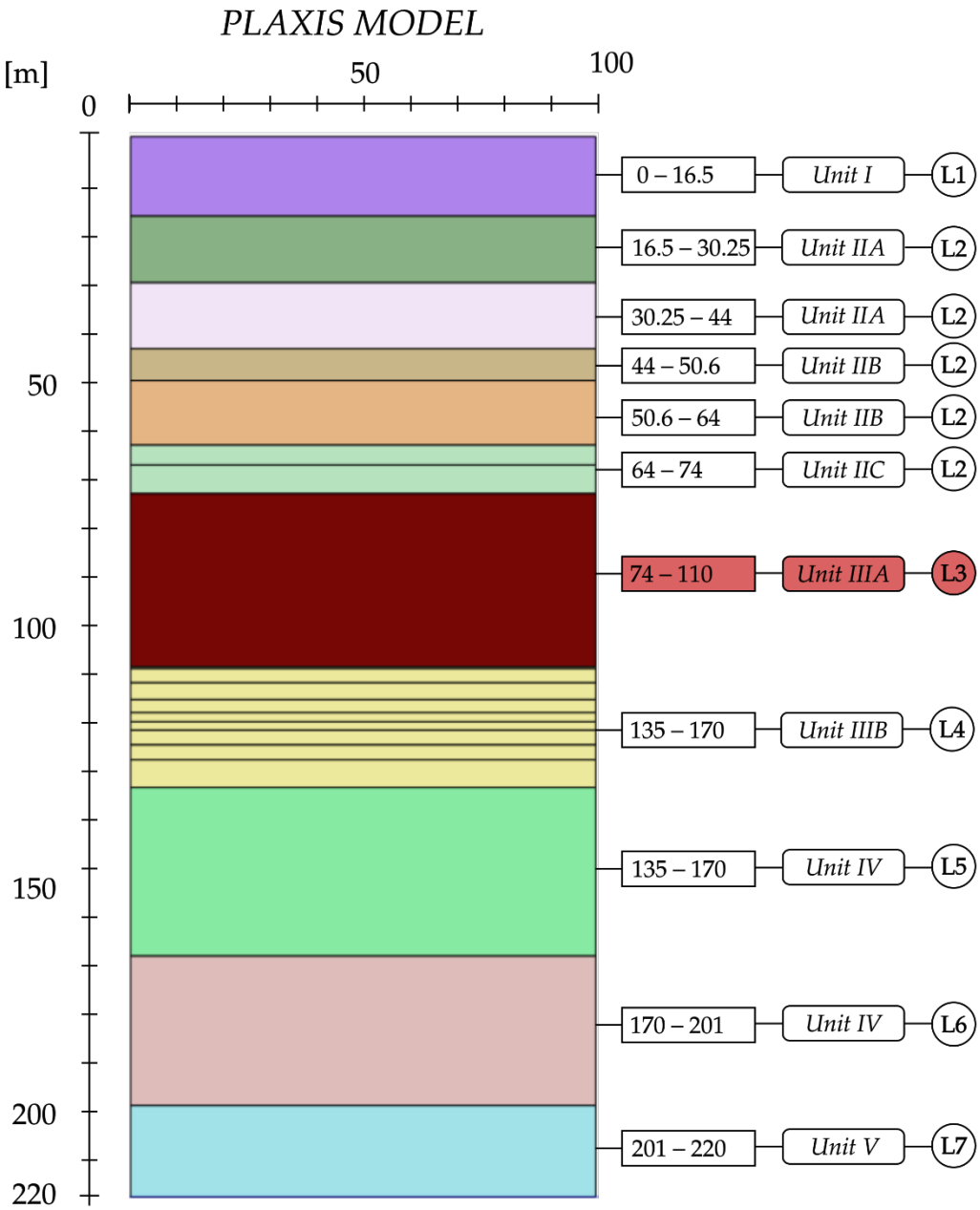

Figure 25: Representation of geometry and soil layers in color with geological lithology in circle, geotechnical units in rounded boxes and depths in boxes. Unit IIIA is highlighted.

3.3 Python automation

PLAXIS' Python API[6] was used to perform parameter variation calculations and to extract results. This is time efficient because extracting results is tedious from the many GUI[7] interactions required from PLAXIS. PLAXIS' integrated Python editor, SciTE[8], was used to run the calculations. In addition, to bring the benefit of working in pair, a GUI for was

[6] API: Application Programming Interface. Enables communication between two or more computer programs.
[7] GUI: Graphical User Interface. Simplifies program interaction through visual input and buttons instead of command or text-based navigation.
[8] General useful editor for building and running programs with plug-in support for Python API

made for convenience use of the automation script without Python knowledge. with the process shown in Figure 26. The input interface is illustrated in Figure 27.

A connection between Python and PLAXIS is made by initiating a remote scripting server with a local address for PLAXIS Input and Output. Using PLAXIS' command and scripting references - a parameter variation script was created. Running the script prompts the user to set parameter values for the HVMCC material model. It then calculates sets of phases from Unit IIIA to the top. After all phases have been calculated, the results on OCR and K_0 were extracted from a vertical, central cross-section, processed into a matrix, appended in a list, and outputted into a text file. An example of such text file can be seen in Appendix 8. Failed calculations are handled by outputting a text file indicating the error. Then the calculation continues to the next set of parameters.

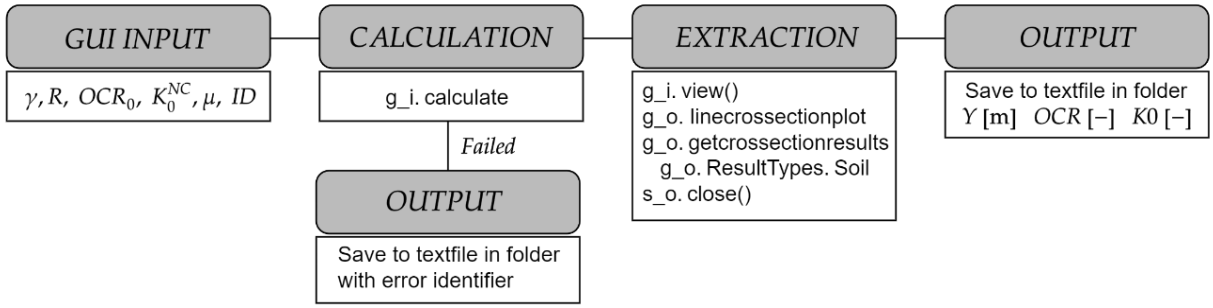

Figure 26: The GUI for input, tailored for set variations for R, γ, OCR_0, K_0^{NC} and μ.

A script was written on Spyder (A Python interpreter) to present the results. To visualize the trends in terms of simulating the field data, a heatmap-plot was used. The actual computation is done by calculating the percentile deviation of OCR and K_0 to the Troll field data. Fortunately, since the Troll field data is heavily discretized, the data is easily parameterized with respect to depth so that each position of the stress point can be compared to Troll. A smoother profile would be digitalized by WebPlotDigitizer[9].

The heatmap plots the percentile deviation from the Troll-data. For readability, each tile is labeled with the deviation. A final heatmap summarizing the deviation from OCR and K_0 helps interpreting an overall improvement of the simulation. The resulting heatmap-plots are shown in Appendix 9A, 9B, 9C, and 9D. Failed calculations are indicated as a cross on the tile of the heatmap.

[9] WebPlotDigitizer: A web-based tool to extract data from plots, pictures, and maps.

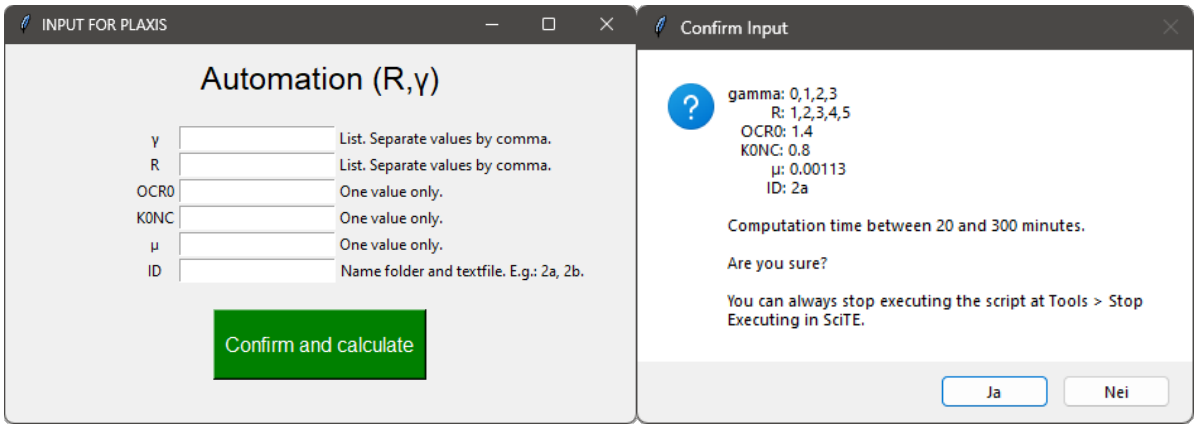

Figure 27: Overview of automation including some applied functions.

3.4 Iteration

The iterative process begins by setting a starting point. SSC parameters in Unit IIIA are translated to HVMCC and applied in Unit IIIA. A series of steps were performed following this process:

1. **Testing**
   Check numerical issues and boundary value problems.
   Mesh analysis.

2. **Starting point**
   Translating SSC parameters to HVMCC and run general calculation at slightly higher OCR_0 to avoid numerical issues.

3. **Analyzing and running targeted calculations**
   Recursively perform targeted calculations based on trial-and-error. Focus on consistent, targeted, and systematic order of calculations. Optimizing calculation workflow and reducing calculation time by reducing the scope of calculation.

4. **Simulating K_0**
   Narrow down on R and γ with best simulation of K_0.

5. **Simulating OCR**
   Narrow down on μ with best simulation of OCR.

3.4.1 Testing

Utilizing a new user-defined model for the first time such as the HVMCC will inevitably run into numerical issues due to the specific problem commonly regarded as boundary value problems. Calculation issues were addressed through frequent troubleshooting with Dadrasajirlou to understand model's limitations. A grossly simplified model from Figure 25 is made to ensure that HVMCC can calculate successfully with the geometry on basic Cam clay parameter values. The results are checked against varying time intervals,

meshing, layer thickness. A mesh analysis is performed as well to cut unnecessary simulating time.

3.4.2 Starting point

To set the conditions for numerical simulations, a qualified guess should be performed. Here, the parameters from SSC in Unit IIIA are translated into HVMCC based on section 2.6.5. These are summarized in Table 4 based on Table 2. Spacing ratio (R) and frictional dissipation (γ) are the main parameters in the simulations.

A practical starting point is setting the parameter in line with SCC. So, $\gamma = 0$ and $R = 2$.

In SSC, the Poisson's ratio was set to 0.46 by back calculation. This practically implies undrained conditions in the model. However, that value would be inconsistent with the drained conditions in Unit IIIA. In addition, a such ratio would return a lower K_0 due to its implied undrained (isotropic) stress conditions. The poison's ratio was therefore set to 0.2 as recommended (Dadras-Ajirloo, Grimstad and Amiri, 2022).

Table 4: Initial input values for HVMCC in Unit IIIA based on the starting point from SSC.

Model parameters	Description	Value	
κ	From SSC	0.01575	
λ	From SSC	0.02592	
g	Calculated	47.62	
M	Calculated	1.135	
R	Set	2	
γ	Set	0	
μ	From SSC	0.00113	
ν	Set	0.2	
τ	Set	0.042 day	
OCR_0	Set	Sedimentation = 1	Consolidation = 1

The first phase of Unit IIIA is a sedimentation phase – meaning the soil is constructed in normally consolidated condition ($OCR_0 = 1$). Provided the extremely long intervals (Appendix 7) this may cause numerical problems in how PLAXIS sets the time steps for the first iterations. In SSC it is recommended to set OCR_0 ~ 1.4 – 1.6 (Nordal, 2020) in the sedimentation phase. This recommendation was based on preventing excessive settlements from creep. However, this is kept in mind when starting from $OCR_0 = 1$.

Then, the proceeding phases, termed consolidation in Table 4, Unit IIIA is assigned OCR_0=1 to reflect a simulation of the normal consolidated stress conditions as the stresses are developing.

3.4.3 Analyzing and running targeted calculations

The starting point gives an idea of the OCR and K_0 in relation to the field data. It provides the basis for which sets of parameters should be calculated. Given the flexibility of the HVMCC it could be argued that good fits to OCR and K_0 can occur on several stationary points across the range of R and γ. Therefore, the process of adjusting the parameters is based on trial-and-error.

The calculation times can vary between one hour and several hours depending on the scope of parameters evaluated. Therefore, it is necessary to perform efficient calculations

to observe changes in OCR and K_0 in relation to the used parameters. A factor in this is maximizing the number of calculations throughout the day. Since calculation of 4 sets of parameters takes about 60 minutes, three methods of calculations were performed.

- **Work hour calculations**
  Daytime calculations lasting about 2 hours were run, giving opportunity to assess the results and perform more targeted sets of parameters. Both personal and office computers were used.

- **Night hour calculations**
  Large calculations lasting about 10 hours were run overnight. Only on personal computer.

- **After work calculations**
  Large calculation lasting about 10 hours were run on the office computer right before leaving office. Only on office computer.

3.4.4 Simulating K_0

The final K_0 is determined by the geometry of the yield surface on the p':q-plane. R and γ is varied between 0 and 6 to see the general trends. Any irrelevant pairs of R and γ will not be calculated. Here it is expected that an increase in γ will increase the loading inclination, attributed to the dilative behavior (softening) of the soil. This would reduce the final K_0. This is observed for oedometer conditions as discussed in chapter 2.6.

Predictions on how the K_0 changes in terms of the spacing ratio are not done due to the limited time of theoretical analysis of the HVMCC, as mentioned in chapter 2.6.

3.4.5 Simulating OCR

The final OCR is mostly determined by creep, given the set vertical loads above Unit IIIA over thousands of years. Knowing this, μ were varied in small increments as this parameter has an exponential effect on OCR. This can be observed in the force potential function (equation 2.20) where the strains are essentially scaled up by the creep index (equation 3.1).

$$\dot{\varepsilon}_V^p = r\left(\frac{p_{eq}}{p_0}\right)^{\frac{\mu}{\lambda-\kappa}} \qquad \textbf{3.1}$$

It is then expected that the OCR is proportional to the creep index.

3.5 Summary

The approach to the numerical work consists of automated calculations on PLAXIS using Python. This enables the benefit of using two systems simultaneously and saving the authors tedious works with the interface on PLAXIS. The model is set in PLAXIS 2D made in what looks like oedometer conditions. Unit IIIA is simulated first by translating soil

parameters from SSC to HVMCC. Noticeably, Poisson's ratio (ν), spacing ratio (R), overconsolidation ratio (OCR_0), and frictional dissipation parameter (γ) are set based on default MCC settings for drained calculations. From there, variations of R, γ, and μ are simulated to find the best simulation to Troll field data. Using Python, the script prompts the user to set the desired variations of the parameters. It then calculates all phases from Unit IIIA to the top and extracts a cross-section profile of OCR and K_0 at the final phase. These profiled are compared with Troll to display deviations on a heatmap plot. It helps visualizes the parameters effects on OCR and K_0 and provide understanding of the shape of the yield surface in HVMCC.

Based on the theoretical discussion, it is expected that OCR_0 >1 in the sedimentation phase due to possible numerical problems with the time intervals of several thousand years. This may have an implication on the plastic strain rates. Also, it is expected that OCR will be quite sensitive to μ, as it was used to adjust OCR in SSC (Jalali, 2022). In return, this implies that OCR may be insensitive to R and K_0, granting more independency between K_0 and OCR.Also, it is expected that OCR will be quite sensitive to μ, as it was used to adjust OCR in SSC (Jalali, 2022). In return, this implies that OCR may be insensitive to R and K_0, granting more independency between K_0 and OCR.

4 Method – Experimental

This chapter will describe the laboratory procedures of the thesis. Here, Onsøy clay is consolidated in various cycles resembling ice loads. An advanced test plan is presented along with how this is achieved. The Atterberg limit properties are tested before and after the consolidation of the samples. Practical challenges and limitations are discussed as well.

4.1 Origin of sample

The sampling was undertaken by NGI in December of 2019 at the Onsøy Norwegian Geo-Test site for soft soil, in the municipality of Fredrikstad. The red box in Figure 28 shows the approximate area of sampling, while a more detailed boring plan is found in Appendix 4. An exact positioning of the sampling provided by Subsea7 is shown in Table 5. The positioning places the borings in what Gundersen *et al.* (2019) refers to as the Southeast corner or "SEC" at the Onsøy site. The cylinders were sent to NTNU Trondheim by NGI.

Table 5: Positions of sampling

Borehole ID	UTM	Datum	CM	Easting	Northing
BH-ONSB-44	32	EUREF89	9°E	608286,38	6566433,19
BH-ONSB-45	32	EUREF89	9°E	608287,88	6566433,19

Two borings were conducted, both 72 mm piston samples, down to a depth of 11 and 12 meters. In connection with this thesis, two pistons spanning depths of 6-8 meters were received for laboratory testing. In the boring card, a comment was made of BH-ONSB-45 that the bottom part of the sample from the cylinder spanning 6-7 meters were missing. It is then reasonable to believe that it was cylinders from BH-ONSB-44 that were sent.

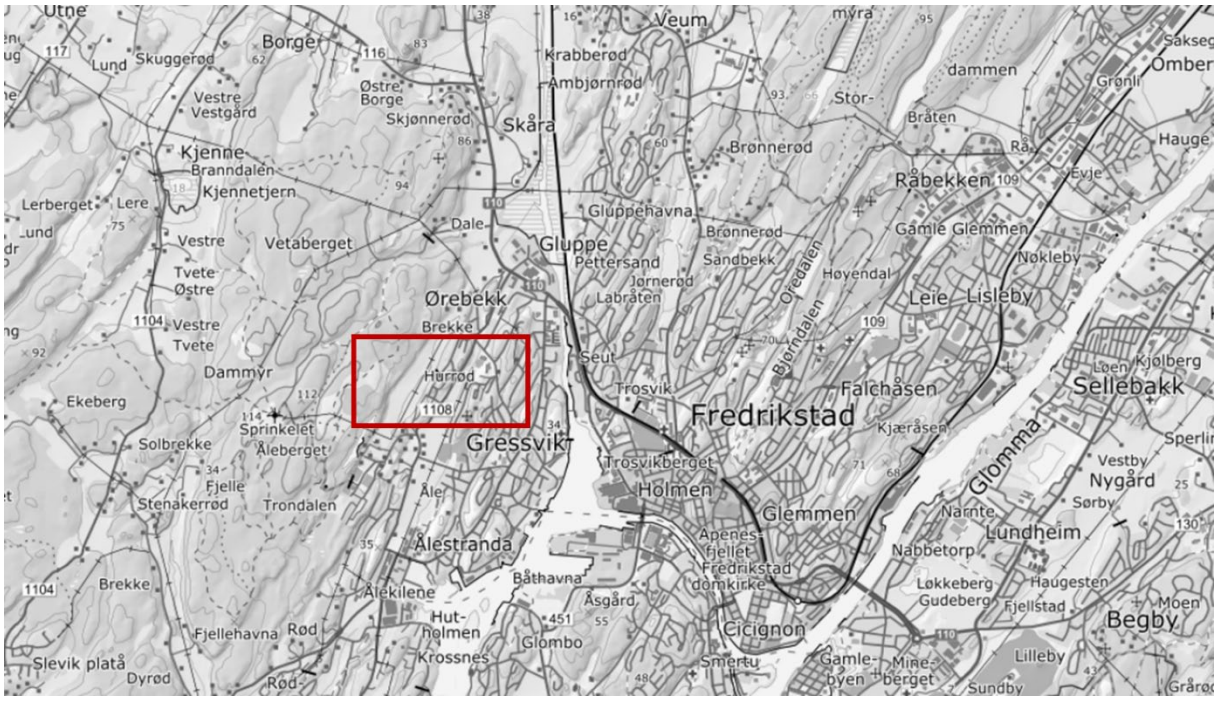

Figure 28: Approximate location of the NGTS Onsøy site (hoydedata.no)

4.2 Oedotriaxial test plan

The laboratory execution follows the design suggested by Lars Grande from NGI. It consists of an anisotropic consolidation in accordance with the Onsøy samples, then three loading/unloading cycles are conducted, before ending with a creep stabilization stage. A total of seven test stages are conducted. A typical test scheme is shown in Table 6. The characteristics of the Onsøy clay is summarized by Gundersen *et al.* (2019). The characteristics of the Troll clay is summarized by Lunne, Long and Uzielli (2006).

Table 6: Oedotriaxial test execution

Stage number	Description
1	Anisotropic consolidation in accordance with the in-situ characteristics of the extracted Onsøy clay
2	K_0 loading to an equivalent of $3 \cdot p_{c,Onsøy}$
3	K_0 unloading to an equivalent of $3 \cdot p_c / OCR_{Onsøy}$
4	K_0 loading to an equivalent of $2 \cdot p_{c,Troll}$ at the desired simulated depth at Troll
5	K_0 unloading to an equivalent of $p_{c,Troll}$, which corresponds to an OCR equal to 2.
6	K_0 loading approaching the maximal load of the apparatus.
7	K_0 unloading corresponding to a desired OCR in relation to the maximal loading in stage 6.
8	Creep stabilization

The testing scheme consists of high stresses which will affect the total testing time. Due to time constraints, only four stages were planned for the last test. This test consisted of an anisotropic consolidation to in-situ Onsøy conditions, loading to the Troll vertical

stress condition, unloading to a desired OCR, before ending the test with a creep stabilization stage and a last loading stage.

4.3 Quality of sample

The sample quality is assessed by the method of Lacasse and Berre (1988), where the volumetric strain when consolidating the sample to its in situ effective stress condition is considered. Volumetric strain is calculated as the change in volume over the starting volume, $^{\delta V}/_{V_0}$. The assessment criteria are as shown in Table 7.

Table 7: Quality assessment criteria (Lacasse and Berre, 1988)

ε_{v0}, %	Test quality
<1	Very good to excellent
1-2	Good
2-4	Fair
4-8	Poor
>8	Very poor

It follows then that good quality samples require less strain to be reverted to its in-situ conditions, speaking to its minimal disturbance before its arrival in the laboratory.

4.4 Index testing

Liquid and plastic limit tests is performed in accordance with NS-EN ISO 17892-12:2018 (Standard Norge, 2018), while the water content tests are performed in accordance with NS-EN ISO 17892-1:2014 (Standard Norge, 2014). The falling cone method of liquid limit testing was used to characterize soil from the NGTS Onsøy test site (Gundersen *et al.*, 2019). Therefore, this method was also used in this instance.

4.5 Oedotriaxial testing

Oedotriaxial testing is a form of drained triaxial testing where the radial strain is kept to zero (Piriyakul and Haegeman, 2005). Similar terms are K_0 testing or K_0 consolidation tests. It enjoys the benefits from independently controlling and measuring the radial stress compared to standard oedometer tests. The testing procedure itself is detailed in chapter 4.5.3. The consolidation is performed with measuring back volume change.

The oedotriaxial testing is performed mostly on 1 kN GDS Triaxial Automated System (GDSTAS) in the geotechnical laboratory in NTNU, Trondheim. It is accompanied by a back pressure controller (2 MPa), cell pressure controller (2 MPa), and an axial displacement transducer from GDS Instruments. The full setup is depicted in Figure 30.

4.5.1 Practical consideratons and limitations

Ideally a high capacity triaxial setup with load cell capacity of at least 10 MPa and cell pressure pump capacity of 5 MPa is required to test stress ranges of interest in Troll with Onsøy samples. Given the similarities of the clay in Unit II and Unit IIIB and Unit V

(Lunne, Long and Uzielli, 2006), consolidating Onsøy samples can provide insights on whether the comparable plasticity and stress states between Onsøy and Troll holds in greater stress regions. Consolidating Onsøy to stresses to Troll requires considerable high levels of stresses which the testing viability will depend on the limitations of the laboratory equipment. Practical aspects related to testing capacity includes, but not limited to:

- Perspex cell rated capacity
- Axial load cell transducer
- Cell and back pressure controller (volume and pressure)
- Axial displacement transducer (length)
- Pore pressure transducer (pressure)

Great emphasis was put on the ability to perform reliable and manageable lab tests within the given time frame. Therefore, it was decided to use a setup with reduced capacity with pressure controllers with 3 MPa capacity. Provided this, these instruments were limited to simulating Unit II. Despite the limitations on the equipment, this will still follow the project goals set by SHARP, according to Lars Grande.

A certain degree of experimentation is expected, especially regarding consolidation time.

4.5.2 Build-in of the sample

As the oedotriaxial test method is a variant of the triaxial test, and is performed in a triaxial test rig, the sample build-in is identical to that of for a triaxial test. The build in follows the method found in R210, the handbook for laboratory tests from the Norwegian Public Roads Administration (Statens Vegvesen, 2014). A GDS triaxial cell, as is used here, is shown in the Figure 30. Here, the components of the triaxial cell are shown.

After being extruded from a cylinder with a diameter of 72 mm, the samples are cut to a height of 100 mm, and a diameter of 54 mm. The process of cutting the sample to a diameter of 54 mm is performed by placing the sample on a pedestal, before cutting it with a wire saw according to Figure 29. It is then clear that the diameter of the samples is marginally larger than 54 mm. The build-in then follows the mentioned method of building in a triaxial sample.

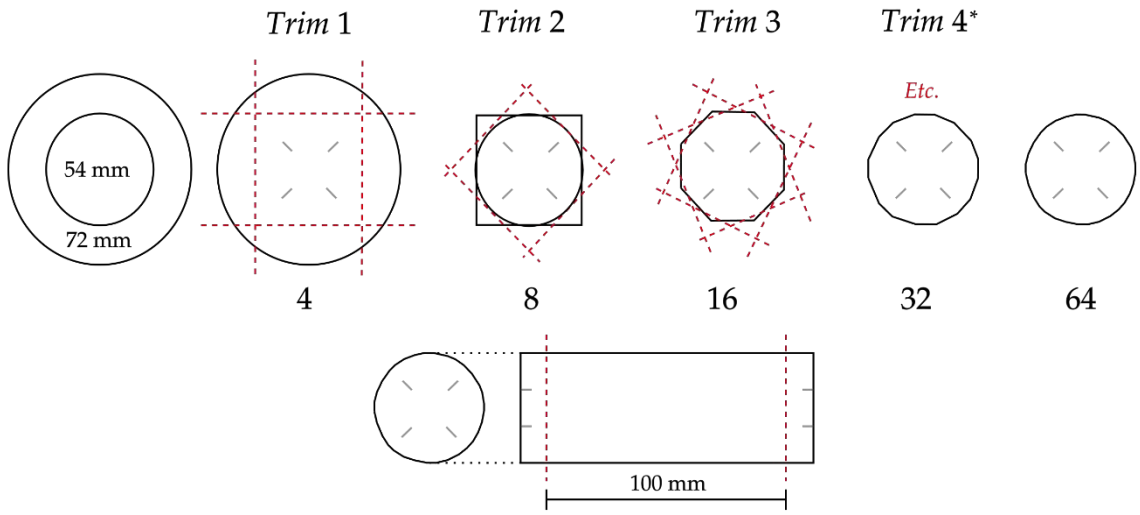

Figure 29: Trimming procedure of the sample. The cross indicates the indent from the sample trimming pedestal.

An important consideration is the use of vertical drainage papers. The theoretical background for the importance of it in our testing is explained in chapter 2.8. The vertical drainage papers are water saturated before being dressed around the sample. Care must be taken for the paper not to slide downwards towards the pedestal as the rubber membrane is dressed over the sample. The papers must have contact with the porous disc on the top of the sample, to get the full effect of the improved consolidation time. This is because the drainage of the sample is found in the two holes of the top socket. The pore pressure is monitored on the one of the holes in the bottom socket.

Assessment of the condition of the rubber membranes also became a focus. Although undergoing the usual test of holding the membrane up to the light, there were some fears of leakage, as possible holes in the membrane were found along the porous discs. This would of course be an hinderance for a test relying on the drainage of excess pore pressure. New membranes were later used to ensure minimal water leakage.

It is important to completely saturate the tubing before starting the test and open the air valve before filling the triaxial cell with water.

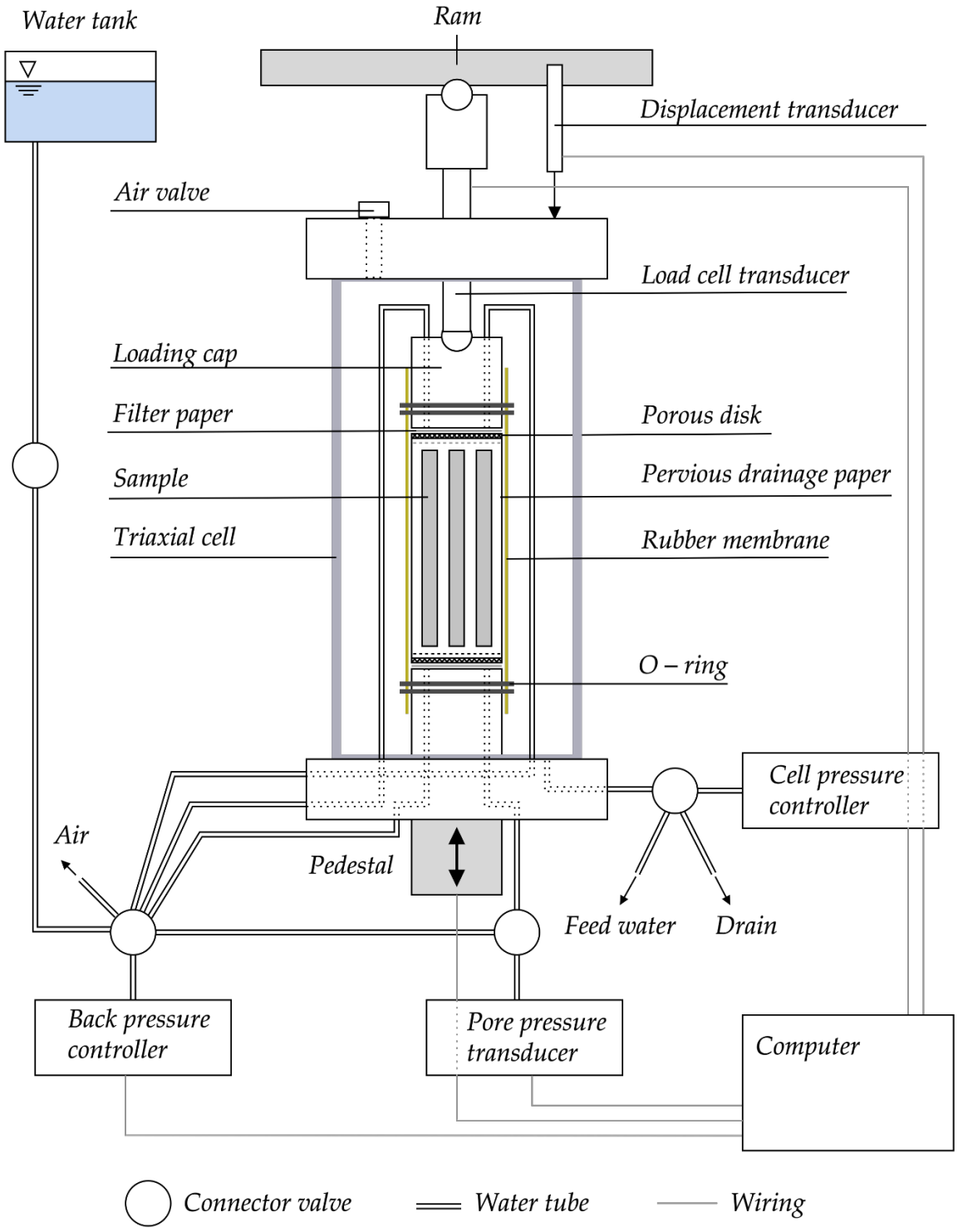

Figure 30: Schematic of the triaxial cell and its setup for the consolidation test. (GDS Instruments, n.d.)

4.5.3 K_0 Module

The oedotriaxial tests uses K_0-module in the GDSLAB software. Figure 31 shows the flowchart of the consolidation procedure. The module is described as follows according to the GDSLab Handbook:

"[…]. Enter the required target value for Radial Stress and set the length of time to reach this target in minutes. During the test, the axial displacement of the sample will be slowly adjusted thus ensuring the diameter of the specimen remains constant, where the specimen diameter change is calculated from the back pressure volume change."

This means radial stress change induces a back volume change. To maintain the cross-sectional area of the sample, the volume change occurs a new ideal sample height which is achieved by slowly adjusting the pedestal of the rig. This is monitored by comparing the water volume expulsed from the sample cell with the theoretical product of axial deformation and the original cross-section area. The change in pore water should be identical to the change in the volume of the sample. The calculation is done recursively until stage termination targets are met.

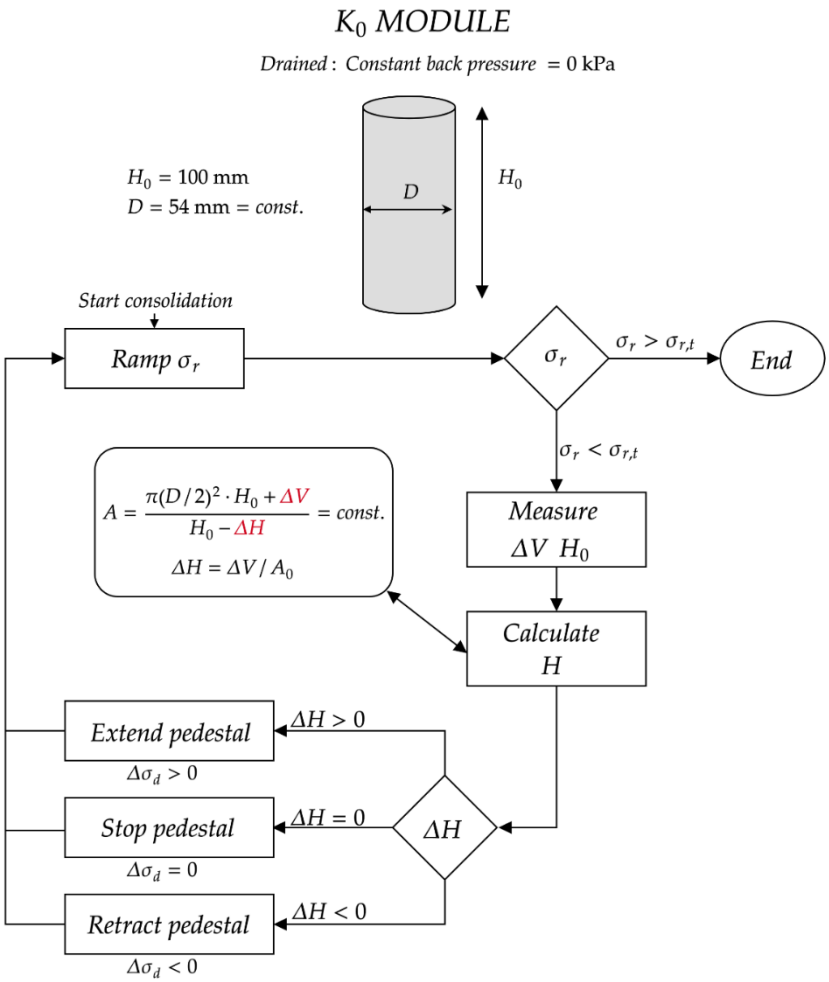

Figure 31: Calculation procedure based on K_0-module description, chart inspired by (Piriyakul and Haegeman, 2005)

The module assumes a fully saturated sample, no excess pore pressure and straight cylinder, i.e.: no barreling.

4.5.4 Approximation of the duration of consolidation

Consolidation time has practical implications for the execution of the lab test. The theoretical background of the approximation of the duration of consolidation is found in chapter 2.8. Drainage from the bottom pedestal must be closed to allow measurement of the pore pressure throughout the test. Tests must then be conducted with one-sided drainage. It follows from chapter 2.8 that one-sided drainage will result long durations for excess pore pressure migration to drainage. Equation 4.1 shows an estimation of the time of consolidation for one-sided drainage without vertical drainage papers.

$$t = {L_{dr}^2}/{c_v} = {(0{,}1\ m)^2}/{1{,}5 \cdot 10^{-7}\ {m^2}/{s}} = 66666\ s \approx 18{,}5\ hrs$$

4.1

As shown in chapter 2.8, vertical drainage papers will greatly reduce the time of consolidation, due to the radial migration of excess pore water towards the drainage paper. One layer of the vertical drainage will result in a consolidation time about 10 times faster. Equation 4.2 estimates the time of consolidation with one layer of vertical drainage paper.

$$t = {66666\ s}/{10} \approx 1{,}9\ hrs$$

4.2

It is important to note that the time of consolidation is controlled for each test. As outlined, a faultily mounted vertical drainage paper will have a great impact on the time of consolidation. The amount of excess pore water expelled is therefore observed throughout the test, and the time spent in consolidation adjusted thereafter.

4.5.5 Approximate time of testing and loading rate

Laboratory handbook R210 by Statens Vegvesen (2014) states that 16-20 hours is the expected time of consolidation for clay samples. As for the oedotriaxial K_0 consolidation, the rate of vertical stress loading must be approximated. A vertical stress rate of 2,5 kPa/h was used successfully in K_0 consolidation on Chinese soft marine clay. It must be strongly noted that these tests were not performed in a triaxial cell (Wang *et al.*, 2019). Applying this rate on a thought Troll loading phase, with a simulated depth of 50 meters and thereby vertical stress of 700 kPa, the equation 4.3 may give an approximate time of a Troll loading oedotriaxial stage.

$$\frac{700kPa}{2{,}5kPa/h} = 280\ h$$

4.3

To ensure a minimal development in excess pore water pressure throughout the test, there must be a balance between the rate of loading and the rate of dissipation. For a clay sample, this would indicate that the rate of loading should be kept low. A rate of 0,2 kN/m2/min was applied successfully by Hayashi *et al.* (2012) when performing an oedotriaxial test on peat and organic clay from Hokkaido. As such, this would only be an indication of the magnitude of loading rate appropriate for the soil considered here.

As noted, the development of excess pore water pressure is undesirable. To quantify this, the Norwegian Public Roads Administration considers a pore water pressure response under 10% of the vertical total stress to be sufficient for constant rate of strain (CRS) oedometer tests (Statens Vegvesen, 2014).

This approximations of time of testing and loading rate held the greatest importance for the earliest tests. The development of excess pore water pressure was observed, and created a basis of whether the rate of loading should be higher or lower for consecutive test stages, and consecutive tests.

4.5.6 Limitations of the laboratory execution

Table 8 lists the limitations which framed the laboratory execution. Most prominent was the limitation of the axial load cell transducer, which had a deviatoric axial stress limit in the vicinity of 345 kPa. This would limit the ability to reach the desired pair of K_0 and axial load. The axial load cell transducer was later changed to one with a higher capacity.

Table 8: Limitations of the oedotriaxial tests

Limitation	Description
Perspex cell	The Perspex cell had a capacity of 3.5 MPa. A cell pressure of 3.5 MPa could then not be exceeded.
Cell pressure pump	The cell pressure pump had a capacity of 2.0 MPa. A cell pressure of 2.0 MPa could then not be exceeded. The pumps had a volumetric capacity of 200 milliliters. Because of this, the back pressure pump had to be emptied, and the cell pressure pump filled, before conducting testing at higher stresses.
Axial load cell transducer	For the first seven tests, the axial load cell had a capacity of 1.0 kN Considering that the samples tested had a diameter in the vicinity of 54 mm, this equates to an axial stress in the vicinity of 345 kPa. This limitation in deviatoric axial load delivered by the load cell would prove to be a challenge. Considering equation 4.4 the limitation of the load cell would restrict the possible simulated depth of K_0 testing at Troll. $$K_0 = \frac{\sigma_{horizontal}}{\sigma_{axial}} = \frac{\sigma_{cell}}{\sigma_{cell} + \sigma_{dev\ load}}$$ **4.4** Considering a value of K_0 in the vicinity of 0.7 and a maximal $\sigma_{dev\ load}$ of 345 kPa, the maximal σ_{axial} would be 805, restricting the simulated depth at Troll to about 80 meters. The cell pressure had to be restricted for the estimated K_0 values to be met. From the eighth test on, a load cell with a capacity of 50 kN was used, allowing a higher cell pressure, and achieved K_0. The calibration of the 50 kN load cell is found in Appendix 3.
Axial displacement transducer	The axial displacement transducer has a maximal measurement capacity of 50 mm of axial retraction.
Pore pressure sensor	It follows from chapter 2.10 that the pore pressure is not evenly distributed within the sample. There is drainage in the top cap, while drainage is closed on the pedestal, where the pore pressure is measured. It is then an incorrect assumption that the measured pore pressure reflects the state throughout the sample. For the test scheme used here, the pore pressures reflective of the whole sample must then be estimated. For tests with high pore pressure readings, equation 2.23 was used to correct the readings, while equation 2.11 was used to correct those of tests with low pore pressure readings.

4.6 Assessment of K_0

The K_0 were assessed in $\sigma_1' - \sigma_3'$-diagrams generated in Microsoft Excel. Assessment in these diagrams plays into the definition of K_0, $K_0 = \sigma_h'/\sigma_v'$, as discussed in chapter 0, with the K_0 being equal to the rate of increase of the graph. Care was taken that the diagram area was as perfectly even sided as possible, so that the K_0 could be read as the height divided by the width of the best fit line. Figure 32 shows an example of a graphical K_0 assessment. All plotting relating to the experimental side of this thesis is done in Microsoft Excel.

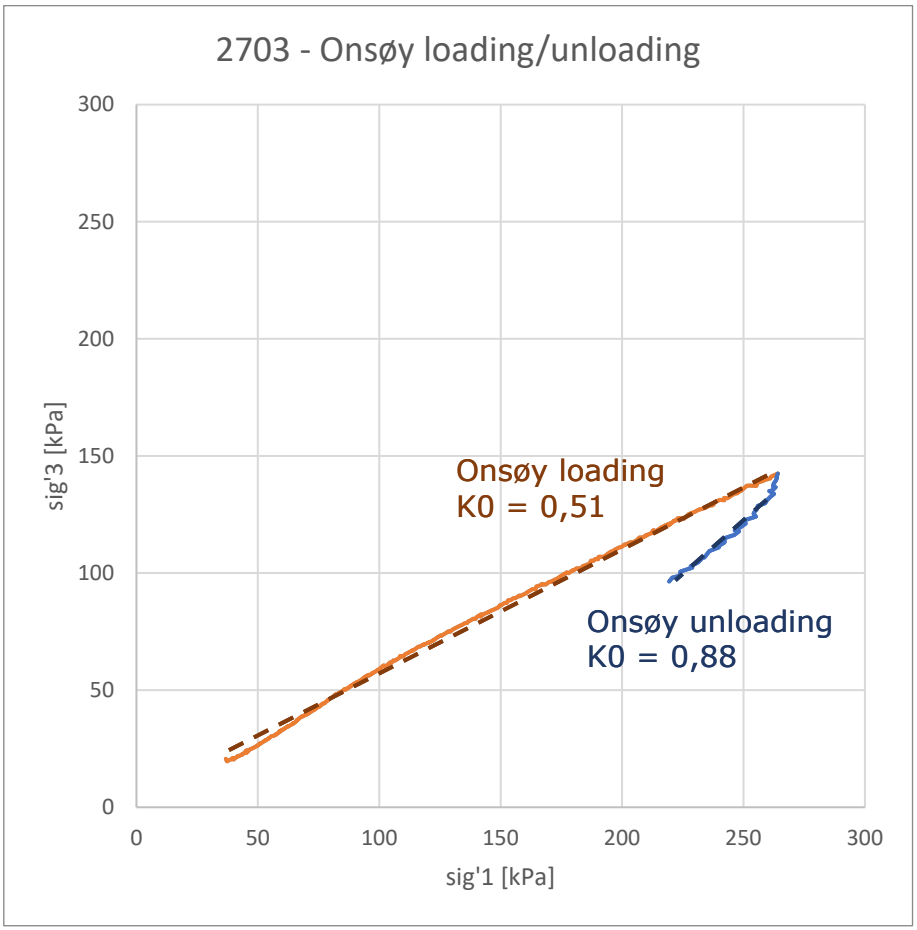

Figure 32: Example of a graphical assessment of K_0

As this a graphical assessment method, some variation between different readings for the same graphs must be expected. To account for this, graphs were assessed by both authors of this thesis, before a common value of K_0 was agreed upon. Care was also taken that relevant parts of the graphs were considered. On some occasions, the maximal limit of the axial load transducer was met. The following readings were regarded as unreliable.

4.7 Summary

The experimental test is performed on Onsøy clay, sampled in December of 2019 at the Norwegian Geo-Test site for soft soil in two 72 mm cylinders.

Oedotriaxial tests are performed in the geotechnical lab in NTNU with a K_0.module by GDS Software. The module slowly increases the cell pressure and keeps back pressure constant. By continuous measurements, it adjusts the displacement of the load cell to accommodate a new sample height based on the volume of the dissipated pore water. This keeps the original cross-section, provided it is a fully saturated sample with uniform pore pressure distribution.

With this module, the clay is subjected to loading-unloading cycles comparable to stress levels in Troll, before normally consolidating at around 1000 kPa cell pressure. Atterberg limit tests are performed before and after consolidation for comparison to Troll.

The entire consolidation is estimated to last 12 days per sample. The graphical assessment of K_0 was agreed by both authors.

5 Results – Numerical

This chapter presents the results of the numerical simulations.

Chapter 5.2 and 5.3 present K_0 and OCR across different configurations of spacing ratio (R), frictional dissipation parameter (γ) and creep index (μ). Chapter 5.6 presents the results of the mesh analysis for OCR and K_0 in terms of improving computational efficiency. The parameters are evaluated and determined for further discussion in relation to the Hyper-viscoplastic Modified Cam Cay Model (HVMCC) and its implication of the stress history in Troll. Chapter 5.7 presents the results of Unit IIIA in the context of the stress profile of Troll, including the previous modelling results by (Jalali, 2022). Chapter 5.8 presents the yield surface of the HVMCC based on the determined parameters R, γ and μ. Chapter 5.9 provides the summary of the results.

5.1 Calculation experiences

The application of Python GUI worked smoothly as both authors enjoyed the benefit of performing both short-term and long-term calculations where the results were shared seamlessly. However, divergent calculations were encountered. Once they were addressed, the calculation continued without any problems.

5.1.1 Divergence

The initial settings were riddled with instantly divergent calculations on the sedimentation calculation of Unit IIIA. The error code was 39, which is according to (Bentley, 2022) is related to severe divergence.(Bentley, 2022) is related to severe divergence. The debug logs (Appendix 9E and 9F) show stress points, highlighted in red, near the top surface of Unit IIIA containing NaN (Non associated number) values of the stresses in the HVMCC (indicated with udsm). By increasing OCR_0 slightly, the divergent stress points moved upwards closer to the surface until at a certain OCR_0 the calculation was successful for the pair of R and γ.

This means the boundary of divergent stress point are affected by OCR_0 which is part of setting up the initial values for p_{eq} and p_0. According to free energy potential, $p < 0$ is an impermissible state. This was quickly addressed in a newer version of the kernel by increasing p_0 slightly to add more stiffness such that new state variables can be defined.

After testing with the relevant parameters connected to the plastic strain rates, it was clear that more pairs of R and γ converged with increasing OCR_0. At $OCR_0 = 1.4$, the trends started to appear, as can be seen in Appendix 9A. Interestingly, the increase in OCR_0 did not affect the resulting OCR and K_0, but only allowed greater pairs of R and γ to converge.

This suggests that the flow direction determined by the yield surface somehow affects the development of p_0 in the first iteration of the sedimentation phase. It was later discovered that the divergence was a pure boundary value issue, exacerbated greatly by long time intervals and the size of the unit.

5.1.2 Calculaton based on general trends

The trend shows unfavorable results on K_0 with $\gamma > 0$. As a result, the scope was reduced to $\gamma = [0,1]$ from $\gamma = [0,1,2,3,4,5]$. On the other hand, increased R showed favorable results, and therefore the range $R = [0,1,2,3,4,5]$ was kept. The initial $\mu = 0.00113$ was

overestimating the OCR. Therefore, it was subsequently decreased until the results improved.

It is important to note that this methodology may return inconsistent material parameters. In practice, the all the chosen parameters should be obtained by recreating the oedometer tests collected by (Lunne, Long and Uzielli, 2006) with PLAXIS' Soil Test.
It is important to note that this methodology may return inconsistent material parameters. In practice, the all the chosen parameters should be obtained by recreating the oedometer tests collected by (Lunne, Long and Uzielli, 2006) with PLAXIS' Soil Test.

5.2 Evaluation of K_0

The results agree with the theoretical limitations in approaching the recommended K_0 values for normal compression in oedometer conditions (Figure 8). Figure 33 show that K_0 approaches 1 asymptotically with increasing spacing ratio, especially from 5. This applies to any creep indexes, although the figure is shown for creep index based on best match for OCR.

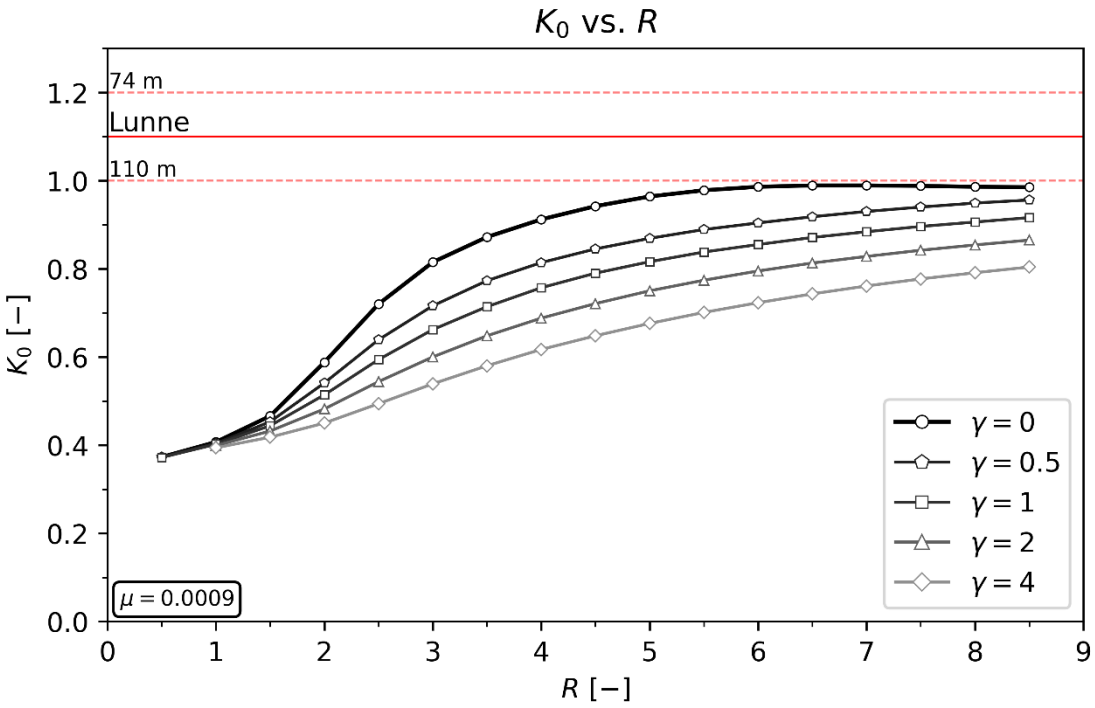

Figure 33: K_0 versus spacing ratio

5.3 Evaluation of OCR

The results in Figure 34 show that OCR increases exponentially with creep index. This agrees with proportionality and exponentiality of p_{eq} from the force potential. From this, it is exacerbated by major time intervals which has great influence on the final OCR. Here, it increases with increasing R and decreases with increasing γ. The influence from Ri s greater than γ. However, their contribution is stronger with increasing creep index.

The best creep index was set to 0.0009, which is considerably higher than the commonly observed creep numbers for marine clay.

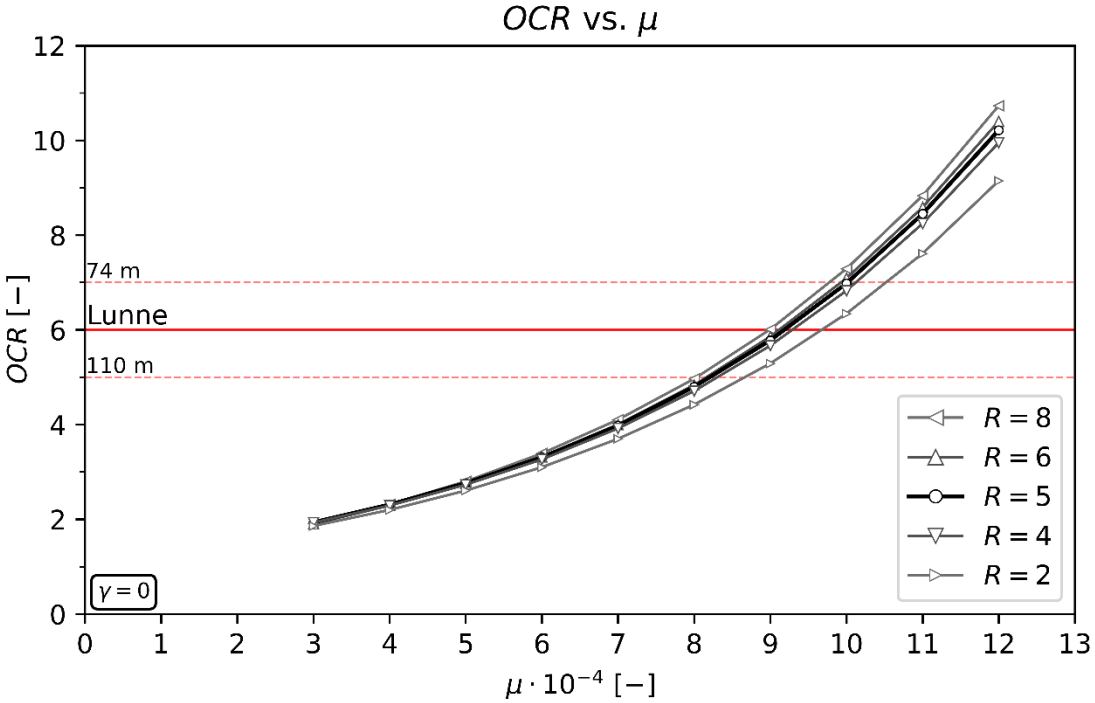

Figure 34: OCR versus creep index

5.4 Spacing ratio (R)

The results in Figure 33 and Figure 34 show that both OCR and K_0 is proportional to the spacing ratio in varying degrees depending on γ and μ. The difference is exacerbated by increased μ but not significantly. (Chen and Yang, 2017) suggests that the spacing ratio for clay is between 1 and 4. Spacing ratio for sand has been measured above 4 as well. Given the classification of the soil in Unit IIIA, this result lies in the boundary between results found in clay and sand. Based on this information, the best spacing ratio is 5.

5.5 Frictional dissipation parameter (γ)

The results show that both OCR and K_0 is inversely proportional to the frictional dissipation. This is an expected response based on the oedometer response in HVMCC (Grimstad *et al.*, 2021). Increasing the frictional dissipation, means the material will have a softer shear response. I.e.: the slope of the CSL increases, which "lifts" the yield surface. Given oedometer conditions in normal consolidation process, the deviatoric stress state on the yield surface will be considerably higher. Therefore, $\gamma = 0$, implying associated flow.

5.6 Mesh analysis

The mesh analysis for Unit IIIA done in the starting point of the iteration show that K_0 and OCR is practically equal between a very fine and a coarser mesh. Figure 35 depicts the calculations with increasingly coarser mesh by the number of total elements in the model. This reduced the computation time significantly from around 60 minutes to 15

minutes. Unit IIIA could not be coarsened any further due to the set mesh resolutions created by the preceding and proceeding layer.

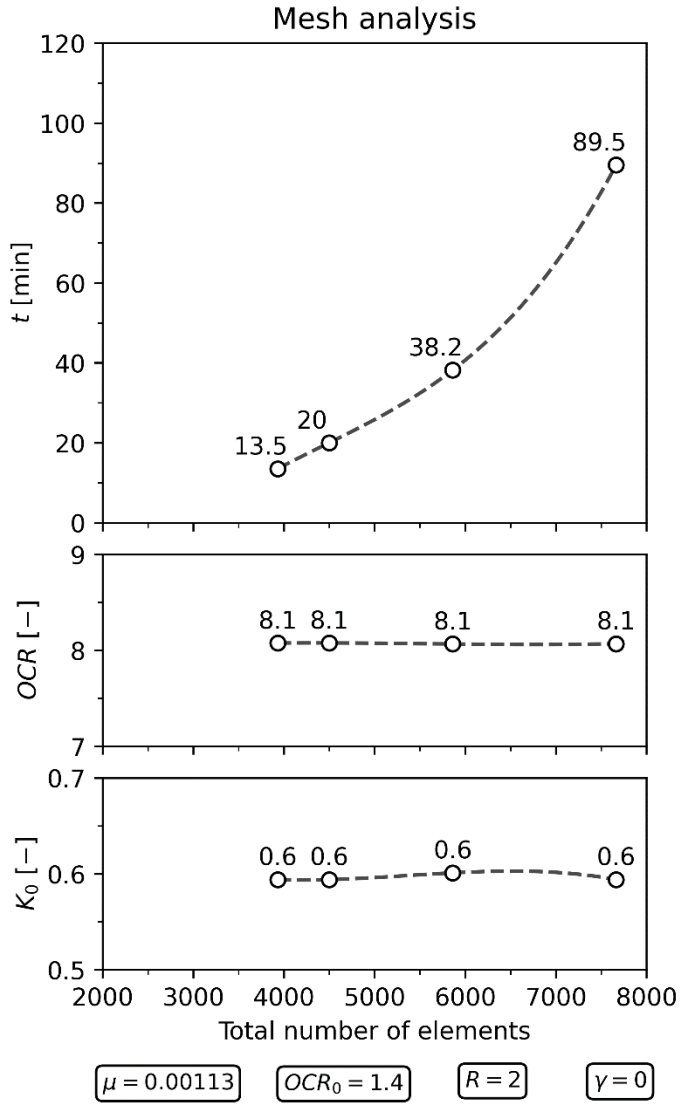

Figure 35: Mesh densities' effect on total computation time in minutes and resulting OCR and K_0 in Unit IIIA. Dashed lines are interpolated.

5.7 Troll

The simulated stress states in Unit IIIA (Figure 36) show improvements in both K_0 and OCR based on the determined spacing ratio ($R = 5$), creep index ($\mu = 0.0009$) and frictional dissipation parameter ($\gamma = 0$). The profile with HVMCC cuts between the two recommended values (OCR: 7,5) and (K_0: 1,1.2). This is accordance with the method of parameter fit. The parameters were set so the average deviation from Unit IIIA was close to 0 %. K_0 seemed to approach near isotropic conditions $K_0 = 1$ before decreasing slightly towards the bottom of Unit IIIA.

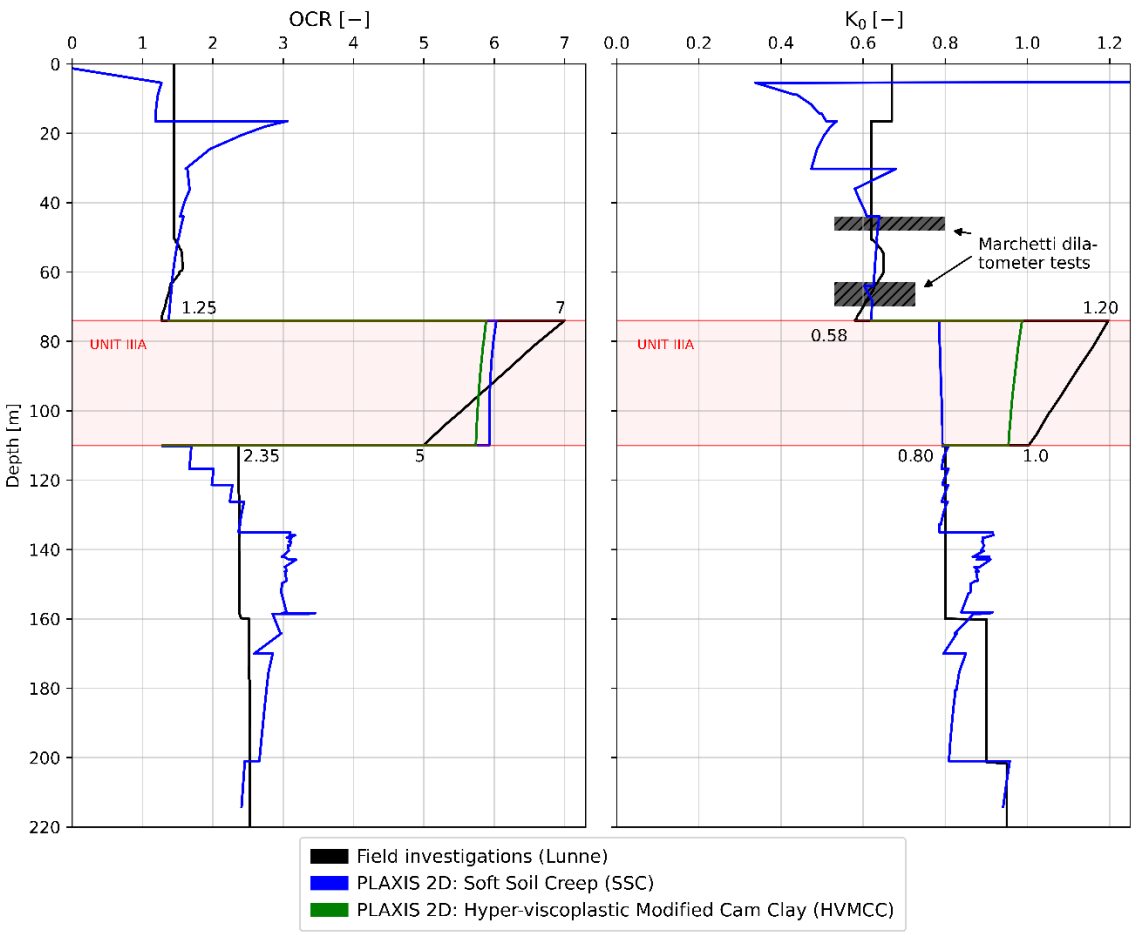

Figure 36: Plot of OCR and K_0 over depth from seabed with field data (Lunne) and numerical calculations from SSC and newly applied HVMCC. Unit IIIA (74- 110 m) is improved with HVMCC.

5.8 Yield surface in HVMCC

The normalised true stress space plane for $R = 5$ and $\gamma = 0$ is shown in Figure 37. The high spacing ratio offsets the location of the critical state giving it a shape resembling a slim guitar pick or a snap hair clip. The inelastic flow direction is considerably vertical with little stress softening on the wet side of the critical state line.

Since spacing ratio determine the location of the critical state on the yield surface, it shifts the maxima of the ellipse leftwards with associated flow. This makes the wet side remain relatively flat. With subsequent oedometer loading on the virgin soil from layers above Unit IIIA, the viscoplastic strains develops isotropic hardening in a rate that increases the OCR.

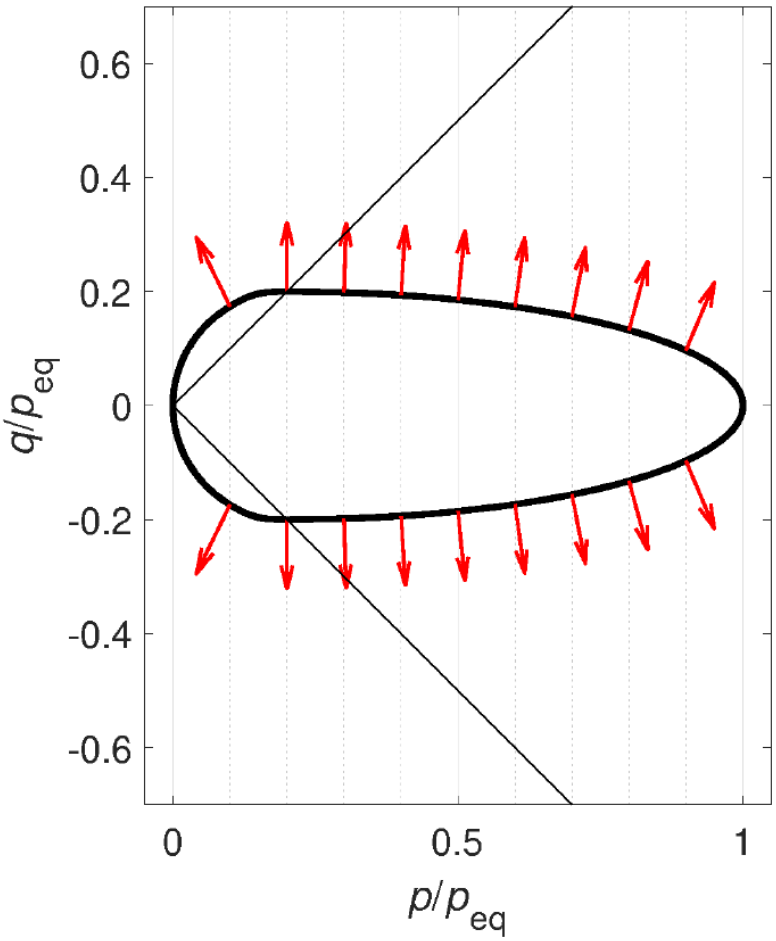

Figure 37: Depiction of yield surface for R=5, γ=0 and M=1.135. Plotted by Dadrasajirlou.

This consistent deviatoric stress level across the normalised mean stress axis may explain the increased K_0 for the oedometer loading condition.

5.9 Summary

The simulations shows that there exist numerical issues related to PLAXIS iteration algorithm. This was mitigated by increasing OCR_0, which returned more convergent sets of R and γ. As the trend became more apparent, the number of variations were reduced. HVMCC shows flexibility in K_0 mostly affected by R and OCR mostly affected by μ. With this, Unit IIIA was successfully simulated within the limitations of being in an oedometer condition ($K_0 \leq 1$) as shown in Table 9.

The main results show that:

- K_0 is sensitive to R and γ and insensitive to μ.
- OCR is very sensitive to μ, however also noticeably affected by R and γ.

Table 9: Determined HVMCC parameters for Unit IIIA.

R	γ	μ
5	0	0.0009

6 Results – Experimental

Two cylinders of NGTS Onsøy clay were provided for laboratory testing. From these two cylinders, 9 samples were cut and trimmed for oedotriaxial testing in the triaxial test rig. Not all these samples were deemed appropriate for testing, and not all tests were successful. Chapter 6.1 gives an overview of the samples and the execution of the tests, and highlights which loading rates gave favorable pore pressures responses throughout the oedotriaxial testing. Chapter 6.2 presents the results from the Atterberg limit testing, along with the unit weights, water content and sample quality of the samples. The results are compared to the Onsøy clay characterization by Gundersen *et al.* (2019). Chapter 6.3 presents the K_0 values evaluated from effective radial stress versus effective axial stress plots shown in Appendix 2. Chapter 6.4 presents plots of effective axial stress against time, and attempts to give an analysis of whether OCR has had an impact on the K_0 presented in chapter 6.3. Two of the tests are presented in axial strain versus effective axial stress plots in chapter 6.5. The chapter briefly presents Moduli M, which is evaluated from each loading stage. Chapter 6.6 rounds of the presentation of the experimental results by presenting two tests in K_0 versus effective axial stress plots, comparing the stabilized K_0 with the ones found in chapter 6.3.

6.1 Oedotriaxial

The oedotriaxial tests were executed in varying degrees of success. This comes from a wide range of occurrences which are detailed in chapter 6.1.1. Most of the occurrences come from quality of execution, test limitations and unforeseen events.

6.1.1 Oedotriaxial sample test details

A common problem for the later stages of tests 1703, 2703, and 1904 were revealed to be a limitation of the axial load transducer, namely the transducer reaching its maximum. Before 0505, an axial load transducer with a higher capacity of 50 kN was mounted. The calibration of this unit is found in Appendix 3. Test 1904 had high pore pressure readings, bringing into question the drained nature of the test. This was corrected for later test by taking more care in mounting the pervious side drain papers, as discussed in chapter 4.5.2. Table 10 summarizes the samples and test executions. The samples that underwent oedotriaxial testing is marked with the date of testing.

Table 10: Summary of samples and test executions.

Sample number (Oedotriaxial test date)	Cylinder number	Description
1	1	The test was ended due to the cell pressure pump volume being too low. The lesson drawn from this, is that the cell pressure pump volume should be maximized before conducting the test, and that the back pressure pump volume should be minimized. This made it clear that a user interaction was necessary before starting maximum load stages of the following tests. This makes it possible to prepare the pumps before this demanding phase.
2	1	The axial displacement device was not mounted. No relevant data was recorded.
3	1	A large rock was found when trimming the sample to size, bringing to question the homogeneity of the soil. The sample was discarded.
4 (1703)	1	The axial displacement device hit one of the mounting screws on top of the of the cell, forcing the test to be ended. This user error came unexpectedly and limited the axial displacement to about half of the available displacement of the device. The solution was found in moving the mount of the device from the load cell to the mounting frame.
5 (2703)	2	A small rock pebble was found when trimming the sample. Due to the scarcity of available samples and the small size of the, the sample went through to testing. The sample went to failure during the maximum load phase of the test. The failure was marked by a sudden increase in pore pressure. The maximal load cell output was met and held before the failure.
6	2	The sample went to failure soon after the start of the in-situ consolidation. After examining the data, the most likely cause was a failure of the load cell transducer. The transducer was plugged in and out before the following test, which solved the problem.
7 (1904)	2	High pore pressure readings, due to the pervious drainage paper not being mounted for highest performance.
8 (0505)	2	Good pore pressure readings, due to pervious drainage paper being mounted for optimal performance. There was a power shortage during the Onsøy loading, necessitating starting the

		test cycle anew from this point on. A load cell of capacity 50 kN was mounted before this test.
9 (2205)	2	Truncated laboratory procedure due to time restraints. Only anisotropic consolidation, an unloading/unloading cycle, creep stabilization and a final loading.

6.1.2 Pore pressure response and loading rate

As mentioned in Table 10, the pore pressure response was high in test 1904, and markedly lowered in the consecutive test 0505. A decent pore pressure response is a premise of a successful oedotriaxial test, and as mentioned in chapter 4.5.5, it should not exceed 10% of the axial load. The pore pressure response of a given sample is governed by the balance between the capacity of draining the excess pore water and the loading rate. The premises of building in a sample for optimal drainage is explained in chapter 2.8. For keeping a successful pore pressure response, good drainage enables a higher rate of loading. Figure 38 shows the pore pressure response relative to axial load for tests 1904 and 0505. Also shown is the 10%-value which should not be exceeded. Both tests were run at similar load rates of 0.15-0.20 kPa/min. This shows that for oedotriaxial testing on Onsøy clay, a load rate of 0.15-0.20 kPa/min will yield favorable excess pore pressure development, given one-sided drainage and that the sample is properly mounted with pervious drainage paper.

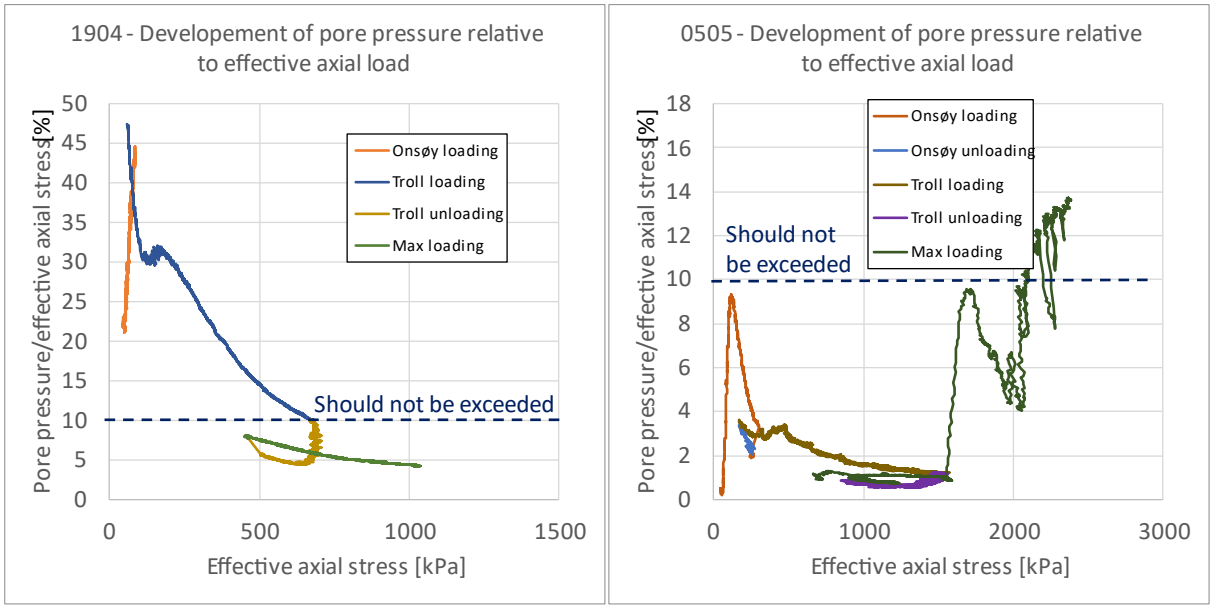

Figure 38: Pore pressure response in tests 1904 and 0505

6.2 Atterberg limits

The index testing and sample quality assessment was conducted as described in chapter 4. Table 11 summarizes the values obtained from the testing. In the "Test number" row, the parenthesized suffix signifies testing done before (1) and after (2) undergoing oedotriaxial testing, where this applies. Appendix 1 contains the background of the presented results.

Table 11: Summary of index testing and sample quality results

Test number	Onsøy depth [m]	w [%]	w_L [%]	w_P [%]	I_P [%]	Unit weight [kN/m³]	Sample quality
1603	6.68	69.0	70.8	27.7	43.1	16.7	-
1703 (1)	6.44	68.9	78.8	31.1	47.9	16.5	Very poor
1703 (2)	6.44	38.3	66.8	27.7	39.1	-	
2703	7.93	65.4	70.1	28.5	41.6	16.8	Good
1904 (1)	7.69	68.2	69.8	26.2	43.6	16.4	Fair/Poor
1904 (2)	7.69	38.2	64.7	27.5	37.2	18.6	
0505 (1)	7.57	63.8	71.6	28.5	43.1	16.2	Good
0505 (2)	7.57	33.2	61.0	28.4	32.6	18.3	
2205 (1)	7.45	67.6	70.5	28.7	41.8	16.0	Good
2205 (2)	7.45	35.9	65.1	28.5	36.6	19.0	

The Atterberg limits obtained from the samples before undergoing the oedotriaxial test largely falls into the range which can be expected due to the previous characterization of the area (Gundersen *et al.*, 2019). A compilation of the previous characterization and the limits obtained in relation to this thesis is shown in Figure 39. The results from testing in relation to this thesis is shown with triangles. As shown in Figure 40, a decrease in the plasticity index is noted after going through the oedotriaxial testing. As also shown in Figure 39, the water content also largely falls into the expected region.

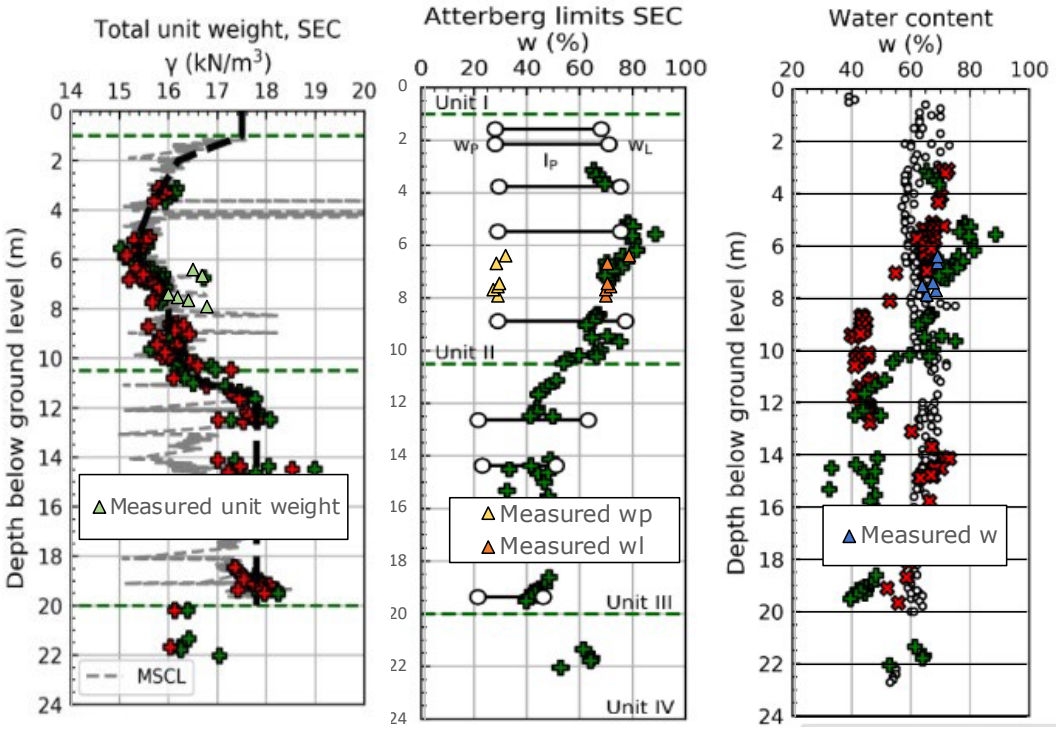

Figure 39: Composition of previous index testing of Onsøy soil and the testing done for this thesis (Gundersen *et al.*, 2019)

The measured unit weights generally exceed the values found in the previous characterization of the soil, as shown in Figure 39. This may be due to the cutting of the sample, as explained in chapter 4.5.2. The samples do not have a perfectly circular cross

section with a diameter of 54 millimeters but are cut with a varying number of edges. A cut sample such as this will have higher weight than a circular sample. This, along with the fact that a perfectly circular diameter of 54 millimeters is used in the calculation of the unit weights, leads to a higher unit weight. Samples 8 and 9 were cut with more edges, closer to a circular cross section. The unit weight of these samples run closer to the values from the previous soil characterization.

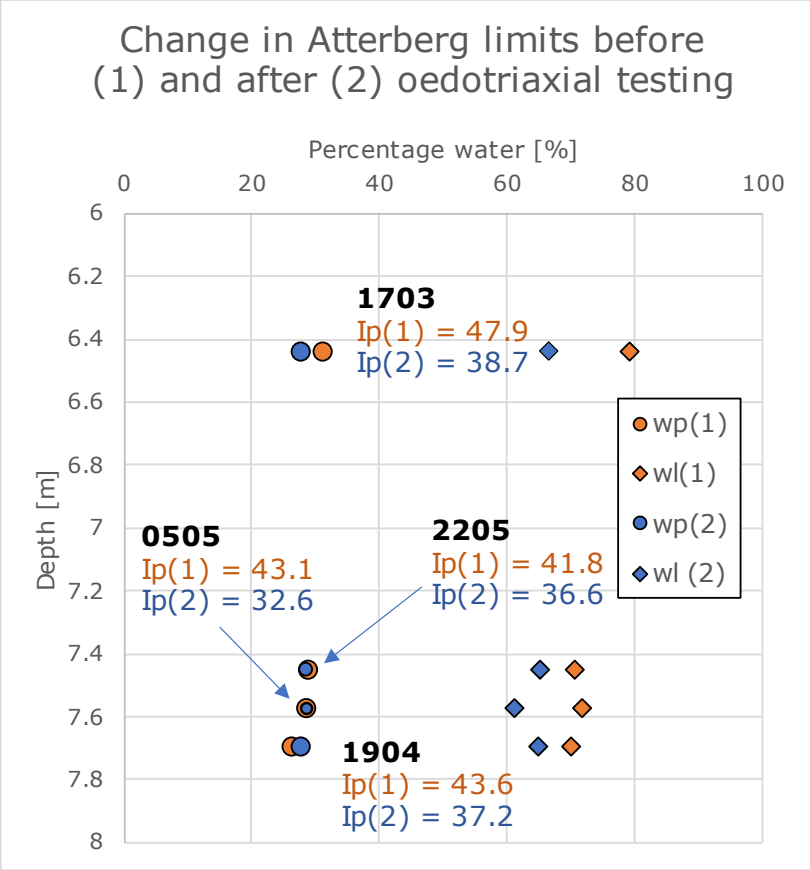

Figure 40: Change in Atterberg limits before and after oedotriaxial testing

As discussed in chapter 2.11, the storage time of the samples may have had an influence on the index properties. Namely, the liquid limit may increase. As shown in the Figure 40, no such effect can be traced to the samples in this instance. This may serve to determine the absence of effects related to storage time. Another point to consider is the storage time in relation to the characterization conducted by Gundersen *et al.* (2019). Mechanical properties of soils can be altered as soon as within the first 10 days of storage (Jean-Sebastien and Kim, 2013). Although the storage time of the soil used in the characterization is not known, it may then be a possibility that the liquid limit was already affected at the time of the characterization. Still, the measured water content is an indication that the samples were stored well.

6.3 Evaluation of K_0

The K_0 values were obtained as discussed in chapter 4.6, with the assessed graphs found Appendix 2. In Table 12, the values obtained from assessment is summarized.

Table 12: Summary of assessed K_0 values

Stage	1703	2703	1904	0505
Quality of sample	Very poor	Good	Fair/Poor	Good
Onsøy loading	0.71	0.49	0.64	0.48
Onsøy unloading	0.96	0.88	-	-
Troll loading	0.80	0.52	0.47	0.53
Troll unloading	0.95	0.81	0.82	0.88
Max loading	0.71	0.65	0.75	0.69 *Must be used with caution due to highly erratic stress path*
Max unloading	-	-		-

The unloading K_0 values assessed from oedotriaxial test data is consistently found to be higher than the K_0 values assessed for loading. This is consistent with what may be expected (Aas and Lacasse, 2022). Although the evidence is limited, the K_0 for first and second unloading may be found to be similar (Aas and Lacasse, 2022). The K_0 values assessed in this instance may reflect this assumption, as the unloading K_0 values do not differ much in assessed values.

A last, truncated oedotriaxial test was performed due to time constraints. The stages planned was an anisotropic consolidation to in-situ Onsøy values, loading-unloading cycle, a creep stabilization stage, and then a last loading stage. The attempted creep stabilization stage was hampered by an unwanted increase in axial stress, bringing into question the veracity of this attempted creep stabilization stage and the subsequent second loading stage. The assessed K_0 values from this test are shown in Table 13.

Table 13: Assessed K_0 values for test 2205.

Stage	**Assessed K_0 values for test 2205**
First loading	0.50
Unloading	0.85
Second loading (After attempted creep stabilization)	0.64

6.4 Development of effective axial stress – assessment of OCR

Figure 41 shows the development of effective axial stress throughout tests 1703, 2703, 1904 and 0505. This is used as a basis of examining whether OCR could have played a role in the assessed K_0 values, which are summarized in Table 12.

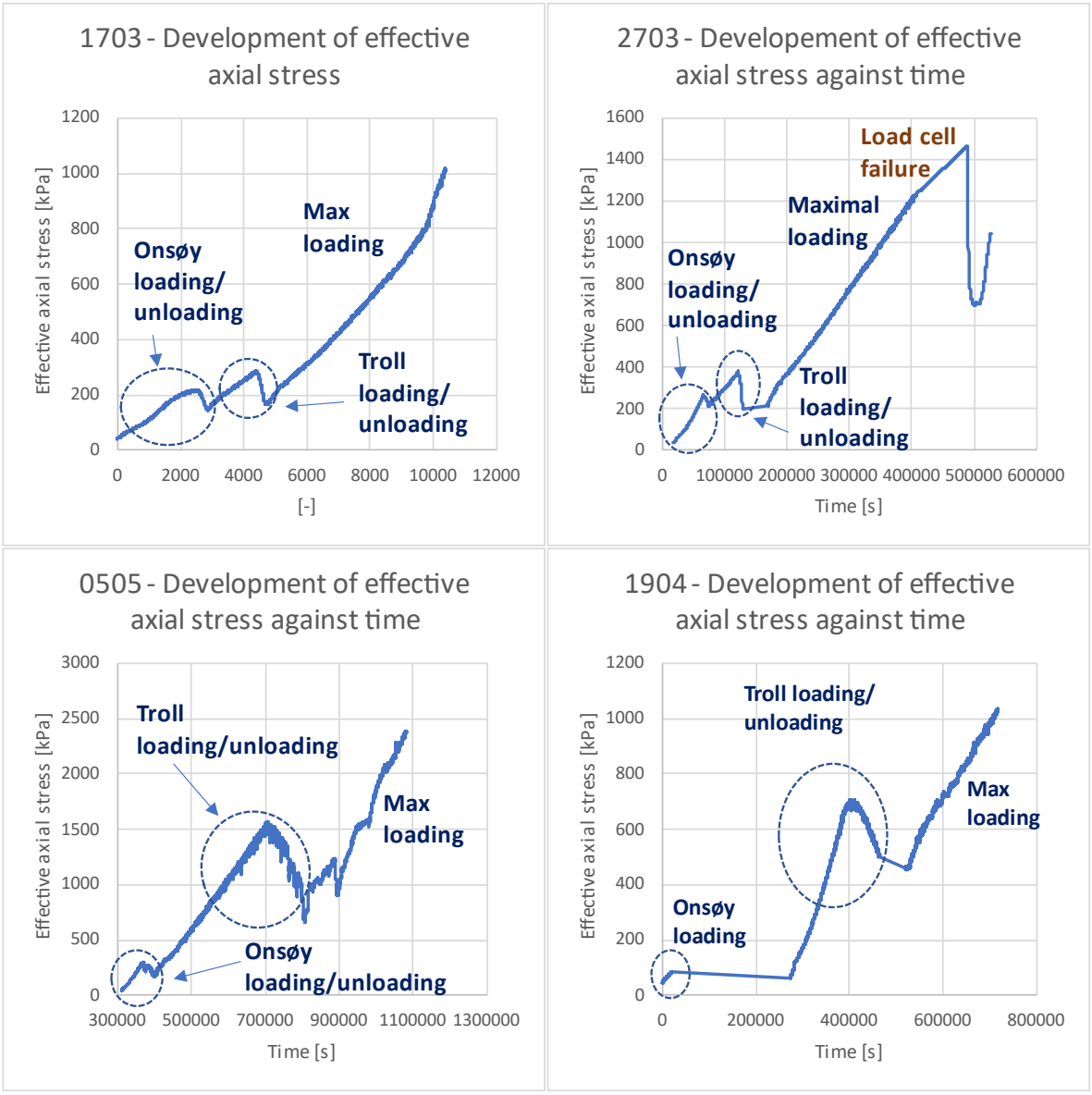

Figure 41: Effective axial stress development in tests 1703, 2703, 1904 and 0505

For tests 1904 and 0505 the previous maximal effective axial stress from the Onsøy loading stage is quickly surpassed in magnitude by the Troll loading stage. The same holds for a majority of test 2703. For test 1703, the previous maximum is surpassed halfway through the Troll loading stage, but this test should in its entirety be viewed with skepticism due to the very poor quality of the sample. For the Onsøy and Troll loading stages, the OCR could then practically be considered as 1.

The results from the maximal loading stage of 0505 must be used with caution, as the sample underwent an unforeseen loss in cell pressure before starting the stage. 1703, 2703, and 1904 underwent mostly successful maximal loading stages, although 1703 and 2703 ended before planned due to reasons summarized in Table 10. The sample qualities in connection with each sample is summarized in Table 11. Only the sample quality of 2703 is good and might therefore be a good test to examine whether OCR might have had an impact on its assessed K_0 from the maximal loading stage.

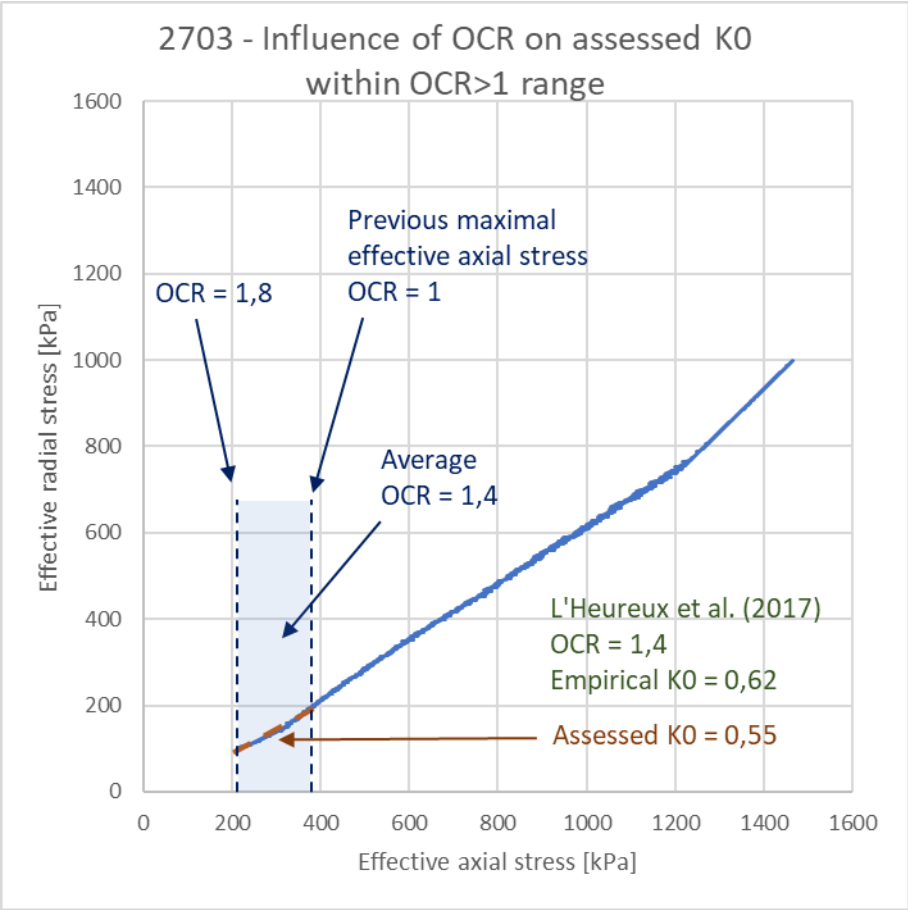

Figure 42: Influence of OCR on assessed K_0 within OCR >1 range.

The maximal loading stage of test 2703 is shown in Figure 42, plotted as effective radial stress against effective axial stress. The area of the test where the OCR is of magnitude higher than 1 is highlighted, and the average OCR of 1.4 within this highlighted area is calculated. The K_0 within the highlighted area is graphically assessed to be 0.55, well under the empirical value given by an OCR of 1.4 as input into equation 2.3. This is all shown in Figure 42. It may note that the K_0 assessed for the whole of the successful execution of test 2703 is 0.65, approaching the empirical value. Still, whether OCR has had any meaningful impact on the assessed K_0 values remain inconclusive.

6.5 Axial strain versus effective vertical load and modulus M

The samples used for tests 2703 and 0505 were of good quality, as shown in Table 11. The two tests also represent two extremes in terms of vertical loading, where 0505 were loaded to a higher magnitude. 2703 and 0505 are therefore two tests assessed considering the axial strain versus the effective vertical load and constrained modulus M. The constrained modulus M represents the deformation properties of a soil in uniaxial vertical loading with the premise of zero lateral strain, and is usually evaluated from oedometer tests (Meyer and Olszewska, 2021). The axial strain versus effective vertical load graphs, along with the evaluated moduli M is shown in Figure 43. Modulus M is evaluated as the slope of each loading stage. Table 14 summarized the evaluated moduli M for the different stages and loading intervals for test 2703, while Table 15 does the same for test 0505. Zero lateral strain is a premise of evaluating modulus M. For this test

regime, there is no way to directly verify this. A possible method of evaluating whether radial strain has occurred would be to compare M moduli obtained from oedotriaxial testing and M moduli obtained from oedometer testing.

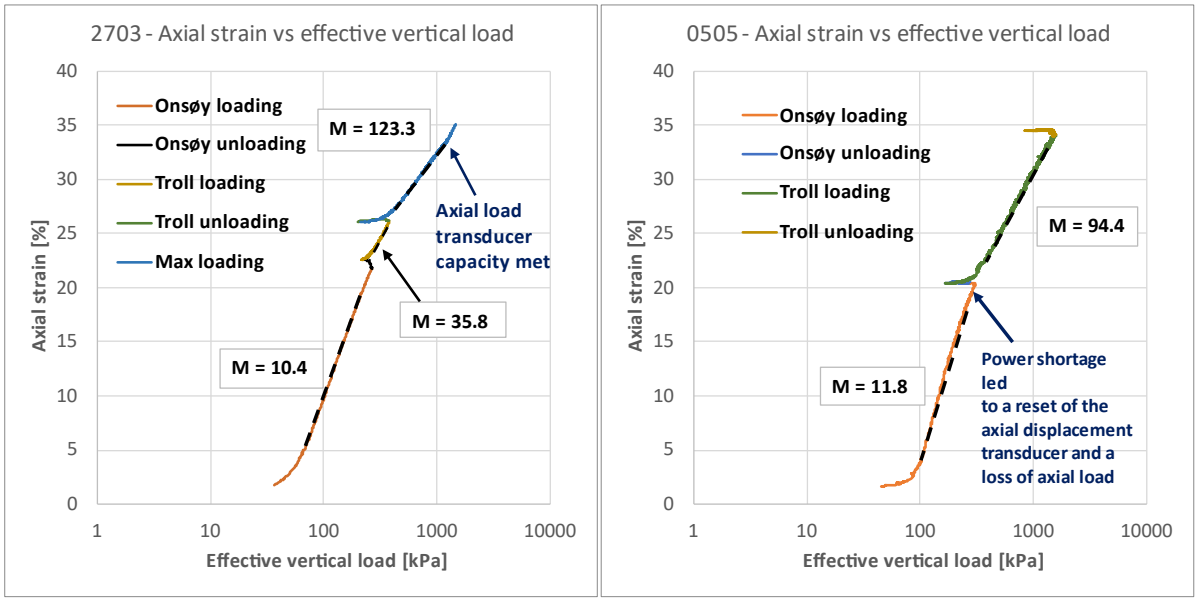

Figure 43: Axial strain versus effective vertical load for tests 2703 and 0505

Table 14: Modulus M evaluation for test 2703

Stage	Approximate loading interval for modulus M evaluation [kPa]	Evaluated modulus M
Onsøy loading	90-270	10.4
Troll loading	250-380	35.8
Max loading	400-1400	123.3

Table 15: Modulus M evaluation for test 0505

Stage	Approximate loading interval for modulus M evaluation [kPa]	Evaluated modulus M
Onsøy loading	100-290	11.8
Troll loading	350-1400	94.4

6.6 K_0 versus effective axial stress

In this section, the results from tests 2703 and 0505 are presented in K_0 versus effective axial stress diagrams. The background for highlighted these two tests is as explained in chapter 6.5. Only the loading stages are presented, as the unloading stages behave highly unreliably when presented in K_0 versus effective axial stress diagrams. Rather than showing an increase in K_0, the show a decrease. This might be due to a swelling of the

sample during unloading, where the swelling sample pushes the load cell, and thereby is subjected to an unwanted axial load. Also presented in the diagrams is the K_0 values at which the test stages seem to stabilize. Figure 44 shows the plots for the Onsøy loading stages, Figure 45 for the Troll loading stages, and Figure 46 the maximal loading stage of test 2703.

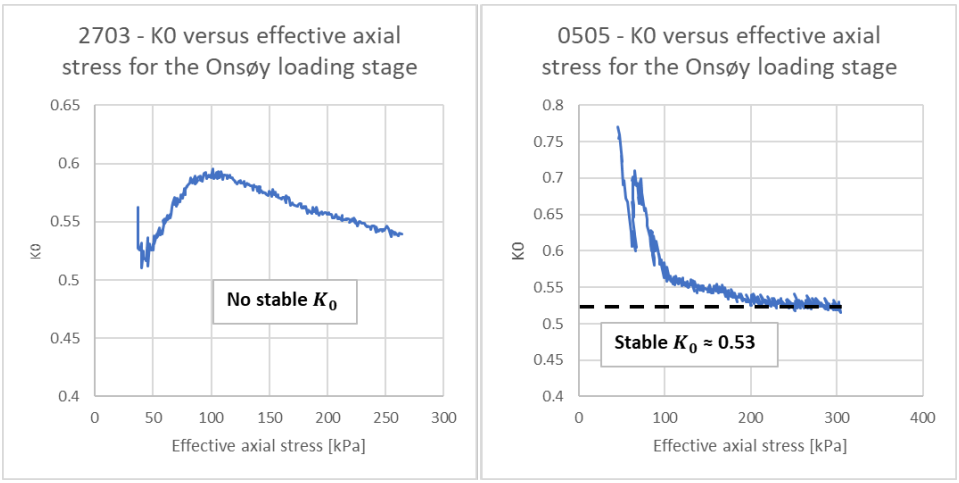

Figure 44: K_0 versus effective axial stress plots for the Onsøy loading stage of test 0505 and 2703.

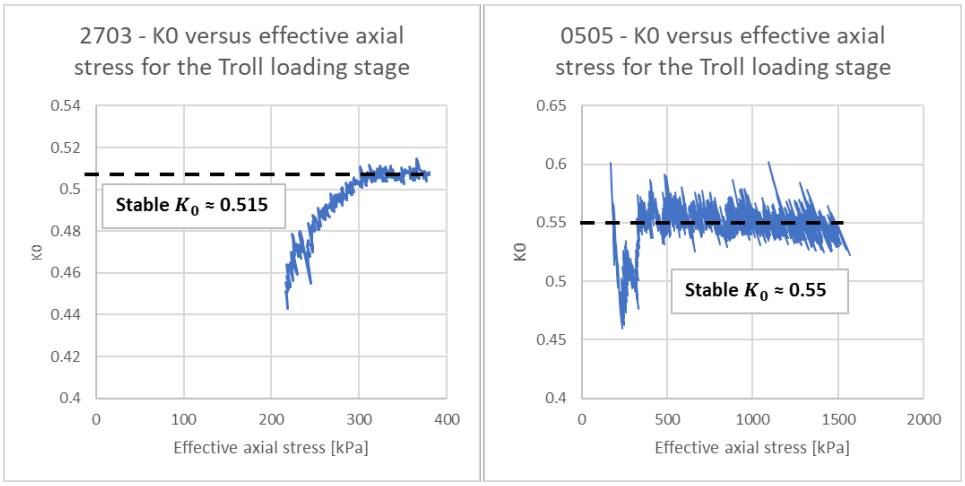

Figure 45: K_0 versus effective axial stress plots for the Troll loading stage of test 0505 and 2703.

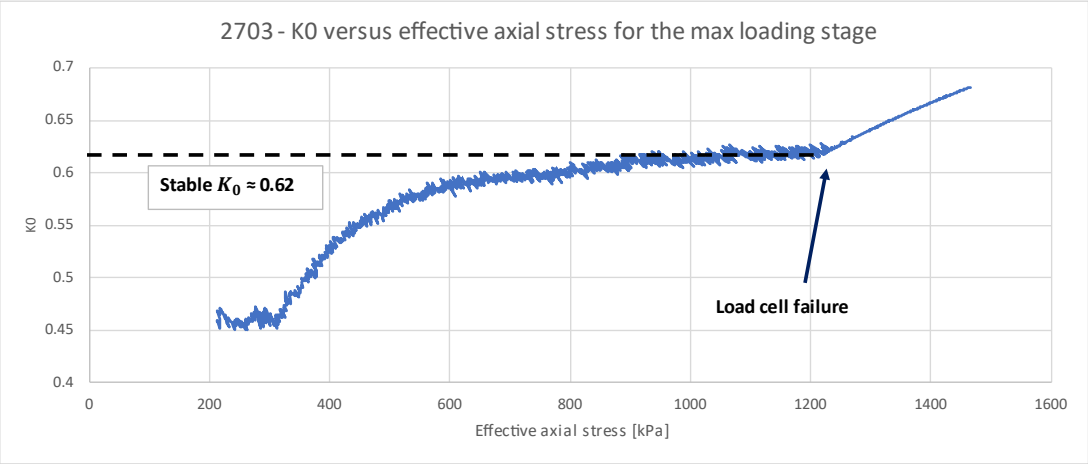

Figure 46: K_0 versus effective axial stress plot for the maximal loading stage of test 2703

Table 16: Summary of K_0 values obtained from graphical evaluation and K0 versus effective axial stress plots.

	Graphically evaluated K_0 Presented in Table 12	**K_0 evaluated from K_0 versus effective axial stress graphs**		
Test number	2703	0505	2703	0505
Onsøy loading	0.49	0.48	-	0.53
Troll loading	0.52	0.53	0.515	0.55
Max loading	0.65	-	0.62	-

Table 16 summarizes the K_0 values obtained from graphical assessments of effective stress plots and the K_0 values evaluated from K_0 versus effective axial stress plots. A decent compliance in K_0 is shown between the values gained from equivalent loading stages.

7 Discussion - Numerical

The modelling work has produced many interesting results that can be connected to main principles in geotechnics, especially regarding the development of K_0 and OCR in Unit IIIA.

Chapter 7.1 discusses the effect of using PLAXIS' Python API for the simulations. Chapter 7.2 discusses the numerical challenges faced during the early stages of simulation. A simple solution is presented overcoming these hurdles. Chapter 7.3 discusses the results of K_0 and representability to the Troll field. Chapter 7.4 discusses the OCR and its relationship with creep. Problematic aspects with creep measurements are also addressed here. Chapter 7.5 investigates identified discrepancies between the soil model and field data from Troll. Chapter 7.6 makes a short comparison with experimental data. Chapter 7.7 discusses the main results considering the SHARP project.

7.1 PLAXIS Automation with Python API

The ability to automate calculations with Python has given many computational benefits. Most importantly, the computations can be run in the background during the day or overnight. This has turned useful since the simulations with HVMCC took several hours to complete. In addition, it is easy to make a graphical user interface for the problem. On the other side, the return on scripting is greater the larger the project is. While it is still possible to use PLAXIS more efficiently with commands, the interface is still good for common engineering problems like slope analysis and retaining walls. Nevertheless, back-calculations with trial-and-error

The ability to automate calculations with Python has given many computational benefits. Most importantly, the computations can be run in the background during the day or overnight. This has turned useful since the simulations with HVMCC took several hours to complete. If this was done manually, then it would take days. In that case, the scope of the parameters would be reduced, possibly preventing further insight into any emerging trends or patterns in the data.

On the other side, scripting for the first time is time-consuming. It may add unnecessary amount of complexity to what could have been a simple project. However, it is the authors belief that the automation in total saved more time in terms of analysis and plotting. Back-calculations with trial-and-error methodology may benefit from the automation.

7.2 Convergence

One of the main challenges encountered was the ability to converge upon initializing of the first calculation of Unit IIIA. It is suspected that simulated surface swelling causes effective stresses to hit the dry side of the yield surface in the p':q-space. This would in turn give negative volumetric strains and subsequently move the iteration towards the mean stress in an impermissible state $p_0 < 0$ according to the Hyper Viscoplasticity theory. This results in a non-associated number in HVMCC kernel. The stiffness matrix cannot be completely generated, and the new state variables are not defined, forcing PLAXIS to abort the calculation due to assumed severe divergence.

The surface swelling effect is shown in the debug log, which specifies which stress point which gave NaN values in the stress vector. By varying OCR_0, stress points from 80 to 74,3 were specified in the log. The erroneous stress points turned shallower when approaching the OCR_0 limit.

The boundary value for divergence is dependent on the geometry of the yield surface controlled by the spacing ratio and frictional dissipation. Then the volumetric strains are exacerbated by layer geometry, time interval and creep number. The convergence is sensitive to time interval, creep number and frictional dissipation.

To prevent divergence, OCR_0 was conveniently increased in the phase construction the layer without affecting the final OCR. Given the high time interval, the calculations would converge into the correct OCR regardless of selected OCR_0. It is important to note that adjusting OCR_0 high may not give accurate strains. However, that is okay because the numerical work is solely focusing on the final stress states. Another kind of remedy was adding a small uniform surface load to increase stiffness in the top surface. This is like adding cohesion in Mohr Coulomb material to test global failure mechanisms.

The SSC does not diverge on similar settings, suggesting that PLAXIS has employed mechanisms to prevent divergent surface stress point. It is assumed that these mechanisms increase the robustness of the model on boundary value problems. However, these kinds of calculations are rarely encountered in real engineering problems.

It is important to note that the surface divergence phenomenon is not limited to HVMCC but observed in other projects related to the development of new constitutive models.

The computational power of HVMCC is considerably poorer compared to SSC. This means the increased flexibility comes at a greater computational cost.

7.3 Coefficient of lateral earth pressure (K_0)

In general, K_0 cannot exceed unity in oedometer loading conditions. Therefore, it is straightforward to assume that simulating K_0 in Unit IIIA to Troll (1 - 1.2) is impossible. With the Cam Clay framework, is it analytically demonstrated that loading $K_0 \leq 1$ seen in Figure 8. The results were taken in the cross-section at the centre of the numerical model. This practically sets up the response in oedometer conditions (Figure 25). Thus, the limitations in K_0 are applicable which coincides with the results (Figure 33).

It is rarely observed K_0>1 for soft clay in the geotechnical field since the rate of lateral relaxation compared to the vertical relaxation is significantly different due to the Poisson's ratio. In such cases, it is the K_0 during unloading.

The highly recorded K_0 begs the question on whether the recorded K_0 in Troll was due to anisotropy or under unloading process. It is possible that the unit had passive loading conditions from glacial thrusting. With subsequent sedimentation the lateral relaxation is restricted, keeping memory the of the lateral stresses.

Unit IIIA is however classified as sandy clay. From glacial till, it is composed of varying degrees of clay, sand, silt, gravel, and even larger aggregates. This classification comes from the variations on erosional material and finer material across the unit (Sejrup *et al.*, 1995).

The paper from (Grimstad *et al.*, 2021) suggests that K_0 increases most rapidly with OCR with $\gamma = 0$ by solving the flow potential (w) (a transformed force potential), evaluated in terms of oedometer conditions, i.e.: $\dot{\varepsilon}_v^p / \dot{\varepsilon}_v^p = 3/2$. The results agree with the simulated K_0, for $OCR = 6$ by extrapolating from the plot with $M = 1.135$ and $\gamma = 0$. However, the flow potential assumes $R = 2$ while the determined spacing ratio is 5. It is possible to solve the flow potential again with the modified spacing ratio and reproduce a plot for higher OCR to examine this effect further. However, this was not done considering the limited time of analysis. Regardless, the K_0 cannot exceed 1 in these conditions.

This suggests that either the recommended K_0 are wrong or that Unit IIIA has a history of anisotropy. Most likely observed K_0>1 comes from anisotropic conditions from passive consolidation by inclined sedimentation, inclined ice loads, mixed principal stress fields, rotation from land heave. Capturing these phenomena require more complex calculations and more research on lateral stresses from glacial advances.

The numerous recommended values may be based on several test data and known correlations from other soil parameters. possibly weighing in factors like sample disturbances. It is well established that there is an empirical relationship between K_0 and OCR. However, the correlation is limited in HVMCC (Grimstad *et al.*, 2021) in oedometer conditions.

7.4 Overconsolidation ratio (OCR)

The final OCR was easily adjustable by varying the creep index (μ) as seen in Figure 34. It might look unfair to match the OCR like this. However, based on (Jalali, 2022), best estimates of the glacial loads from the literature is insufficient in simulating the recorded vertical effective preconsolidation stresses. This led to the suspicion that the jump in OCR must have gotten a large contribution from creep. Given the enormous time span of the simulation, attributing OCR to creep must be evaluated carefully (Grimstad *et al.*, 2021). For example, Unit IIIA has since its sedimentation been creeping in-situ for about hundred thousand of years as noted in (Appendix 7). It begs to question whether it would be fair to simulate this layer with the laboratory measured creep now. This adds new perspective to the comments on the measured secondary compression index by (Lunne, Long and Uzielli, 2006), where the creep decreased by the depth until it turned negligible after Unit II. With offshore conditions, it is reasonable to assume that the creep time is linear with sedimentation depth. A proper way to investigate this is to perform long-term creep tests and compare it to in-situ measurements, which is also the main conclusion of (Grimstad *et al.*, 2021).

7.5 Discreprancy between field numerical results

Several inconsistencies were identified for the SSC parameters. For all units, the λ^*, κ^* were interpreted from (confidential) data sets from oedometer and triaxial tests for Troll (Jalali, 2022). The model parameters for SSC are found in Appendix 7. It was found that the rate sensitivity parameter $\alpha = (\lambda^* - \kappa^*)/\mu^*$ was set constant with $\alpha = 100$. (Lunne, Long and Uzielli, 2006) suggested that creep may occur in Unit I and Unit II, but negligible for lower units. However, these values were not used. Instead μ^* was determined solely on the set rate (α). The calculated creep indexes imply negligible creep in all units. One

exception is made for Unit IIIA, where the rate is changed to attribute the high OCR to creep with $\alpha = 9$. The set rate was likely set for SSC to model the crown of the yield surface. The Poisson's ratio (ν) was back calculated based on equation in Table 2 using reasonable assumptions for K_0^{NC}. Here, further inconsistencies are found. For example, the ratio was all around very high. For Unit IIIA, it was calculated to be 0.46, which implies undrained, isotropic conditions. The SSC for Unit IIIA, produces a K_0~0.8, which is in line with the estimation from oedometer normal consolidation $\nu_{ur}/(1-\nu_{ur}) = 0.82$.

In order to simulate high K_0 in oedometer conditions, the Poisson's ratio should be $\nu_{ur} \approx 0.2$ (Bentley, 2022). Understanding this, the back calculated ν_{ur} from Unit IIIA was therefore not used in the HVMCC. However, the interpreted λ^* and κ^* from (Jalali, 2022) was reproducible from the data sets and carried on to HVMCC.

7.6 Connection to experimental data

In the discussion of Soft Soil Creep model, it was suggested some estimations between the plasticity index (I_p) and of λ^*, κ^* and μ^*. For Unit IIIA, (Lunne, Long and Uzielli, 2006) suggested $I_p = (13-28)\,\%$. For Unit IIIA, (Lunne, Long and Uzielli, 2006) suggested $I_p = (13-28)\,\%$. The interpreted $\lambda = 0.02592$ corresponds to $I_P = 13\,\%$, which is at the lowest range. However, the next two estimates are not approachable.

7.7 SHARP

The importance of shear in glacial tills as the glacier advances, have been a contested subject among researchers (Gareau *et al.*, 2005). One-dimension consolidation have typically been thought to have the major impact on the stress state of the soil, but laboratory testing has brought forward the importance of shearing on the glacial front. Testing in a lateral stress oedometer found glacial tills samples to have anisotropic horizontal stress response when loaded vertically, with the directions of the anisotropy coinciding with glacial advance directions. This, expectedly, has a great impact on the K_0 values. While isotropic values of K_0 are the typical assumption, this may not hold in analyzing glacial tills, as the difference between minimum and maximum K_0 values have been found to be as much as 2.

Other contributions to the SHARP project indicate great scatter in OCR for Unit IIIA in other boreholes around Troll. This suggests that Unit IIIA is not uniformly distributed, likely related to geological processes like complex folding within the shallow subsurface sediments. The results are consequently more relevant for soil in the Norwegian Channel based on the seismicity of the area. In any regard, there are still uncertainties in these depths related to sample disturbances due to the challenging offshore environments.

7.8 Summary

Automated simulations with Python has provided many computational benefits and is worth developing further for more complex engineering problems. Numerical problems due to erratic surface behaviour for normal consolidation condition are remedied by increasing OCR_0. This phenomenon is not uncommon for user-defined soil models. The K_0

cannot be higher than unity in normal consolidated oedometer conditions for clay. However, it is possible to observe this during unloading or after passive loading. The increase in μ in Unit IIIA was necessary since the estimated glacial loads were insufficient in simulating OCR. However, (Lunne, Long and Uzielli, 2006) suggests that layers lower than Unit II has negligible creep. This begs the question whether it is fair to assume this in the simulation when the material measured has already creeped for tens of thousands of years. The compression parameters in SSC is reproducible from the confidential data set and ν is corrected in HVMCC. Adds new perspective on Unit IIIA SHARP project.

8 Discussion - Experimental

To which degree do then the assessed K_0 values attained from oedotriaxial testing reflect the stress state of Troll? Upon an immediate comparison between the recommended K_0 profile from Troll as shown in Figure 3 and the assessed K_0 values shown in chapter 6.3, it is clear that the assessed K_0 values from the oedotriaxial testing do not directly capture the Troll stress state.

As explained in chapter 2.1, the K_0 is interlinked with the stress history of the soil, hereunder the OCR. As the Onsøy soil has not been subjected to the same geological processes as having undergone at Troll, a direct comparison of the K_0 between the two may then be a cumbersome task. Upon loading, the values of OCR are quickly go towards 1, as the soil is always loaded to values higher than its previous preconsolidation stress. Keeping chapter 2.1 in mind, one could expect the laboratory assessed loading K_0 values to shoot lower than the K_0 values of Troll, as the OCR at Troll is consistently higher than 1. With these precautions, some basis of comparison reveals itself.

The OCR throughout the oedotriaxial testing can practically be of value 1. A point of interest is then that the assessed K_0 values for Onsøy and Troll loading for tests 2703 and 0505 is in the realm of what can be expected according to equation 2.3 in chapter 2.1 for OCR =1. This is shown in Table 17.

Table 17: Comparison between assessed K_0 and theoretical K_0

	Laboratory assessed K_0 OCR = 1		**Equation 2.3 L'Heureux *et al.* (2017)**
Test number	2703	0505	OCR = 1
Sample quality	Good	Good	K_0 = 0.53
Onsøy loading	0.49	0.48	
Troll loading	0.52	0.53	

Having found that the assessed Onsøy and Troll loading K_0 values largely follow what can be expected from the empirical equation by L'Heureux *et al.* (2017), a possible link between the Onsøy and Troll material reveals itself. The recommended K_0 profile from Troll is mainly derived from a relationship between K_0, OCR and I_P developed by E.W. Brooker and H.O. Ireland (Lunne, Long and Uzielli, 2006). As explained in chapter 2.1, the relationship between K_0 and OCR developed by L'Heureux *et al.* (2017) takes greater care to reflect Norwegian soils, and finds the I_P negligible. Using this approach along with the OCR profile from Troll yields a K_0 profile which is similar to the recommended Troll K_0 profile. One could then raise the question whether assessed K_0 values from oedotriaxial testing with higher OCR would approach values given by equation 2.3, and thereby approach the recommended K_0 profile at Troll. If such an association could be found, one might be closer to a definite answer to whether oedotriaxial testing of Onsøy clay can approach the stress state at Troll.

The assessed K_0 values of the maximum loading stages are markedly increased in comparison to the Onsøy and Troll loading stages. A possible venue of exploration to explain this is creep. As outlined in chapter 2.3, K_0 may rise with creep, although this assumption is disputed. Using equation 2.7 and values recommended by Mesri and Castro (1987), one might examine whether the assessed rise in K_0 follows what might be expected due to creep. A ratio of secondary compression index to compression index of $\frac{C_\alpha}{C_c} = 0.04 \pm 0.01$ reportedly holds for most inorganic soft clays. Mesri and Castro (1987) used a ratio of recompression index to compression index of $\frac{C_r}{C_c} = 0.05$, and is also used here. As no oedometer tests were performed, possible values for time t and time of primary consolidation t_p was chosen for the sake of the examination. The same goes for the friction angle φ'. A summation of the values used and the resulting K_0 due to creep is shown in Table 18. Although it may have been a contributing factor, creep can then not be said to the main cause of the increase in loading K_0 in the maximal loading stages.

Table 18: A possible rise in K_0 due to creep

$[K_0]_{primary}$	$t\ [hrs]$	$t_p[hrs]$	C_α/C_c	C_r/C_c	$\varphi'[°]$	$[K_0]_{creep}$
0.53	24	300	0.5	0.5	30	0.57

The heightened K_0 values of the maximum loading stages may also be due to the consecutive loading of the soil. As stated in chapter 2.1, the soil has a capacity of retaining horizontal stresses. Coupled with the assumption that the Onsøy soil has not been subjected to a significant loading event after its deposition (Gundersen *et al.*, 2019), this opens the possibility of the consecutive loading and some retention of horizontal stresses being a cause of the recorded phenomenon.

As a delivery to work package 3.1 of the SHARP project, the findings of the oedotriaxial testing on Onsøy clay shows some promise. During the work on this thesis, the authors encountered students that had gained access to Troll core samples, which may bring to question the need for testing on analogous materials such as Onsøy clay. Still, the availability of clay from the NGTS Onsøy site clay may be a good argument for further development of the usefulness of this material for approaching Troll stress states.

As for the reliability of the findings, the time of storage was a subject of discussion before undergoing the laboratory testing, as the sampling was undertaken roughly 4 years before the time of testing. As shown in chapter 6.2, the recorded Atterberg limits, and the water content, shows good compliance with the Onsøy soil characterization by Gundersen *et al.* (2019). This is a good indication that the storage time did not have a notable impact on the findings of this thesis. The assessed sample qualities, shown in Table 11, ranges from very poor to good, according to the classification of Lacasse and Berre (1988). The results from samples where the quality was poor must be read with a skeptical eye.

9 Conclusion and further work

9.1 Numerical

- The recommended parameters simulating K_0 and OCR in Unit IIIA (74- 110 m) is a spacing ratio of 5 with associated flow rule ($\gamma = 0$) with creep index of 0.0009.

- It is impossible to simulate a loading $K_0 \geq 1$ in oedometer conditions for clay within the family of Cam Clay

- The Hyper-viscoplastic Modified Cam Clay model demonstrated the potential to simulate different pairs of K_0 and OCR better than the Soft Soil Creep model. It also addresses thermodynamical issues with unloading-reloading processes from the Cam Clay family.

- It is plausible to observe $K_0 > 0$ only if Unit IIIA has been subjected to passive loading or undergoing unloading conditions. Evidence of glacial thrusts and land uplifts support this theory.

- Automation with Python combined with a graphical input interface provided greater computational capacity and user-friendliness.

It is recommended to investigate the geomechanical implications of materials with high spacing ratio with associative flow rule. Reconstituting materials with this behavior could be useful to learn more about these types of material.

As previously recommended by (Jalali, 2022), more high-quality tests are needed in order increase the models' accuracy. Long-term creep tests are particularly useful.As previously recommended by (Jalali, 2022), more high-quality tests are needed in order increase the models' accuracy. Long-term creep tests are particularly useful.

9.2 Experimental

- Atterberg limits and water content does not indicate adverse effects due to time in storage for the 72 mm Onsøy soil samples.

- Whether Onsøy clay can capture stress states found at Troll remains inconclusive. An updated laboratory plan may better capture the importance of OCR on K_0.

- The K_0 values assessed from oedotriaxial testing largely confirms the value found by the empirical approach by (L'Heureux *et al.*, 2017) for the Onsøy and Troll loading stages with an OCR of 1.

- In terms of keeping a low pore pressure response, a loading rate of 0.15-0.20 $^{\mathrm{kPa}}/_{\mathrm{min}}$ yielded successful oedotriaxial tests for Onsøy clay, given that the pervious drainage paper is correctly mounted along the circumference of the sample.

Results from the experimental testing shows no sign of adverse effects stemming from time in storage for the NGTS Onsøy clay for the use of oedotriaxial testing. This indicates that NGTS Onsøy clay sampled at a similar date, and stored similarly, may be used in further testing. Coupled with the findings that the evaluated K_0 values for loading correspond well with empirical values by L'Heureux *et al.* (2017), this makes oedotriaxial testing on Onsøy clay an option for further approaching Troll stress states in relation to the SHARP project.

Throughout the oedotriaxial testing conducted in relation to this thesis, a loading rate of 0.15-0.20 kPa has been found to yield favorable pore pressure responses and thereby successful stages throughout the tests. It is vital the pervious drainage paper is dressed well around the sample, being in contact with the top and bottom porous discs. This may be a contribution towards further oedotriaxial testing on NGTS Onsøy clay.

A possibility of further work, if the oedotriaxial laboratory side of this thesis is to be investigated further, is to attempt to design a laboratory testing plan which better accounts for OCR throughout the test stages. A clear possibility in this realm is to load heavier, and then let the samples reload even further, so that the samples spend a greater time of loading in an overconsolidated state. If a standard triaxial setup is to be used in the furthering of the work, Appendix 6 sums up the central learnings attained to conduct successful oedotriaxial laboratory tests. An oedotriaxial test laboratory guide is found in Appendix 5. This may be a useful for any undertaking of oedotriaxial testing in the future. A possible method of assessing whether a sample has undergone lateral strain, is to perform parallel oedometer tests, and evaluate moduli M. If moduli M evaluated from oedotriaxial test are similar to those evaluated from oedometer testing, it would possibly be an indication that the samples did not experience lateral strain in the oedotriaxial testing.

The oedotriaxial method in a standard triaxial rig may itself pose as a limitation in trying to approach the stress states of deeper soil layers of Troll. As shown in Figure 5, the preconsolidation stresses below Unit II ranges roughly from 2500 kPa to 5000 kPa. Holding this against the fact that capacity of the cell pressure pumps in the setup used for this thesis was 2000 kPa, and the capacity of 3500 kPa for the Perspex cell, a standard triaxial setup would struggle with reach in situ Troll stress states at deeper levels than unit 2.

References

Bellwald, B. *et al.* (2020) Meltwater sediment transport as the dominating process in mid-latitude trough mouth fan formation, *Nature Communications*, 11(1), pp. 4645. doi: 10.1038/s41467-020-18337-4.

Bentley (2022) *Material Models Manual*. Available at: https://communities.bentley.com/cfs-file/__key/communityserver-wikis-components-files/00-00-00-05-58/5315.2D_2D00_3_2D00_Material_2D00_Models.pdf (Accessed: June 12 2022).

Brooker, E. W. and Ireland, H. O. (1965) Earth Pressures at Rest Related to Stress History, *Canadian Geotechnical journal*, 2(1), pp. 1-15. doi: 10.1139/t65-001.

By, T. and Skomedal, E. (1993) *Soil parameters for foundation design, Troll platform*. (NGI Publication). Oslo: Norwegian Geotechnical Institute.

Chen, Y. N. and Yang, Z. X. (2017) A family of improved yield surfaces and their application in modeling of isotropically over-consolidated clays, *Computers and Geotechnics*, 90, pp. 133-143. doi: https://doi.org/10.1016/j.compgeo.2017.06.007.

Dadras-Ajirloo, D., Grimstad, G. and Amiri, S. A. G. (2022) On the isotache viscous modelling of clay behaviour using the hyperplasticity approach, *Géotechnique*, 0(0), pp. 1-13. doi: 10.1680/jgeot.21.00245.

Dadrasajirlou, D. (2022) *Hyper-Viscoplastic Modelling of Clay Behaviour*. Doctoral, Norwegian University of Science and Technology.

Gareau, L. *et al.* (2005) Anisotropic geomechanical parameters as a result of glacial shearing, *International Conference on Soil Mechanics and Geotechnical Engineering*, *Osaka, Japan*. IOS Press BV, pp. 365-368.

GDS Instruments (n.d.) GDS Triaxial Compression/Extension Cells. Available at: https://www.gdsinstruments.com/__assets__/Products/00109/Triaxial_cell_datasheet.pdf.

Grimstad, G., Dadrasajirlou, D. and Ghoreishian Amiri, S. A. (2020) Modelling creep in clay using the framework of hyper-viscoplasticity. doi: https://doi.org/10.1680/jgele.20.00004.

Grimstad, G. *et al.* (2021) Investigation of Development of the Earth Pressure Coefficient at Rest in Clay During Creep in the Framework of Hyper-Viscoplasticity, *International Journal of Geomechanics*, 21(1), pp. 04020235. doi: doi:10.1061/(ASCE)GM.1943-5622.0001883.

Gundersen, A. S. *et al.* (2019) Characterization and engineering properties of the NGTS Onsøy soft clay site, *AIMS Geosciences*, 5(3), pp. 665-703. doi: 10.3934/geosci.2019.3.665.

Hayashi, H. *et al.* (2012) Coefficient of earth pressure at rest for normally and overconsolidated peat ground in Hokkaido area, *Soils and Foundations*, 52(2), pp. 299-311. doi: https://doi.org/10.1016/j.sandf.2012.02.007.

Head, K. H. and Epps, R. (2011) *Manual of Soil Laboratory Testing Volume 2: Permeability, Shear Strength and Compressibility tests*. Caithness, Scotland: Whittles Publishing.

Head, K. H. and Epps, R. J. (2014) *Manual of Soil Laboratory Testing Volume 3: Effective Stress Tests*. Caithness, Scotland: Whittles Publishing.

Houlsby, G. T., Amorosi, A. and Rojas, E. (2005) Elastic moduli of soils dependent on pressure: A hyperelastic formulation, *Géotechnique*, 55(5), pp. 383-392. doi: 10.1680/geot.2005.55.5.383.

Houlsby, G. T. and Puzrin, A. M. (2006) *Principles of hyperplasticity : an approach to plasticity theory based on thermodynamic principles*. Springer.

Jaky, J. (1944) *The Coefficient of Earth Pressure at Rest*. Unpublished paper presented at Journal Society of Hungarian Architects and Engineers. Budapest.

Jalali, R. (2022) *Consolidation and stress history in shallow sediments in the northern North Sea*. Master's thesis, Norwegian University of Science and Technology.

Jean-Sebastien, L. H. and Kim, Y. (2013) *Effect of storage time on sample quality*. (NIFS - N.6.4.3 - Effect of storage time on sample quality): NGI.

Karstunen, M. and Amavasai, A. (2017) *BEST SOIL: Soft soil modelling and parameter determination*. (Big Project A2015-06): Chalmers University of Technology.

Knappett, J. and Craig, R. F. (2019) *Craig's Soil Mechanics*. CRC Press.

L'Heureux, J.-S. *et al.* (2017) *A revised look at the coefficient of earth pressure at rest for Norwegian Clays*. Unpublished paper presented at Geoteknikkdagen. Oslo.

L'Heureux, J.-S. (no date) *NGTS - Nasjonale Geoforsøksfelt*. Available at: https://www.ngi.no/prosjekter/ngts/ (Accessed: May 15 2023).

Lacasse, S. and Berre, T. (1988) *Triaxial Testing methods for Soils*. Unpublished paper presented at Advanced Triaxial Testing of Soil and Rock. Louisville.

Larsen, T. B. (2023) *Work Package 5 : Risk quantification*. Available at: https://sharp-storage-act.eu/work-packages/wp-5/.

Lunne, T., Long, M. and Uzielli, M. (2006) Characterisation and engineering properties of Troll Clay, *International Workshop on Characterisation and Engineering Properties of Natural Soils*, *Singapore*.

Mackinnon, P. *et al.* (2010) Effectiveness of filters in reducing consolidation time in routine laboratory testing, *Géotechnique*, 60, pp. 949-956. doi: 10.1680/geot.9.T.013.

Mesri, G. and Castro, A. (1987) Ca/Cc Concept and K0 During Secondary Compression, *Journal of Geotechnical Engineering*, 113(3), pp. 230-247. doi: doi:10.1061/(ASCE)0733-9410(1987)113:3(230).

Meyer, Z. and Olszewska, M. (2021) Methods Development for the Constrained Elastic Modulus Investigation of Organic Material in Natural Soil Conditions, *Materials*, 14(22), pp. 6842. Available at: https://www.mdpi.com/1996-1944/14/22/6842.

NGI (2023) *SHARP Storage Objectives*. Available at: https://sharp-storage-act.eu/objectives/.

Nilmar, J. (1969) *The resistance concept applied to deformations of soils*. Mexico City.

Nordal, S. (2020) *TBA4116 Geotechnical Engineering Advanced Course Lecture Notes*. Norwegian University of Science and Technology - Geotechnical Engineering Group.

Olsen, L. *et al.* (2013) Quaternary glaciations and their variations in Norway and on the Norwegian continental shelf, *Geological Survey of Norway Special Publication*, 13, pp. 27-78.

Piriyakul, K. and Haegeman, W. (2005) Automated K0 consolidation in stress path cell, *International Conference on Soil Mechanics and Geotechnical Engineering*, *Osaka, Japan*. IOS Press.

Sejrup, H. P. *et al.* (1995) *Quaternary of the Norwegian Channel: glaciation history and palaeoceanography*. (Norwegian Journal of Geology). Oslo: Norwegian Geological Society.

SINTEF (no date) *CCS*. Available at: https://www.sintef.no/en/sintef-research-areas/ccs/ (Accessed: 24.01.2023 2023).

Sivakumar, V. *et al.* (2002) Relationship between K0 and overconsolidation ratio: A theoretical approach, *Géotechnique*, 52(3), pp. 225-230. doi: 10.1680/geot.52.3.225.41017.

Standard Norge (2014) Laboratory testing of soil Part 1: Determination of water content *NS-EN ISO 17892-1:2014*.

Standard Norge (2018) Geotechnical investigation and testing *Part 12: Determination of liquid and plastic limits*: Standard Norge.

Statens Vegvesen (2014) Håndbok R210 Laboratorieundersøkelser *Geoteknikk* (pp. 112-176): Vegdirektoratet.

Statens Vegvesen (2022) Håndbok V220 Geoteknikk i vegbygging *Kapittel 2 Laboratorieundersøkelser*. Oslo, Norway: Vegdirektoratet.

Suklje, L. (1957) *The Analysis of the Consolidation Process by the Isotaches Method*. Unpublished paper presented at International Conference on Soil Mechanics and Foundation Engineering. London.

UiB (2023) *Geological processes and sediment properties of the Sørlige Nordsjø II offshore wind area, interpreted from TOPAS and vibrocore data*. Available at: https://www.uib.no/geo/157867/geological-processes-and-sediment-properties-s%C3%B8rlige-nordsj%C3%B8-ii-offshore-wind-area.

Wang, J. *et al.* (2019) Anisotropic and Noncoaxial Behavior of K0-Consolidated Soft Clays under Stress Paths with Principal Stress Rotation, *Journal of Geotechnical and Geoenvironmental Engineering*, 145(9), pp. 04019036. doi: doi:10.1061/(ASCE)GT.1943-5606.0002103.

Wood, D. M. (2007) *Soil Behavior and Critical State Soil Mechanics*. Cambridge University Press.

Yeo, S.-S., Shackelford, C. and Evans, J. (2005) Consolidation and Hydraulic Conductivity of Nine Model Soil-Bentonite Backfills, *Journal of Geotechnical and Geoenvironmental Engineering*, 131. doi: 10.1061/(ASCE)1090-0241(2005)131:10(1189).

Aas, G. and Lacasse, S. (2022) K0 as Function of Changes in Stress and Strain Conditions during Consolidation, Unloading and Reloading, i Institute, N. G. (ed.) *Publication* (vol. 209). Oslo: Norwegian Geotechnical Institute.

Appendices

Appendix 1: Atterberg limit test results.

Appendix 2: K_0 assessments.

Appendix 3: Calibration of the 50 kN load cell.

Appendix 4: NGTS Onsøy boring plan.

Appendix 5: Oedotriaxial testing guide.

Appendix 6: Oedotriaxial testing experience note.

Appendix 7: PLAXIS Model Information.

Appendix 8: PLAXIS Cross-section data – OCR and K_0.

Appendix 9: PLAXIS Numerical Results.

A: Varying OCR_0 with constant K_0^{NC}, μ.
B: Further inspection of A.
C: Varying K_0^{NC} with constant OCR_0, μ.
D: Varying μ and OCR_0 with constant K_0^{NC}.
E: Debug log 1 of failed calculation.
F: Debug log 2 of failed calculation.
G: Debug log of successful calculation.

Appendix 1: Atterberg limit test results

ATTERBERG LIMITS - 1703 (1)

Crib and sample	930.1	g
Crib	545.8	g
Sample	384.3	g
	0.3843	kg
Weight of sample	0.00376998	kN
Sample volume	0.00022902	m3
Unit weight	16.4613702	kN/m3

Water content			
Container and moist	153.3	g	m1
Container and dry	145.1	g	m2
Container	133.2	g	mc
Weight of water	8.2	g	mw
Weight of dry sample	11.9	g	md
Water content w	68.91	%	

Plastic limit

Portion A (3 sub-portions)			
Container + moist	28.8	g	m1
Container + dry	27.3	g	m2
Container	22.1	g	mc
Water	1.5	g	mw
Dried specimen	5.2	g	md
Plastic limit A	28.85	%	wp A
Portion B (3 sub-portions)			
Container + moist	31.3	g	m1
Container + dry	30	g	m2
Container	26.1	g	mc
Water	1.3	g	mw
Dried specimen	3.9	g	md
Plastic limit B	33.33	%	wp B
Plastic limit	**31.09**	**%**	**wp**

Liquid limit

Point A			
Container + moist	145.6	g	m1
Container + dry	137.6	g	m2
Container	126.8	g	mc
Water	8	g	mw
Dried specimen	10.8	g	md
Water content A	74.07	%	w A
Point B			
Container + moist	84.2	g	m1
Container + dry	75.7	g	m2
Container	64.6	g	mc
Water	8.5	g	mw
Dried specimen	11.1	g	md
Water content B	76.58	%	w B
Point C			
Container + moist	91.6	g	m1
Container + dry	80.5	g	m2
Container	66.7	g	mc
Water	11.1	g	mw
Dried specimen	13.8	g	md
Water content C	80.43	%	w C
Point D			
Container + moist	88.8	g	m1
Container + dry	77.2	g	m2
Container	63.6	g	mc
Water	11.6	g	mw
Dried specimen	13.6	g	md
Water content D	85.29	%	w D

Point	Cone penetration [mm]	Water content [%]	Read liquid limit [%]
A	7.5	74.07	79
B	9.1	76.58	
C	11.2	80.43	
D	13.5	85.29	

SAMPLE QUALITY

Berre, 1988 (Volumetric strain in the consolidation phase)

OCR	Depth [m]	εvol [%]	Quality
1.71	6.44	8.059	Very poor

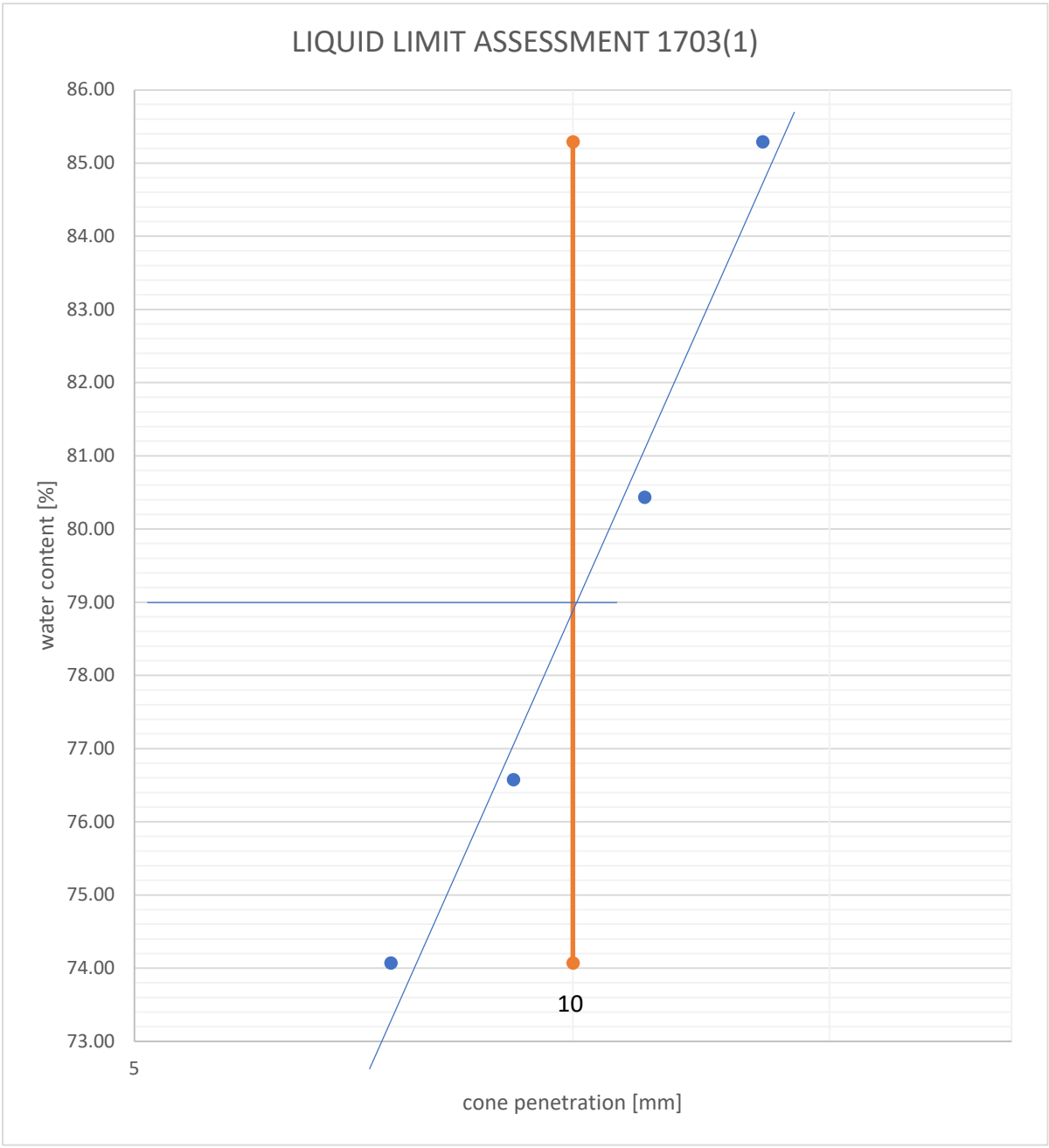
LIQUID LIMIT ASSESSMENT 1703(1)
86.00
85.00
84.00
83.00
82.00
81.00
80.00
79.00
78.00
77.00
76.00
75.00
74.00
73.00
water content [%]
10
5
cone penetration [mm]

ATTERBERG LIMITS - 1703(2)

Water content			
Container and moist	142.3	g	m1
Container and dry	138.7	g	m2
Container	129.3	g	mc
Weight of water	3.6	g	mw
Weight of dry sample	9.4	g	md
Water content w	38.30	%	

Plastic limit

Portion A (3 sub-portions)			
Container + moist	39.3	g	m1
Container + dry	37.1	g	m2
Container (6)	29.4	g	mc
Water	2.2	g	mw
Dried specimen	7.7	g	md
Plastic limit A	28.57	%	wp A
Portion B (3 sub-portions)			
Container + moist	34.8	g	m1
Container + dry	33.3	g	m2
Container (3)	27.7	g	mc
Water	1.5	g	mw
Dried specimen	5.6	g	md
Plastic limit B	26.79	%	wp B
Plastic limit	**27.68**	**%**	**wp**

Liquid limit

Point A			
Container + moist	46.4	g	m1
Container + dry	42.4	g	m2
Container	36	g	mc
Water	4	g	mw
Dried specimen	6.4	g	md
Water content A	62.50	%	w A
Point B			
Container + moist	52	g	m1
Container + dry	49.6	g	m2
Container	45.8	g	mc
Water	2.4	g	mw
Dried specimen	3.8	g	md
Water content B	63.16	%	w B
Point C			
Container + moist	68.3	g	m1
Container + dry	60.8	g	m2
Container	49.9	g	mc
Water	7.5	g	mw
Dried specimen	10.9	g	md
Water content C	68.81	%	w C
Point D			
Container + moist	61.8	g	m1
Container + dry	56.4	g	m2
Container	48.9	g	mc
Water	5.4	g	mw
Dried specimen	7.5	g	md
Water content D	72.00	%	w D

Point	Cone penetration [mm]	Water content [%]	Read liquid limit [%]
A	7.5	62.50	66.8
B	9.1	63.16	
C	11.2	68.81	
D	13.5	72.00	

SAMPLE QUALITY

Berre, 1988 (Volumetric strain in the consolidation phase)

OCR	Depth [m]	εvol [%]	Quality
1.71	6.44	8.059	Very poor

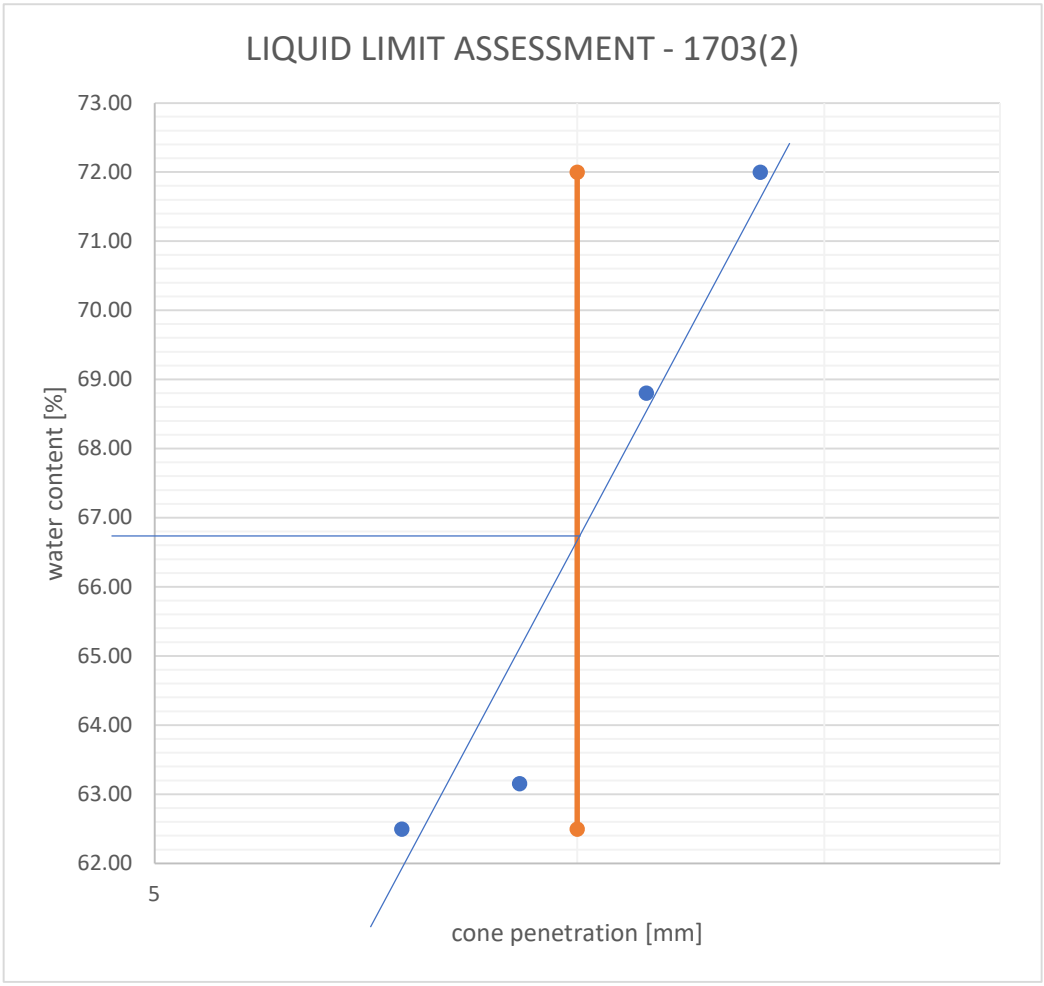
LIQUID LIMIT ASSESSMENT - 1703(2)
73.00
72.00
71.00
70.00
69.00
68.00
67.00
66.00
65.00
64.00
63.00
62.00
water content [%]
5
cone penetration [mm]

ATTERBERG LIMITS - 2703

UNIT WEIGHT

Crib and trimmed sample	937	g
Crib	545.8	g
Trimmed sample	391.2	g
	0.3912	kg
Tyngde av prøve	0.00383767	kN
Trimmed sample	0.00022902	m3
Unit weight	**16.76**	**kN/m3**

WATER CONTENT

Container + moist	150.9	g	m1
Container + dry	142.4	g	m2
Container	129.4	g	mc
Water	8.5	g	mw
Dried specimen	13	g	md
Water content	**65.38**	**%**	**w**

Plastic limit

Portion A (3 sub-portions)			
Container + moist	28.7	g	m1
Container + dry	27.4	g	m2
Container	22.5	g	mc
Water	1.3	g	mw
Dried specimen	4.9	g	md
Plastic limit A	26.53	%	wp A
Portion B (3 sub-portions)			
Container + moist	33.1	g	m1
Container + dry	31.7	g	m2
Container	27.1	g	mc
Water	1.4	g	mw
Dried specimen	4.6	g	md
Plastic limit B	30.43	%	wp B
Plastic limit	**28.48**	**%**	**wp**

Liquid limit

Point A			
Container + moist	47.2	g	m1
Container + dry	42.6	g	m2
Container	36	g	mc
Water	4.6	g	mw
Dried specimen	6.6	g	md
Water content A	69.70	%	w A
Point B			
Container + moist	66.3	g	m1
Container + dry	59.1	g	m2
Container	48.9	g	mc
Water	7.2	g	mw
Dried specimen	10.2	g	md
Water content B	70.59	%	w B
Point C			
Container + moist	64.9	g	m1
Container + dry	58.6	g	m2
Container	49.9	g	mc
Water	6.3	g	mw
Dried specimen	8.7	g	md
Water content C	72.41	%	w C
Point D			
Container + moist	65.8	g	m1
Container + dry	56.9	g	m2
Container	45.8	g	mc
Water	8.9	g	mw
Dried specimen	11.1	g	md
Water content D	80.18	%	w D

Point	Cone penetration [mm]	Water content [%]	Read liquid limit [%]
A	9	69.70	70.1
B	9.6	70.59	
C	11.7	72.41	
D	14.2	80.18	

SAMPLE QUALITY

Berre, 1988 (Volumetric strain in the consolidation phase)

OCR	Depth [m]	εvol [%]	Quality
1.66	7.93	1.775	Good

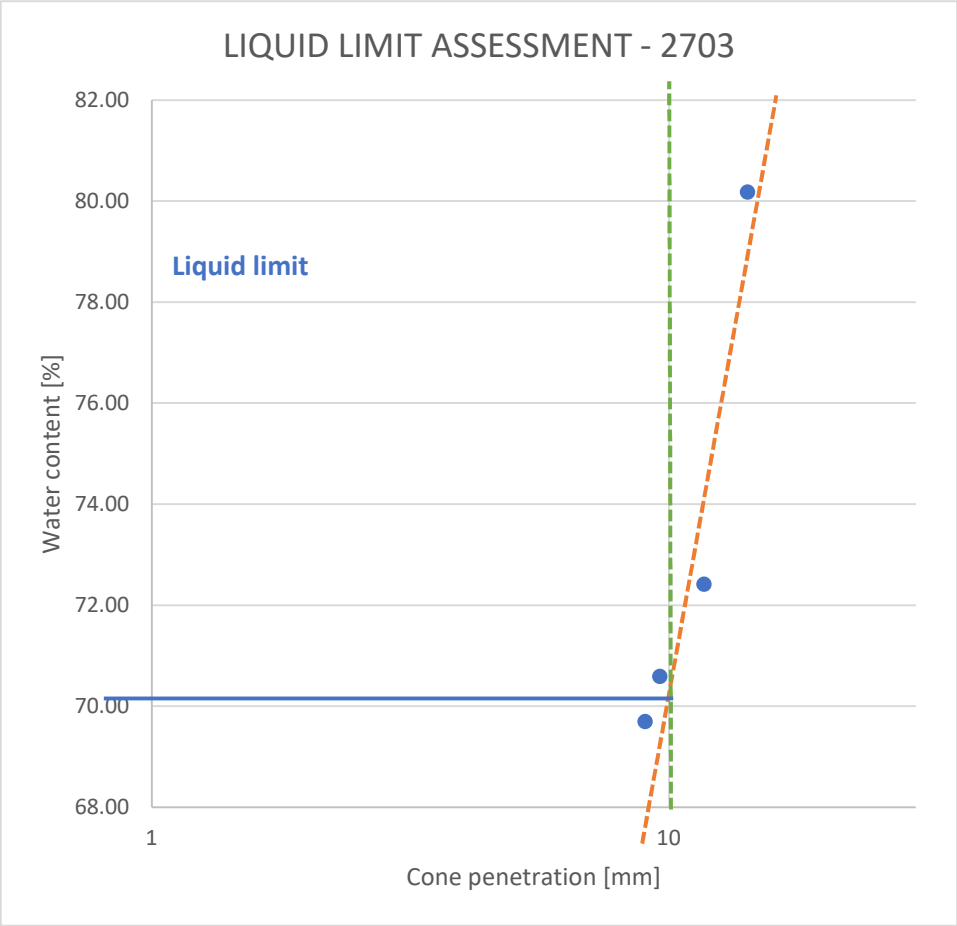
LIQUID LIMIT ASSESSMENT - 2703
82.00
80.00
78.00
76.00
74.00
72.00
70.00
68.00
Water content [%]
Liquid limit
1
10
Cone penetration [mm]

ATTERBERG LIMITS - 1904 (1)

UNIT WEIGHT

Crib and trimmed sample	929	g
Crib	545.8	g
Trimmed sample	383.2	g
	0.3832	kg
Tyngde av prøve	0.00375919	kN
Trimmed sample	0.00022902	m3
Unit weight	**16.41**	**kN/m3**

WATER CONTENT

Container + moist	149.9	g	m1
Container + dry	143.9	g	m2
Container	135.1	g	mc
Water	6	g	mw
Dried specimen	8.8	g	md
Water content	**68.18**	**%**	**w**

Plastic limit

Portion A (3 sub-portions)			
Container + moist	34.9	g	m1
Container + dry	33.4	g	m2
Container (3) m lokk	27.7	g	mc
Water	1.5	g	mw
Dried specimen	5.7	g	md
Plastic limit A	26.32	%	wp A
Portion B (3 sub-portions)			
Container + moist	35.6	g	m1
Container + dry	34.3	g	m2
Container (6) m lokk	29.3	g	mc
Water	1.3	g	mw
Dried specimen	5	g	md
Plastic limit B	26.00	%	wp B
Plastic limit	**26.16**	**%**	**wp**

Liquid limit

Point A			
Container + moist	32.2	g	m1
Container + dry	29.2	g	m2
Container	24.7	g	mc
Water	3	g	mw
Dried specimen	4.5	g	md
Water content A	66.67	%	w A
Point B			
Container + moist	40.6	g	m1
Container + dry	33.1	g	m2
Container	22.5	g	mc
Water	7.5	g	mw
Dried specimen	10.6	g	md
Water content B	70.75	%	w B
Point C			
Container + moist	41.9	g	m1
Container + dry	33.9	g	m2
Container	23	g	mc
Water	8	g	mw
Dried specimen	10.9	g	md
Water content C	73.39	%	w C
Point D			
Container + moist	44.9	g	m1
Container + dry	35.3	g	m2
Container	22.8	g	mc
Water	9.6	g	mw
Dried specimen	12.5	g	md
Water content D	76.80	%	w D

Point	Cone penetration [mm]	Water content [%]	Read liquid limit [%]
A	8.9	66.67	69.8
B	9.9	70.75	
C	12	73.39	
D	13.9	76.80	

SAMPLE QUALITY

Berre, 1988 (Volumetric strain in the consolidation phase)

OCR	Depth [m]	εvol [%]	Quality
1.65	7.7	4.095	Fair/Poor

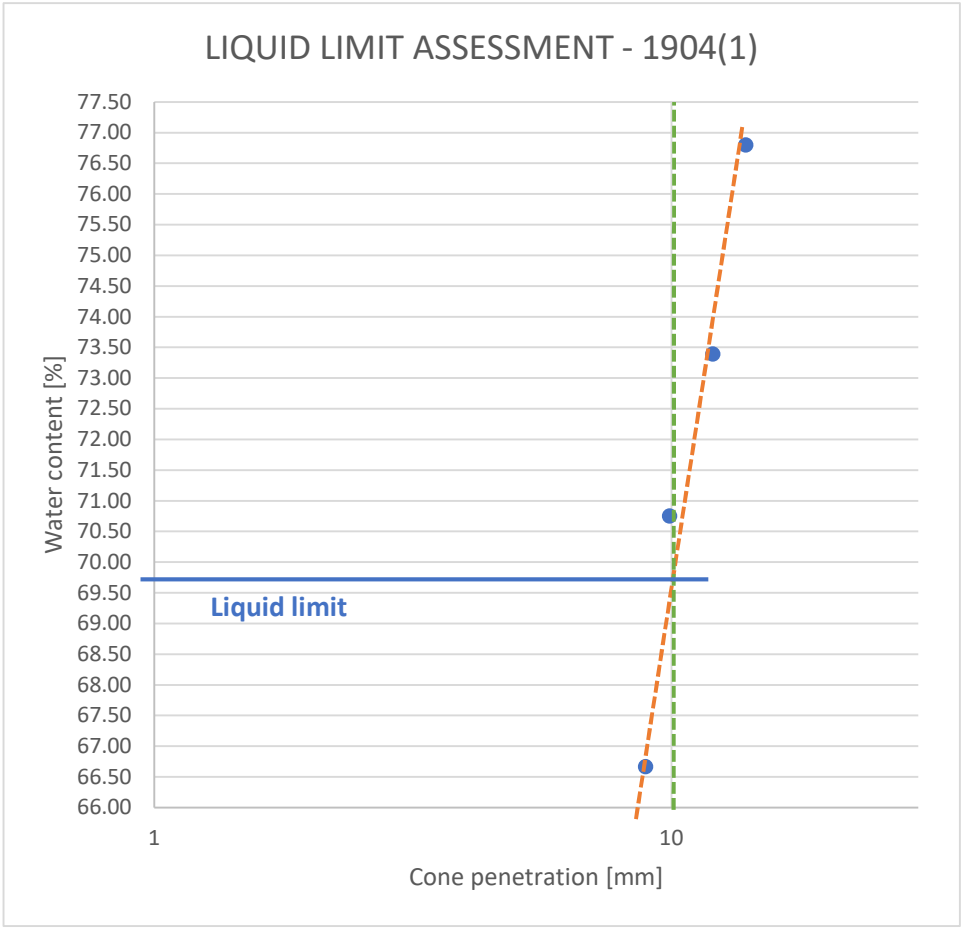
LIQUID LIMIT ASSESSMENT - 1904(1)
77.50
77.00
76.50
76.00
75.50
75.00
74.50
74.00
73.50
73.00
72.50
72.00
71.50
71.00
70.50
70.00
69.50
69.00
68.50
68.00
67.50
67.00
66.50
66.00
Water content [%]
Liquid limit
1
10
Cone penetration [mm]

ATTERBERG LIMITS - 1904 (2)

UNIT WEIGHT

Trimmed sample		310.37	g
		0.31037	kg
Tyngde av prøve		0.00304473	kN
Trimmed sample	*updated height*	0.00016374	m3
Unit weight		**18.60**	**kN/m3**

WATER CONTENT

Container + moist	86.22	g	m1
Container + dry	80.82	g	m2
Container	66.68	g	mc
Water	5.4	g	mw
Dried specimen	14.14	g	md
Water content	**38.19**	**%**	**w**

Plastic limit

Portion A (3 sub-portions)			
Container + moist	35.19	g	m1
Container + dry	33.55	g	m2
Container (3) m lokk	27.68	g	mc
Water	1.64	g	mw
Dried specimen	5.87	g	md
Plastic limit A	27.94	%	wp A
Portion B (3 sub-portions)			
Container + moist	36.25	g	m1
Container + dry	34.79	g	m2
Container (6) m lokk	29.39	g	mc
Water	1.46	g	mw
Dried specimen	5.4	g	md
Plastic limit B	27.04	%	wp B
Plastic limit	**27.49**	**%**	**wp**

Liquid limit

Point A			
Container + moist	57.37	g	m1
Container + dry	54.15	g	m2
Container	48.95	g	mc
Water	3.22	g	mw
Dried specimen	5.2	g	md
Water content A	61.92	%	w A
Point B			
Container + moist	49.38	g	m1
Container + dry	44.16	g	m2
Container	36.1	g	mc
Water	5.22	g	mw
Dried specimen	8.06	g	md
Water content B	64.76	%	w B
Point C			
Container + moist	58.72	g	m1
Container + dry	55.19	g	m2
Container	49.93	g	mc
Water	3.53	g	mw
Dried specimen	5.26	g	md
Water content C	67.11	%	w C
Point D			
Container + moist	58.94	g	m1
Container + dry	53.57	g	m2
Container	45.78	g	mc
Water	5.37	g	mw
Dried specimen	7.79	g	md
Water content D	68.93	%	w D

Point	Cone penetration [mm]	Water content [%]	Read liquid limit [%]
A	7.5	61.92	64.7
B	10.5	64.76	
C	11.9	67.11	
D	13.9	68.93	

SAMPLE QUALITY

Berre, 1988 (Volumetric strain in the consolidation phase)

OCR	Depth [m]	εvol [%]	Quality
1.65	7.7	4.095	Fair/Poor

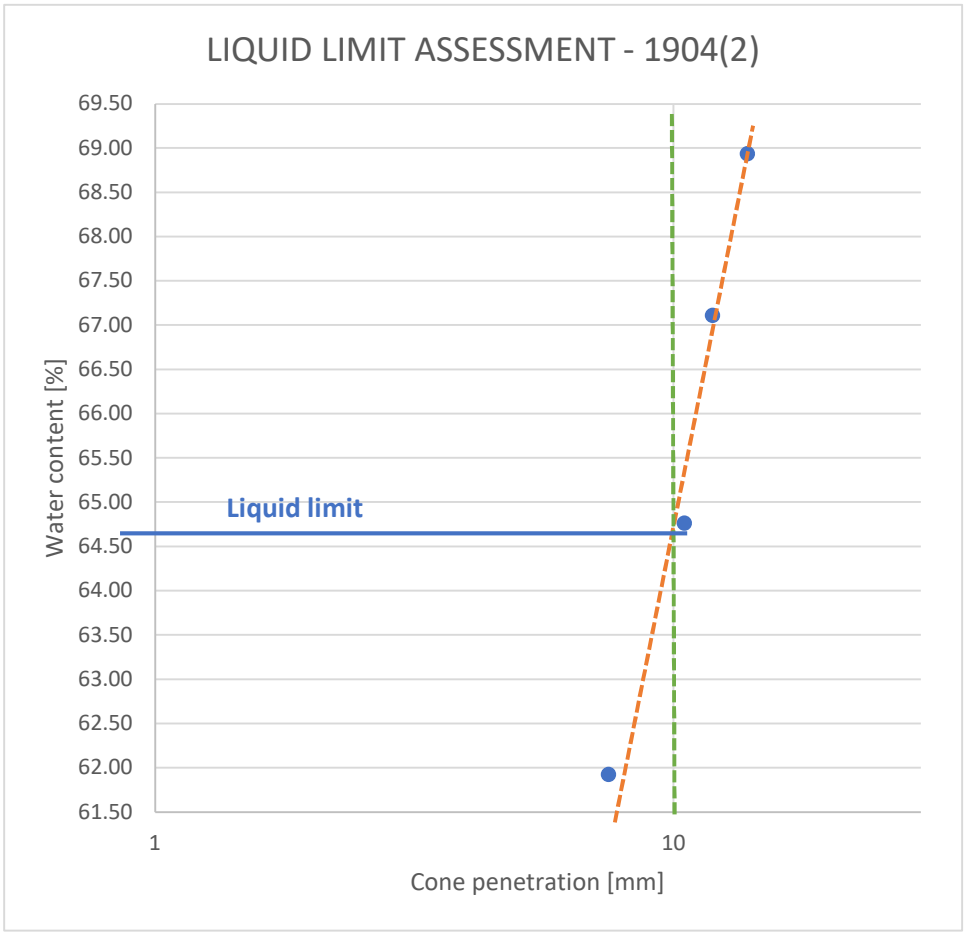
LIQUID LIMIT ASSESSMENT - 1904(2)
69.50
69.00
68.50
68.00
67.50
67.00
66.50
66.00
65.50
65.00
64.50
64.00
63.50
63.00
62.50
62.00
61.50
Water content [%]
Liquid limit
1
10
Cone penetration [mm]

ATTERBERG LIMITS - 0505 (1)

UNIT WEIGHT

Crib and trimmed sample	924.9	g
Crib	545.8	g
Trimmed sample	379.1	g
	0.3791	kg
Tyngde av prøve	0.00371897	kN
Trimmed sample	0.00022902	m3
Unit weight	**16.24**	**kN/m3**

WATER CONTENT

Container + moist	139.54	g	m1
Container + dry	132.98	g	m2
Container	122.7	g	mc
Water	6.56	g	mw
Dried specimen	10.28	g	md
Water content	**63.81**	**%**	**w**

Plastic limit

Portion A (3 sub-portions)			
Container + moist	34.91	g	m1
Container + dry	33.32	g	m2
Container 3	27.68	g	mc
Water	1.59	g	mw
Dried specimen	5.64	g	md
Plastic limit A	28.19	%	wp A
Portion B (3 sub-portions)			
Container + moist	36.15	g	m1
Container + dry	34.64	g	m2
Container 6	29.39	g	mc
Water	1.51	g	mw
Dried specimen	5.25	g	md
Plastic limit B	28.76	%	wp B
Plastic limit	**28.48**	**%**	**wp**

Liquid limit

Point A			
Container + moist	44.38	g	m1
Container + dry	41.05	g	m2
Container	36.09	g	mc
Water	3.33	g	mw
Dried specimen	4.96	g	md
Water content A	67.14	%	w A
Point B			
Container + moist	55.78	g	m1
Container + dry	51.69	g	m2
Container	45.77	g	mc
Water	4.09	g	mw
Dried specimen	5.92	g	md
Water content B	69.09	%	w B
Point C			
Container + moist	61.65	g	m1
Container + dry	56.29	g	m2
Container	48.95	g	mc
Water	5.36	g	mw
Dried specimen	7.34	g	md
Water content C	73.02	%	w C
Point D			
Container + moist	65.19	g	m1
Container + dry	58.51	g	m2
Container	49.87	g	mc
Water	6.68	g	mw
Dried specimen	8.64	g	md
Water content D	77.31	%	w D

Point	Cone penetration [mm]	Water content [%]	Read liquid limit [%]
A	7.5	67.14	71.6
B	9	69.09	
C	10.9	73.02	
D	13.1	77.31	

SAMPLE QUALITY

Berre, 1988 (Volumetric strain in the consolidation phase)

OCR	Depth [m]	εvol [%]	Quality
1.67	7.57	1.705	Good

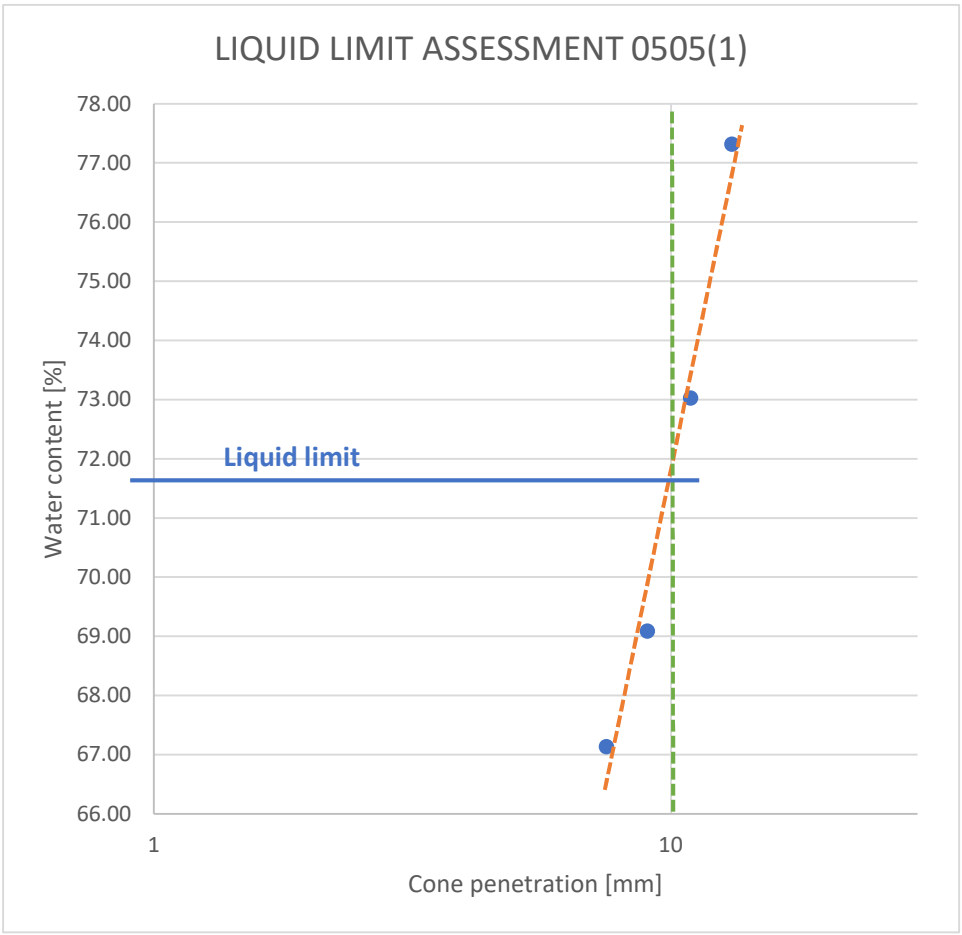
LIQUID LIMIT ASSESSMENT 0505(1)
78.00
77.00
76.00
75.00
74.00
73.00
72.00
71.00
70.00
69.00
68.00
67.00
66.00
Water content [%]
Liquid limit
1
10
Cone penetration [mm]

ATTERBERG LIMITS - 0505 (2)

UNIT WEIGHT

Dish and sample	693.07	g
Dish	348.5	g
Sample	344.57	g
	0.34457	kg
Tyngde av prøve	0.00338023	kN
Approximate volume of sample	0.000185	m3
Unit weight	**18.27**	**kN/m3**

WATER CONTENT

Container + moist	89.07	g	m1
Container + dry	83.49	g	m2
Container	66.69	g	mc
Water	5.58	g	mw
Dried specimen	16.8	g	md
Water content	**33.21**	**%**	**w**

Plastic limit

Portion A (3 sub-portions)			
Container + moist	35.73	g	m1
Container + dry	33.97	g	m2
Container 3	27.68	g	mc
Water	1.76	g	mw
Dried specimen	6.29	g	md
Plastic limit A	27.98	%	wp A
Portion B (3 sub-portions)			
Container + moist	39.75	g	m1
Container + dry	37.43	g	m2
Container 6	29.39	g	mc
Water	2.32	g	mw
Dried specimen	8.04	g	md
Plastic limit B	28.86	%	wp B
Plastic limit	**28.42**	**%**	**wp**

Liquid limit

Point A			
Container + moist	47	g	m1
Container + dry	43.07	g	m2
Container	36.12	g	mc
Water	3.93	g	mw
Dried specimen	6.95	g	md
Water content A	56.55	%	w A
Point B			
Container + moist	56.98	g	m1
Container + dry	53.98	g	m2
Container	49.01	g	mc
Water	3	g	mw
Dried specimen	4.97	g	md
Water content B	60.36	%	w B
Point C			
Container + moist	57.51	g	m1
Container + dry	52.99	g	m2
Container	45.79	g	mc
Water	4.52	g	mw
Dried specimen	7.2	g	md
Water content C	62.78	%	w C
Point D			
Container + moist	62.45	g	m1
Container + dry	57.47	g	m2
Container	49.96	g	mc
Water	4.98	g	mw
Dried specimen	7.51	g	md
Water content D	66.31	%	w D

Point	Cone penetration [mm]	Water content [%]	Read liquid limit [%]
A	7.8	56.55	61
B	10	60.36	
C	11	62.78	
D	13.5	66.31	

SAMPLE QUALITY

Berre, 1988 (Volumetric strain in the consolidation phase)

OCR	Depth [m]	εvol [%]	Quality
1.67	7.57	1.705	Good

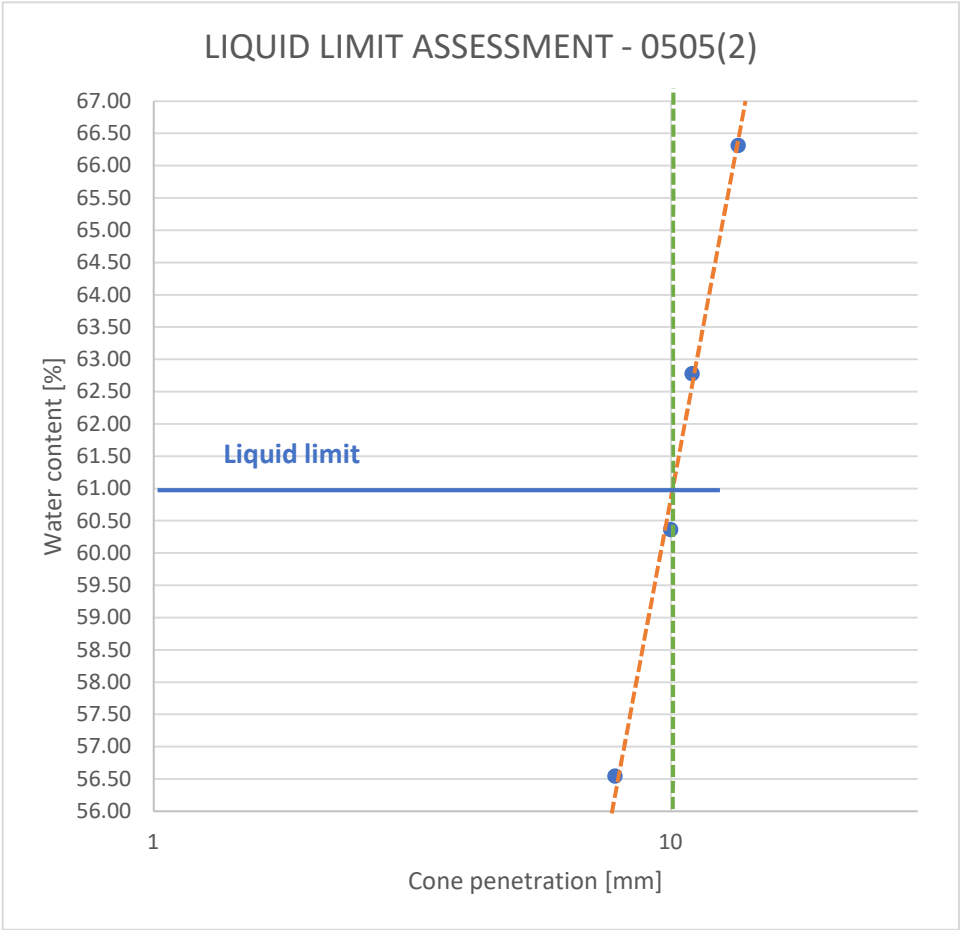
LIQUID LIMIT ASSESSMENT - 0505(2)
67.00
66.50
66.00
65.50
65.00
64.50
64.00
63.50
63.00
62.50
62.00
61.50
61.00
60.50
60.00
59.50
59.00
58.50
58.00
57.50
57.00
56.50
56.00
Water content [%]
Liquid limit
1
10
Cone penetration [mm]

ATTERBERG LIMITS - 2205 (1)

UNIT WEIGHT

Crib and trimmed sample	918.75	g
Crib	545.31	g
Trimmed sample	373.44	g
	0.37344	kg
Tyngde av prøve	0.00366345	kN
Trimmed sample	0.00022902	m3
Unit weight	**16.00**	**kN/m3**

WATER CONTENT

Container + moist	129.87	g	m1
Container + dry	104.39	g	m2
Container	66.7	g	mc
Water	25.48	g	mw
Dried specimen	37.69	g	md
Water content	**67.60**	**%**	**w**

Plastic limit

Portion A (3 sub-portions)			
Container + moist	35.45	g	m1
Container + dry	33.74	g	m2
Container (3)	27.69	g	mc
Water	1.71	g	mw
Dried specimen	6.05	g	md
Plastic limit A	28.26	%	wp A
Portion B (3 sub-portions)			
Container + moist	38.86	g	m1
Container + dry	36.73	g	m2
Container (6)	29.40	g	mc
Water	2.13	g	mw
Dried specimen	7.33	g	md
Plastic limit B	29.06	%	wp B
Plastic limit	**28.66**	**%**	**wp**

Liquid limit

Point A			
Container + moist	48.47	g	m1
Container + dry	43.52	g	m2
Container	36.11	g	mc
Water	4.95	g	mw
Dried specimen	7.41	g	md
Water content A	66.80	%	w A
Point B			
Container + moist	60.87	g	m1
Container + dry	56.04	g	m2
Container	48.97	g	mc
Water	4.83	g	mw
Dried specimen	7.07	g	md
Water content B	68.32	%	w B
Point C			
Container + moist	59.97	g	m1
Container + dry	55.7	g	m2
Container	49.91	g	mc
Water	4.27	g	mw
Dried specimen	5.79	g	md
Water content C	73.75	%	w C
Point D			
Container + moist	59.96	g	m1
Container + dry	53.88	g	m2
Container	45.77	g	mc
Water	6.08	g	mw
Dried specimen	8.11	g	md
Water content D	74.97	%	w D

Point	Cone penetration [mm]	Water content [%]	Read liquid limit [%]
A	7.9	66.80	70.5
B	8.6	68.32	
C	12	73.75	
D	13.5	74.97	

SAMPLE QUALITY

Berre, 1988 (Volumetric strain in the consolidation phase)

OCR	Depth [m]	εvol [%]	Quality
1.66	7.45	1.26	Good

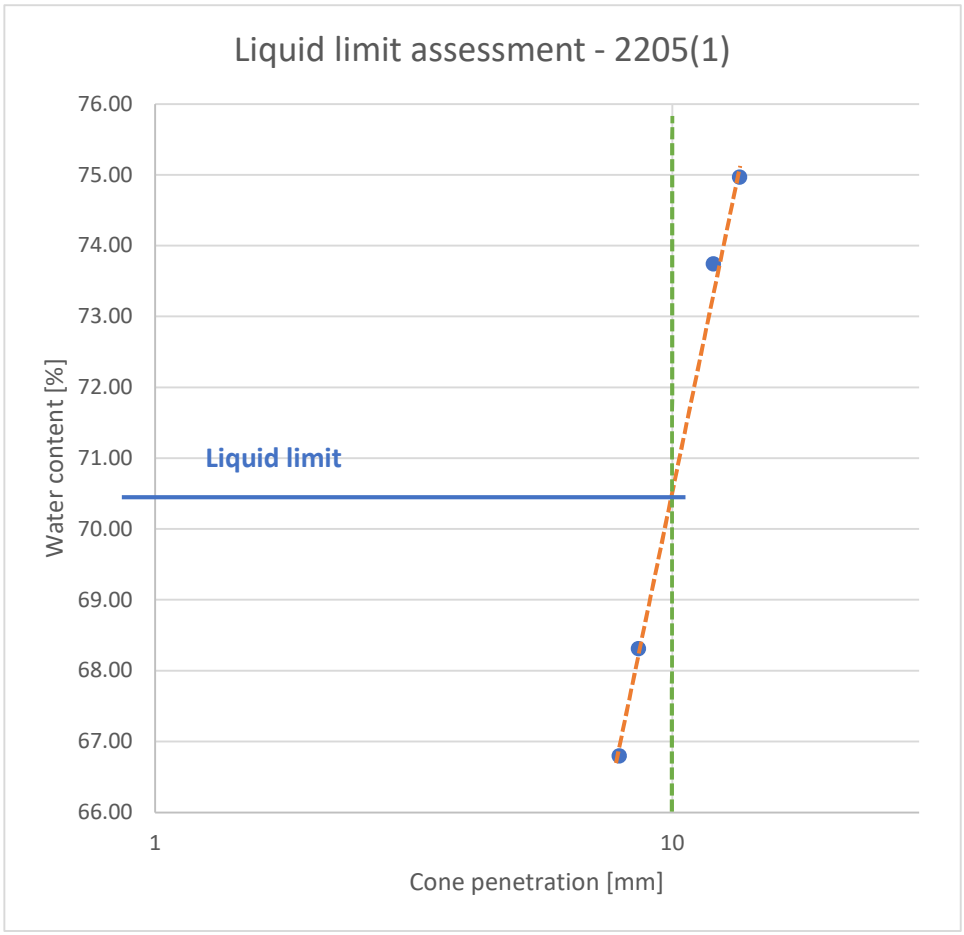
Liquid limit assessment - 2205(1)
76.00
75.00
74.00
73.00
72.00
71.00
70.00
69.00
68.00
67.00
66.00
Water content [%]
Liquid limit
1
10
Cone penetration [mm]

ATTERBERG LIMITS - 2205 (2)

UNIT WEIGHT

Trimmed sample	355.16	g
	0.35516	kg
Tyngde av prøve	0.00348412	kN
Trimmed sample	0.0001836	m3
Unit weight	**18.98**	**kN/m3**

WATER CONTENT

Container + moist	196.35	g	m1
Container + dry	182.8	g	m2
Container	145.04	g	mc
Water	13.55	g	mw
Dried specimen	37.76	g	md
Water content	**35.88**	**%**	**w**

Plastic limit

Portion A (3 sub-portions)			
Container + moist	36.21	g	m1
Container + dry	34.33	g	m2
Container (3)	27.69	g	mc
Water	1.88	g	mw
Dried specimen	6.64	g	md
Plastic limit A	28.31	%	wp A
Portion B (3 sub-portions)			
Container + moist	37.51	g	m1
Container + dry	35.7	g	m2
Container (6)	29.40	g	mc
Water	1.81	g	mw
Dried specimen	6.3	g	md
Plastic limit B	28.73	%	wp B
Plastic limit	**28.52**	**%**	**wp**

Liquid limit

Point A			
Container + moist	61.2	g	m1
Container + dry	56.66	g	m2
Container	48.89	g	mc
Water	4.54	g	mw
Dried specimen	7.77	g	md
Water content A	58.43	%	w A
Point B			
Container + moist	58.69	g	m1
Container + dry	55.34	g	m2
Container	49.89	g	mc
Water	3.35	g	mw
Dried specimen	5.45	g	md
Water content B	61.47	%	w B
Point C			
Container + moist	58.06	g	m1
Container + dry	53.25	g	m2
Container	45.78	g	mc
Water	4.81	g	mw
Dried specimen	7.47	g	md
Water content C	64.39	%	w C
Point D			
Container + moist	101.15	g	m1
Container + dry	95.49	g	m2
Container	87.26	g	mc
Water	5.66	g	mw
Dried specimen	8.23	g	md
Water content D	68.77	%	w D

Point	Cone penetration [mm]	Water content [%]	Read liquid limit [%]
A	7.2	58.43	65.1
B	9	61.47	
C	10	64.39	
D	11.6	68.77	

SAMPLE QUALITY

Berre, 1988 (Volumetric strain in the consolidation phase)

OCR	Depth [m]	εvol [%]	Quality
1.66	7.45	1.26	Good

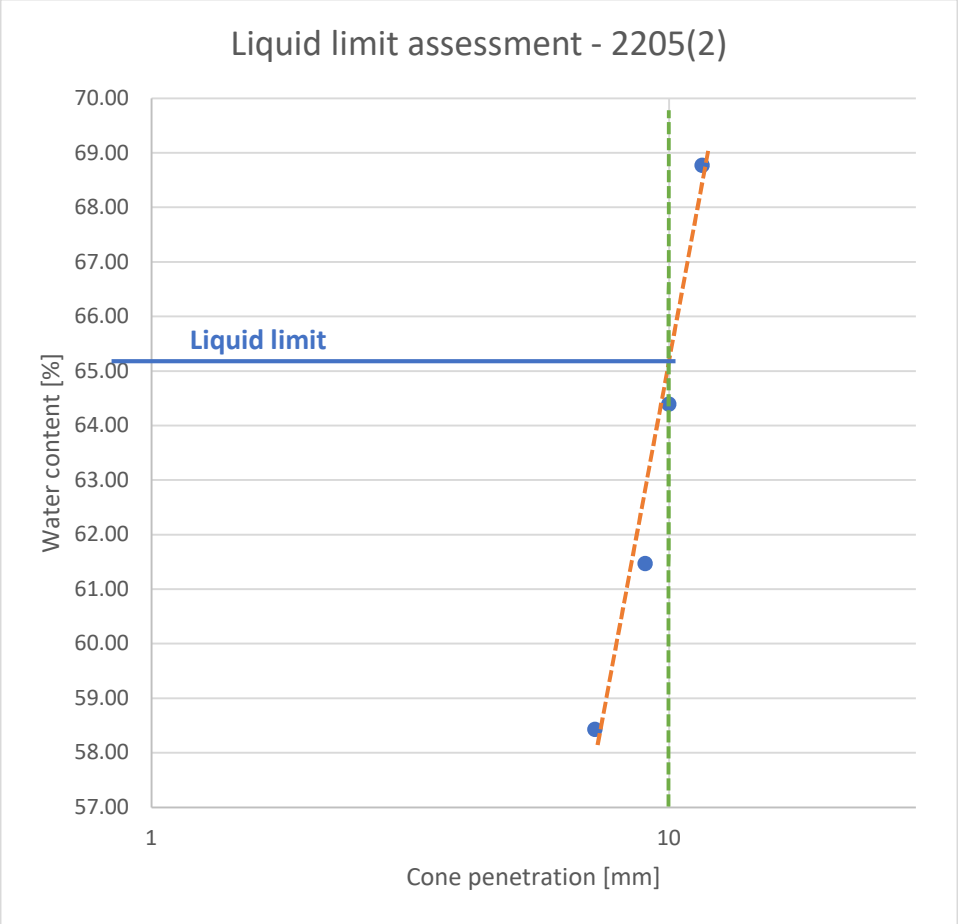
Liquid limit assessment - 2205(2)
70.00
69.00
68.00
67.00
66.00
65.00
64.00
63.00
62.00
61.00
60.00
59.00
58.00
57.00
Water content [%]
Liquid limit
1
10
Cone penetration [mm]

Appendix 2: K_0 assessments

1703 - K0 stress paths

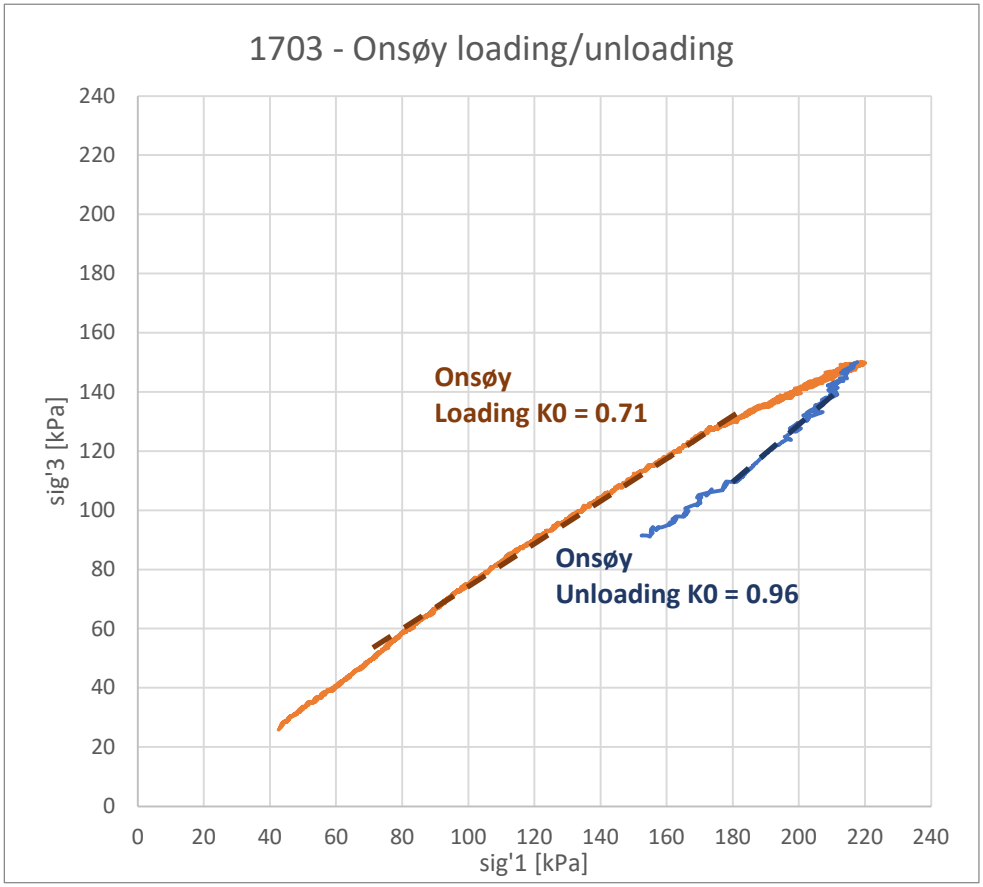

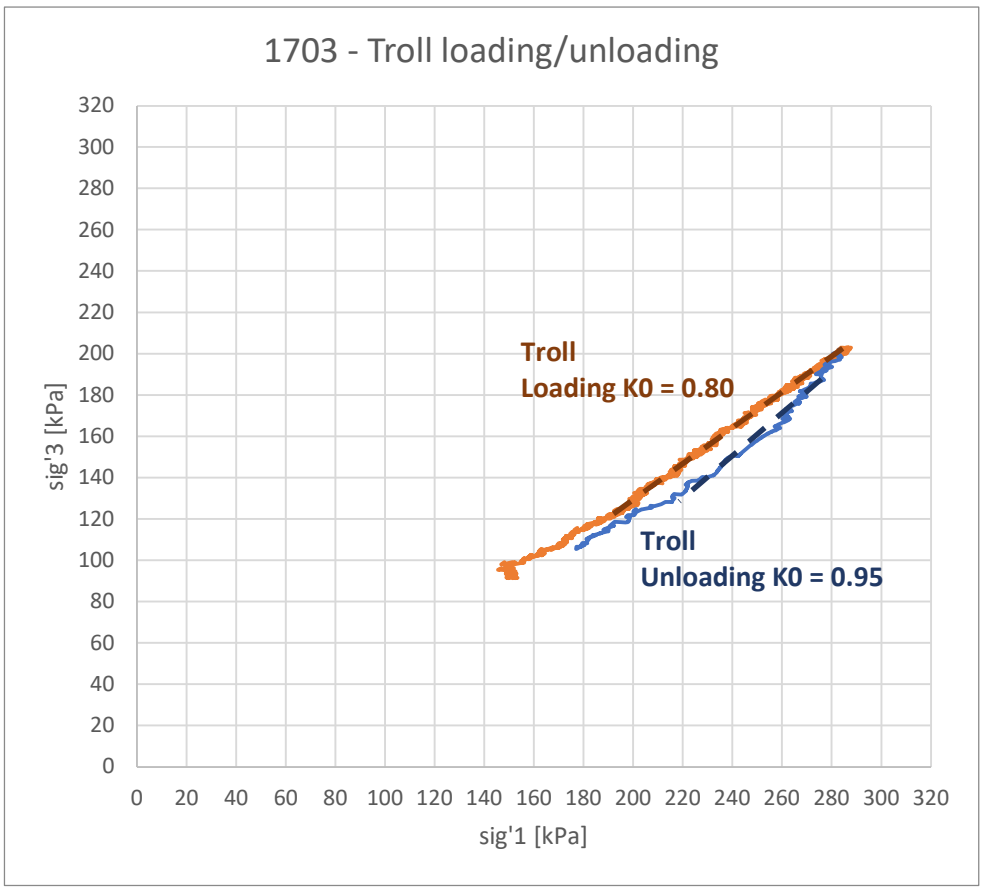
1703 - Troll loading/unloading
sig'3 [kPa]
sig'1 [kPa]
0
20
40
60
80
100
120
140
160
180
200
220
240
260
280
300
320
Troll
Loading K0 = 0.80
Troll
Unloading K0 = 0.95

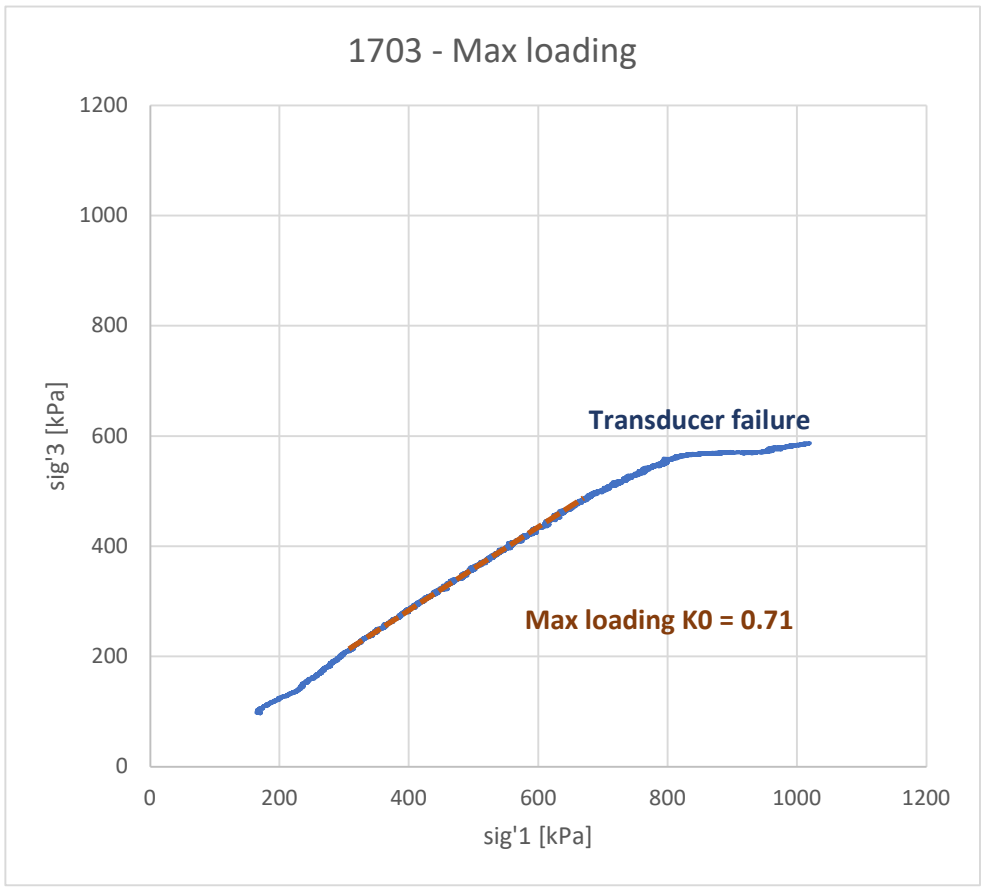
1703 - Max loading
sig'3 [kPa]
sig'1 [kPa]
0
200
400
600
800
1000
1200
Transducer failure
Max loading K0 = 0.71

2703 - K0 stress paths

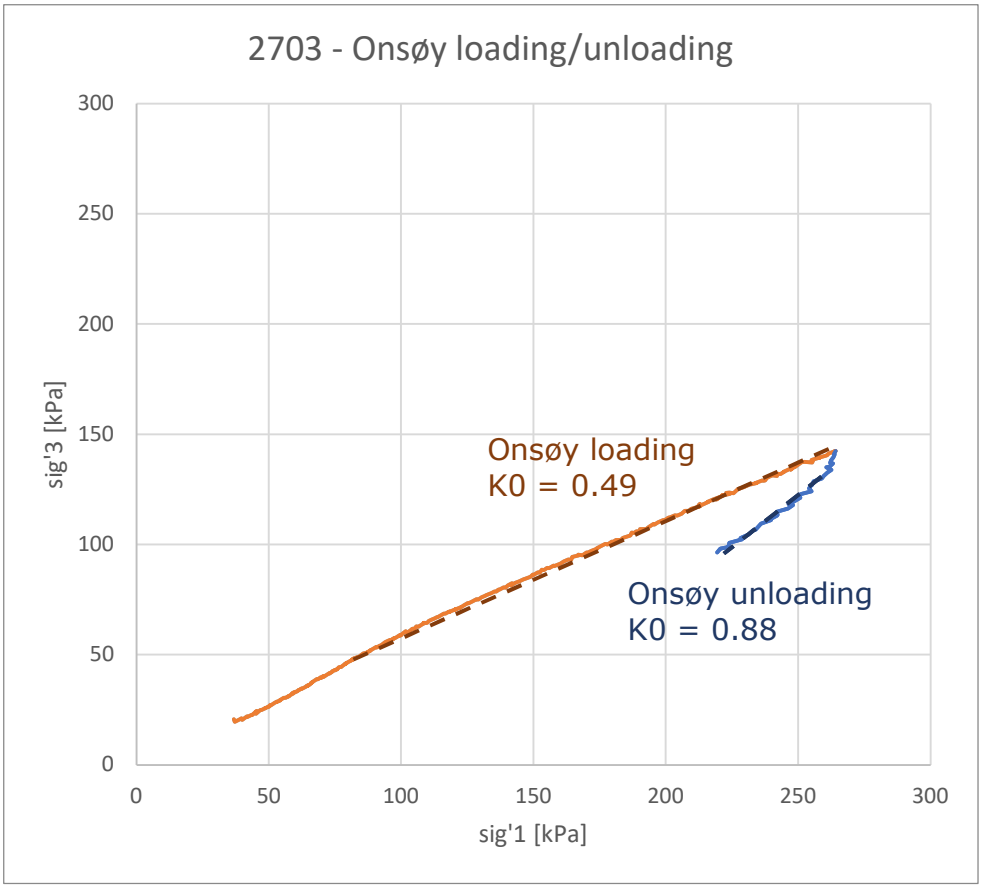

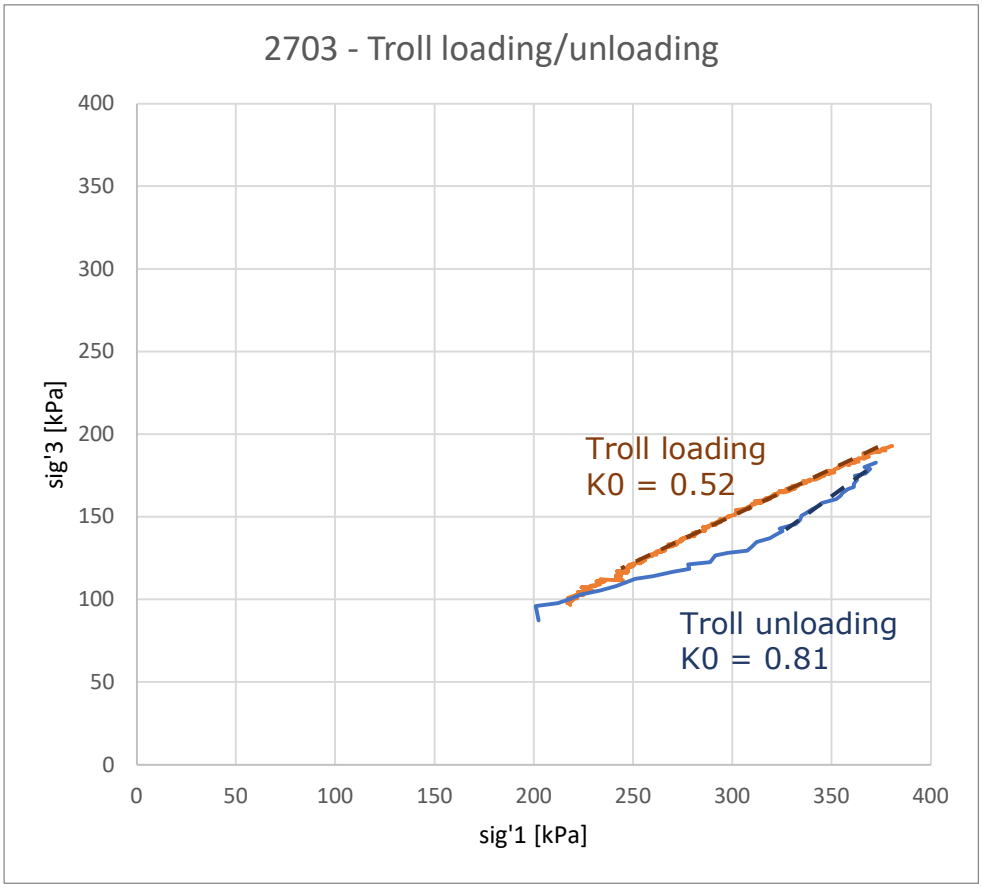

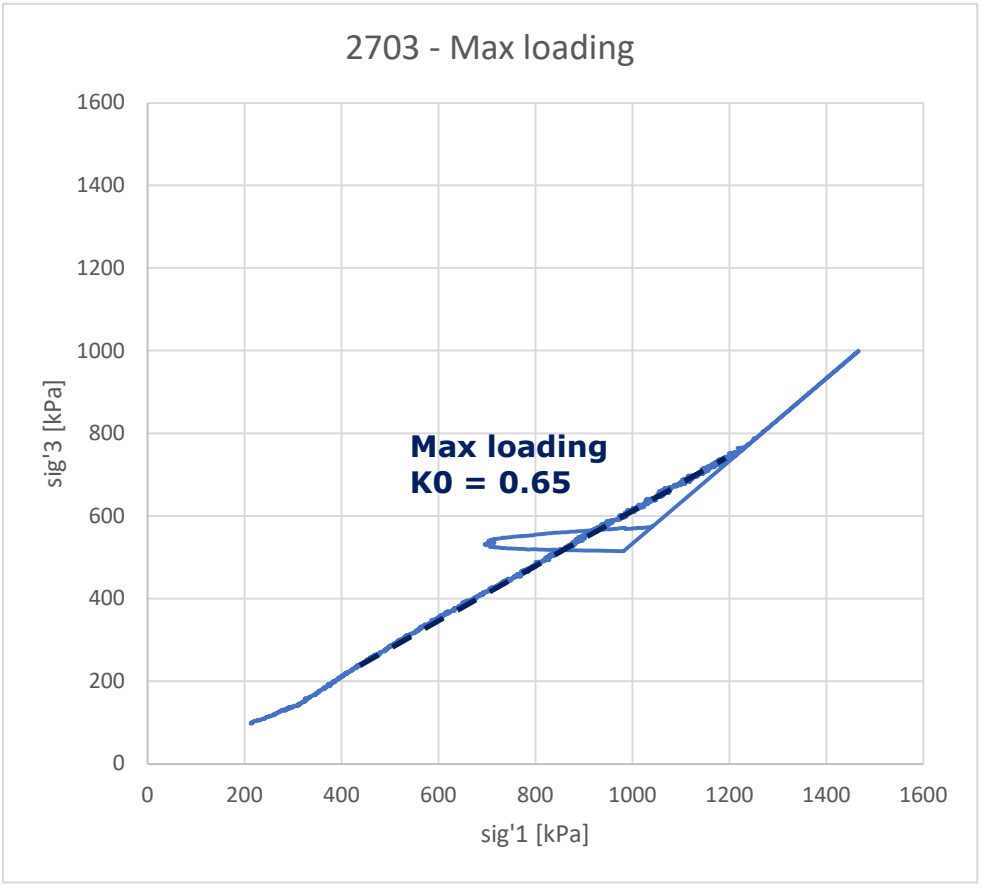
2703 - Max loading
1600
1400
1200
1000
800
600
400
200
0
sig'3 [kPa]
Max loading
K0 = 0.65
0
200
400
600
800
1000
1200
1400
1600
sig'1 [kPa]

1904 - K0 stress paths

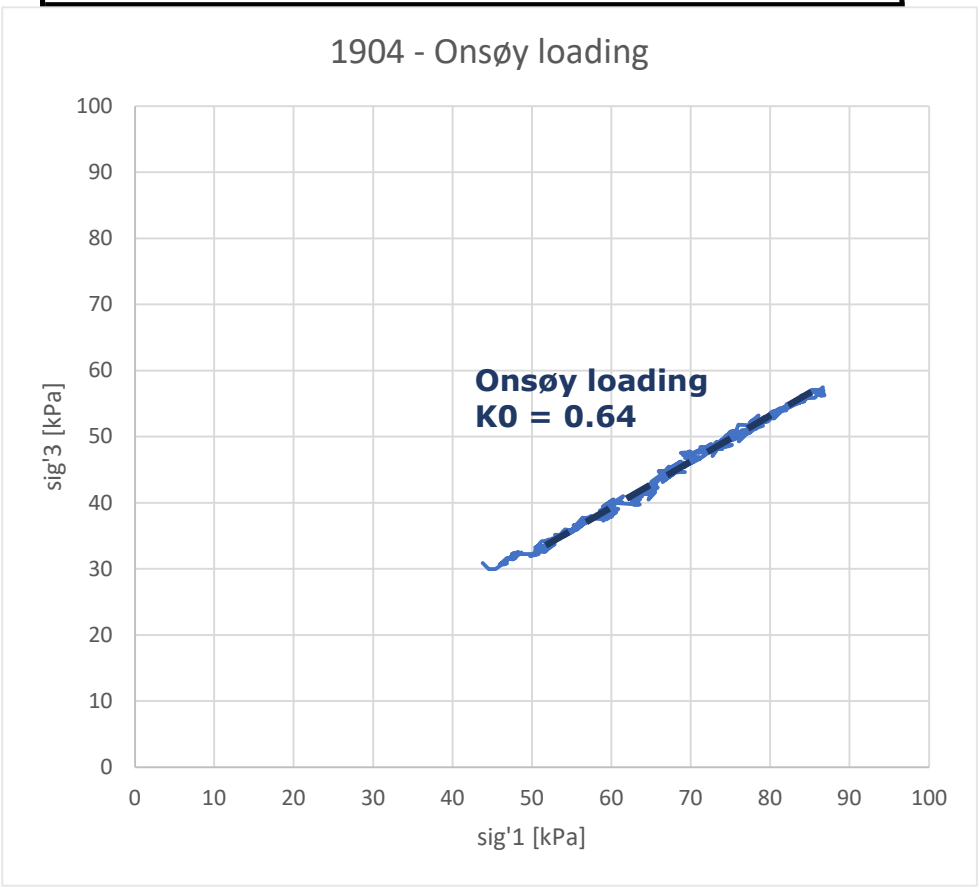

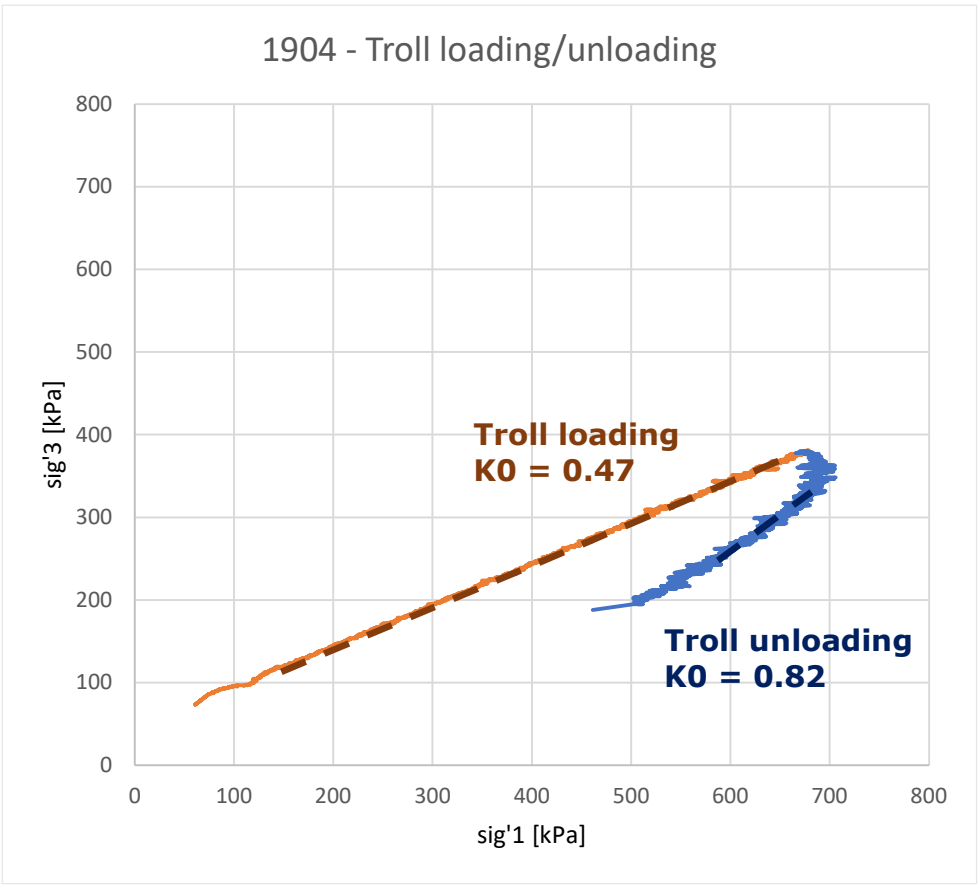

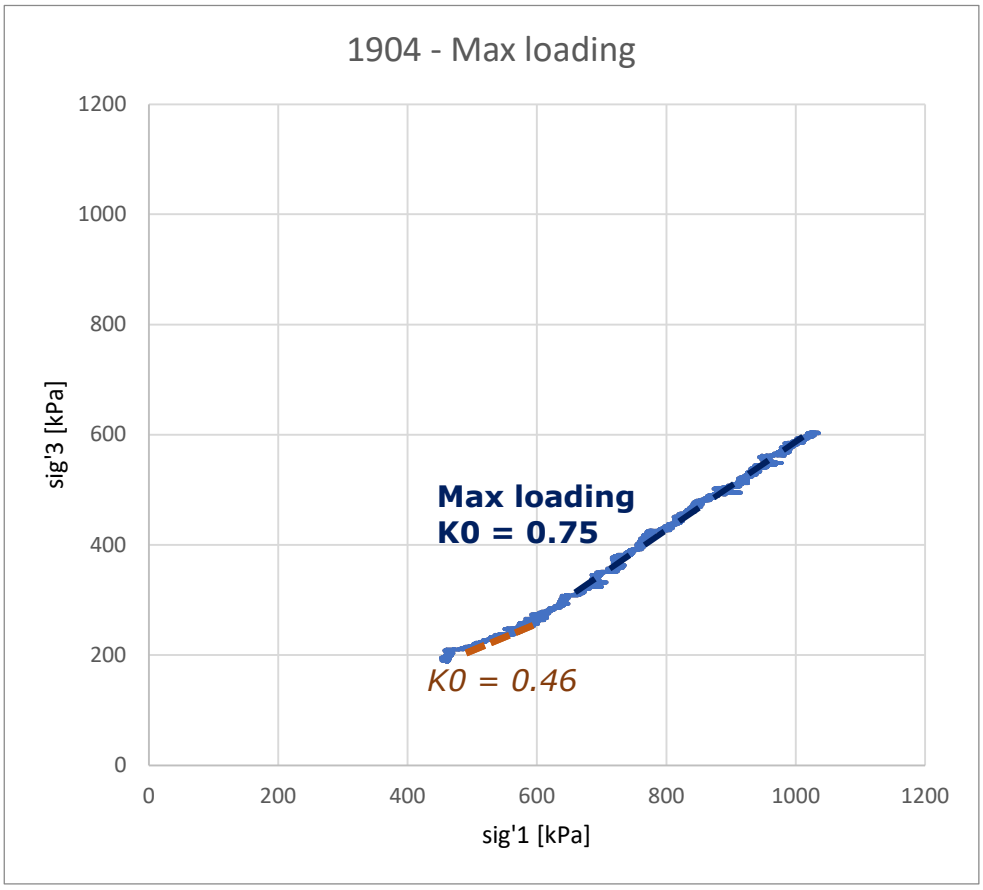
1904 - Max loading
1200
1000
800
600
400
200
0
sig'3 [kPa]
0
200
400
600
800
1000
1200
sig'1 [kPa]
Max loading
K0 = 0.75
K0 = 0.46

0505 - K0 stress paths

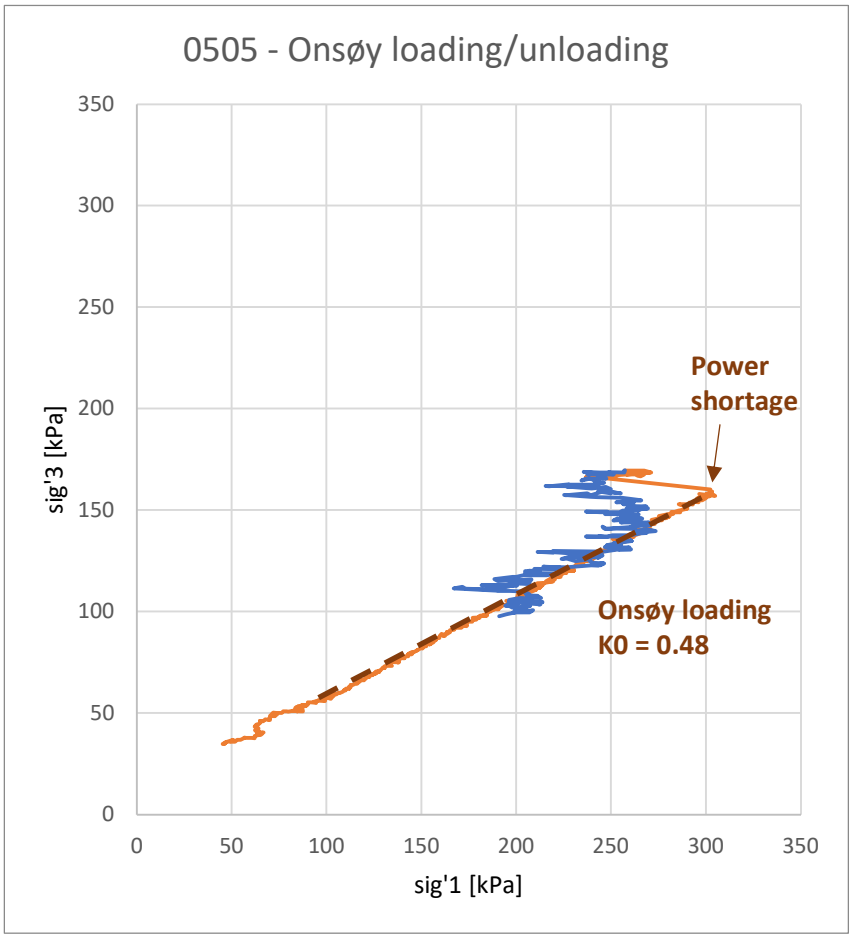

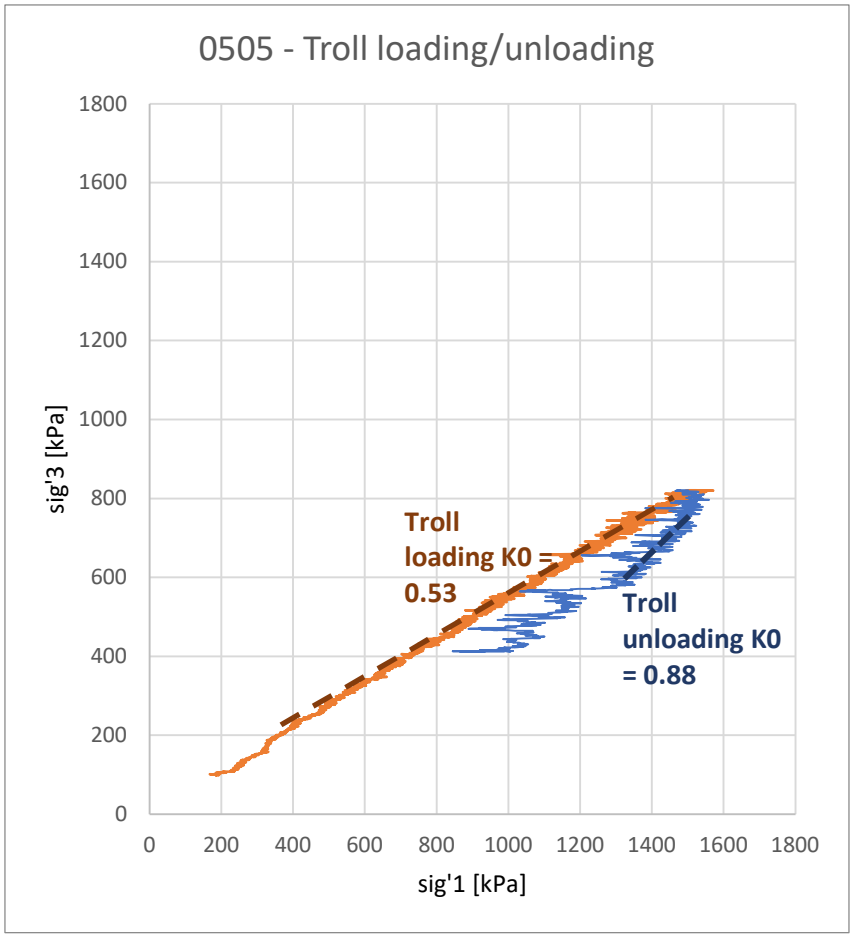
0505 - Troll loading/unloading
sig'3 [kPa]
sig'1 [kPa]
0
200
400
600
800
1000
1200
1400
1600
1800
Troll loading K0 = 0.53
Troll unloading K0 = 0.88

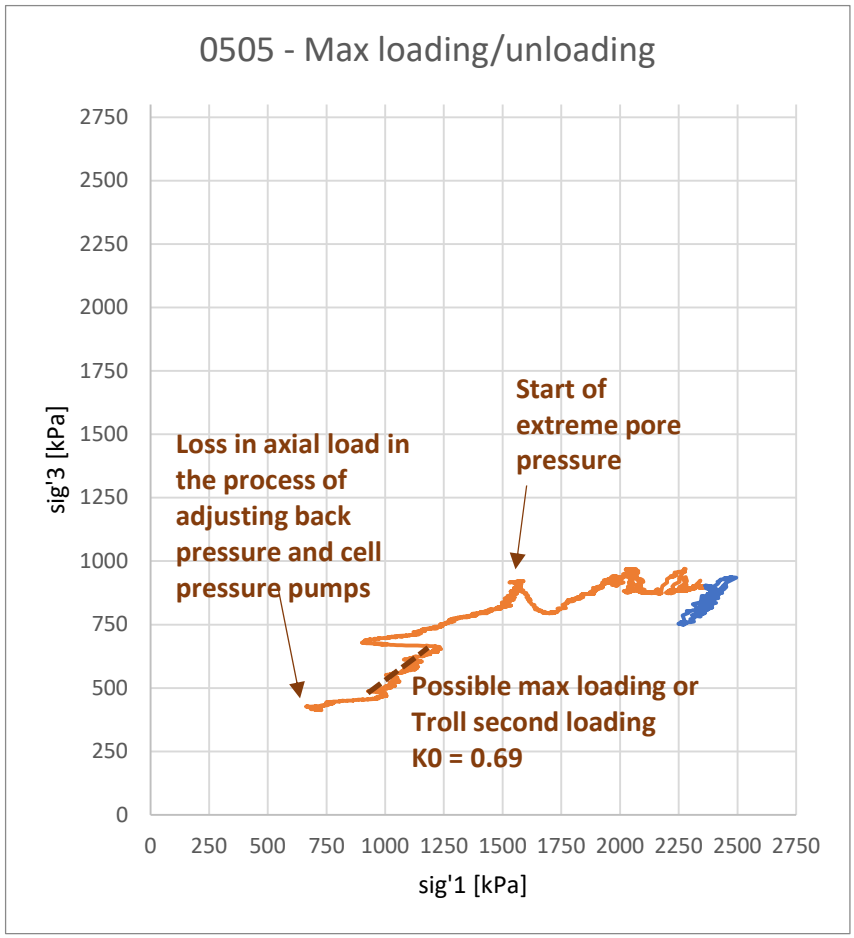
0505 - Max loading/unloading
sig'3 [kPa]
sig'1 [kPa]
0
250
500
750
1000
1250
1500
1750
2000
2250
2500
2750
Loss in axial load in the process of adjusting back pressure and cell pressure pumps
Start of extreme pore pressure
Possible max loading or Troll second loading K0 = 0.69

2205 - K0 stress paths

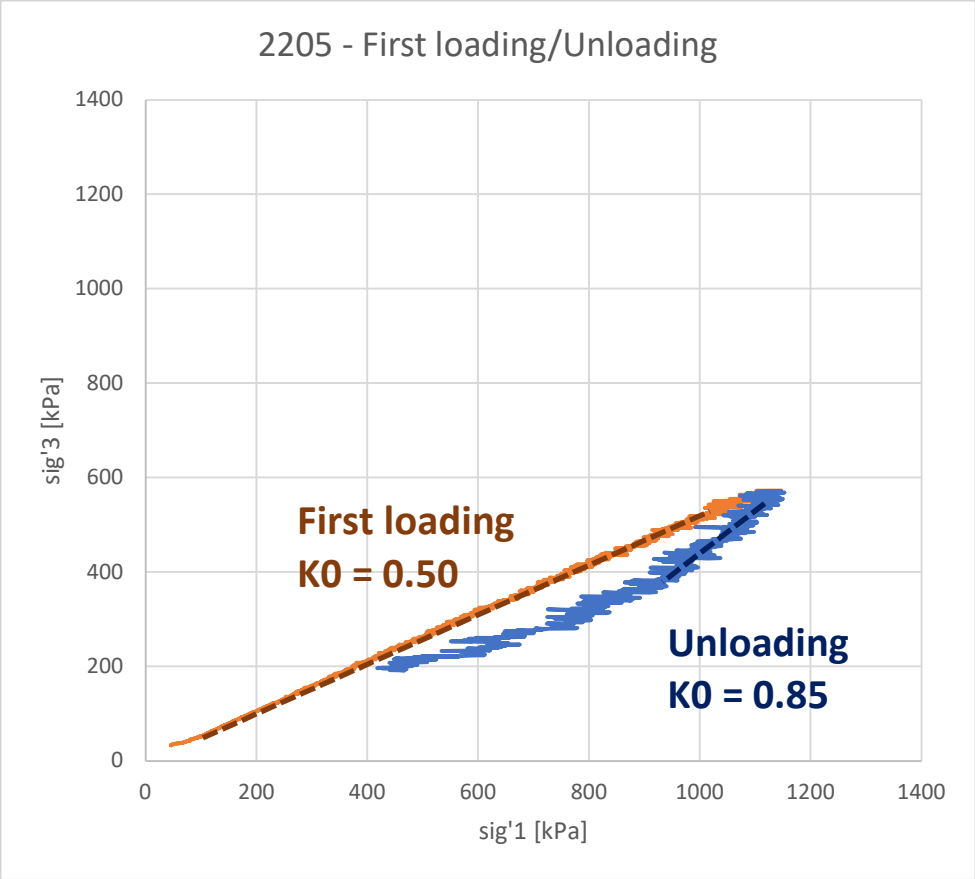

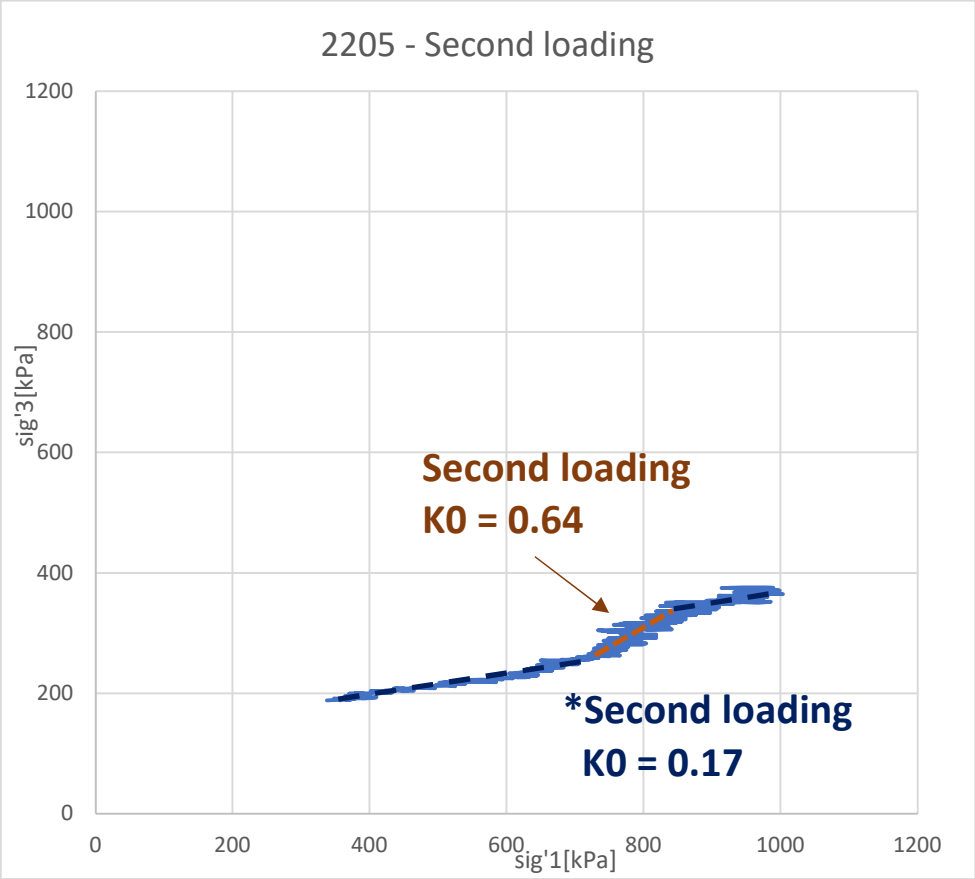

Appendix 3: Calibration of 50 kN load cell

$$Full\ Scale\ Output = 2.1218\ mV/V \cdot 10\ V = 21.218\ mV$$

$$Sensitivity = \frac{Load\ Range}{Full\ Scale\ Output} = \frac{50\ kN}{21.218\ mV} = \underline{2.356489\ \ kN/mV}$$

125 Helpsheet

GDS INSTRUMENTS LIMITED

World Leaders in Computer Controlled Testing Systems for Geotechnical Engineers and Geologists

Hardware

Transducers

Calculating Sensitivity and Full Scale Output

1 Introduction

Many GDS transducers work using an excitation voltage, and return a linear output in millivolts directly proportional to the parameter being measured. To correlate this millivolt output with an actual quantity trying to be measured it is necessary to calibrate the transducer.

The full-scale output value, the excitation voltage and the range of the transducer enables the sensitivity of the transducer to be calculated.

All transducers calibrated by GDS have the sensitivity value shown on the calibration certificate, but some certificates require a calculation to be made.

Copies of all calibration certificates are kept at GDS UK, so do not hesitate to contact us if you have mislaid one.

2 Full Scale Output

All GDS transducers are supplied with a calibration certificate, which shows the millivolts that the transducer will output when at it's maximum range. This is the **full scale output** and is usually given as a the value at full scale in millivolts.

Some transducer calibration certificates give this full scale output value as *millivolts **per** volt*. In this case this value will need to be multiplied by the excitation voltage used (usually 10 Volts) to give the full scale output at that specific excitation voltage.

Example 1

Full Scale Output = 29.95mV
Excitation Voltage used at calibration = 10V

So long as we are ALSO using the transducer with 10V excitation, the transducer FULL SCALE OUTPUT = 29.95mV.

Example 2

Full Scale Output = 2.995mV/V
Excitation Voltage used at calibration = 10V

Here, the full scale output is given ***per volt excitation***. Here we must multiply the full scale output supplied by the excitation voltage used. Using an excitation of 10V therefore fives a FULL SCALE OUTPUT = 2.995 x 10 = 29.95mV.

3 Calculating the Sensitivity of the Transducer

To calculate the sensitivity value of a transducer, simply divide the **range in units** of the transducer by the **full scale output** value (as calculated in section 2).

$$Sensitivity = \frac{Transducer\,Range}{Full\,Range\,Output}$$

4 Example sensitivity calculations

GDS Load Cell (required units are kN)

Example1:
GDS BA4958 Submersible Load Cell
Range = 4kN Full scale output = 19.55mV
Excitation Voltage used at calibration = 10V
Excitation Voltage that will be used in Lab = 10V

$$Sensitivity = \frac{kN}{mV} = kN/mV$$

$$Sensitivity = \frac{4}{19.55} = 0.2kN/mV$$

Example2:
GDS BA4958 Submersible Load Cell
Range = 4kN Full scale output = 1.955mV/V
Excitation Voltage used at calibration = 10V
Excitation Voltage that will be used in Lab = 10V

$$Sensitivity = \frac{kN}{mV/V \times V} = kN/mV$$

$$Sensitivity = \frac{4}{1.955 \times 10} = 0.2kN/mV$$

GDS Pressure Transducer (required units are kPa)

Range = 500psi Full scale output = 200mV
Excitation Voltage used at calibration = 10V
Excitation Voltage that will be used in Lab = 10V

To convert from PSI to kPa multiply by 6.8948

$$Sensitivity = \frac{psi \times 6.8948}{mV} = kPa/mV$$

$$Sensitivity = \frac{500 \times 6.8948}{200} = 17.237 kPa/mV$$

GDS Displacement Transducer (required units are mm)

Range = 50mm Full Scale Output = 1000mV/V
Excitation Voltage used at calibration = 10V
Excitation Voltage that will be used in Lab = 10V

Sensitivity value is shown on calibration certificate = 0.005mm/mV

$$Sensitivity = \frac{mm}{mV} = mm/mV$$

$$Sensitivity = \frac{50}{10000} = 0.005 mm/mV$$

GDS Hall Effect Transducer (required units are mm)

Range = 6mm Full Scale Output = 2727mV
Excitation Voltage used at calibration = 10V
Excitation Voltage that will be used in Lab = 10V

Sensitivity value shown on calibration certificate = 2.2micron/mV = .0022mm/mV

$$Sensitivity = \frac{mm}{mV} = mm/mV$$

$$Sensitivity = \frac{6}{2727} = 0.0022 mm/mV$$

GDS Mid Plane Pore Pressure Transducer (required units are kPa)

Range = 15bar g Full Scale Output = 1.13mV/V/bar
Excitation Voltage used at calibration = 5V
Excitation Voltage that will be used in Lab = 5V

To convert from bar to kPa multiply by 100

$$Sensitivity = \frac{bar \times 100}{mV \times V \times bar} = kPa/mV$$

$$Sensitivity = \frac{15 \times 100}{1.13 \times 5 \times 15} = 17.699 kPa/mV$$

THE QUEEN'S AWARDS FOR ENTERPRISE: INTERNATIONAL TRADE 2011

GDS
www.gdsinstruments.com

World Leaders in Computer Controlled Testing Systems for Geotechnical Engineers and Geologists

CALIBRATION CERTIFICATE

Calibration of Transducer

Calibration Results:

Date:	10th January 2016
Transducer Type:	STALC9-50kN-003-000
Serial No:	53365
Load Rating:	50kN
Proof Rating:	75kN
Calibration Mode:	Compression
Zero Output:	0.054mV @ 10Vdc
Sensitivity:	2.1218mV/V
Non-linearity	< ±0.040 % FS
Hysteresis:	< -0.042% FS
Supply Voltage:	10.0000Vdc
Input Resistance:	750 Ohms
Insulation Resistance:	> 20 GOhms at 100Vdc
Reference Standard:	TE159C

Electrical connections:

3m Cable Assy

Red	+ve excitation
Blue	-ve excitation
Green	+ve signal
Yellow	-ve signal

This product is hereby certified to have been inspected, tested and calibrated – using UKAS traceable test equipment - in all respects with the requirements of the customer's order.

GDS Instruments, an operating division of Global Digital Systems Ltd,
Unit 32 Murrell Green Business Park, London Road, Hook, Hampshire, RG27 9GR.
Tel: +44 (0)1256 382450 Fax: +44 (0)1256 382451 Web: www.gdsinstruments.com
Company Registered No. 1459108. VAT Registered No. GB 335 5934 41

Appendix 4: NGTS Onsøy boring plan

Boring plan - NGTS Onsøy

-
M = ~
-
-
-

-
-

Rapport nr. -	Figur nr.
Tegner	Dato:
Kontrollert	
Godkjent	

Appendix 5: Oedotriaxial testing guide

25.01.2023
Jan Alexander Tubid Myhrvold
Alf Valle Eirik Kopperud
Elias

GDS 2000 installasjonsnotis (IBM)

FORORD

Det er finnes mange anbefalte prosedyrer, basert på erfaringer. Av og til kan disse være basert på den enkelte treaksrigg, som kan være omstendelige for best mulig resultater. Disse er inspirert fra anbefalinger fra R210 og NGI, men aller viktigst, erfaringer fra den aktuelle riggen. Denne notisen er basert på Elias sine forklaringer – som har plukket opp diverse metoder. Også inspirert fra guider fra *GDS Triaxial* for leire på YouTube, Det aller viktigste er å bli kvitt alle luftboblene i systemet, og sørge for god tetting.

25.01.2023
Jan Alexander Tubid Myhrvold
Alf Valle Eirik Kopperud
Elias

FØR INNBYGGING

Sørg for at:

- Alle delene til treakscellen er til stede. Se gjerne under bordet om ev. gummiringer eller hetter har falt av bordet.
- Topp- og bunn filtersteinen er rengjort via sonisk bad – og fullstendig mettet med luftfritt vann via eksikkatoren. Begge ligger i hver sin kopp vann.
- Den store O-ringen på bunnsiden av treaksriggen er fuktet og i god stand. Ev. erstatt eller smør med O-ringfett (Molykote).
- Gummimembranen er tilstrekkelig rengjort inn- og utvendig, og tilført talkumpulver. Se etter skader som hull, riper, osv. ved å føre den mot taklyset. Hvis mistanke om skade – kast og bruk en ny.
- Innbyggingsformen er teipet med god tetning på hver side, samt med to fettete gummiringer på hver side av vakuumventilen.
- Baktrykk- og celletrykkontrollen og GDS er påslått før innlogging i PCen.

Til sist:

- Leirprøven er tilskåret til 10 cm med rengjort trådsag i krybben. Merk topp- og bunnside samt in-situ dybdene på disse. Tildekk prøven med krybben i med plastfolie for å hindre uttørking av prøven under forberedelsene.
- Merk alle ventiler og slanger med etiketter!

25.01.2023
Jan Alexander Tubid Myhrvold
Alf Valle Eirik Kopperud
Elias

INNBYGGING 1 – Mette bunnsokkelen med luftfritt vann

Her må vi mette alle vannkanalene til bunnsokkelen før prøven settes på.

1. Åpne ventil til luftfritt vann (i en beholder over cellen)
2. La det renne vann til det ikke lenger dukker opp luftbobler.
3. Lukk bunnventil.
4. Gjøres på den andre vannkanalen.
5. Man ender opp med en hinne av vann på toppen av bunnsokkelen.
6. Lukk ventil til bunnsokkelen.

NGI metter ikke filtersteinen.

INNBYGGING 2 – Gummimembran og filterstein

1. Sett inn gummimembran på innsiden av prøveformen og trekk over topp- og bunnkantene slik at de sitter høvelig stramt til. Rull begge O-ringene fra hver side over membranen før vakuumpumpa brukes.
2. Skru inn én stang i riggen – den hjelper å trekke prøveformen med membranen inn. Stangen i den delen av riggen der vakuumventilen er lettest tilgjengelig.
3. Sett inn nederste filterstein fra siden, mens den fortrenger vannet slik at ingen luft blir fanget.
4. Sett på et tørt filterpapir på filtersteinen. Den trekker i seg vann via filtersteinen. Klem ut luftrom fra midten.

NGI fukter filtrerpapiret i forkant. Dessuten benyttes ikke filtrerpapirene på siden av prøven.

25.01.2023
Jan Alexander Tubid Myhrvold
Alf Valle Eirik Kopperud
Elias

INNBYGGING 3 – Trekning




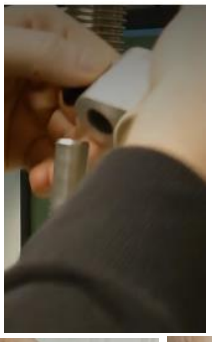
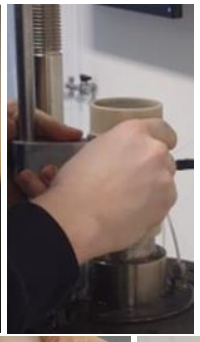



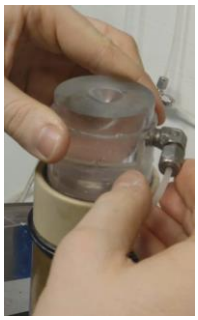


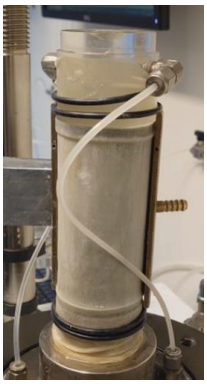
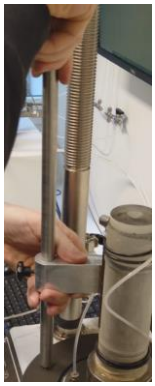


1. Prøven tas forsiktig ut av krybben, og settes på filtrerpapiret med bunnsiden ned.
2. Smøre på gult fett i rundt sokkelen. Dette hjelper med å feste gummimembranen og tette mot lekkasjer.
3. Koble luftslangen fra vakuumpumpa til prøveformen og slå på pumpen.
    a. Sørg for at gummimembranen suges helt inn mot prøveformen når pumpen virker.
4. Nå kan gummimembranen med ventil festes i stangen.

OBS 1: Formen med gummimembran kan slå til prøven. Forsiktig! Sjekk at prøven faktisk kan trekkes gjennom.

5. Trekk ned formen forsiktig slik at leirprøven kommer gjennom mens vakuumpumpen går
6. Stopp når formen er midtstilt prøven slik at formen dekker over den nedre filtersteinen.

OBS 2: Formen må dekke over filtersteinen, fordi gummimembranen skal brettes ned til topp og bunnsokkelen. Da må O-ringen rulle direkte ned til sokkelen, ikke på prøven eller filtersteinen.

7. Slå av vakuumpumpa og fjern luftslangen fra formen – nå skal gummimembranen automatisk trekke seg til leirprøven på innsiden.

25.01.2023
Jan Alexander Tubid Myhrvold
Alf Valle Eirik Kopperud
Elias

8. Rull opp begge nedre O-ringene – deretter trekk ned gummimembranen over bunnsokkelen.
    a. Rull ned begge O-ringene, og legg dem tett under leppen på prøveformen.
9. Sett på tørt filterpapir på toppsiden – glatt forsiktig ut ev. hulrom.
10. Sett inn øverste filterstein – formen skal dekke over den øverste filtersteinen.
11. Mett toppsokkelen med luftfritt vann med de riktige kanalene som utført i **INNBYGGING 1**.
12. Vend toppsokkelen ned og legg forsiktig på filtersteinen ovenfra.
13. Utfør **steg 8** og **steg 8a** for toppsokkelen.
14. Fjern teiingen på siden av formen. Nå kan den ytre halvdelen av formen fjernes. Formen mot stangen kan enkelt roteres unna, og fjernes.

OBS 3: Pass på at vannslangene til toppsokkelen ikke berører prøven på sidene.

Nå er prøven ferdig inntrukket og cellen kan nå installeres.

CELLE 1 – Montering av cellen

Her monteres cellen og sørger for kontakt mellom stempel og toppsokkel. Sørg for at den øvre armen til treaksriggen er koblet fra slik at cellen kan komme til.

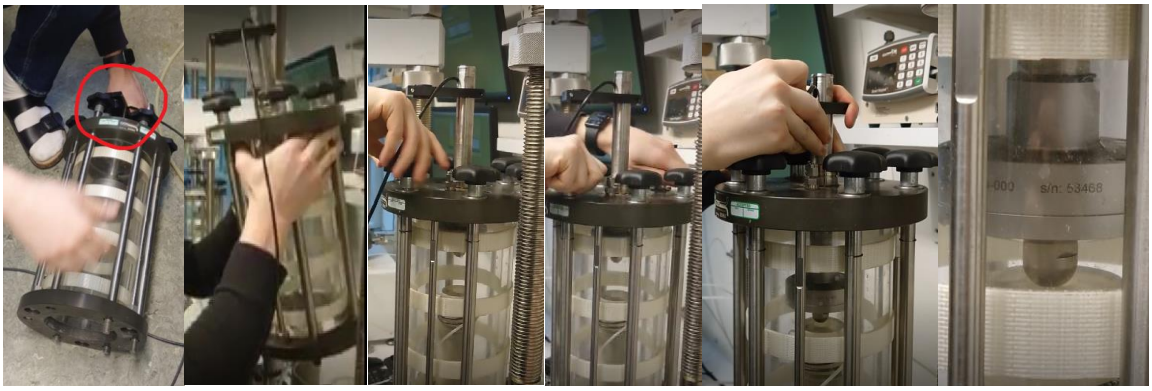

1. Sørg for at stempelet er fullstendig slått ut av cellen og festet slik. Løft opp cellen og tre stengene forsiktig inn i riggen.
2. Skru til stengene med sort håndtak **hardt**.
3. Stram til alle bolter, med tang og klut.
4. Før stempelet forsiktig inn på toppsokkel til man har kontrakt. Man observerer dette når toppsokkelen endrer litt posisjon.

OBS 4: Pass på at stempelet ikke slår inn i prøven når cellen settes inn! I tillegg – ikke skru på metallhetten til luftventilen

25.01.2023
Jan Alexander Tubid Myhrvold
Alf Valle Eirik Kopperud
Elias

CELLE 2 – Metning av cellen

Her fyller vi cellen med vann. Vannet vil komme fra springen inn til bunnen av cellen. Ventil til sluken skal være stengt her.

OBS 5: Pass på at luftventilen på toppen er åpen – slik at luften evakueres mens vannet sakte fortrenger luften inne i cellen.

1. Identifiser vannslangen og alle relevante ventiler. Identifiser springventilen
2. Sørg for at luftventilen over er åpen
3. Sørg for at slukventilen er lukket
4. Sørg for at ventil til celletrykkspumpen er lukket.
5. Åpne forsiktig springventilen – deretter åpne forsiktig ventil til bunncellen (lukket i bilde 2).
6. Påse at ingen luftbobler ligger fanget i slangene.

Det er normalt å observere luftbobler under toppsiden av cellen.

OBS 6: Lukk forsiktig igjen bunnventilen før vannet når toppen – slik at vannet pipler ut av luftventilen. Hvis ikke, vil en sterk vannstråle skyte ut av cellen og treffe himlingen – dessuten utsettes prøven for unødvendig trykk som kan forstyrre prøven.

7. Steng igjen springventilen – men hold åpen ventil for celletrykkspumpen. Dette sørger for å mette slangene med vann før nullstilling.

25.01.2023
Jan Alexander Tubid Myhrvold
Alf Valle Eirik Kopperud
Elias

CELLE 2 – Montering av slutt av cellen

Her forbinder vi rammen med stempelet til cellen og skaper kontakt med prøven. I tillegg monteres en forskyvningsmåler.

1. Tre inn metallhodet til stempelet.
2. Juster rammen slik at den er nær hodet til stempelet med begge metallhjulene.

Nå skjer fininnstillingen slik at vi har kontakt.

3. Beveg metallhodet sidelengs, mens hele cellen og bunnsokkelen heves via GDS panelet.
4. Når metallhodet ikke kan beveges sidelengs– har vi kontakt med prøven.
5. Skru til hodet.
6. Monter forskyvningsmåleren

Nå er cellen mettet – og riggen har kontakt med stempelet, som igjen har kontakt med prøven.

25.01.2023
Jan Alexander Tubid Myhrvold
Alf Valle Eirik Kopperud
Elias

NULLSTILLING 1 – Nullstilling av celletrykk- og baktrykk-pumpene

Disse stegene består av å manuelt nullstille det faktiske trykket i celletrykk- og baktrykk-kontrollene – og følge steg for å fjerne ev. luft og mette slangene. Gjennom dette kommuniserer cellen med pumpene. Observer trykket via skjermen som står på kontrolleren.

BAKTRYKKSPUMPEN

Vi skal nå koble sammen baktrykkspumpen og cellen.

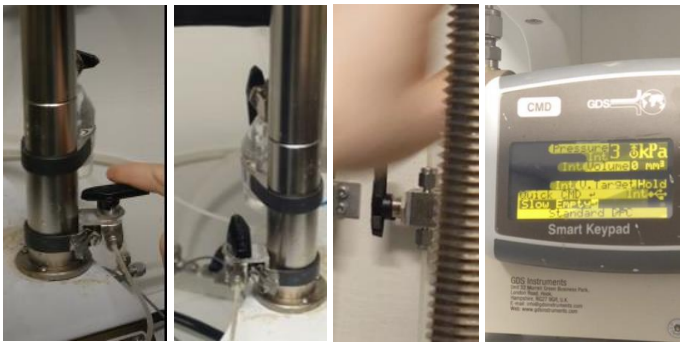

1. Steng ventil til luftfri vann
2. Åpne ventil til atmosfærisk trykk (bilde 2)
3. Åpne ventil til baktrykk (bilde 3)
4. ???????
5. Det kan hjelpe å tappe ut trykket ved å innblåsing i ventilene for å skape undertrykk.

OBS 7: Rengjør først før innblåsing!

6. Når trykket har gått ned. Steng ventil til baktrykk (bilde 3, men lukket).

25.01.2023
Jan Alexander Tubid Myhrvold
Alf Valle Eirik Kopperud
Elias

CELLETRYKKSPUMPEN

Vi skal nå koble sammen celletrykkspumpen og cellen.

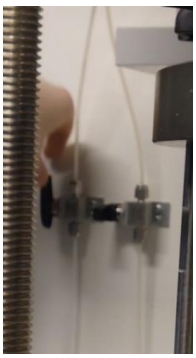

1. Steng ventil til luftfri vann
2. Åpne ventil til atmosfærisk trykk
3. Åpne ventil til celletrykk (bilde 1)
4. ???????
5. Det kan hjelpe å tappe ut trykket ved å innblåsing i ventilene for å skape undertrykk.

OBS 8: Rengjør først for innblåsing!

NULLSTILLING 2 – Nullstilling av poretrykkssensoren

Samme idé som **Nullstilling 2**

1. Se at ventilene for celletrykk og baktrykk er lukket ettersom de er nå nullstilte.
2. Ventilen til poretrykksmåleren åpnes???
3. Åpne hetten til poretrykkssensoren med en skiftenøkkel.

Det vil være en viss trykk til sensoren slik at det renner ut vann – og ev. luftbobler.

4. Mens vannet rennes skrus til hetta.

25.01.2023
Jan Alexander Tubid Myhrvold
Alf Valle Eirik Kopperud
Elias

NULLSTILLING 3 – Kommunisere med pumpene før testing

(video 64)

B-TESTING – Er prøven fullstendig mettet?

B-testing angir forholdet mellom endring i celle- og poretrykk. Celletrykket økes med ca. 10 kPa i en viss varighet. Etter dette registreres økning i poretrykk. Deretter går celletrykket ned til normalt nivå.

HVILEPERIODE – Dissipering av poreovertrykk

Selv om lasthastigheten er lav nok – kan det fremdeles være poreovertrykk i prøven. For minst mulige forstyrrelser ilegges en «hvileperiode» på ca. 40 min mellom hvert steg av testen.

DEMONTERING 1 – Fjerne celletrykket

Før vi henter ut prøven, må vi sørge for at trykket i systemet er nullstilt til atmosfærisk trykk. For sikkerhets skyld reduseres trykket trinnvis.

1. I panelet til celle- og baktrykkspumpen: Gå til Main Menu -> System Menu -> Lock/Unlock -> Unlock Device
2. På begge pumpene: Main Menu -> Set Volume / Pressure -> Set Pressure -> Target Pressure [kPa].
3. Når begge pumpene har samme inntasta verdi, trykk kjør på begge pumpene samtidig ved å trykke på den grønne knappen.
4. Gjenta steg 2 og 3 inntil trykket går mot 0. I demonstrasjonen ble det stilt fra 620 – 500 – 350 kPa.

OBS 9: Reduser trykket på begge pumpene samtidig!

25.01.2023
Jan Alexander Tubid Myhrvold
Alf Valle Eirik Kopperud
Elias

DEMONTERING 2 – Stille inn ventilene

Ventilene stilles inn slik at cellen kan tappes for vann. Trykket må være null!







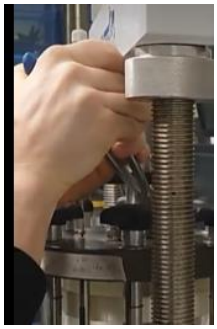


1. Baktrykksventilen lukkes.
2. Alle ventilene i baktrykksystemet lukkes.
3. Ventilen (bilde 5) lukkes deretter.
4. Lukk celletrykksventilen.
5. Åpne hetta til luftventilen på toppen av cella. Hvis det er gjenværende trykk, vil vannet sprute ut.
6. Nå kan cellen tappes ut ved å vri ventil til sluk.

25.01.2023
Jan Alexander Tubid Myhrvold
Alf Valle Eirik Kopperud
Elias

DEMONTERING 3 – Tappe ut cellen for vann

Når cellen tappes for vann, vil dette skje sakte. Dette er fordi i luftventilen øverst er ganske liten. En luftpumpe settes på for å hjelpe til tappinga.

1. Under bordet ved tastaturene ligger en luftpumpe, koblet til slange med rødfarget ventil.
2. Vri den røde ventilen opp.
3. Deretter før slangen (grå) til luftventilen (bilde 2). Sjekk at ventil til sluk er åpnet.

Appendix 6: Oedotriaxial testing experience note

Oedotriaxial testing experience note

Situation	Description
Holding pressures between test stages	On some occasions it was decided that pressures were to be held in between test stages, for instance to let excess pore pressure dissipate. This proved to present problems. When holding pressures for a longer period, the samples would experience axial displacement and the load cell would lose its contact with the sample. Furthermore, holding the pressures, and thereby not having an active stage running, meant that data were not recorded. Starting a subsequent stage, the deviatoric axial load would then sometimes have trouble with catching up to the stress changes, and there would be gaps in the recorded data.
Importance of vertical pervious drainage paper	The importance of vertical pervious drainage paper on drainage, and thereby consolidation time, is discussed in within the thesis. In practice, it also shown itself as an important factor of success. Although the authors were aware that pervious paper should be mounted along the periphery of the samples, its full importance was not understood until after the seventh sample was mounted. The seventh sample did not get its paper mounted optimally, with the result being problematic pore pressure response throughout the test. For the eighth sample, it was taken care that the paper was mounted to the best of the authors' abilities. The paper sat snug along the periphery of the sample, and were in contact with both the pervious stone on the pedestal and on the top cap. The resulting pore pressure response was much less, and a more successful consolidation were conducted at a faster rate.
Axial displacement transducer hitting mounting screws	On one occasion, the axial displacement transducer hit one of the mounting screws of the Perspex cell. The transducer was then mounted as is standard to the triaxial cell. Upon further examination, it was found that this setup would only track about 50% of the range of the displacement transducer, before hitting the screw. For the stress levels used in this thesis, it was found that about 90% of the range would be needed. The solution was found in mounting the displacement transducer on the loading frame, circumventing the mounting screws of the Perspex cell.
Load cell transducer capacity	For the majority of the tests, a load cell transducer with a capacity of 1.0 kN was used. A common problem with this transducer was that the capacity was met, and thereafter gave unreliable readings. A load cell transducer with a capacity of 50 kN was later mounted. The heightened load capacity was welcome, although it came with the expense of lower resolution of the recorded values.

Appendix 7: PLAXIS model information

Overview of discretised layers based on ice sheet presence. Unit IIIA is highlighted.

Lithology	Unit	Depth [m]	Time interval [ka]	Ice sheets
L1	I	0 – 16.5	11 – 17	**No**
L2	IIA	16.5 – 30.25	17 – 27	**Yes**
		30.25 – 44	27 – 37	**No**
	IIB	44 – 50.6	37 – 47	**Yes**
		50.6 – 64	47 – 67	**No**
	IIC	64 – 68.1	67 – 83	**Yes**
		68.1 – 74	83 – 106	**No**
L3	IIIA	74 – 110	106 – 123	**No**
L4	IIIB	110 – 110.31	123 – 127	**No**
		110.31 – 113.25	127 – 183	**Yes**
		113.25 – 116.8	183 – 260	**No**
		116.8 – 119.5	260 – 303	**Yes**
		119.5 – 121.4	303 – 340	**No**
		121.4 – 123.1	340 – 373	**Yes**
		123.1 – 126.17	373 – 430	**No**
		126.17 – 129.25	430 – 490	**Yes**
		129.25 – 135	490 – 600	**No**
L5	IV	135 – 170	600 – 1100	**Yes**
L6	IV	170 – 201	1100 – 3070	**No**
L7	V	201 – 220	3070 – 15947	No information

All phases based on the overview above, with estimated time interval and loading. Unit IIIA is highlighted in red.

Unit	Depth [m]	Time interval [day]	Loading [kPa]
I	0 – 16.5	2.19 E6	**None**
IIA	16.5 – 30.25	1.824 E6	Unloading
		1.824 E6	220
	30.25 – 44	3.65 E6	**None**
IIB	44 – 50.6	1.825 E6	Unloading
		1.825 E6	250
	50.6 – 64	7.3 E6	**None**
IIC	64 – 68.1	2.920 E6	Unloading
		2.920 E6	500
	68.1 – 74	8.395 E6	**None**
IIIA	74 – 110	6.205 E6	10
IIIB	110 – 110.31	1.46 E6	**None**
	110.31 – 113.25	20.44 E6	Unloading
		20.44 E6	2000
	113.25 – 116.8	24.46 E6	**None**
	116.8 – 119.5	17.16 E6	Unloading
		19.35 E6	2500
	119.5 – 121.4	13.51 E6	**None**
	121.4 – 123.1	12.05 E6	Unloading
		12.05 E6	2800
	123.1 – 126.17	20.81 E6	**None**
	126.17 – 129.25	21.9 E6	Unloading
		21.9 E6	3000
	129.25 – 135	40.15 E6	**None**
IV	135 – 170	182.5 E6	Unloading
		182.5 E6	4000
IV	170 – 201	719 E6	**None**
V	201 – 220	4.7 E9	No information

All units had $\psi = 0$. Cohesion was set to 10 due for numerical reasons. Unit weight (γ) applies for saturated and unsaturated soil. The pore pressures are reflected in the unit weight.

Unit	**Model parameters from SSC (Jalali, 2022)**								
	λ^*	κ^*	$\mu^* \cdot 10^{-3}$	ν_{ur}	ϕ	K_0^{NC}	γ [kN/m^3]	< 2 µm [%]	$2 - 50$ µm [%]
I	0.08877	0.01969	0.0006908	0.3	29	0.6	4.96	40	45
IIA	0.08877	0.01969	0.691	0.3	29	0.37	10.21	27	38
	0.02785	0.02202	0.0583	0.2	28.5	0.55	10.74	27	38
IIB	0.02828	0.00818	0.2	0.3	29	0.6	11.60	23	27
	0.04902	0.01081	0.38	0.3	29	0.6	11.75	23	26
IIC	0.06029	0.02097	0.39	0.3	28.5	0.6	11.43	23	37
IIIA	0.02592	0.01575	0.00113	0.46	28.5	0.8	12.81	14	43
IIIB	0.02534	0.02120	0.041	0.45	26.5	0.8	11.00	27	38
IV	0.0565	0.01334	0.41	0.48	28.55	0.8	8.52	67	28
IV	0.014086	0.00616	0.079	0.3	30.6	0.6	7.11	77	18
V	0.0111	0.0023	0.088	0.27	30.6	0.63	8.35	66	29

Appendix 8: PLAXIS cross section data – OCR and K_0

Troll (8903)					
Jalali			Myhrvold & Kopperud		
SSC			HVMCC		
Y [m]	OCR [-]	K0 [-]	Y [m]	OCR [-]	K0 [-]
0	-0,396	34,515	0	-0,263	7,057
5,44	1,27	0,339	5,44	1,276	0,339
5,44	1,27	0,338	5,44	1,277	0,339
8,88	1,218	0,433	8,88	1,111	0,434
8,88	1,218	0,435	8,88	1,238	0,433
8,88	1,218	0,435	8,88	1,237	0,433
8,88	1,217	0,435	8,88	1,213	0,433
8,88	1,217	0,435	8,88	1,213	0,433
8,88	1,219	0,439	8,88	1,001	0,453
11,81	1,198	0,475	11,81	1,195	0,472
11,81	1,198	0,474	11,81	1,195	0,471
14,3	1,188	0,494	14,3	1,186	0,493
14,3	1,189	0,495	14,3	1,186	0,494
14,3	1,189	0,495	14,3	1,186	0,494
14,3	1,188	0,495	14,3	1,185	0,495
14,3	1,188	0,495	14,3	1,185	0,495
14,3	1,189	0,499	14,3	1,186	0,494
16,5	1,182	0,51	16,5	1,179	0,506
16,5	3,062	0,536	16,5	3,19	0,539
17,2	2,907	0,529	17,2	3,023	0,532
17,2	2,907	0,528	17,2	3,022	0,532
18,2	2,722	0,52	18,2	2,823	0,523
18,2	2,723	0,52	18,2	2,823	0,523
20,64	2,393	0,505	20,64	2,471	0,508
20,64	2,393	0,505	20,64	2,471	0,508
20,91	2,365	0,504	20,91	2,441	0,506
20,91	2,365	0,504	20,91	2,441	0,506
21,07	2,347	0,503	21,07	2,428	0,506
21,07	2,35	0,503	21,07	2,426	0,505
24,49	1,964	0,488	24,49	1,966	0,489
24,49	1,963	0,488	24,49	1,954	0,488
30,25	1,613	0,474	30,25	1,712	0,479
30,25	1,638	0,68	30,25	1,754	0,685
35,97	1,668	0,581	35,97	1,711	0,584
35,97	1,677	0,58	35,97	1,709	0,583
39,41	1,604	0,592	39,41	1,643	0,593
39,41	1,605	0,593	39,41	1,643	0,593
39,58	1,602	0,593	39,58	1,64	0,594
39,58	1,601	0,593	39,58	1,641	0,594
39,84	1,597	0,594	39,84	1,636	0,595
39,84	1,597	0,594	39,84	1,636	0,595
42,32	1,559	0,604	42,32	1,595	0,605
42,32	1,559	0,604	42,32	1,595	0,605
43,34	1,545	0,607	43,34	1,58	0,608
43,34	1,545	0,607	43,34	1,58	0,608
44	1,536	0,609	44	1,571	0,61

44	1,583	0,64	44	1,585	0,639
45,03	1,57	0,638	45,03	1,571	0,638
45,03	1,57	0,638	45,03	1,571	0,638
45,86	1,559	0,637	45,86	1,561	0,637
45,86	1,559	0,637	45,86	1,561	0,637
50,6	1,509	0,633	50,6	1,51	0,633
50,6	1,506	0,634	50,6	1,508	0,634
56,19	1,46	0,63	56,19	1,461	0,63
56,19	1,46	0,63	56,19	1,461	0,63
59,53	1,438	0,628	59,53	1,439	0,628
59,53	1,438	0,628	59,53	1,439	0,628
59,7	1,436	0,628	59,7	1,438	0,628
59,7	1,436	0,628	59,7	1,438	0,628
59,97	1,435	0,628	59,97	1,436	0,628
59,97	1,435	0,628	59,97	1,436	0,627
62,34	1,421	0,626	62,34	1,422	0,626
62,34	1,421	0,626	62,34	1,422	0,626
63,31	1,416	0,626	63,31	1,417	0,626
63,31	1,416	0,626	63,31	1,417	0,626
64	1,412	0,625	64	1,413	0,625
64	1,418	0,603	64	1,419	0,604
68,1	1,396	0,621	68,1	1,397	0,621
68,1	1,396	0,622	68,1	1,397	0,622
74	1,372	0,62	74	1,373	0,62
74,01	6,031	0,785	74	5,885	0,987
79,42	5,992	0,786	81,07	5,845	0,978
79,42	5,992	0,786	81,07	5,84	0,978
84,82	5,965	0,788	81,07	5,84	0,978
84,82	5,965	0,788	81,07	5,841	0,978
84,84	5,965	0,788	81,07	5,841	0,978
84,84	5,965	0,788	81,07	5,843	0,978
84,86	5,965	0,788	88,14	5,807	0,971
84,86	5,965	0,788	88,14	5,807	0,971
90,25	5,947	0,789	95,22	5,779	0,964
90,25	5,947	0,789	95,22	5,779	0,964
93,63	5,94	0,79	95,22	5,779	0,964
93,63	5,94	0,79	95,22	5,779	0,964
93,64	5,94	0,79	95,22	5,779	0,964
93,64	5,94	0,79	95,22	5,779	0,964
93,66	5,94	0,79	100,37	5,762	0,96
93,66	5,94	0,79	100,37	5,762	0,96
96,52	5,935	0,791	100,37	5,762	0,96
96,52	5,936	0,791	100,37	5,762	0,96
98,87	5,933	0,792	103,59	5,753	0,958
98,87	5,933	0,792	103,59	5,753	0,958
98,93	5,933	0,792	107,3	5,745	0,955
98,93	5,933	0,792	107,3	5,745	0,955
98,99	5,933	0,792	107,3	5,745	0,955
98,99	5,933	0,792	107,3	5,745	0,955
100,99	5,931	0,792	107,3	5,745	0,955

100,99	5,931	0,792	107,3	5,745	0,955
102,53	5,931	0,792	110	5,739	0,954
102,53	5,931	0,792	110	1,282	0,795
102,79	5,93	0,792	110,31	1,282	0,795
102,79	5,93	0,792	110,31	1,693	0,808
103,01	5,93	0,792	110,51	1,692	0,807
103,01	5,93	0,792	110,51	1,692	0,807
104,42	5,93	0,793	110,72	1,692	0,806
104,42	5,93	0,793	110,72	1,692	0,806
104,98	5,93	0,793	111,41	1,689	0,803
104,98	5,93	0,793	111,41	1,689	0,803
105,66	5,93	0,793	111,62	1,688	0,802
105,66	5,93	0,793	111,62	1,688	0,802
106,48	5,93	0,793	111,73	1,688	0,802
106,48	5,93	0,793	111,73	1,688	0,802
106,69	5,93	0,793	113,25	1,683	0,796
106,69	5,93	0,793	113,25	1,683	0,796
107,22	5,93	0,793	115,16	1,673	0,793
107,22	5,93	0,793	115,16	1,674	0,793
107,57	5,93	0,793	115,16	1,674	0,793
107,57	5,93	0,793	115,16	1,674	0,793
107,72	5,93	0,793	115,16	1,674	0,793
107,72	5,93	0,793	115,16	1,674	0,793
108,39	5,93	0,793	116,8	1,665	0,792
108,39	5,93	0,793	116,8	2,01	0,808
108,91	5,931	0,793	118,15	2,004	0,803
108,91	5,931	0,793	118,15	2,003	0,803
109,15	5,931	0,793	118,15	2,003	0,803
109,15	5,931	0,793	118,15	2,003	0,803
109,59	5,931	0,793	118,15	2,003	0,803
109,59	5,931	0,793	118,15	2,003	0,803
109,66	5,931	0,794	119,5	1,996	0,798
109,66	5,931	0,794	119,5	1,996	0,798
110	5,931	0,794	120,45	1,991	0,795
110,01	1,281	0,801	120,45	1,991	0,795
110,16	1,281	0,793	121,4	1,985	0,793
110,16	1,281	0,793	121,4	2,278	0,807
110,31	1,281	0,794	122,11	2,272	0,805
110,31	1,693	0,808	122,11	2,273	0,805
110,51	1,692	0,807	123,1	2,265	0,801
110,51	1,692	0,807	123,1	2,265	0,801
110,72	1,691	0,806	124,73	2,251	0,796
110,72	1,692	0,806	124,73	2,254	0,796
111,41	1,689	0,803	124,73	2,254	0,796
111,41	1,689	0,803	124,73	2,253	0,796
111,62	1,689	0,803	124,73	2,253	0,796
111,62	1,688	0,802	124,73	2,252	0,796
111,73	1,688	0,802	126,2	2,242	0,791
111,73	1,688	0,802	126,2	2,44	0,806
113,25	1,683	0,796	127,29	2,433	0,802

113,25	1,683	0,796	127,29	2,43	0,802
115,16	1,673	0,793	127,29	2,43	0,802
115,16	1,674	0,793	127,29	2,431	0,802
115,16	1,674	0,793	129,25	2,414	0,796
115,16	1,674	0,793	129,25	2,412	0,796
115,16	1,674	0,793	132,82	2,381	0,789
115,16	1,674	0,793	132,82	2,39	0,788
116,8	1,665	0,792	132,82	2,39	0,788
116,8	2,01	0,808	132,82	2,383	0,785
118,15	2,004	0,803	135	2,364	0,786
118,15	2,003	0,803	135	3,103	0,915
118,15	2,003	0,803	135,91	3,093	0,917
118,15	2,003	0,803	135,91	3,175	0,915
118,15	2,003	0,803	136,51	3,051	0,898
118,15	2,003	0,803	136,51	3,121	0,891
119,5	1,996	0,798	137,74	3,082	0,891
119,5	1,996	0,798	137,74	3,106	0,89
120,45	1,991	0,795	138,79	3,101	0,894
120,45	1,991	0,795	138,79	3,066	0,895
121,4	1,985	0,793	140,4	3,08	0,887
121,4	2,278	0,807	140,4	3,077	0,894
122,11	2,272	0,805	142,12	2,982	0,867
122,11	2,273	0,805	142,12	3,017	0,907
123,1	2,265	0,801	142,91	3,079	0,877
123,1	2,265	0,801	142,91	3,184	0,91
124,73	2,251	0,796	145,04	3,023	0,884
124,73	2,254	0,796	145,04	3,034	0,871
124,73	2,254	0,796	146,29	3,048	0,882
124,73	2,253	0,796	146,29	3,025	0,875
124,73	2,253	0,796	149,03	3,048	0,879
124,73	2,252	0,796	149,03	3,047	0,874
126,2	2,242	0,791	149,77	2,982	0,863
126,2	2,44	0,806	149,77	2,986	0,862
127,29	2,433	0,802	152,52	2,968	0,861
127,29	2,43	0,802	152,52	2,976	0,857
127,29	2,43	0,802	158,13	3,047	0,839
127,29	2,431	0,802	158,13	3,037	0,915
129,25	2,414	0,796	158,36	2,986	0,909
129,25	2,412	0,796	158,36	3,454	0,893
132,82	2,381	0,789	158,56	3,371	0,887
132,82	2,39	0,788	158,56	2,85	0,869
132,82	2,39	0,788	164,18	2,96	0,823
132,82	2,383	0,785	164,18	2,973	0,828
135	2,364	0,786	170	2,588	0,796
135	3,103	0,915	170	2,851	0,85
135,91	3,093	0,917	175,3	2,792	0,834
135,91	3,175	0,915	180,61	2,761	0,827
136,51	3,051	0,898	180,61	2,761	0,824
136,51	3,121	0,891	180,61	2,761	0,824
137,74	3,082	0,891	180,61	2,762	0,825

137,74	3,106	0,89	185,5	2,736	0,82
138,79	3,101	0,894	190,4	2,712	0,816
138,79	3,066	0,895	190,4	2,712	0,816
140,4	3,08	0,887	190,4	2,712	0,816
140,4	3,077	0,894	190,4	2,712	0,816
142,12	2,982	0,867	195,7	2,686	0,812
142,12	3,017	0,907	201	2,661	0,809
142,91	3,079	0,877	201	2,455	0,957
142,91	3,184	0,91	207,31	2,432	0,949
145,04	3,023	0,884	207,31	2,432	0,949
145,04	3,034	0,871	210,76	2,42	0,945
146,29	3,048	0,882	210,76	2,42	0,945
146,29	3,025	0,875	214,22	2,408	0,941
149,03	3,049	0,879	214,22	2,408	0,941
149,03	3,047	0,874	220	2,388	0,934
149,77	2,982	0,863			
149,77	2,986	0,862			
152,52	2,968	0,861			
152,52	2,976	0,857			
158,13	3,047	0,839			
158,13	3,037	0,915			
158,36	2,986	0,909			
158,36	3,454	0,893			
158,56	3,371	0,887			
158,56	2,85	0,869			
164,18	2,96	0,823			
164,18	2,973	0,828			
170	2,588	0,796			
170	2,851	0,85			
175,3	2,792	0,834			
180,61	2,761	0,827			
180,61	2,761	0,824			
180,61	2,761	0,824			
180,61	2,762	0,825			
185,5	2,736	0,82			
190,4	2,712	0,816			
190,4	2,712	0,816			
190,4	2,712	0,816			
190,4	2,712	0,816			
195,7	2,686	0,812			
201	2,661	0,809			
201	2,455	0,957			
207,31	2,432	0,949			
207,31	2,432	0,949			
210,76	2,42	0,945			
210,76	2,42	0,945			
214,22	2,408	0,941			
214,22	2,408	0,941			
220	2,388	0,934			

Appendix 9A: PLAXIS Numerical Results. Varying OCR_0 with constant K_0^{NC}, μ.

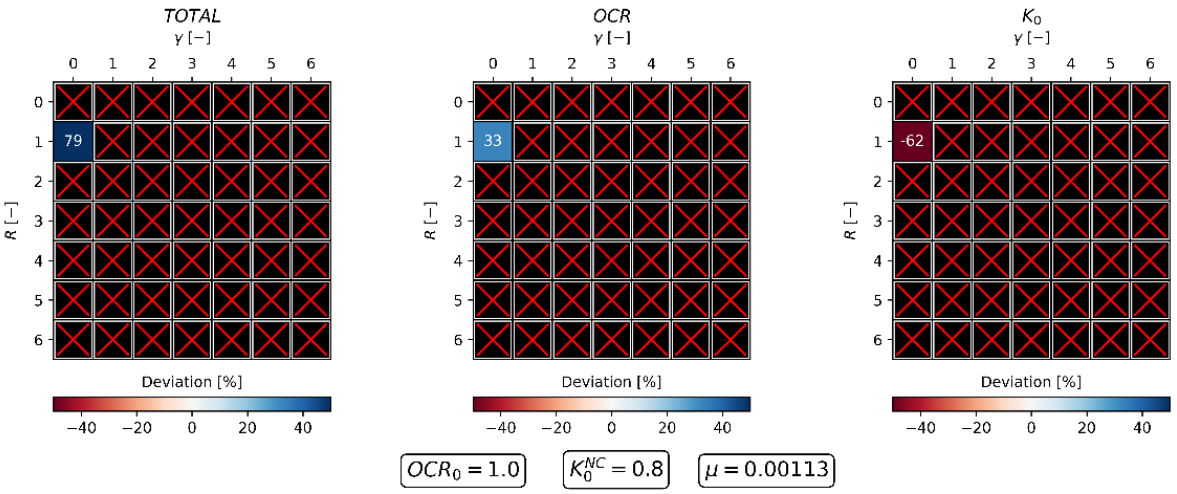

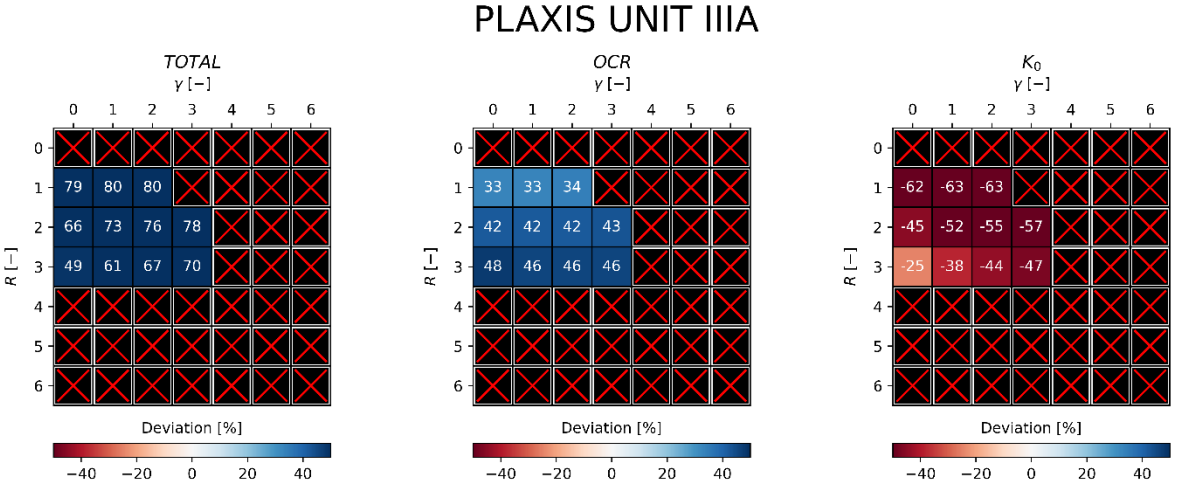

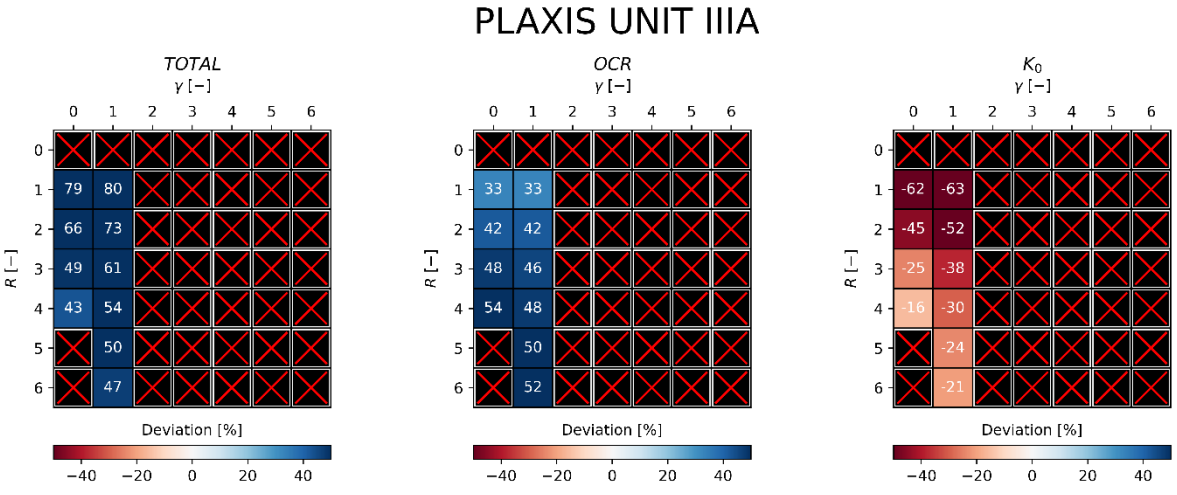

The crossed fields represent numerical divergence on the set of variating parameters with set parameter in boxes. The color bar represents the total percentile deviation from the field data.

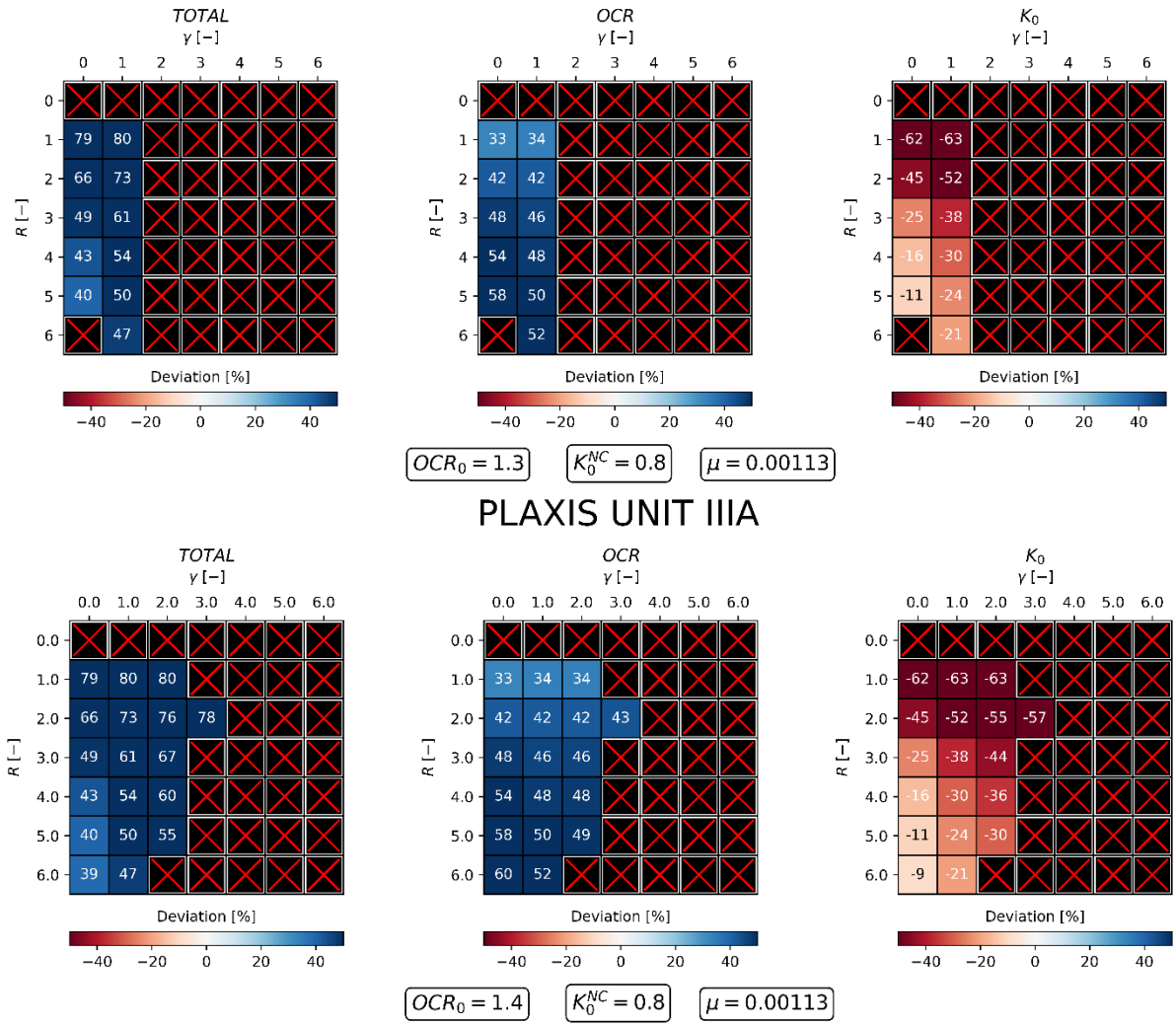

The crossed fields represent numerical divergence on the set of variating parameters with set parameter in boxes. The color bar represents the total percentile deviation from the field data.

Appendix 9B: PLAXIS Numerical Results. Further inspection of A.

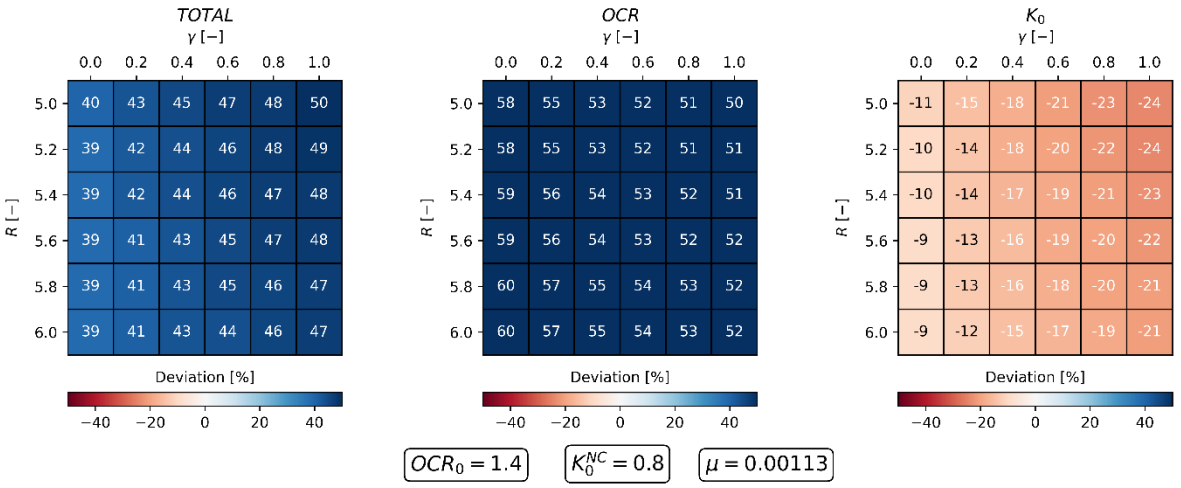

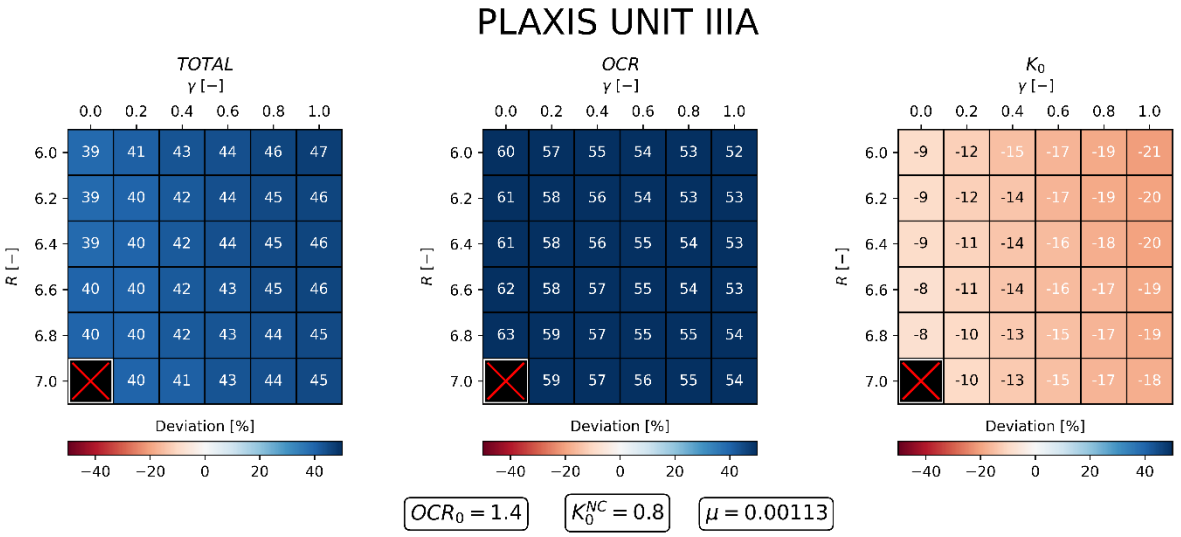

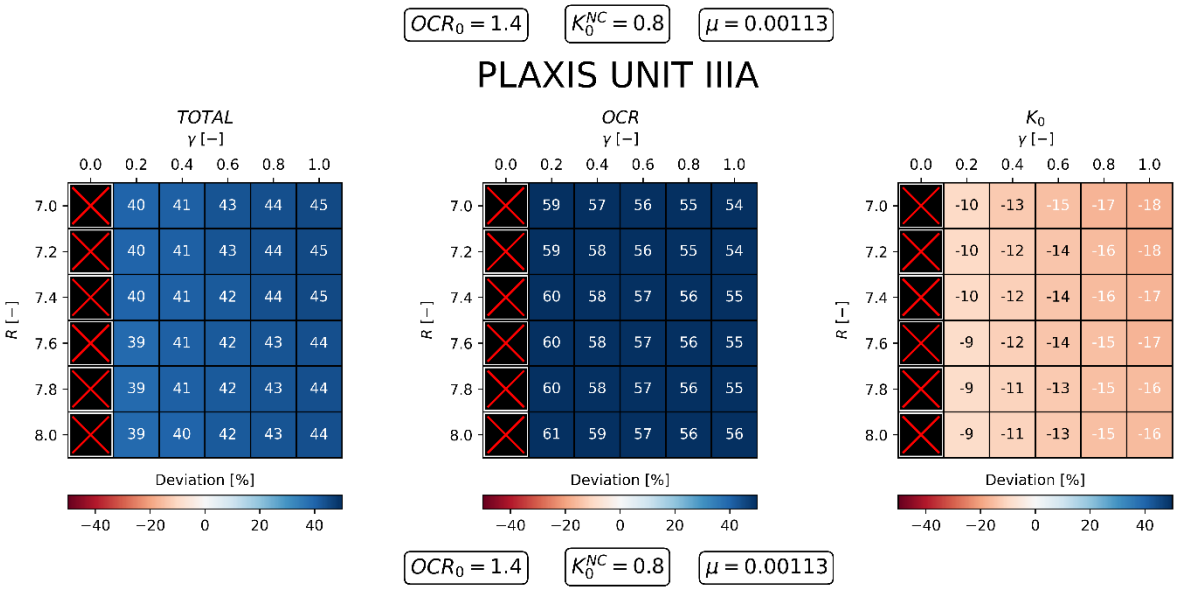

The crossed fields represent numerical divergence on the set of variating parameters with set parameter in boxes. The color bar represents the total percentile deviation from the field data.

PLAXIS UNIT IIIA

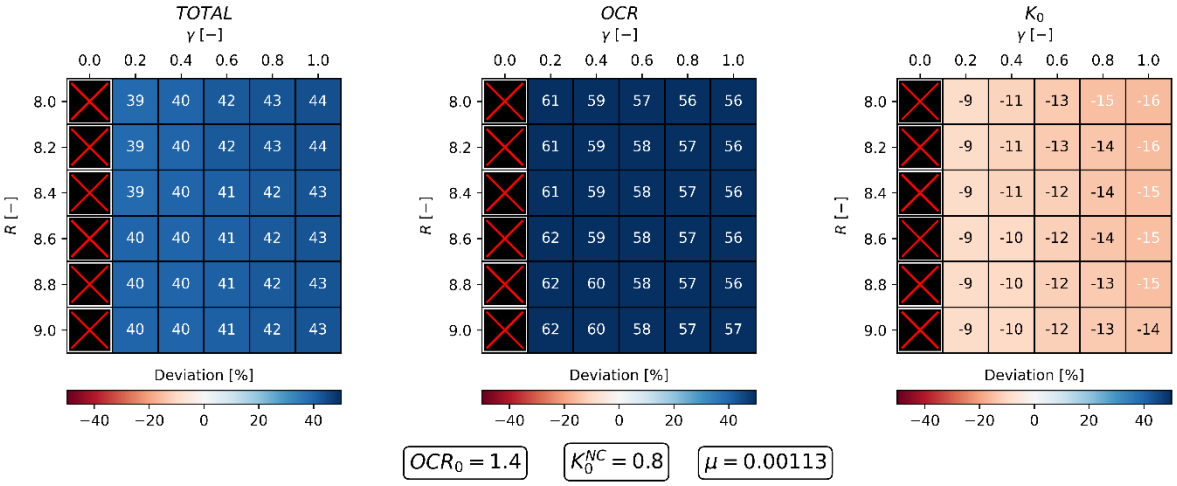

$OCR_0 = 1.4$ $K_0^{NC} = 0.8$ $\mu = 0.00113$

The crossed fields represent numerical divergence on the set of variating parameters with set parameter in boxes. The color bar represents the total percentile deviation from the field data.

Appendix 9C: PLAXIS Numerical Results. Varying K_0^{NC} with constant OCR_0, μ.

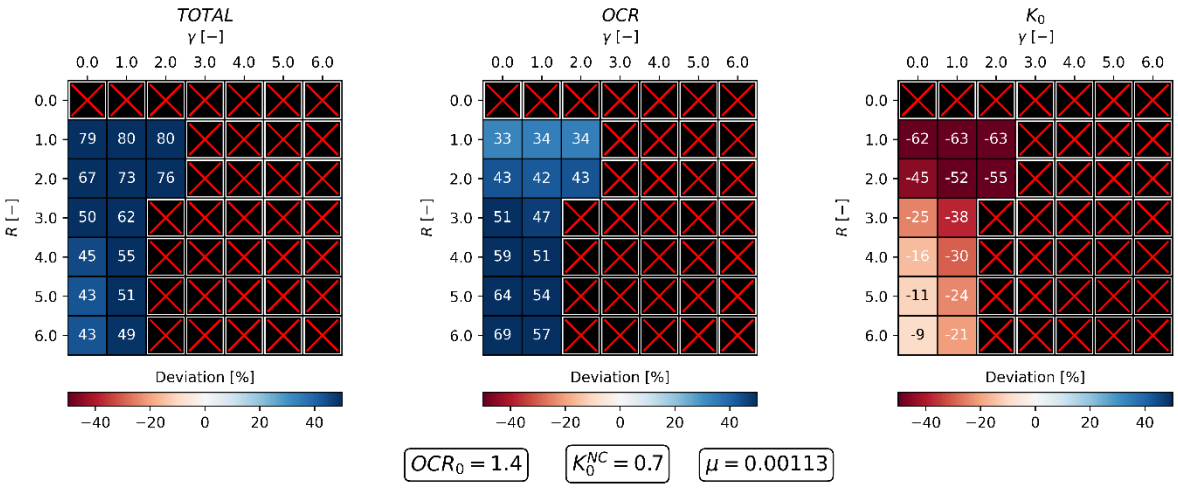

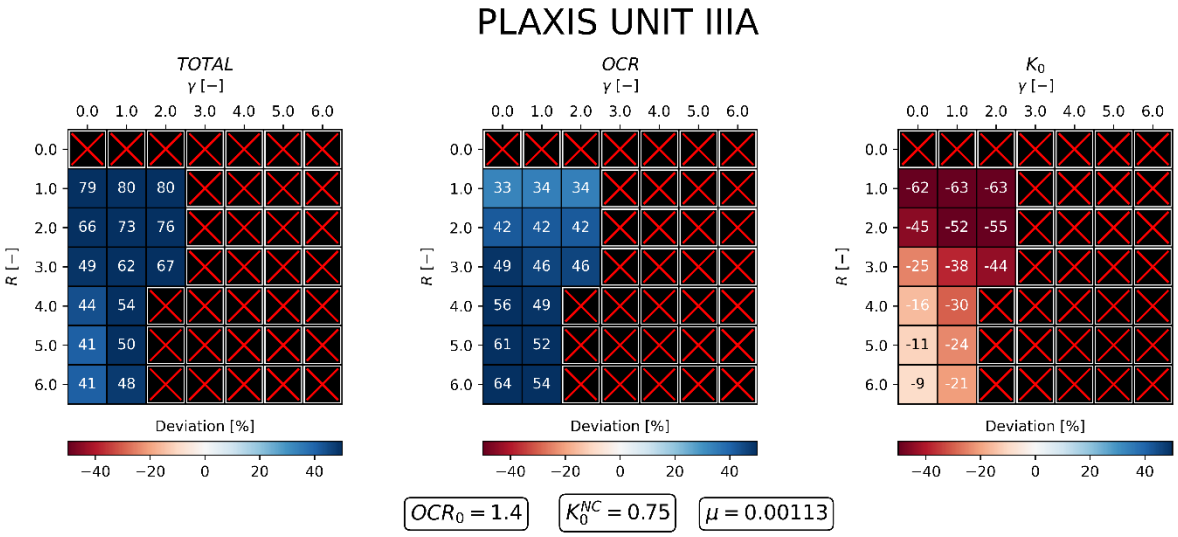

The crossed fields represent numerical divergence on the set of variating parameters with set parameter in boxes. The color bar represents the total percentile deviation from the field data.

PLAXIS UNIT IIIA

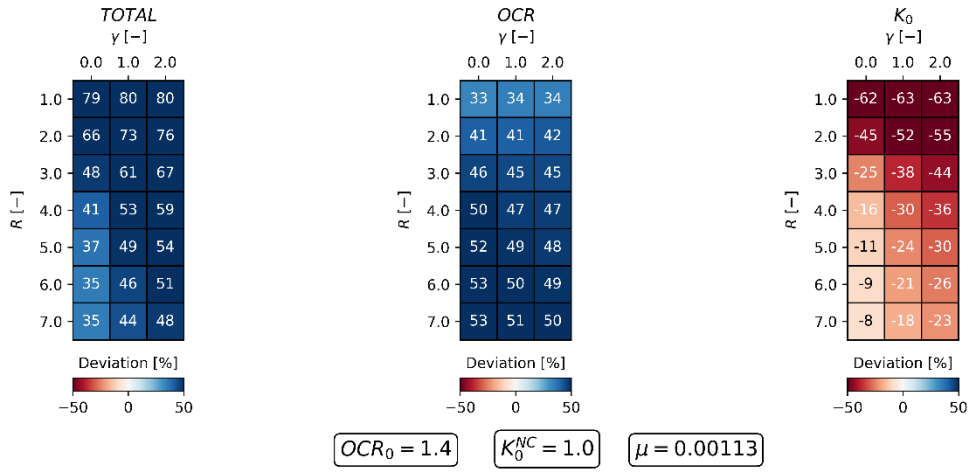

$OCR_0 = 1.4$ $K_0^{NC} = 1.0$ $\mu = 0.00113$

PLAXIS UNIT IIIA

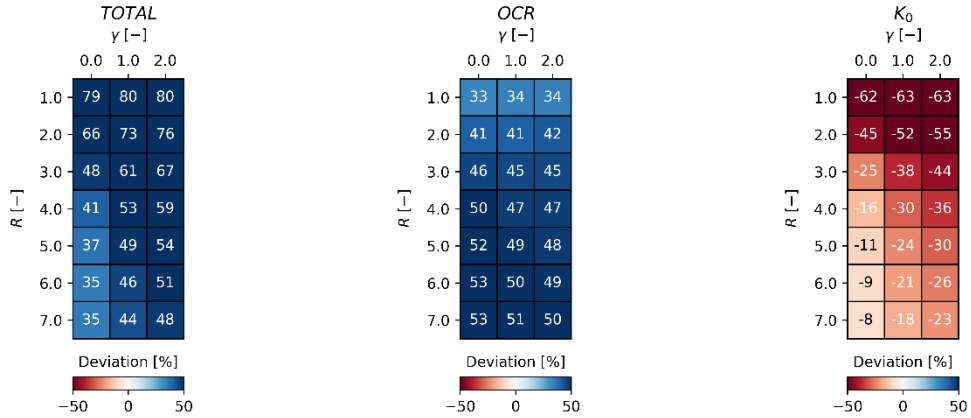

$OCR_0 = 1.4$ $K_0^{NC} = 1.0$ $\mu = 0.00113$

The crossed fields represent numerical divergence on the set of variating parameters with set parameter in boxes. The color bar represents the total percentile deviation from the field data.

Appendix 9D: PLAXIS Numerical Results. Varying μ and OCR_0 with constant K_0^{NC}.

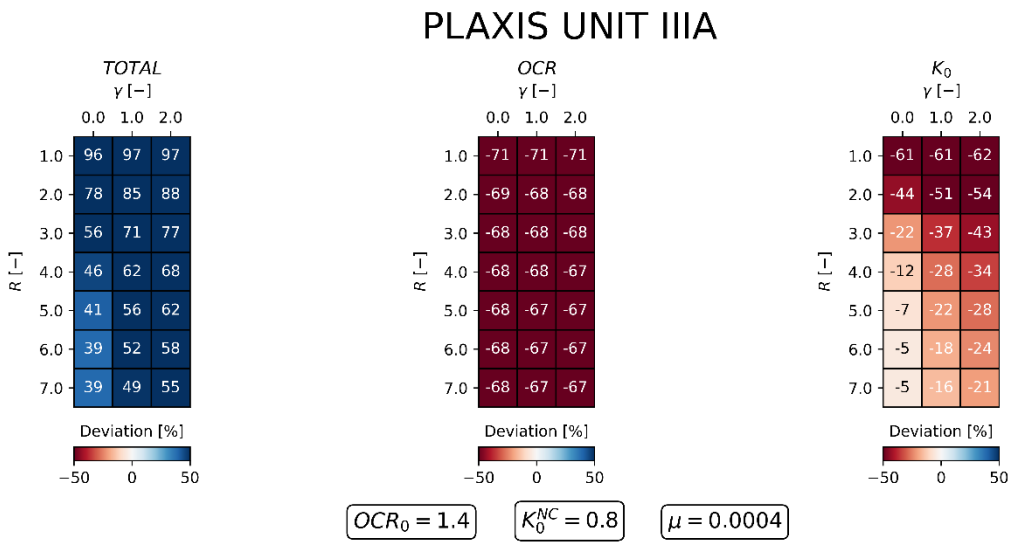

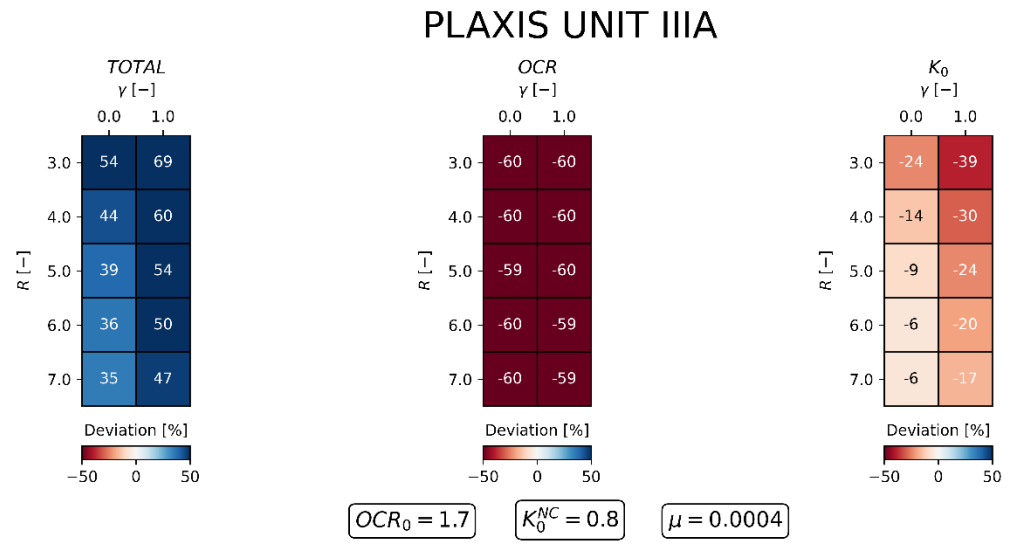

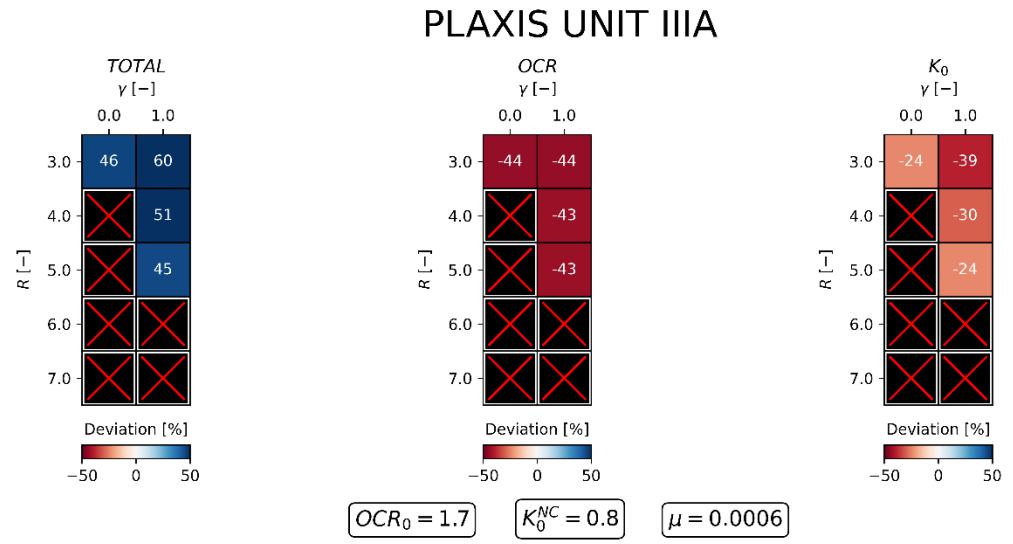

The crossed fields represent numerical divergence on the set of variating parameters with set parameter in boxes. The color bar represents the total percentile deviation from the field data.

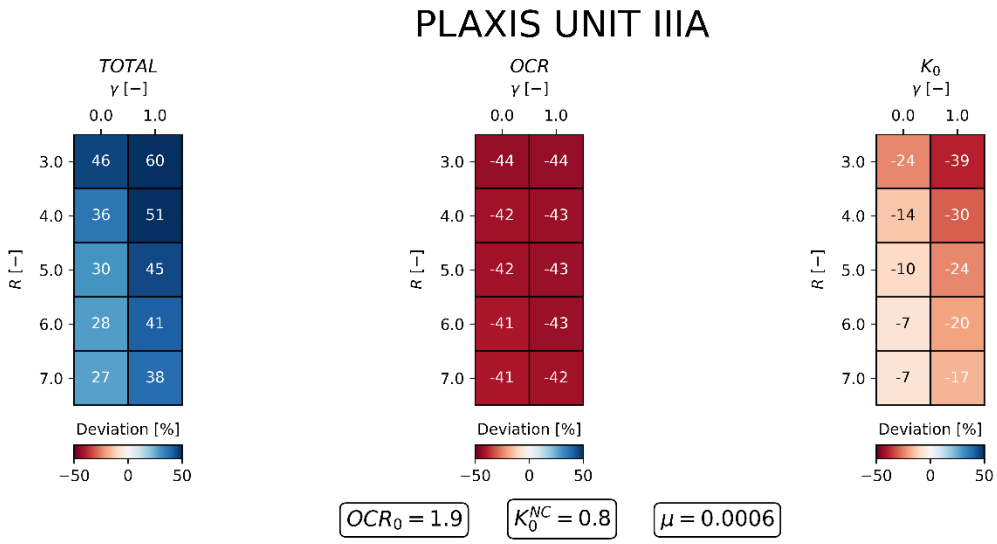

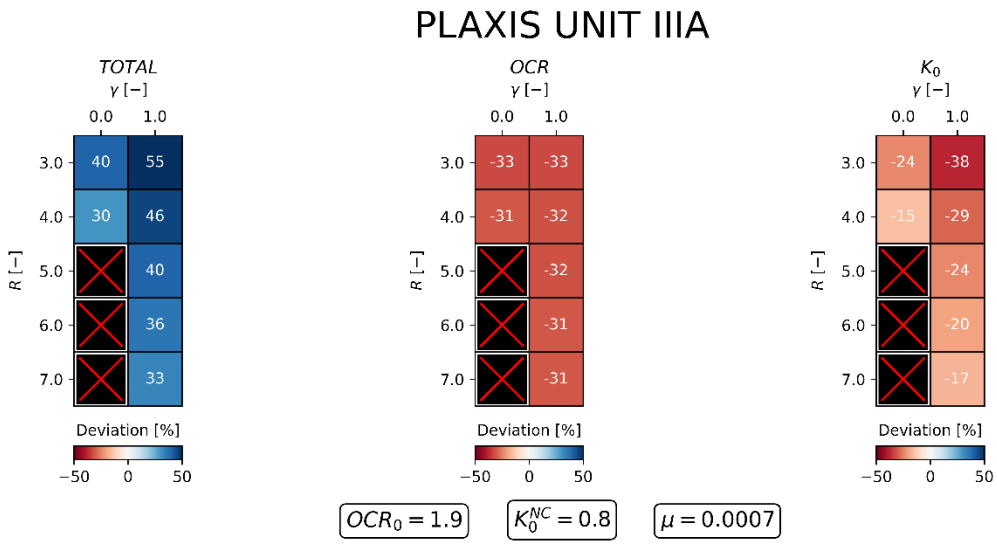

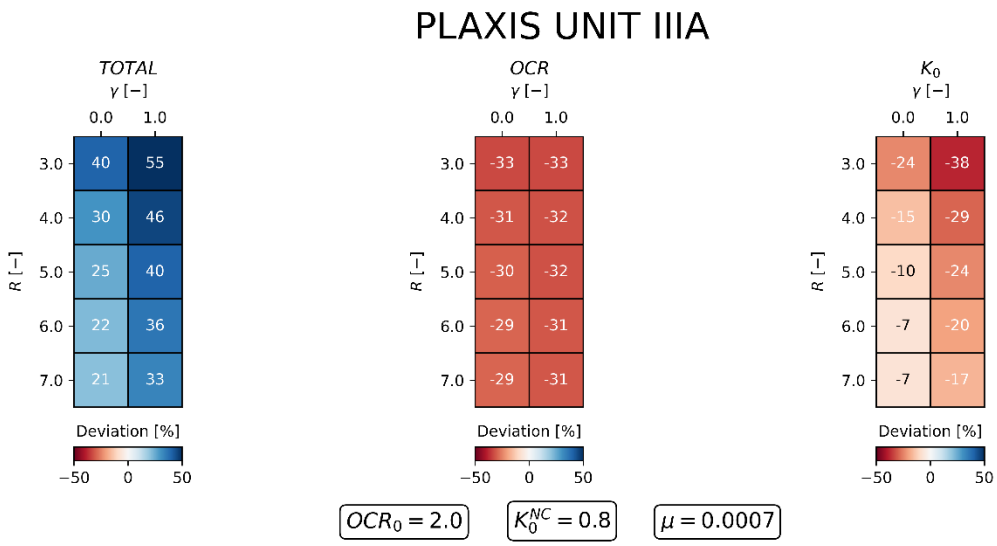

The crossed fields represent numerical divergence on the set of variating parameters with set parameter in boxes. The color bar represents the total percentile deviation from the field data.

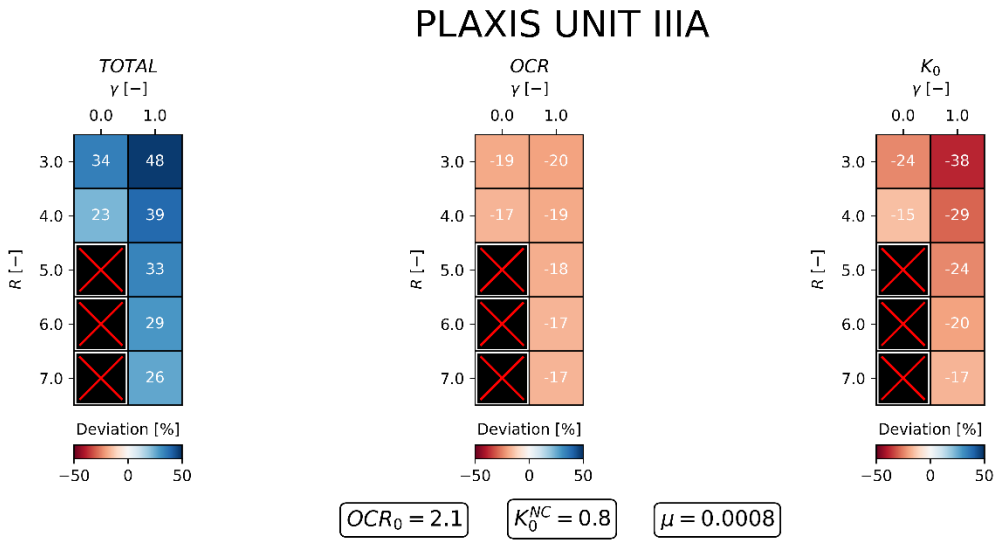

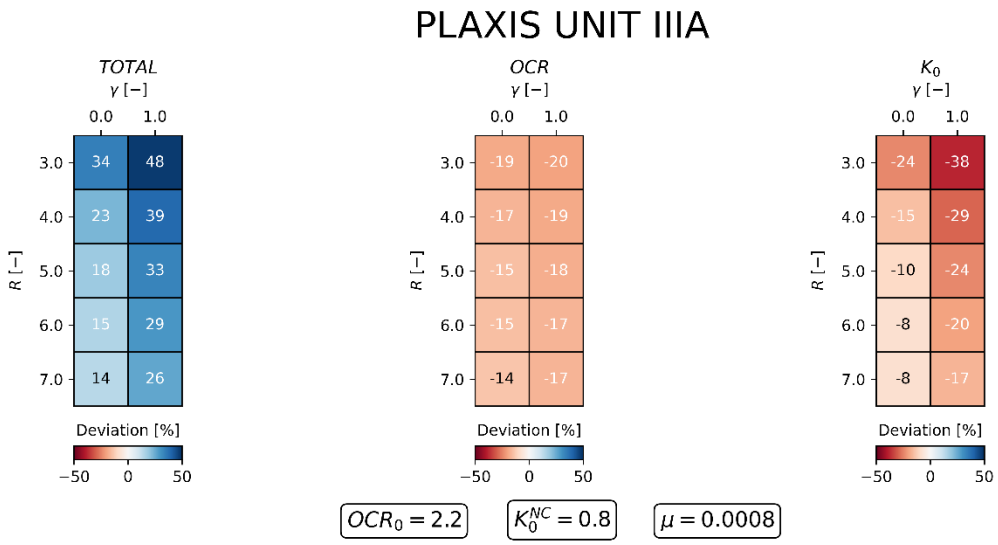

The crossed fields represent numerical divergence on the set of variating parameters with set parameter in boxes. The color bar represents the total percentile deviation from the field data.

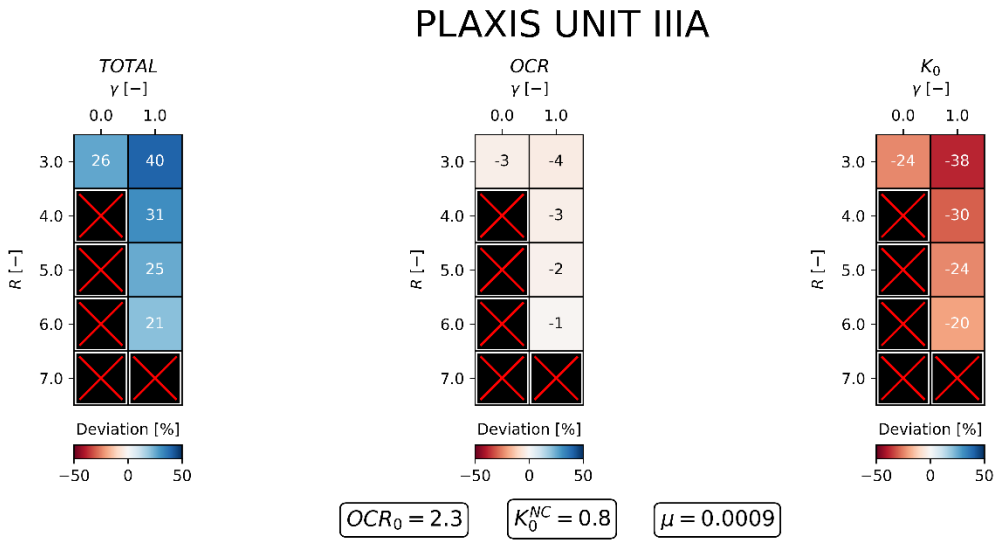

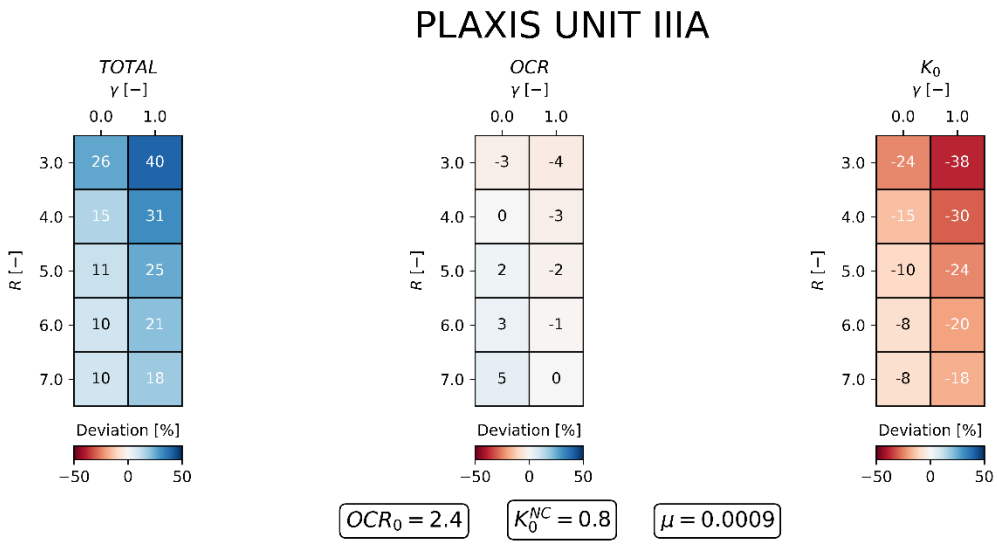

The crossed fields represent numerical divergence on the set of variating parameters with set parameter in boxes. The color bar represents the total percentile deviation from the field data.

Appendix 9E: PLAXIS Numerical Results. Debug log 1 of failed calculation.

Excerpt from debug-file of failed calculation

$\mu = 0.0009$ $R = 2$ $\gamma = 0$

Stvar0 = $[OCR, e, Flag, p_0, r]$
Sig0 = $[\sigma'_{xx,0}, \sigma'_{yy,0}, \sigma'_{zz,0}, \sigma'_{xy,0}, \sigma'_{yz,0} = 0, \sigma'_{zx,0} = 0,\ldots,]$
IDTask = 2 = Calculate constitutive stresses.
nStat = Number of state variables
UDSM = User-Defined Soil Model = HVMCC

$$\boldsymbol{OCR_0 = 2.2}$$

```
NSTEP=   1
 100A : dT :    1551250.00000000       6035917568.54789
 LoadAc start Active
   0.000E+00  0.000E+00  0.000E+00   1.000E+00  0.000E+00  0.000E+00
   0.000E+00  0.000E+00  0.000E+00   0.000E+00  0.000E+00
 LoadAc end   Active
   0.000E+00  0.000E+00  0.000E+00   1.000E+00  0.000E+00  0.000E+00
   0.000E+00  0.000E+00  0.000E+00   0.000E+00  0.000E+00
Active   0.000E+00  0.000E+00  0.000E+00   1.000E+00  0.000E+00  0.000E+00
       0.000E+00  0.000E+00  0.000E+00   0.000E+00  0.000E+00
 iel,prev:       1214       1458          0          6
 SumG:    393479706.699562
 AA dT :    1551250.00000000
 BB dT :    1551250.00000000
 Before MakMat :    1551250.00000000       T
 iTest, MakMat          0 T
Time 11:11:44         2.00
 dTime in matrix :    1551250.00000000
 FMAMAT T   1551250.00000000
 iel,prev:       1214       1458          0          3
 SymDif/Sum   :   4.06869E-06  4.71677E+10  1.06021E+10
 Determine_Sp_i0A_i1A          3           94107472          1922471716
       5453         20
          1          0        115
      33021       1108       5453
 dasum AA:   28521709891.9264
 dasum AA:   27041673094.2564
 bound3n:          4
 Time for forming matrix:
Time 11:11:44         0.00
 Process ID, MemMB : 37552 187
 PASSMBMEM 187
  iMat     :          3
 iUsePardiso:          1
 iUsePardiso:          1
 Fill_Pard T          1
 try SpMtx
 Size iiA:       43847      63419
 Size jjA:     1225741     154877
 Size  AA:     1045749     154877
 nnz:     1045749
 Size ia_Pard:       63419      43847
 Size ja_Pard:     1045749    1225741
 Size  a_Pard:     1045749    1045749
 end fill          4
 size amat  :    18651125
```

```
 size a_pard:     1045749
 dasum a_Pard:   27041673094.2564         1032024   27041673094.2597
 Filter SpMtx:           5
      iUsePardiso:          1
 GetFreeMem
 Tot. Int.:     16119096  kB       15741  Mb
 Internal :      5612952  kB        5481  Mb free
 InSwap   :      7872180  kB        7687  Mb free
 Total    :     13485132  kB       13169  Mb free
 mkl_get_max_threads          3
 n_in, nthr :        43846          2     1045750
 iParm(2):           2
 iparm(3):           2
 call pardiso 11
 pardiso         11        117
 iparm(3):           2
 done pardiso 11, error=           0
 kbused, kbpeak:       35742      72619
 nnz L :     3295541         25  Mb
 MFlops:        505
 Mem_Internal:     5612952
 iUsePardiso :          1
 sym-pos-def
 Checking unrelated dofs
        386  dofs only used once of       43846
        242  max dofs for dof      33313
 First infected dof      33313        242
         1 nDone :       5390 of       43846      38456 T
         1 nDone :      43846 of       43846          0 T
 Check time           4 ms
 Dof    33313 found, node:   16657      1     79.4118   -110.0000
 about to call pardiso_dec
 Mem: 2 15741 (5455) MB (free) physical memory
 Process ID, MemMB : 37552 232
 call pardiso 22, ityp          2
 sec0:   40304.9296875000
 size ia:       63419        2678832185536
 size ja:     1045749        2678854976256
 size  a:     1045749        2678905900160
 pardiso         22         55
 pardecomp:  6.250000000000000E-002  5.468750000000000E-002
 done pardiso 22, error=           0
 back from pard_gg
Decomp :   0.18 s
 Process ID, MemMB : 37552 259
 PASSMBMEM 259
Time 11:11:44         0.00
 dsT:  0.000000000000000E+000  0.000000000000000E+000
  GNORM=   159686.462411482
 idVolOpt          0
 iel,prev:       1214       1458          0          3
 SumRnew1=   294025.480966638
 SumRnew2=   294025.480966638
 iOutbal, |SC|          2   22592.0969277677       1601.20651028317
 SumRnew3=   73506.3702416596
 SumRload1,:   13276.8208529125
 pardiso mtype          2
 dTime()   1551250.00000000
 dTime in Constit :    1551250.00000000
 iel,prev:       1214       1458          0          3
 NaN in UDSM:       1214          1
sig0     0.000E+00  0.000E+00  0.000E+00   0.000E+00
stvar0   2.200E+00  4.400E-01  5.550E+02   4.400E+00  2.086E+00
```

dEps 7.413E-08 -8.888E-02 0.000E+00 1.356E-07 0.000E+00 0.000E+00
-5.053E-03 1.457E-03 0.000E+00 5.428E-03 0.000E+00 0.000E+00
0.000E+00 0.000E+00 0.000E+00 0.000E+00 0.000E+00 0.000E+00
0.000E+00 0.000E+00 0.000E+00 0.000E+00
D
1 2.540E+02 6.349E+01 6.349E+01 0.000E+00 0.000E+00 0.000E+00
2 6.349E+01 2.540E+02 6.349E+01 0.000E+00 0.000E+00 0.000E+00
3 6.349E+01 6.349E+01 2.540E+02 0.000E+00 0.000E+00 0.000E+00
4 0.000E+00 0.000E+00 0.000E+00 9.524E+01 0.000E+00 0.000E+00
5 0.000E+00 0.000E+00 0.000E+00 0.000E+00 9.524E+01 0.000E+00
6 0.000E+00 0.000E+00 0.000E+00 0.000E+00 0.000E+00 9.524E+01
sig NaN NaN NaN NaN
stvar NaN 4.398E-01 5.550E+02 NaN 2.086E+00
2 IDTask
1 iMod
0 isUndr
1 iStep
1 iTer
1214 iEl
1 int
13.9548607707615 x
-80.2677202194893 y
0.00000000000000 z
6029712568.54789 Time0
1551250.00000000 dTime
50 Props
1.13481281000000 47.6190476000000 1.5750000000000000E-02
2.5920000000000000E-02 0.800000000000000 9.0000000000000000E-04
4.2000000000000000E-02 2.20000000000000 2.00000000000000
100.000000000000 0.440000000000000 0.00000000000000
0.00000000000000 0.00000000000000 0.00000000000000
0.00000000000000 0.00000000000000 0.00000000000000
0.00000000000000 0.00000000000000 0.00000000000000
0.00000000000000 0.00000000000000 0.00000000000000
0.00000000000000 0.00000000000000 0.00000000000000
0.00000000000000 0.00000000000000 0.00000000000000
0.00000000000000 0.00000000000000 0.00000000000000
0.00000000000000 0.00000000000000 0.00000000000000
0.00000000000000 0.00000000000000 0.00000000000000
0.00000000000000 0.00000000000000 0.00000000000000
0.00000000000000 0.00000000000000 0.00000000000000
0.00000000000000 0.00000000000000
50 Sig0
0.00000000000000 0.00000000000000 0.00000000000000
0.00000000000000 0.00000000000000 0.00000000000000
0.00000000000000 0.00000000000000 0.250000000000000
1.00000000000000 1.00000000000000 0.00000000000000
0.00000000000000 1.00000000000000 1.00000000000000
1.00000000000000 1.00000000000000 0.00000000000000
0.00000000000000 0.00000000000000 0.00000000000000
0.00000000000000 0.00000000000000 0.00000000000000
0.00000000000000 0.00000000000000 0.00000000000000
0.00000000000000 0.00000000000000 0.00000000000000
0.00000000000000 0.00000000000000 0.00000000000000
0.00000000000000 0.00000000000000 0.00000000000000
0.00000000000000 0.00000000000000 0.00000000000000
0.00000000000000 0.00000000000000 0.00000000000000
0.00000000000000 0.00000000000000
0.00000000000000 swp0
5 nStatV0

```
 2.20000000000000     0.440000000000000      555.000000000000
 4.40000000000000      2.08627374249605
  6  dEps
7.412569802272960E-08 -8.887870645784091E-02   0.00000000000000
1.356475959219426E-07   0.00000000000000      0.00000000000000
 1551250.00000000     dTime
 36  D
 253.968253917460      63.4920635174603      63.4920635174603
 0.00000000000000      0.00000000000000      0.00000000000000
 63.4920635174603      253.968253917460      63.4920635174603
 0.00000000000000      0.00000000000000      0.00000000000000
 63.4920635174603      63.4920635174603      253.968253917460
 0.00000000000000      0.00000000000000      0.00000000000000
 0.00000000000000      0.00000000000000      0.00000000000000
 95.2380952000000      0.00000000000000      0.00000000000000
 0.00000000000000      0.00000000000000      0.00000000000000
 0.00000000000000      95.2380952000000      0.00000000000000
 0.00000000000000      0.00000000000000      0.00000000000000
 0.00000000000000      0.00000000000000      95.2380952000000
 12698.4126984127      BulkW
  6  Sig
           NaN             NaN             NaN
           NaN             NaN             NaN
 0.00000000000000     swp
  5  nStatV
           NaN  0.439804467008869      555.000000000000
           NaN   2.08627374249605
  0  ipl
  0  iAbort
MyStop        39
Total cpu  :   1.45312500010000
Total wall :   2.40200000000000

+------+--------+-------------+--------+-------------+--------+----------+
| Task |  Count |      CPU    |   %    |  Wall clock |    %   | Name     |
+------+--------+-------------+--------+-------------+--------+----------+
|    0 |      1 |       1.45 | 100.00 |        2.40 | 100.00 | Total    |
+------+--------+-------------+--------+-------------+--------+----------+
|    1 |      2 |       0.08 |   5.38 |        0.09 |   3.54 | FrmMtx   |
|    5 |      2 |       0.62 |  43.01 |        0.47 |  19.36 | GetSig   |
|    6 |      4 |       0.06 |   4.30 |        0.02 |   0.92 | Bt_Sig   |
|    8 |      1 |       0.00 |   0.00 |        0.00 |   0.08 | WtCXX    |
|   30 |      2 |       0.00 |   0.00 |        0.00 |   0.04 | mtx_scl2 |
|   51 |      2 |       0.33 |  22.58 |        0.23 |   9.70 | Reorder  |
|   52 |      2 |       0.08 |   5.38 |        0.06 |   2.62 | Factor   |
|   53 |      2 |       0.03 |   2.15 |        0.01 |   0.25 | Backsub  |
|   63 |      2 |       0.00 |   0.00 |        0.01 |   0.25 | fill_ijA |
|   64 |      1 |       0.00 |   0.00 |        0.00 |   0.08 | clean    |
|   67 |      2 |       0.03 |   2.15 |        0.03 |   1.08 | FillLMat |
+------+--------+-------------+--------+-------------+--------+----------+
|  100 |      1 |       0.22 |  15.05 |        1.49 |  62.07 | Rest     |
+------+--------+-------------+--------+-------------+--------+----------+
NaN found during calculation, probably severe divergence
p_DLL_CE 3:       140726902259712       140726902264352
FFUninitialize
Calc_Ready 0
```

Appendix 9F: PLAXIS Numerical Results. Debug log 2 of failed calculation.

Excerpt from debug-file of failed calculation

$\mu = 0.0009$ $R = 2$ $\gamma = 0$

Stvar0 = $[OCR, e, Flag, p_0, r]$
Sig0 = $[\sigma'_{xx,0}, \sigma'_{yy,0}, \sigma'_{zz,0}, \sigma'_{xy,0}, \sigma'_{yz,0} = 0, \sigma'_{zx,0} = 0,\ldots,]$
IDTask = 2 = Calculate constitutive stresses.
nStat = Number of state variables
UDSM = User-Defined Soil Model = HVMCC

$$\boldsymbol{OCR_0 = 2.277}$$

```
NSTEP=   1
 100A : dT :    1551250.00000000       6035917568.54789
 LoadAc start Active
   0.000E+00  0.000E+00  0.000E+00   1.000E+00  0.000E+00  0.000E+00
   0.000E+00  0.000E+00  0.000E+00   0.000E+00  0.000E+00
 LoadAc end   Active
   0.000E+00  0.000E+00  0.000E+00   1.000E+00  0.000E+00  0.000E+00
   0.000E+00  0.000E+00  0.000E+00   0.000E+00  0.000E+00
Active   0.000E+00  0.000E+00  0.000E+00   1.000E+00  0.000E+00  0.000E+00
       0.000E+00  0.000E+00  0.000E+00   0.000E+00  0.000E+00
 iel,prev:       1214       1458         0         6
 SumG:    393479706.699562
 AA dT :    1551250.00000000
 BB dT :    1551250.00000000
 Before MakMat :    1551250.00000000       T
 iTest, MakMat          0 T
Time 11:55:48         2.00
 dTime in matrix :    1551250.00000000
 FMAMAT T   1551250.00000000
 iel,prev:       1214       1458         0         3
 SymDif/Sum   :  4.06869E-06  4.71677E+10  1.06021E+10
 Determine_Sp_i0A_i1A         2          94107472          1922471716
       5453         20
          1         0       115
      33021       1108       5453
 dasum AA:   28521709891.9264
 dasum AA:   27041673094.2564
 bound3n:          3
 Time for forming matrix:
Time 11:55:48         0.00
 Process ID, MemMB : 25544 182
 PASSMBMEM 182
  iMat    :          3
 iUsePardiso:          1
 iUsePardiso:          1
 Fill_Pard T          1
 try SpMtx
 Size iiA:      43847      63419
 Size jjA:     1225741     154877
 Size  AA:     1045749     154877
 nnz:     1045749
 Size ia_Pard:      63419      43847
 Size ja_Pard:     1045749    1225741
 Size  a_Pard:     1045749    1045749
 end fill          2
 size amat  :    18651125
```

```
 size a_pard:     1045749
 dasum a_Pard:   27041673094.2564         1032024   27041673094.2597
 Filter SpMtx:          3
      iUsePardiso:          1
 GetFreeMem
 Tot. Int.:     16119096  kB       15741  Mb
 Internal :      5196200  kB        5074  Mb free
 InSwap   :      6911380  kB        6749  Mb free
 Total    :     12107580  kB       11823  Mb free
 mkl_get_max_threads         3
 n_in, nthr :       43846         2     1045750
 iParm(2):          2
 iparm(3):          2
 call pardiso 11
 pardiso         11        148
 iparm(3):          2
 done pardiso 11, error=          0
 kbused, kbpeak:       35742      72619
 nnz L :     3295541         25  Mb
 MFlops:        505
 Mem_Internal:     5196200
 iUsePardiso :          1
 sym-pos-def
 Checking unrelated dofs
        386  dofs only used once of       43846
        242  max dofs for dof      33313
 First infected dof      33313        242
         1 nDone :       5390 of       43846      38456 T
         1 nDone :      43846 of       43846          0 T
 Check time          3 ms
 Dof    33313 found, node:   16657      1     79.4118   -110.0000
 about to call pardiso_dec
 Mem: 2 15741 (5054) MB (free) physical memory
 Process ID, MemMB : 25544 227
 call pardiso 22, ityp          2
 sec0:   42948.5390625000
 size ia:       63419        2574439366848
 size ja:     1045749        2574462157568
 size  a:     1045749        2574513212544
 pardiso         22         71
 pardecomp:  0.125000000000000       7.031250000000000E-002
 done pardiso 22, error=          0
 back from pard_gg
Decomp :   0.23 s
 Process ID, MemMB : 25544 255
 PASSMBMEM 255
Time 11:55:48         0.00
 dsT:  0.000000000000000E+000  0.000000000000000E+000
  GNORM=   159686.462411482
 idVolOpt          0
 iel,prev:       1214       1458          0          3
 SumRnew1=   294025.480966638
 SumRnew2=   294025.480966638
 iOutbal, |SC|          2   22592.0969277677       1601.20651028317
 SumRnew3=   73506.3702416596
 SumRload1,:   13276.8208529125
 pardiso mtype          2
 dTime()   1551250.00000000
 dTime in Constit :    1551250.00000000
 iel,prev:       1214       1458          0          3
 NaN in UDSM:       1214          2
sig0     0.000E+00  0.000E+00  0.000E+00   0.000E+00
stvar0   2.277E+00  4.400E-01  5.550E+02   4.554E+00  2.086E+00
```

dEps -5.228E-09 -1.555E-02 0.000E+00 2.162E-08 0.000E+00 0.000E+00
-5.432E-03 1.358E-03 0.000E+00 5.257E-04 0.000E+00 0.000E+00
0.000E+00 0.000E+00 0.000E+00 0.000E+00 0.000E+00 0.000E+00
0.000E+00 0.000E+00 0.000E+00 0.000E+00
D
1 2.540E+02 6.349E+01 6.349E+01 1.270E+02 7.777E+02 0.000E+00
2 6.349E+01 2.540E+02 6.349E+01 1.270E+02 7.777E+02 0.000E+00
3 6.349E+01 6.349E+01 2.540E+02 1.270E+02 7.777E+02 0.000E+00
4 1.270E+02 1.270E+02 1.270E+02 2.222E+02 7.777E+02 0.000E+00
5 7.777E+02 7.777E+02 7.777E+02 7.777E+02 4.859E+03 0.000E+00
6 0.000E+00 0.000E+00 0.000E+00 0.000E+00 0.000E+00 9.524E+01
sig NaN NaN NaN NaN
stvar NaN 4.400E-01 5.550E+02 NaN 2.086E+00
2 IDTask
1 iMod
0 isUndr
1 iStep
1 iTer
1214 iEl
2 int
17.3445085922206 x
-74.4525227161498 y
0.00000000000000 z
6029712568.54789 Time0
1551250.00000000 dTime
50 Props
1.13481281000000 47.6190476000000 1.5750000000000000E-02
2.5920000000000000E-02 0.800000000000000 9.0000000000000000E-04
4.2000000000000000E-02 2.27700000000000 2.00000000000000
100.000000000000 0.440000000000000 0.00000000000000
0.00000000000000 0.00000000000000 0.00000000000000
0.00000000000000 0.00000000000000 0.00000000000000
0.00000000000000 0.00000000000000 0.00000000000000
0.00000000000000 0.00000000000000 0.00000000000000
0.00000000000000 0.00000000000000 0.00000000000000
0.00000000000000 0.00000000000000 0.00000000000000
0.00000000000000 0.00000000000000 0.00000000000000
0.00000000000000 0.00000000000000 0.00000000000000
0.00000000000000 0.00000000000000 0.00000000000000
0.00000000000000 0.00000000000000 0.00000000000000
0.00000000000000 0.00000000000000 0.00000000000000
0.00000000000000 0.00000000000000
50 Sig0
0.00000000000000 0.00000000000000 0.00000000000000
0.00000000000000 0.00000000000000 0.00000000000000
0.00000000000000 0.00000000000000 0.250000000000000
1.00000000000000 1.00000000000000 0.00000000000000
0.00000000000000 1.00000000000000 1.00000000000000
1.00000000000000 1.00000000000000 0.00000000000000
0.00000000000000 0.00000000000000 0.00000000000000
0.00000000000000 0.00000000000000 0.00000000000000
0.00000000000000 0.00000000000000 0.00000000000000
0.00000000000000 0.00000000000000 0.00000000000000
0.00000000000000 0.00000000000000 0.00000000000000
0.00000000000000 0.00000000000000 0.00000000000000
0.00000000000000 0.00000000000000 0.00000000000000
0.00000000000000 0.00000000000000 0.00000000000000
0.00000000000000 0.00000000000000
0.00000000000000 swp0
5 nStatV0

```
 2.27700000000000     0.440000000000000      555.000000000000
 4.55400000000000      2.08627374249605
  6  dEps
-5.228477921352944E-09 -1.554998926991658E-02   0.00000000000000
 2.162360646852834E-08   0.00000000000000      0.00000000000000
 1551250.00000000     dTime
 36  D
 253.968253917460      63.4920635174603      63.4920635174603
 126.984126984127      777.737836909760      0.00000000000000
 63.4920635174603      253.968253917460      63.4920635174603
 126.984126984127      777.737836909760      0.00000000000000
 63.4920635174603      63.4920635174603      253.968253917460
 126.984126984127      777.737836909760      0.00000000000000
 126.984126984127      126.984126984127      126.984126984127
 222.222222184127      777.737836909760      0.00000000000000
 777.737836909760      777.737836909760      777.737836909760
 777.737836909760      4858.63772101845      0.00000000000000
 0.00000000000000      0.00000000000000      0.00000000000000
 0.00000000000000      0.00000000000000      95.2380952000000
 12698.4126984127      BulkW
  6  Sig
           NaN             NaN             NaN
           NaN             NaN             NaN
 0.00000000000000     swp
  5  nStatV
           NaN  0.439965790012104      555.000000000000
           NaN   2.08627374249605
  0  ipl
  0  iAbort
MyStop        39
Total cpu  :   1.53125000010000
Total wall :   2.43400000000000

+------+--------+-------------+--------+-------------+--------+----------+
| Task |  Count |      CPU    |   %    |  Wall clock |    %   | Name     |
+------+--------+-------------+--------+-------------+--------+----------+
|    0 |      1 |       1.53 | 100.00 |       2.43 | 100.00 | Total    |
+------+--------+-------------+--------+-------------+--------+----------+
|    1 |      2 |       0.08 |   5.10 |       0.09 |   3.66 | FrmMtx   |
|    5 |      2 |       0.64 |  41.84 |       0.44 |  18.24 | GetSig   |
|    6 |      4 |       0.06 |   4.08 |       0.03 |   1.15 | Bt_Sig   |
|    8 |      1 |       0.00 |   0.00 |       0.00 |   0.08 | WtCXX    |
|   30 |      2 |       0.00 |   0.00 |       0.00 |   0.08 | mtx_scl2 |
|   51 |      2 |       0.31 |  20.41 |       0.26 |  10.81 | Reorder  |
|   52 |      2 |       0.12 |   8.16 |       0.08 |   3.20 | Factor   |
|   53 |      2 |       0.03 |   2.04 |       0.01 |   0.29 | Backsub  |
|   63 |      2 |       0.00 |   0.00 |       0.00 |   0.16 | fill_ijA |
|   64 |      1 |       0.00 |   0.00 |       0.00 |   0.08 | clean    |
|   67 |      2 |       0.05 |   3.06 |       0.03 |   1.07 | FillLMat |
+------+--------+-------------+--------+-------------+--------+----------+
|  100 |      1 |       0.23 |  15.31 |       1.49 |  61.18 | Rest     |
+------+--------+-------------+--------+-------------+--------+----------+
NaN found during calculation, probably severe divergence
p_DLL_CE 3:       140726902259712       140726902264352
FFUninitialize
Calc_Ready 0
```

Appendix 9G: PLAXIS Numerical Results. Debug log 2 of successful calculation.

Excerpt from debug-file of successful calculation

$\mu = 0.0009$ $R = 2$ $\gamma = 0$

Stvar0 = $[OCR, e, Flag, p_0, r]$
Sig0 = $[\sigma'_{xx,0}, \sigma'_{yy,0}, \sigma'_{zz,0}, \sigma'_{xy,0}, \sigma'_{yz,0} = 0, \sigma'_{zx,0} = 0,\ldots,]$
IDTask = 2 = Calculate constitutive stresses.
nStat = Number of state variables
UDSM = User-Defined Soil Model = HVMCC

$$\boldsymbol{OCR_0 = 2.4}$$

```
NSTEP=   1
 100A : dT :    1551250.00000000       6035917568.54789
 LoadAc start Active
   0.000E+00  0.000E+00  0.000E+00   1.000E+00  0.000E+00  0.000E+00
   0.000E+00  0.000E+00  0.000E+00   0.000E+00  0.000E+00
 LoadAc end   Active
   0.000E+00  0.000E+00  0.000E+00   1.000E+00  0.000E+00  0.000E+00
   0.000E+00  0.000E+00  0.000E+00   0.000E+00  0.000E+00
Active   0.000E+00  0.000E+00  0.000E+00   1.000E+00  0.000E+00  0.000E+00
       0.000E+00  0.000E+00  0.000E+00   0.000E+00  0.000E+00
 iel,prev:       1214       1458          0          6
 SumG:    393479706.699562
 AA dT :    1551250.00000000
 BB dT :    1551250.00000000
 Before MakMat :    1551250.00000000       T
 iTest, MakMat          0 T
Time 11:13:31         2.00
 dTime in matrix :    1551250.00000000
 FMAMAT T   1551250.00000000
 iel,prev:       1214       1458          0          3
 SymDif/Sum   :   4.06869E-06  4.71677E+10  1.06021E+10
 Determine_Sp_i0A_i1A          3           94107472          1922471716
       5453         20
          1         0       115
      33021       1108       5453
 dasum AA:   28521709891.9264
 dasum AA:   27041673094.2564
 bound3n:          4
 Time for forming matrix:
Time 11:13:31         0.00
 Process ID, MemMB : 24048 184
 PASSMBMEM 184
  iMat     :          3
 iUsePardiso:          1
 iUsePardiso:          1
 Fill_Pard T          1
 try SpMtx
 Size iiA:       43847      63419
 Size jjA:     1225741     154877
 Size  AA:     1045749     154877
 nnz:     1045749
 Size ia_Pard:       63419      43847
 Size ja_Pard:     1045749    1225741
 Size  a_Pard:     1045749    1045749
 end fill         10
 size amat  :    18651125
```

```
 size a_pard:     1045749
 dasum a_Pard:   27041673094.2564         1032024   27041673094.2597
 Filter SpMtx:         11
      iUsePardiso:          1
 GetFreeMem
 Tot. Int.:     16119096  kB       15741  Mb
 Internal :      5716908  kB        5582  Mb free
 InSwap   :      7863796  kB        7679  Mb free
 Total    :     13580704  kB       13262  Mb free
 mkl_get_max_threads          3
 n_in, nthr :       43846          2     1045750
 iParm(2):          2
 iparm(3):          2
 call pardiso 11
 pardiso         11        127
 iparm(3):          2
 done pardiso 11, error=          0
 kbused, kbpeak:       35742      72619
 nnz L :     3295541         25  Mb
 MFlops:        505
 Mem_Internal:     5716908
 iUsePardiso :          1
 sym-pos-def
 Checking unrelated dofs
        386  dofs only used once of       43846
        242  max dofs for dof      33313
 First infected dof      33313        242
         1 nDone :       5390 of       43846      38456 T
         1 nDone :      43846 of       43846          0 T
 Check time           4 ms
 Dof    33313 found, node:   16657      1     79.4118   -110.0000
 about to call pardiso_dec
 Mem: 2 15741 (5559) MB (free) physical memory
 Process ID, MemMB : 24048 229
 call pardiso 22, ityp          2
 sec0:   40411.9257812500
 size ia:       63419        1863464272064
 size ja:     1045749        1863487062784
 size  a:     1045749        1863538052224
 pardiso         22         80
 pardecomp:  0.156250000000000       7.812500000000000E-002
 done pardiso 22, error=          0
 back from pard_gg
Decomp :   0.22 s
 Process ID, MemMB : 24048 257
 PASSMBMEM 257
Time 11:13:32         1.00
 dsT:  0.000000000000000E+000  0.000000000000000E+000
  GNORM=   159686.462411482
 idVolOpt          0
 iel,prev:       1214       1458          0          3
 SumRnew1=   294025.480966638
 SumRnew2=   294025.480966638
 iOutbal, |SC|          2   22592.0969277677       1601.20651028317
 SumRnew3=   73506.3702416596
 SumRload1,:   13276.8208529125
 pardiso mtype          2
 dTime()   1551250.00000000
 dTime in Constit :    1551250.00000000
 iel,prev:       1214       1458          0          3
SUB:max,IP,avg,mLev:      5  17497  1.49   0
 SumRnew1=   10526078561.0515
 SumRnew2=   10526078561.0515
```

```
 thermal line search relax=   1.00000000000000      F
 ActiveUWC= F
ITER=    1 ERROR = 1.749E+04  ERRLOC= 1.780E-04  NPLAS=  6552  NINAC=  3612
        FACTOR= 1.000E+00  ERRLCI= 0.000E+00  NPINT=     0  INACI=     0
        CSP   = 9.981E-01  EGLM  = 0.000E+00  NPLBM=     0

iTest :          1
FSTULT,SCF =    1.00000000000000       0.125000000000000
DTime (BBB)=   775625.000000000
```

Series of iterations later:

```
ITER=    7 ERROR = 3.833E-03  ERRLOC= 3.357E-06  NPLAS=  6552  NINAC=     0
        FACTOR= 1.000E+00  ERRLCI= 0.000E+00  NPINT=     0  INACI=     0
        CSP   = 5.687E-01  EGLM  = 0.000E+00  NPLBM=     0

 EGLQtOld=  0.000000000000000E+000  0.000000000000000E+000
 UWC_Div_Indication=          0          3
 EGLQtOld=  0.000000000000000E+000
 LADV0=          1
 isTHM= F
 EGLN1=  3.832650359134970E-003  1.137412973677932E-002
 RNORM=   2014.31322349371       5977.86330284996
 ICHK :          1 F
 iel,prev:       1214       1458         0         6
 UITIT,ULTNIL: F F
 CSP :   6.21146E-01  1.92398E+04  3.09746E+04
 ICHK :          2 F
 ISTSUB, NSUBT  :         1         1
 ULTLEV, ULTCONS: T F
 iRes:           1
 WrtLog:  T
 Tot, Av Gb: 952.622 107.417
 iSpace:   112634948       6566
  99  8237825      32   257432 B/ms
 Tot, Av Gb: 952.622 107.409
 Used kB:        8045  kB       8045
 AddCxx
 bkhead:$$S000010H##        440
 end cxx
 Call Step_Ready
 After Call Step_Ready
 ParmT :    6035917568.54789
 flTUlt:    6035917568.54789
Time for this step :      4.109 s
Calculation time :      35.090 s
Time 11:14:04        35.00
 p_DLL_CE 3:       140726902259712       140726902264352
 FFUninitialize
Time 11:14:04         0.00
Total time :      35.210 s
CPU   time :      39.672 s
 Total cpu  :    39.6718750001000
 Total wall :    35.2090000000000
```

Task	Count	CPU	%	Wall clock	%	Name
0	1	39.67	100.00	35.21	100.00	Total
1	23	1.66	4.17	1.87	5.32	FrmMtx
5	47	33.47	84.36	27.99	79.49	GetSig
6	116	1.06	2.68	0.64	1.82	Bt_Sig
7	10	0.09	0.24	0.37	1.05	WtXXX
8	11	0.00	0.00	0.01	0.03	WtCXX
30	23	0.02	0.04	0.04	0.11	mtx_scl2
51	2	0.28	0.71	0.28	0.78	Reorder
52	23	1.92	4.84	1.13	3.20	Factor
53	29	0.17	0.43	0.14	0.41	Backsub
63	23	0.14	0.35	0.08	0.22	fill_ijA
64	1	0.00	0.00	0.00	0.01	clean
67	2	0.09	0.24	0.03	0.07	FillLMat
71	10	0.00	0.00	0.02	0.06	Genucht
100	1	0.77	1.93	2.62	7.44	Rest

Calc_Ready 0

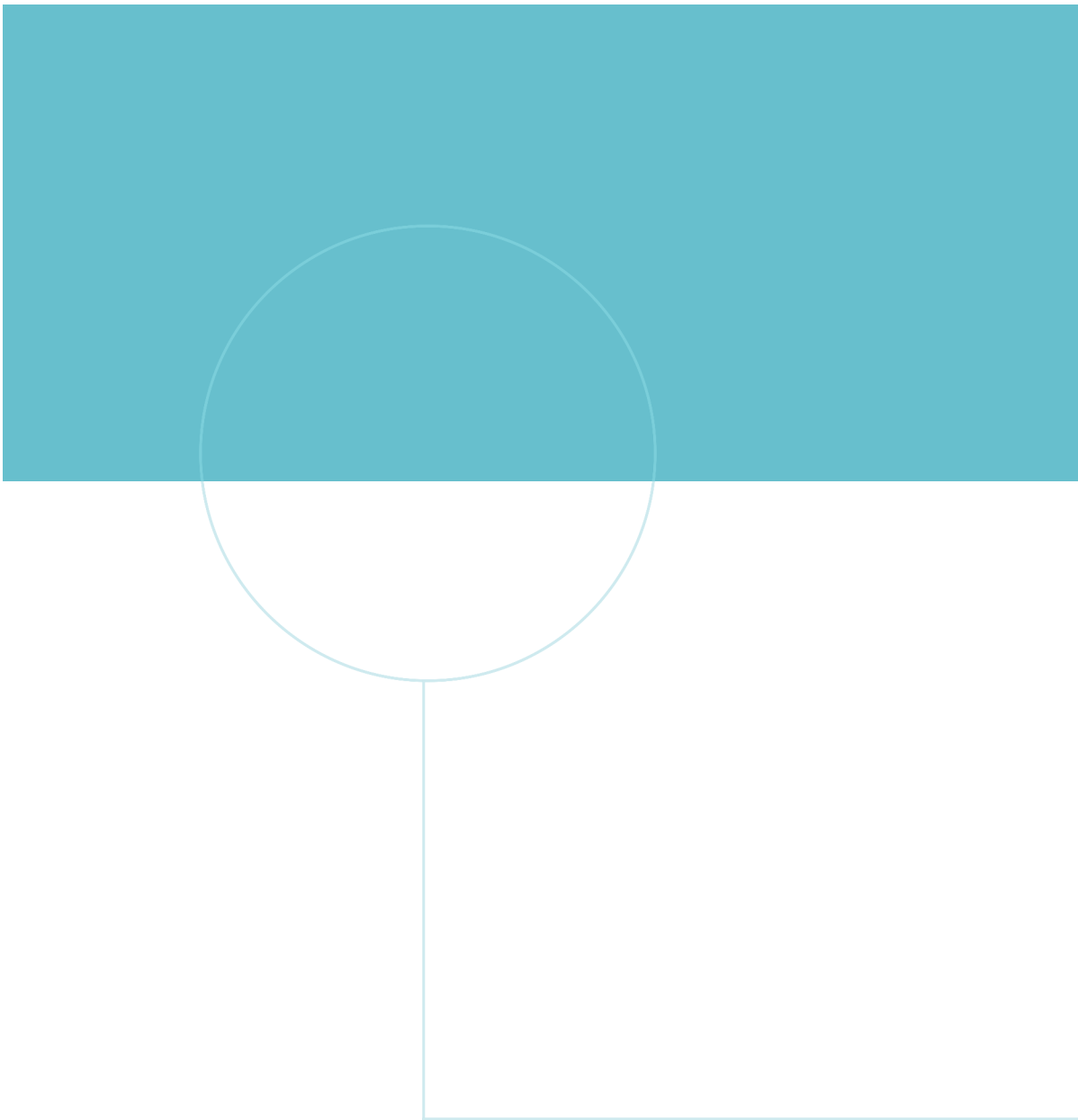

NTNU

Norwegian University of
Science and Technology